A METHODOLOGY FOR DYNAMIC SIZING OF ELECTRIC POWER GENERATION AND DISTRIBUTION ARCHITECTURES

A Dissertation
Presented to
The Academic Faculty

By

Gökçin Çınar

In Partial Fulfillment
of the Requirements for the Degree
Doctor of Philosophy in the
Daniel Guggenheim School of Aerospace Engineering

Georgia Institute of Technology

December 2018

A METHODOLOGY FOR DYNAMIC SIZING OF ELECTRIC POWER GENERATION AND DISTRIBUTION ARCHITECTURES

Approved by:

Professor Dimitri N. Mavris, Advisor
School of Aerospace Engineering
Georgia Institute of Technology

Professor Daniel P. Schrage
School of Aerospace Engineering
Georgia Institute of Technology

Dr. Elena Garcia
School of Aerospace Engineering
Georgia Institute of Technology

Dr. Soumya S. Patnaik
Aerospace Systems Directorate
Air Force Research Laboratory

Mr. John G. Nairus
Power and Control Division
Air Force Research Laboratory

Date Approved: September 7, 2018

“The future is in the skies.”

Mustafa Kemal Atatürk

To my parents, for their unconditional love, support and sacrifice.

And to my husband, for being the joy of my life.

ACKNOWLEDGEMENTS

Now that I am at the end of my six year-long PhD journey, I can unhesitatingly say that it has been an incredibly challenging, emotionally consuming but at the same time an extremely rewarding adventure. Looking back, I could have never imagined the amount of opportunities I was going to come across. Of course, each opportunity came with multiple challenges I had to overcome. I consider myself very lucky, as I had the support of some truly amazing people who have helped me make my dreams come true.

First of all, I would like to thank my advisor, mentor and role model, Professor Dimitri Mavris. There are no words to describe my gratitude and appreciation to him, for making me a part of the ASDL family, taking me under his wings, and being my "surrogate father", just like he is to hundreds of his students. His knowledge and passion for his job, his patience, caring and understanding for the people around him, and his dedication to share and teach will always inspire me to *strive to fulfill my unrealized potential*.

I wish to express my heartfelt appreciation to Dr. Elena Garcia, who spent hours and hours of her time to review and critique this research and steered me to the right direction every time I felt stuck, got lost in the details and couldn't see the "bigger picture" anymore. I am also grateful to her for providing invaluable advice not only on this work but also on many other areas in life.

I would like to gratefully acknowledge my valuable committee members, Professor Schrage, Dr. Patnaik and Mr. Nairus for their support of this work, and for taking the time from their busy schedule to review this three-hundred-plus-pages thesis. I greatly benefited from their expertise, guidance and feedback.

During this journey, I have made many intelligent, inspiring and amusing friends without whom my graduate school experience would have been very dull and lonely. I would like to take this opportunity to sincerely thank my confidants Dr. Derya Aksaray and Dr. Can Temel for always being there fore me, and helping me overcome the cultural shock

I was having in my first few months at graduate school. I am also deeply grateful for my good friends Dr. Burak Bağdatlı, Emre Yılmaz, and Fatma Karagöz for their endless support especially during the "dark days" of PhD qualifying exams and the defense.

I must also thank my ASDL family. To name a few: Nathalie Antunes, Clélia Level, Emily Kollin and Coleby Friedland for not losing touch so many years after graduation and for being crazy enough to travel a great distance to come to my wedding; Dr. Shai Bernstein for being a good "komşu"; Dr. Imon Chakraborty, Dr. Mohammed Hassan, Dr. Matthew LeVine, Dr. Christopher Frank, and Dr. Holger Pfaender for sharing their valuable experiences and technical insights, but more importantly, for their friendship. I would also like to thank to my very first friend from Georgia Tech, Eliya Wing, with whom I had the pleasure to work with in our Georgia Tech-METU team for the 2012 AHS Student Design Competition (and we won!).

I would like to thank to Professor Ümit Çatalyürek and Gamze Çatalyürek for their friendship, kindness and support. I very much enjoy our board game nights! I am also grateful to Professor Çatalyürek for letting me use his high performance computer (a "New Hope") so that I could run thousands of time-consuming simulations for my thesis in a fraction of the time.

There have been many other people who have helped me improve myself in my career, and I wish to extend my sincere appreciation to all of them. My dear physicist cousin, Dr. Tuna Yıldırım, not only catalyzed my interest in astrophysics but also kick-started my U.S.A. experience by helping me get an internship in physics. Dr. Jared Leisner and Professor Donald Gurnett gave me the opportunity to work with them in the Radio and Plasma Wave Group at University of Iowa, where I first got a taste of academic research and learned a great deal from it. Professor Ilkay Yavrucuk and my many other undergraduate professors guided and supported me in my decision to sail to the land of opportunities to pursue a PhD degree. Mathias Emeneth and Alexander Schneegans gave me the great opportunity to work with them at PACE for three months in Germany where I gained valuable experience

and got to learn about yet another amazing culture. And last but not least, Dr. Hernando Jimenez was an exceptional researcher, teacher and friend who although no longer with us, continues to inspire by his example and dedication.

Special thanks goes to my best friend, my rock, my husband, Efe Yamaç Yarbaşı. I could not have come this far without his kindness, patience, witty spirit and love. He wholeheartedly supported my decision to move to a far, far away country across the ocean to follow my dreams. For four long years being apart, in spite of the thousands of miles and seven hours of time difference between us, he was always there for me. And ever since our love overcame all the obstacles in our way and reunited us, he continues empowering me by spending many nights by my side while I was working on my thesis, by playing my favorite songs on his guitar, by taking me to a bicycle ride, and by just being himself, the most wonderful human being I have ever known. Thank you Efe, the love of my life, for being my brightest star in the darkest of nights.

Finally, I would like to express my deepest gratitude to my parents, Filiz and Ertuğrul, for *everything*. It is funny how hard I find it to express my feelings when it comes to the two most influential people in my life. I came this far because of their hard work, energy and faith in me. I was able to pull through because they stayed awake through countless nights just to be there for me, on the other end of the video call when I was studying for the PhD Quals, so that they could cheer me up, so that I wouldn't feel lonely. I am receiving this degree because I have the most amazing, loving and caring family I could ever wish for. *Anne, baba, sizi tahmin edemeyeceğiniz kadar çok seviyorum.*

Gökçin Çınar

Atlanta, GA

October 2018

TABLE OF CONTENTS

LIST OF TABLES

LIST OF FIGURES

SUMMARY

In recent years, there have been increasing efforts to reduce aviation related greenhouse gas emissions and fuel burn. To meet the increasing demand for greener aviation, the aerospace industry is working on a cutting-edge aircraft concept: electric aircraft. Although electric propulsion is an enabler for CO_2, NO_x and noise reduction, as well as higher propulsive efficiency, aircraft which solely depend upon electric motors and batteries are unlikely to achieve similar flight performance to conventional propulsion systems in the near future. Hence, a hybrid-electric propulsion system is envisioned as a middle step towards fully electric propulsion.

Electric and hybrid electric aircraft (EA/HEA) pose a significant architecture challenge, as these concepts not only deal with considerably high electrical loads, but are also extremely weight-sensitive. Therefore, the architectural choices must be made carefully. However, the majority of performance characteristics and dynamic behavior of electric power generation and distribution subsystems (EPGDS) are neglected at the aircraft conceptual design stage, and left to later design phases where the design freedom is limited.

Additionally, the traditional aircraft sizing and synthesis approach has two major shortcomings when it comes to such revolutionary aircraft concepts. First, the aircraft weight estimations and the sizing of its major subsystems are typically performed at early design stages based on historical data pertaining to existing aircraft. However, there is a lack of historical data for unconventional vehicle concepts which do not necessarily conform to standard fixed-wing or rotary-wing vehicle configurations. Second, the traditional mission performance analysis approach is inadequate for unconventional energy sources, such as rechargeable batteries, which are the focus of this thesis.

The over-arching objective of this thesis is to develop a methodology to perform the sizing, integration and performance evaluation of electric power generation and distribution subsystems and architectures within electric and hybrid electric aircraft concepts. To this

end, this dissertation presents a methodological framework which integrates EPGDS considerations into the aircraft sizing and synthesis process to enable quantitative comparisons between different types of electric and hybrid electric propulsion architectures.

To overcome the aforementioned limitations, the traditional sizing and synthesis approach is modified to incorporate a modular weight estimation technique along with an energy-based mission analysis approach which stems from conservation laws. The new, generalized approach enables the design and performance evaluation of any vehicle configuration, including electric and hybrid electric aircraft.

Subsystem considerations are included within the aircraft sizing and synthesis by the development of bi-level, physics-based, parametric EPGDS models. These models increase the dimensionality of the analysis, reduce the epistemic uncertainty due to modeling assumptions, and enable technology projections. Moreover, a model-based propulsion architecture characterization method is presented to enable rapid architecture comparisons through automatic relationship establishment among the major subsystems.

Architectural comparisons are meaningful provided that the candidate architectures are evaluated while being operated under their optimal power management schedule. To ensure fair architectural comparisons, a power split optimizer is wrapped around the sizing and synthesis capability. This way, both design and off-design missions can be optimized during the sizing and/or the performance evaluation of the candidate architectures.

The dynamic nature of EPGDS is taken into account by the adaptive step sizing capability which enables performing transient analysis at the conceptual design stage without sacrificing valuable computational resources. A significant transient definition based on transient constraint violations is introduced. This definition is used to create categorical surrogate models to predict the probability of triggering significant transient responses due to operational changes. The predictions are made based on mission level factors only, and do not require detailed knowledge about the subsystem dynamics during mission performance analysis.

A conditional rule set is established based on the categorical surrogate model to determine whether the aircraft conditions necessitate transient analysis at any point in the mission. If they do, the conditional rule set adjusts the step size of the computations to switch from mission analysis to the higher fidelity transient analysis using the proper timescale. This way, the transient analyses are performed only when required so that the knowledge about the subsystem design is maximized while minimizing the computational burden.

A controller gain tuning approach is also presented to perform design space explorations within the subsystem domain. This approach utilizes Monte Carlo simulations to assess variable importance and to modify the optimization algorithm in such a way that it is biased to yield a solution acceptable for the majority of the cases in the design space. A gain scheduling technique is then used to simulate the dynamic subsystem response while minimizing the optimization efforts.

The created methodology, called *Electric Propulsion Architecture Sizing and Synthesis* (*E-PASS*), incorporates these elements and provides a capability to integrate subsystem performance and dynamics of novel architectures to the aircraft sizing process at early design phases.

The sizing and synthesis capabilities of E-PASS were validated against aircraft sizing and performance data obtained from literature. Significant transient responses predicted by the categorical surrogate model approach within E-PASS were compared against high fidelity transient analysis simulations. Comparisons between the predicted and simulated responses proved that this new approach can predict the occurrence of significant transients based only on information available at the mission analysis, with a high success rate.

Finally, it was presented that E-PASS ensured proper sizing and performance evaluation of the aircraft regardless of its propulsion system type. Therefore, by integrating the aforementioned elements and bringing the subsystem and architecture considerations into the aircraft conceptual design stage, E-PASS enables adequate comparisons between competing architectures.

CHAPTER 1
INTRODUCTION

1.1 The Need for a Greener Aviation

The global aviation industry is an important contributor to climate change. This contribution is due to the products emitted by fossil fuel combustion primarily at cruise altitudes. [1]

Aircraft emissions as well as cloud effects alter the chemical and particle microphysical atmospheric properties throughout the upper troposphere and lower stratosphere (between altitudes of 8-13 km) where the atmospheric changes associated with these emissions can have a lifetime of minutes (in case of contrails), to years (in case of changes in methane). These alterations change radiative forcing and hence, potentially lead to climate change, which in turn damages social welfare. [2, 3, 4]

The impacts of CO_2 on radiative forcing and climate change are well characterized and quantitatively calculated from fuel burn and emission data over time.[4] In 2015, worldwide aircraft operations produced 781 million tonnes of CO_2, out of over 36 billion tonnes anthropogenic CO_2 production. [5, 6] This means that aviation as a whole is responsible for approximately 2% of global human-induced CO_2 emissions and for 12% among all transportation sources. [3] Although 2% is rather a small contribution, global aircraft fuel consumption and CO_2 emissions are expected to increase as aviation demand increases rapidly in the upcoming years. [7]

1.2 Future Aircraft Emission Goals

As a response to the forecasted rise in demand, the aviation industry has committed to take action in order to prevent the potential increase of aircraft fuel consumption and emissions. At the 37th session of the International Civil Aviation Organization (ICAO) Assembly in

2010, the member states agreed to set a goal of 2% annual fuel efficiency improvement through the year 2050. [3] In 2010, international aviation had an approximately 65% share in global aviation fuel consumption and is expected to grow to about 70% by 2050. [7] Figure 1.1 demonstrates the expected fuel burn trends for international aviation from 2005 to 2040, with an extrapolation to 2050, as illustrated by ICAO [1]. The fuel burn results in the case when the 2% annual fuel efficiency goal is also reached are provided in the figure. Moreover, the analysis considers the improvements that are expected to come from advances in aircraft technology, air traffic management and infrastructure use. Note that, in general, CO_2 emissions are assumed to be proportional to the total fuel usage. [1]

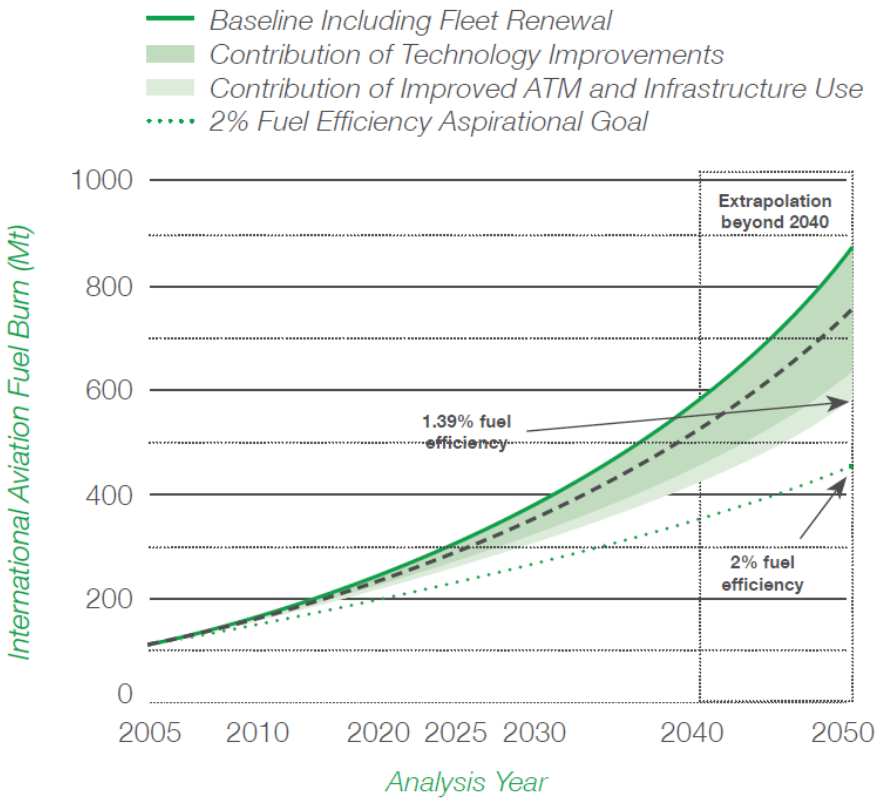

Figure 1.1: ICAO fuel burn trends from international aviation, 2005 to 2050. Results were modeled for 2005, 2006, 2010, 2020, 2025, 2030, and 2040 then extrapolated to 2050.[1]

Furthermore, at the 37th session of the ICAO Assembly, the member states also adopted a global aspirational goal to keep the net CO_2 emissions at 2020 levels and subsequently to reduce net CO_2 emissions by 50% by 2050 relative to 2005 levels. To help achieve these

goals, the Assembly defined a "basket of measures" which includes technology improvements, operational changes, alternative fuels, and market-based measures. [3, 7] Figure 1.2 (illustrated by IATA [8]) demonstrates a roadmap to reduce CO_2 emissions reflecting these aspirational goals. In the absence of new policies, CO_2 emissions are expected to grow by 1.9 to 4.5 times the 2005 levels by 2050. [3]

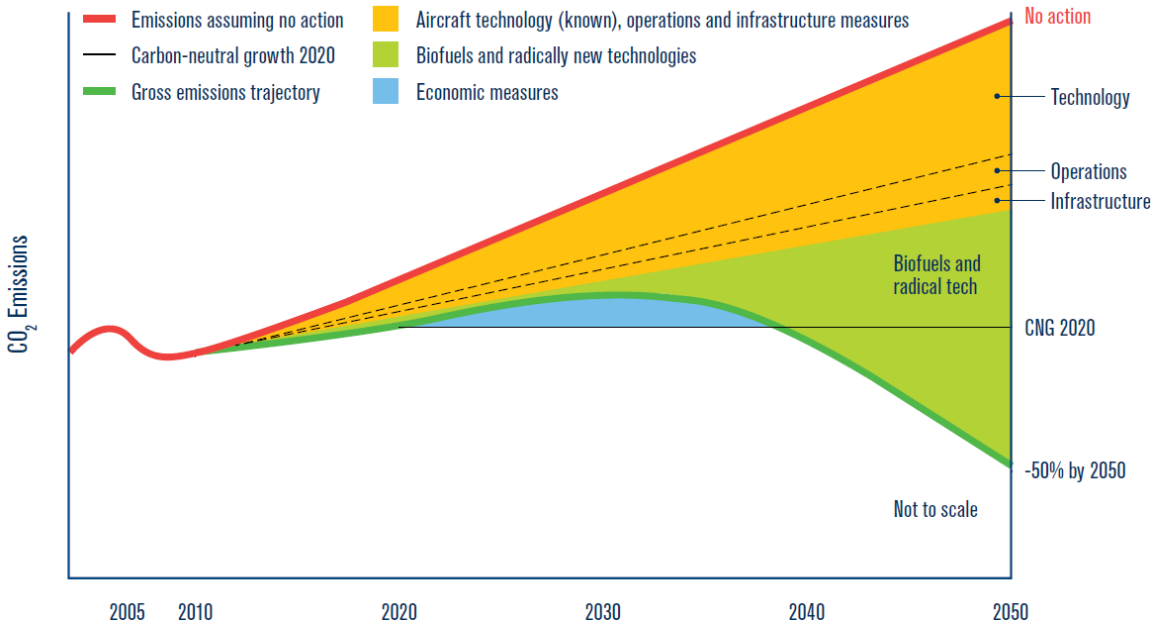

Figure 1.2: Schematic of CO_2 emissions reduction roadmap by IATA[8].

NASA has two primary areas of technical focus to realize these future low-carbon propulsion scenarios. The first one is to characterize and develop commercially available alternative fuels to lower the carbon use of standard turbofan engines in the near term. The second and the long term focus is to explore radically different propulsion systems that can achieve very low to no carbon emissions, such as hybrid electric and fully electric propulsion.[9] Although alternative fuels approach seems more viable in the near term, it does not help with the local air quality impact, the very long lifetime of CO_2 emissions or the NO_x emissions throughout the upper troposphere and lower stratosphere.[10] This thesis will focus on the long term solution: electric and hybrid electric aircraft.

1.3 Research Objective

The literature survey conducted on electric and hybrid electric aircraft concepts revealed that while there is a lot of effort on the propulsion aspect of the problem, incorporation of detailed architecture analyses into sizing considerations are missing. Moreover, the dynamic behavior of the electric power generation and distribution subsystems (EPGDS) are not taken into account at early design phases. To fill this gap, the over-arching research objective of this thesis is to **develop a methodology to perform sizing, integration and performance evaluation of electric power generation and distribution subsystems and architectures within electric and hybrid electric aircraft concepts.** The methodology will capture the impact of individual subsystem performance characteristics at subsystem, aircraft and mission levels; and evaluate architectures for different types of system level requirements under varying levels of hybridization; subject to the constraint that the level of complexity must be suitable for rapid, low-cost analyses at the conceptual design stage.

The stated research objective may be realized by addressing the main research question presented below:

The Overarching Research Question: How can the aircraft sizing and synthesis process be more generalized so that adequate comparisons between different types of primary power generation and distribution subsystems and candidate architectures are made available?

The answer to the main research question will yield the over-arching hypothesis of this thesis. This question can be broken down into the following research questions:

- What modifications should be done on the aircraft sizing and mission analysis process so that it is inclusive of any type of aircraft design, propulsion system, architecture and the energy storage type?
- What capabilities are needed to enable rapid changes in the subsystem characteristics and architectures?

- How can EPGDS be represented to demonstrate various characteristics related to different types of subsystems?
- How can the dynamic EPGDS characteristics be integrated into the sizing process?
- How can the technological sensitivities be captured?
- How can the best performing hybrid electric architecture be determined under varying levels of hybridization?
- How can the optimum operating conditions be obtained for different types of architectures?
- What impact does the level of hybridization have on choosing the best performing architecture?
- Does every operational change trigger a significant transient response in the electrical system of the aircraft?
- How can a balance between smaller and larger time steps be found so that significant transients at the subsystem level are captured at the conceptual design stage without bringing the associated computational burden?
- Can the transient behavior of an electrical system be related to the mission level parameters?
- If they are related, how can the relationship be captured between the significant transients of a given electrical system which could occur under a wide range of inputs which are expected to be given to the electrical system during a mission?
- If they are related, can the relationship be generalized for the given electrical system so that the whether a significant transient occurs could be estimated with only the limited amount of information obtained from the mission performance analysis?

Each of these questions must be addressed to realize the research objective. The answers to these questions will collectively yield the formulation of a repeatable methodology to perform sizing, integration and performance evaluation of electric power generation and distribution subsystems and architectures within electric and hybrid electric aircraft concepts.

The following chapters are organized as follows: Chapter 2 provides a literature review and seeks answers to the research questions given above. Chapter 3 maps the observations driven from this literature survey to the research questions, identifies the gaps and lays out the formulation of research arguments which include proposed hypotheses and experiments. Chapter 4 introduces the proposed methodology and its building blocks. Chapters 5 and 6 present further technical details on the proposed approach. Chapters 7 and 8 present the results of the experiments outlined in Chapter 3. Finally, Chapter 9 summarizes the conclusions derived from these experiments, highlights the contributions of this work, and provides a list of recommendations for future work.

CHAPTER 2
BACKGROUND AND LITERATURE REVIEW

2.1 Overview of Electric and Hybrid Electric Aircraft Concepts

In recent years, NASA's long term focus to fly electrically has gained a high interest especially due to the technology advancements in electric power generation and distribution components. Advanced concept studies commissioned by NASA for the N+3/N+4 generation have identified promising aircraft and propulsion systems, such as Bauhaus Luftfahrt's fully electric Ce-Liner, NASA's SCEPTOR distributed electric propulsion, Boeing's SUGAR parallel hybrid electric aircraft and NASA's N3X blended wing body with distributed turboelectric propulsion system concepts.[8, 10, 11] Among these, Boeing's SUGAR concept promises about 60% fuel burn reduction, 53% energy use reduction, 77-87% NO_x reduction compared to its baseline Boeing 737-800.[12]

2.1.1 Electrifying an Aircraft: Terminology

It is important to clarify the terminology in terms of electric and hybrid electric concepts before getting deeper into the details of electric propulsion and its examples. Electric aircraft (EA) and hybrid electric aircraft (HEA) concepts are sometimes confused with more electric aircraft (MEA) and all electric aircraft (AEA) concepts, although they are fundamentally different.

For AEA, the end goal is to replace all of the mechanical, hydraulic, and pneumatic subsystems that provide *non-propulsive (secondary) power* with electric counterparts. MEA is a middle step towards AEA where only some of these secondary subsystems are replaced with electric or more-electric alternatives, such as the case for Airbus A380 and Boeing 787.[13]

On the other hand, for electric aircraft (sometimes referred as electric propulsion aircraft, fully electric aircraft or universally electric aircraft), all of the *propulsive (primary) power* is provided by electric means, such as Airbus E-Fan and Pipistrel Alpha Electro aircraft. Since aircraft which solely depend upon electric motors and batteries are unlikely to achieve similar flight performance of conventional propulsion systems in the near future, turboelectric and hybrid electric propulsion (HEP) systems are envisioned as a middle step towards electric propulsion (EP) systems. In hybrid electric aircraft, only partial propulsive power is supplied by an electrical energy source; whereas in turboelectric aircraft, a gas turbine engine drives electric motor(s) which in turn drive(s) the fan(s).[14, 15, 16]

2.2 Real Life Applications of Electric Aircraft

Electric and hybrid electric aircraft concepts gained popularity especially in the last few years due to the aforementioned aggressive emission goals and advances in electric power generation and distribution subsystems technology. There are a number of unmanned aerial vehicles (UAVs) powered by electric motors, such as the solar powered and world altitude record setter Helios UAV. [17] However, the number of inhabited electric aircraft are still limited to low-power and low-range aircraft specifically designed for the flight training market.[18]

Below is an overview of the two successfully flown electric aircraft: Alpha Electro (Figure 2.1a) and E-Fan 2.0 (Figure 2.1b). These aircraft were used to benchmark the appropriate mission duration and the modeling capabilities developed as part of this thesis.

2.2.1 Pipistrel Alpha Electro

The Alpha Electro (also known by its prototype's name, WATTsUP), is a 2-seater electric trainer especially built to be used in flight schools. It can fly up to 1 hour with an extra 30 minutes reserve, and the cruise range is 200 km.

It is powered by a Siemens electric motor which has a continuous power output of

(a) Pipistrel Alpha Electro. Image Credit: [19]

(b) Airbus E-Fan. Image Credit: [20]

Figure 2.1: Electric aircraft applications.

65 kW and weighs 14 kg (almost a power-to-weight ratio of 5kW/kg, including inverter and gearbox).[21, 18] It runs on dual-redundant lithium battery pack which can be either swapped easily or can be recharged in less than an hour. [19] Some prominent characteristics regarding of the Alpha Electro are listed in Table 2.1 and compared with the E-Fan.

2.2.2 Airbus E-Fan 2.0

The E-Fan 2.0 is also a two-seater electric aircraft. Its twin-engines can provide a maximum power of 30 kW each. Its endurance is also 1 hour, the same as that of Alpha Electro, but its battery pack stores a higher total energy of 29 kWh. The system voltage of E-Fan is 270V.

It runs on lithium-ion batteries, (18650 by KOKAM) which has a specific energy of 207 Wh/kg per cell. The battery pack consists of 120 cells with 40 Ah capacity and 4 V voltage per cell.

The operating costs of E-Fan is only one-third of traditional piston-engine light aircraft. Its battery pac can be charged to 100% in 1.5 hours. Airbus also stated that there has been a 60% increase in E-Fans battery capacity since 2014, proving that significant improvements in these subsystems are possible in relatively short amount of time. [20]

As a continuum of its electric propulsion program, Airbus converted the E-Fan 2.0 to E-Fan Plus, a hybrid electric variant. In addition to the twin electric motors, a two-stroke

Table 2.1: Prominent Characteristics of Airbus E-Fan and Pipistrel Alpha Electro.

	E-Fan 2.0	Alpha Electro
MTOW [kg]	600	550
Motor Power [kW]	30x2	85
Battery Weight [kg]	168	126
Total Energy [kWh]	29	17
Endurance [min]	60	60

internal combustion engine (ICE) is installed on the E-Fan Plus. The ICE extends the range and increases the endurance to approximately 2 hours and 15 minutes.

There have been also some changes in the electric propulsion architecture of E-Fan Plus. The system voltage was increased from 270V to 400V. Airbus states that the new voltage provides better electrical performance in powering E-Fans electric motors. The electric batteries on E-Fan 2.0 were also replaced by higher-intensity and 15% more powerful lithium-ion batteries from LG. The battery weight reduced from 168 kg to 63 kg in order to compensate for the additional weight from the ICE system. A passive cooling system was also added for better thermal management of the batteries.[22] At the time of this thesis proposal, there is not much further information on E-Fan Plus, and therefore it could not be compared with E-Fan 2.0 and Alpha Electro except for its endurance.

2.3 Literature Review on the EA/HEA Conceptual Design and Feasibility Studies

Although the electric propulsion applications are limited to UAVs and general aviation sized airplanes so far, there are many conceptual studies being conducted for various sizes of aircraft. Among many other conceptual studies conducted by academia and industry, an overview of only the most notable ones are presented here: NASA SCEPTOR (Figure 2.2a), Bauhaus Luftfahrt Ce-Liner (Figure 2.2b), Boeing SUGAR Volt (Figure 2.2c) and

NASA N3X (Figure 2.2d).

(a) NASA SCEPTOR. Image Credit: [23]

(b) Bauhaus Luftfahrt Ce-Liner. Credit: [10]

(c) Boeing SUGAR. Image Credit: [24]

(d) NASA N3X. Image Credit: [25]

Figure 2.2: Electric and Hybrid electric aircraft concepts.

These aircraft also represent distinct types of electric and hybrid electric propulsion. SCEPTOR is a distributed electric propulsion concept, Ce-Liner is an electric aircraft concept, SUGAR is a hybrid electric propulsion concept and N3X is a turbo-electric one. Hence, in addition to introducing these aircraft, other research on these related concepts will also be included to investigate different electric and hybrid-electric propulsion architectures and the related challenges. Similar to the Alpha Electro and E-Fan, the following aircraft concepts were used to benchmark the modeling capabilities developed as part of this thesis.

2.3.1 NASA SCEPTOR - Distributed Electric Propulsion

NASA SCEPTOR project (which stands for Scalable Convergent Electric Propulsion Technology Operations Research) investigates the implications and performance of distributed electric propulsion (DEP). DEP consists of multiple propulsors which are driven by elec-

tric motors and distributed along the airframe, as seen on the wings of SCEPTOR in Figure 2.2a. This research does not focus on a single integration strategy, but rather a suit of various airframe-propulsion integrations which could lead to net efficiency benefits over fewer and larger engines. [26] Therefore, the concept seen in Figure 2.2a is just one of many configurations being studied in the SCEPTOR project.

There are various advantages of DEP. Moore and Fredericks [27] discuss a NASA Langley investigation which revealed that placing multiple propellers across the leading edge of the wing provided enhanced dynamic pressure, which in turn yielded a lift enhancement by about 2 times. Moore and Fredericks further explain that distributing many small diameter propellers over the wing results in the highest propeller induced velocities and the greatest lift augmentation compared to using a few large diameter propellers.

DEP is also beneficial in terms of propulsion sizing. A comparison between the LEAPTech concept (with 12 propellers) to the Cirrus SR-22 which is a conventional reciprocating general aviation aircraft revealed that the conventional engine looses around 20% of its available power on a hot summer day with a take-off at a high altitude, whereas the electric motors on the LEAPTech concept do not suffer from any power reduction as their performance is independent of temperature and altitude. [27]

Borer et al. [26] also demonstrate these advantages by comparing the electric DEP architecture to a conventional one, concluding that the high-lift system enables a 2.5 times reduction in wing area over the baseline aircraft, which in turn reduces drag during cruise and increases the velocity for maximum lift-to-drag ratio while maintaining low-speed performance. The final aircraft requires 4.8 times less energy at the selected cruise point compared to the baseline aircraft.

For more detailed analysis and findings on the DEP concept, the interested reader is referred to References [28, 29, 30].

To sum up, these papers provide detailed information about the increased aerodynamic efficiency, potentially decreased drag, power sizing benefit which can replace the penalty

associated with the heavier energy storage, and propeller design. However, they do not cover a detailed architecture analysis except for the selection of number of propellers.

During this comprehensive literature survey, only a NASA presentation by Clarke [31] was found to include the system architecture, as depicted in Figure 2.3. However, there is no study regarding the impacts of subsystem sizing on the overall vehicle design. Architectural implications of choosing the number of propulsors are also unknown.

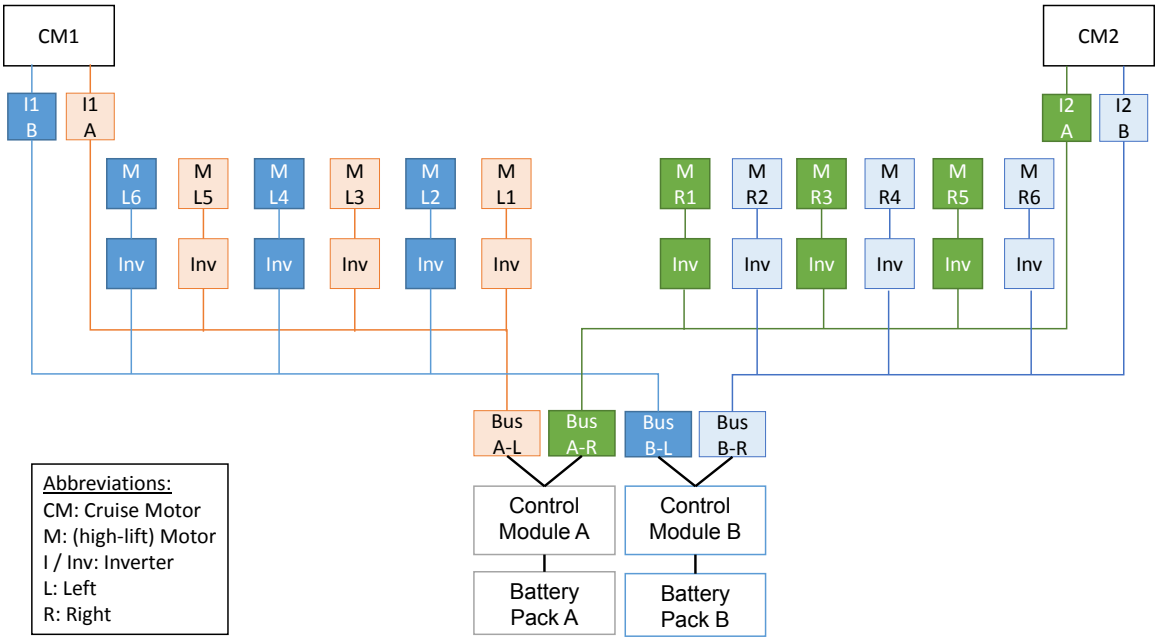

Figure 2.3: SCEPTOR Traction power system architecture. Reproduced from [31].

OBSERVATION 1: Electric aircraft research in literature does not incorporate detailed architecture analyses into sizing considerations.

2.3.2 Bauhaus Luftfahrt Ce-Liner - Electric Propulsion

The Ce-Liner is an electrical aircraft concept developed by the German non-profit research institution Bauhaus Luftfahrt as a response to the zero-CO_2emission goals. It is a tricycle, monoplane, low-winged twin-fan with podded mountings located on the aft fuselage. It has a design payload range of 900 NM with a payload capacity of around 190 passengers (PAX). [10] Figure 2.4 shows a cutaway view of the Ce-Liner.

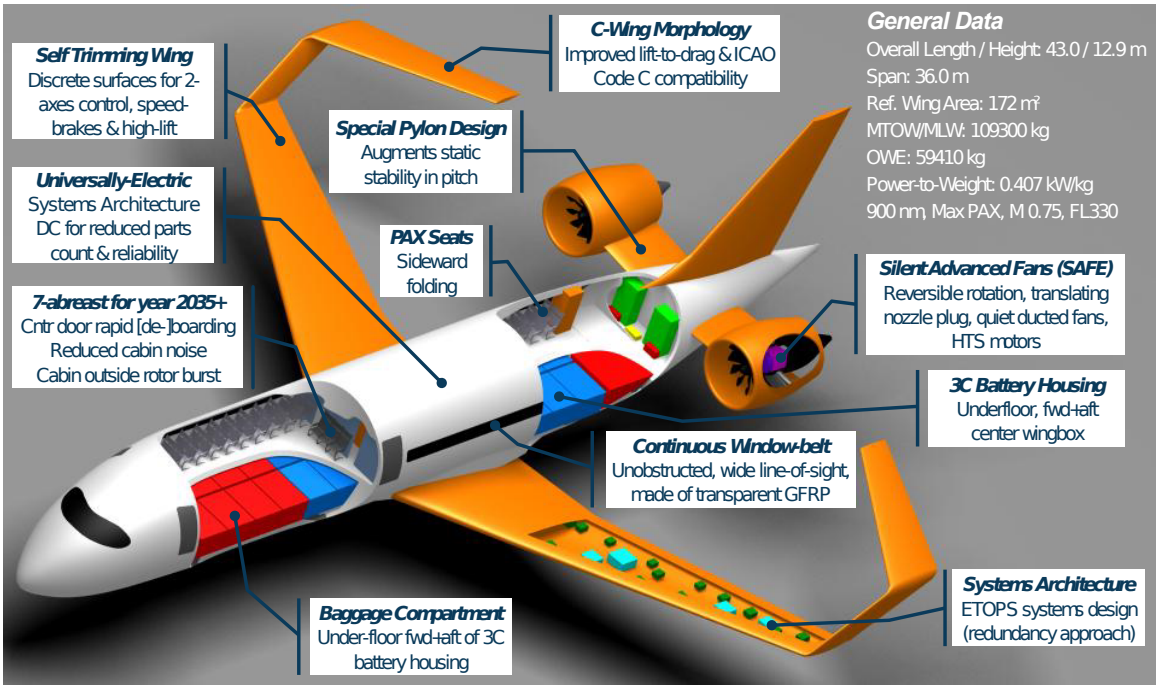

Figure 2.4: Ce-Liner cutaway views. Source:[32]

Hornung et al. [10] provide a high-level case study for the conceptual design of the Ce-Liner. It is stated that the most critical enabling technology in electric propulsion is the energy storage, i.e. the batteries, especially in terms of specific energy. They argue that the second key metric in quantifying battery performance is specific power (or power density). The power required to accelerate within given runway and operational constraints, then to perform take-off and climb can be provided by the current batteries. The specific power of SOA lithium batteries goes beyond 2 kW/kg which is enough for providing the power required during take-off and climb for the Ce-Liner. However, there exists a tradeoff between battery specific power and specific energy.

Their analysis lays out that the maximum power demand for the Ce-Liner is around 34.1 MW during take off and 16.55 MW during cruise (including power off-takes). The total energy requirement is 47 MWh for the whole mission (excluding power off-takes). These requirements can be delivered with a battery specific energy of 1.7 kWh/kg and specific power of 1.2 kW/kg. When the power off-takes and safety measurements are included, the battery technology target is extended to a specific energy of 2 kWh/kg and specific power

of 2 kW/kg. This is quite an aggressive goal for the EIS year of 2035.

The architecture considerations of the Ce-Liner are presented by Isikveren et al. [32] in another publication. Isikveren et al. divides the electric systems architecture into three main systems based on the power and voltage levels: high power and voltage (propulsion system), medium power and voltage (associated to on-board consumer system requirement), and low power and voltage (avionics), as demonstrated in Figure 2.5. They argue that this categorization is generic and hence can be applied to various transport aircraft categories.

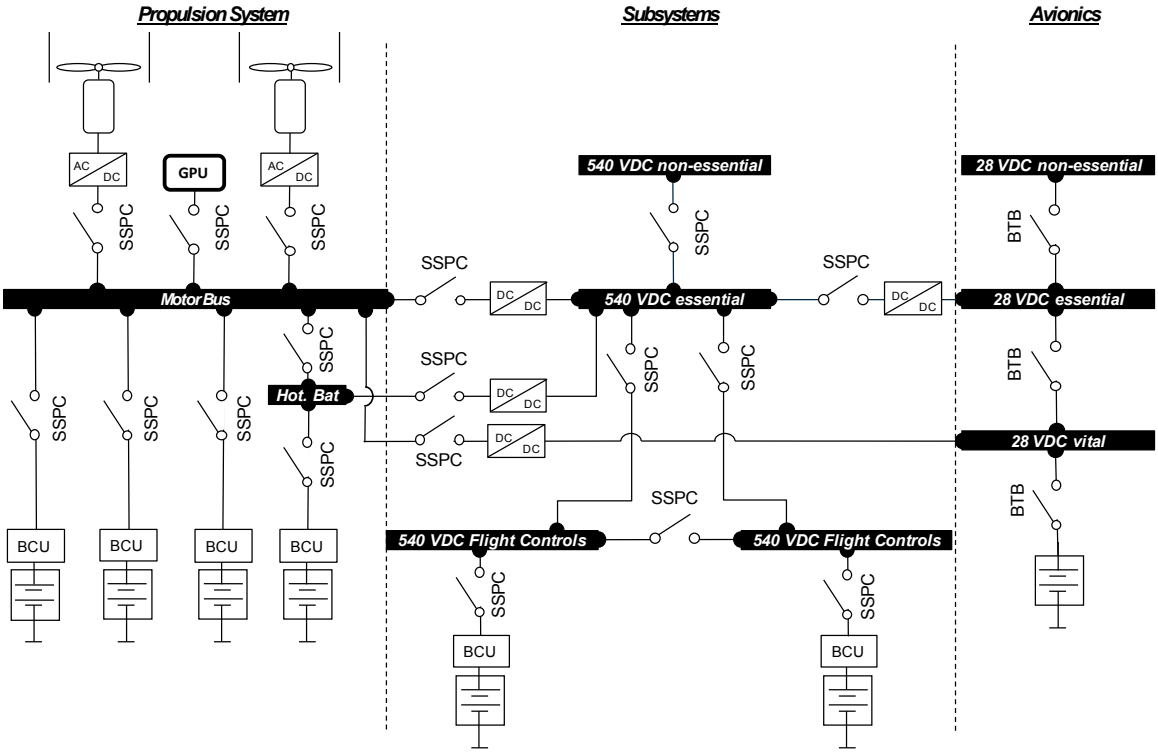

Figure 2.5: Bauhaus Luftfahrt's universally electric systems architecture. Source:[32]

It can be seen from Figure 2.5 that direct current (DC) voltage was chosen for power transmission. This is because of the fact that DC systems minimize electro-magnetic interference, reduce power losses in the cables, and are compatible with batteries without requiring conversion into another type of voltage. The authors explain that since the first category is runs on high power, a high voltage level is necessary to reduce the cable sizing (i.e. weight). They point out that voltage levels between 1000-3000 VDC are currently being investigated and that the common-place for contemporary terrestrial locomotive trans-

portation systems to work with voltages of up to 15 kVDC.

In this power transmission architecture, power is supplied by the batteries to the propulsors through a motor bus in order to connect multiple power loads to the electrical system. Moreover, battery control units (BCU) are placed to monitor the battery and prevent it from discharging under a certain level. It also regulates the voltage such that the voltage at the BCU output is constant.

The second category is the medium power medium voltage one. The voltage here was chosen to be 540 VDC as it is claimed to be the common voltage level for future subsystems. Components used in this category are similar to those of the first category. The third one is the low power low voltage category which represents the avionics. The voltage level was chosen to be 28 VDC and since both the power demand and voltage level are low, standard Bus Tie Breakers are utilized instead of SSPCs to decrease the weight penalty.

The authors estimated the mass of each power transmission subsystem from their predicted specific power and efficiency for 2035. They then carry on with sizing analysis. They point out that the take-off power is the driving factor for this type of electric aircraft; in fact it has a greater effect on the sizing compared to the conventional aircraft. This means that if the electric propulsion architecture is sized for low-speed operations, there will be a dramatic weight penalty due to the oversized battery. Hence, the required power for low-speed operations (specifically, take-off and initial climb) must be minimized for a successful design.

OBSERVATION 2: Electric aircraft are significantly more weight sensitive than conventional ones because of the tremendous difference between the specific power/energy of conventional fuels and the specific power/energy of batteries.

2.3.3 Boeing SUGAR Volt - Hybrid Electric Propulsion

Subsonic Ultra Green Aircraft Research (SUGAR) conducts an advanced concept and technology study which examines various alternative fuel and energy technologies. One of the concepts developed in this study is the SUGAR Volt, a medium-size hybrid electric aircraft concept. SUGAR is a collaboration among Boeing, General Electric, Virginia Tech, and Georgia Tech. [33]

A research by Perullo et al. [34] applies hybrid electrical elements developed within the Numerical Propulsion System Simulation (NPSS) for the SUGAR project. They perform a parametric investigation into the engine cycle design. The authors find that the effects of efficiency and weight of the electric system are mainly seen at the vehicle level as they are independent of the engine cycle. Hence, the engine cycle can be chosen without detailed attention to the electrical architecture.

There is not much detailed information on the SUGAR Volt concept in literature, but a plenty of sizing methodologies for hybrid electric propulsion exist. The ones that are most related to the scope of this proposal were provided in the following paragraphs.

Nam et al. [35, 36] propose a generalized aircraft sizing formulation applicable to non-traditional energy sources and propulsion systems. The authors first categorize energy sources as consumable energy (such as fuel) and non-consumable energy (such as batteries). Then, they present a power-based formulation based on multiple "power-paths" that make up the propulsion system when integrated. In this approach, a power path is decomposed into power generation and distribution subsystems. Each subsystem is represented by its individual specific energy, specific power and efficiency. Hybrid electric propulsion is represented as a set of power paths for electric and fuel burning engine branches.

Pornet et al. [37] present a methodology for sizing and performance assessment of hybrid electric aircraft. Traditionally, thrust and fuel-flow look-up tables are used for performance evaluation of conventional aircraft. Pornet et al. extends these look-up tables and add electrical system characteristics; specifically by including the required electric power

as additional output parameter. Then, the energy required from the battery and the fuel to fly the mission can be determined. However, this methodology is only for sizing the power systems and not for determining an optimum hybridization factor. It also does not consider a detailed architecture. In fact, the methodology provided would need modifications for hybrid configurations other than the parallel hybrid one.

Perullo and Mavris [38] provide a literature survey of the existing methodologies and propose an environment for a hybrid-electric design by combining high fidelity conceptual design tools with energy management optimization for a full mission. They select NPSS as the modeling framework and a two-level optimization environment which combines distributed optimization with detailed analysis modules. The analysis modules are executed concurrently instead of sequentially. They also decouple the sizing process from the mission analysis so that the optimization takes place for two problems which are high level design parameters (e.g. aspect ratio, engine cycle parameters, etc.) and degrees of freedom available to the system during a mission (e.g. power split from multiple sources, etc.) using model predictive control technique. They do not include the architectural implications of optimizing the level of hybridization.

OBSERVATION 3: Energy management optimization should be performed during vehicle sizing. Architectural implications of optimizing the level of hybridization have yet to be discovered.

2.3.4 NASA N3X - Turboelectric Propulsion

NASA N3X is a conceptual turboelectric distributed aircraft based on the Boeing 777-200. It is estimated that this concept will enable about 63% energy savings, 90% NO_x reduction and 32-64 EPNdB cum noise reduction. [39]

In a turboelectric propulsion architecture is essentially similar to a hybrid one, where a hydrocarbon fuel-burning turbomachinery is coupled to a generator which distributes

power to propulsors. Different from the hybrid electric propulsion, there are no on board energy storage devices other than fuel.

The turboelectric distributed propulsion architecture decouples the power producing components from the thrust producing components. This way, each can operate at their peak efficiency rather than a compromise between the two, increasing the overall thermal efficiency. There are losses associated with turboelectric propulsion due to the power conversion from mechanical to electrical, the transmission of electrical power and conversion from electrical power back to mechanical power. However, this system architecture enables technologies to help overcome the efficiency losses, such as distributed fans and boundary layer ingestion. [40]

N3X concept utilizes large and efficient engines with freestream inlets which drive superconducting generators. These generators provide electric power to multiple electric motor driven propulsors. The propulsors ingest boundary layer which increases the overall vehicle efficiency through a propulsive efficiency increase and reduced vehicle wake dissipation. The distributed fans increase the total fan area and effective bypass ratio while reducing fan pressure ratio. [39]

2.4 A Look From the Architecture Perspective

This section summarizes the prominent subsystems and architecture types of electric and hybrid electric propulsion systems. Throughout the document, these subsystems will be referred as electric power generation and distribution subsystems (EPGDS). Each of these subsystems will be covered in detail in Chapter 5.

The prominent subsystems of a fully electric propulsion architecture are energy source (such as a battery or fuel cell), electric motor, and power converter (or power electronics, or power management and distribution system), as demonstrated in Figure 2.6. The energy source transfers energy in the form of electricity to the power converter. Electricity propagates through the power converter and reaches to the electric motor which converts

this electrical power to mechanical (shaft power). Then, a propeller speed reduction unit (PSRU, shown as a gearbox in Figure 2.6) transfers the rotational motion of the motor output shaft to the propeller via a speed reduction. If the electric motor is direct-drive, such as the Siemens SP260D electric motor for aircraft [41], then a PSRU is not needed in between the motor and the propeller.

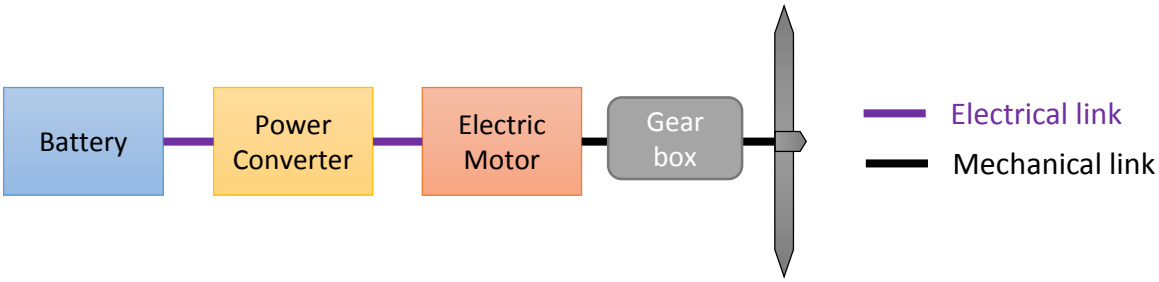

Figure 2.6: Notional subsystem components and power-train for fully electric propulsion

The electric motor adjusts its torque and rotational speed to supply enough shaft power which varies based on the variations in the power required by the propeller. In order to change the output mechanical energy of the electric motor, the incoming current and motor voltage must be regulated. Moreover, a conversion from/to alternating current (AC) to/from direct current (DC) might also be necessary. Power converters are responsible for performing this regulation and/or conversion between the input and output stations, i.e. between the battery and electric motor as given in Figure 2.6.[42, 43]

Hybrid electric propulsion architectures incorporate a fuel burning engine, such as gas turbine or internal combustion engines. HEP requires fewer changes in the energy supply infrastructure than EP, however also brings increased complexity. It also is not emissionless, but is vastly less polluting and has less fuel consumption than a conventional propulsion system. HEP is accepted as a middle step between the conventional systems and EP as it can deliver similar, if not the same, range performance of a fuel burning aircraft. The fuel burning engine in HEP can be operated in its most efficient mode which results lower emission and fuel consumption. Alternatively, the fuel burning engine can be shut down and the vehicle can be operated as a fully electric one.[44] The ratio of the power extracted

from the electric motor(s) to the total power is determined by the "hybridization factor" (a.k.a. "level of hybridization"). [45]

Similar to the EP architecture, electrical energy is transmitted through common subsystems in all four HEP concepts, but they can be connected in different configurations. These HEP configurations can be mainly categorized into 4 types of architectures: series, parallel, series-parallel and complex hyrbid; as shown in Figure 2.7.

- **Series Architecture:** In this architecture, the mechanical energy at the output of the fuel burning engine is first converted into electricity by the generator. This electrical energy can be used to charge the battery or to generate shaft power by the electric motor. One of the advantages of the series architecture is that the fuel burning engine is decoupled from the transmission system and thus it can run at its peak efficiency independent of the RPM of the transmission system. It also has the advantage of flexibility in terms of locating the engine-generator set. The powertrain is also not as complex as the other architectures.

  As it can be seen from Figure 2.7a, there are three propulsion devices (fuel burning engine, generator and electric motor) in this architecture. All these three propulsion devices need to be sized for the maximum sustained power for high performance flight; which brings increased weight penalty. Although a torque amplification device can be integrated to improve the performance of the motor and hence reduce its size, the motor must still be significantly more powerful than a motor used in parallel hybrid architecture. [44, 46]

- **Parallel Architecture:** Contrary to the series architecture, the fuel burning engine and the electric motor are coupled to the shaft, as demonstrated in Figure 2.7b. Therefore, the propulsive power can be delivered to the propeller by only the engine (conventional propulsion), only the electric motor (fully electric propulsion) or both of them simultaneously (hybrid propulsion).

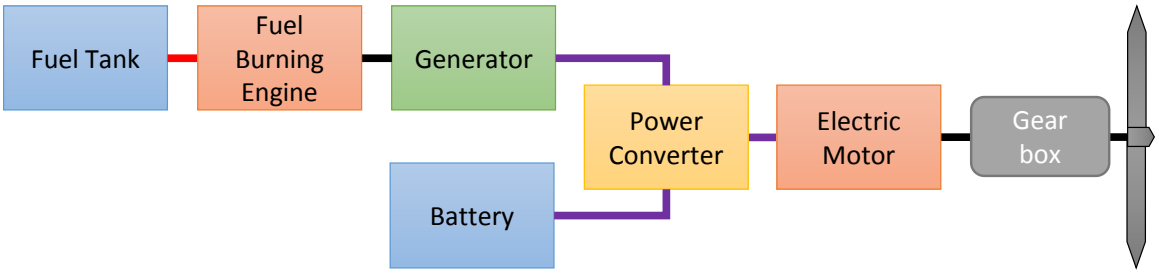

(a) Series configuration.

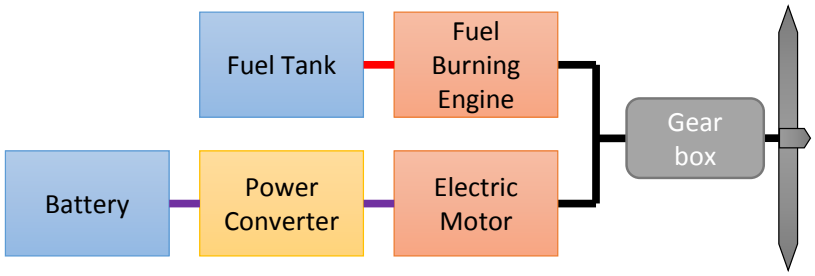

(b) Parallel configuration.

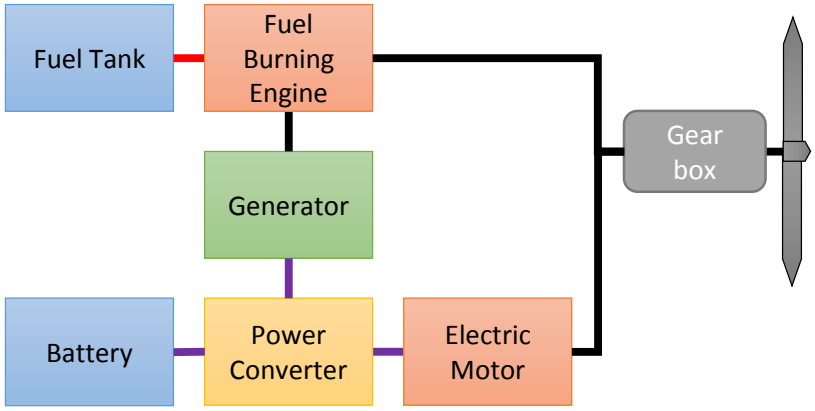

(c) Series-parallel configuration.

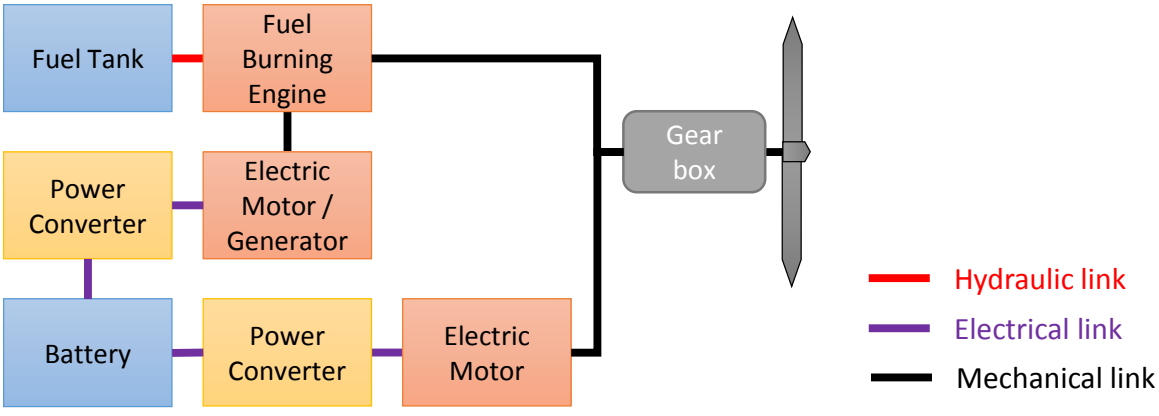

(d) Complex configuration.

Figure 2.7: Notional subsystem components and powertrain for hybrid electric propulsion in four different configurations. [44, 46]

There is no need for a generator in parallel architecture. When the output power of the engine is greater than the required power, the electric motor can be used as a generator to charge the battery by absorbing power from the engine. Furthermore, either the engine or the motor can be downscaled and still deliver the same performance and maximum power. The main disadvantages over the series hybrid is that this architecture increases the control complexity, requires more complex and expensive transmission system, and brings mechanical couplings. [44, 46]

- **Series-parallel Architecture:** This architecture (displayed in Figure 2.7c) possesses the advantages of both series and parallel architectures. However, when compared to the series hybrid, it involves an additional mechanical link; and when compared to the parallel hybrid, it requires an additional generator. Therefore, even though it takes advantages of the features of both series and parallel architectures, it suffers from significantly higher complexity and costliness.[44, 47]

- **Complex Architecture:** The main difference between the complex architecture (shown in Figure 2.7d) and series-parallel architecture is that in complex architecture, the power flow of the electric motor is bidirectional, whereas in the series-parallel architecture the power flow of the generator is unidirectional. The bidirectional power flow allows for versatile operations, especially with the addition of an extra electric motor. However, it suffers from the weight penalty coming from the additional propulsion devices and is also relatively more complex and costlier than the series and parallel architectures. [44, 47]

Due to the increased complexity, weight penalty and cost of the series-parallel and complex hybrid configurations, they are usually not preferred in hybrid electric vehicle applications with a few exceptions in the automotive industry.[44] In fact, both series and parallel hybrid architectures are successfully used in the automotive industry, but the parallel hybrid configuration is the most popular one.[46]

The divergence in the HEP architectures leads to the following observation:

OBSERVATION 4: HEP architecture types have different benefits and drawbacks, and therefore each will perform differently. Comparisons among different vehicles and architectures only makes sense if they are operated under their optimum performance.

2.4.1 Selection of the Energy Source

The two options to provide electrical energy in EP are fuel cells and batteries. A fuel cell converts the chemical energy stored in chemical reactions of hydrogen and oxygen into electrical energy. Fuel cells provide electrical energy as long as the active chemicals are supplied to the electrodes and hence do not store energy like batteries. In most cases, fuel cells require a battery during start up as they cannot deliver electrical energy until they approach to their operating point. They also have a rather slow dynamic performance and are well suited for continuous operations. Therefore, in the case where temporary power boosts under sudden demands are necessary, fuel cells are usually connected with batteries in parallel. [48]

Battery cells convert chemical energy to electrical energy through electrochemical reactions and generate DC electricity. This is called a "discharge" process. Rechargeable battery cells can reverse this chemical reaction when current is sent into the battery. This is called a "charge" process. Although they come with much lower specific energy than fuel cells, batteries can provide higher power although only for short periods. [42, 48]

A lot of research has already been conducted on fuel cell powered electric vehicle applications for electric and hybrid electric cars and aircraft (specifically for small unmanned aerial vehicles). [48, 49, 50, 51, 52, 47, 53] As the battery technology advances, there is a shift to employing rechargeable batteries in electric aircraft applications, such as the case for Airbus E-fan and Pipistrel Alpha Electro aircraft. For these reasons, and noting the nu-

merous advantages including the high specific energy of fuel cells, this research will only focus on the rechargeable battery technology as the electrical energy source.

Batteries have a dynamic discharge behavior, such as depicted in Figure 2.8. Each curve in this plot shows the discharge behavior under a certain current draw in terms of battery voltage and discharge time (or sometimes capacity). Figure 2.8 shows a representative Lithium-Ion (Li-Ion) type of battery discharge characteristics. These type of batteries usually have an exponential zone at the beginning of discharge, and then the discharge curves remain almost constant for a considerable amount of battery run time. Voltage starts to drop very rapidly somewhere around the cutoff voltage, and continues to drop even more as the battery is fully discharged. The nature of these curves depend on the battery type and properties. But the main idea behind these curves is that voltage drops as battery is discharged, and increases as battery is charged. In many cases, charge characteristics can be assumed the same as discharge characteristics although they might not be exactly the same.[54]Different types of batteries yield different dynamic behaviors and performance characteristics.

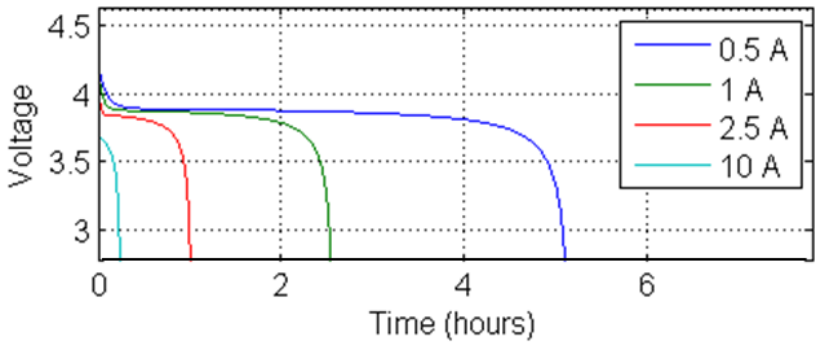

Figure 2.8: Dynamic discharge behavior for a lithium-ion battery.

It can be seen from the different colored curves in Figure 2.8 that drawing a high amount of current (e.g. the red curve) over a short amount of time decreases the battery run time whereas drawing a low amount of current (e.g. the blue curve) over a longer time increases the run time, as described previously. This phenomenon has a vital impact on the aircraft

performance, because the power requirement can vary from flight segment to segment, and even within the segment. This means that in the case of excessive high power demands, the battery current spikes up and run time on a single charge significantly decreases, reducing the battery capacity and hence limiting the performance (especially in terms of endurance or range) of the aircraft. [42, 54]

Aircraft mission analysis usually incorporates large time steps, in the order of minutes. However, the literature survey on battery characteristics necessitates that the battery must be sized by considering its dynamics within shorter time steps and integrating the energy requirement of each time step. Otherwise, its performance and weight cannot be estimated correctly, resulting to an under or over-sized battery. An over-sized battery penalizes aircraft's range capability as it essentially becomes a dead-weight which will be carried throughout the whole flight.

2.4.2 The Transient Nature of Electric Machines

The type of dynamic response of electric machines are classified as "steady-state" and "transient" response. For electrical circuits, steady-state behavior is the dynamic response where quantities such as currents, voltages, power, energy, etc. do not change in time in direct current (DC) operation, or remain periodical with constant amplitudes and phase angles in alternating current (AC) operation. On the contrary, during transient behavior, these quantities vary with time and sometimes exceed the boundaries and may destroy the circuit equipment. [55]

Although transient regimes do not necessarily break an electric machine, they can severely impact the operation of an aircraft. [56] Especially for cases where high electrical loads are unavoidable, such as the case for electric and hybrid electric applications, degradation of electric power quality becomes a significant concern. [57] Voltage dips or bursts that only last for just a few milliseconds can cause significant damage on electrical equipment, and spike up the overall wasted energy. [56, 57]

This is why, transient regimes which an electric machine is expected to experience during normal operations must be analyzed during the design and development process of that machine. If an EPGDS is not capable of bearing the loads the aircraft is expected to experience, the aircraft performance can suffer as a result. For instance, in a hybrid electric aircraft, if the pilot suddenly demands significantly high power from the electric motor, the change in the power quantity in the powertrain might cause (among many things) a voltage unbalance in an AC machine, which in turn can cause excessive heat and might damage the machine.

The transient regimes gain more significance in EA/HEA concepts as the EPGDS architecture experiences much larger loads than those subsystems in secondary power systems. There exist standards and regulations on aircraft electric power characteristics for both AC and DC machines, such as MIL-STD-704F published by Department of Defense. [58] This standard establishes the requirements and characteristics for electric utilization equipment. Although specific requirements for electric machines used as primary power sources in EA/HEA have not been established yet, the constraints given in existing standards can be used as a reference to ensure the power quality of the aircraft electrical system.

The amount of time a transient occurs vary for each EPGDS, but are several orders of magnitude smaller than the aircraft dynamics. [38, 59] Therefore, much smaller time steps are needed for transient analysis compared to the time steps used in mission performance analysis (which are generally in the order of minutes). However, transient analyses are performed within a duration of time usually not exceeding a couple of seconds [58, 57] in accordance with the definition of a transient. Combining the subsystem level transient analysis with mission performance analysis require simulations and computations to be performed at a scale of millionth of a second, which would bring enormous computational burden to otherwise high-level analysis.

Due to this tradeoff between required computational resources and desired accuracy, the transients are usually neglected in mission performance analysis at aircraft conceptual

design stage. [38]

These discussions lead to the following observations:

OBSERVATION 5: The appropriate timescales are different at mission and subsystem levels, especially when transient regimes are concerned. This discrepancy might result in performance degradation due to inaccurate approximation of subsystem dynamics using large time steps, or computational burden due to selecting very small time steps for the entire mission in mission performance analysis.

2.5 Advantages and Challenges of Electric and Hybrid Electric Aircraft

There are various advantages of EA/HEA, including but not limited to reduced or zero emissions. However, there are also challenges associated mainly with the technology levels and lack of experience in this area. The next two sections summarize the advantages and discuss the drawbacks.

2.5.1 Advantages

There are numerous advantages that come with electrically propelled aircraft other than the reduced (for HEP) to zero (for EP) emissions. In some instances, the use of an electric motor as a source of shaft power can be superior to combustion-based engines thanks to the power and efficiency characteristics of electric motors. Electric propulsion systems offer dramatic energy savings as the conversion from electric power to shaft power is much more efficient.[27]

Recent advances in electric motors enabled higher power-to-weight ratios, such as the Siemens electric motor for aircraft which has a state-of-the-art power-to-weight ratio of 5 kW/kg and delivers a continuous output of about 260 kW.[41] Moreover, electric motor efficiency is independent of operational altitude and also has a relatively scale-free efficiency and power-to-weight ratio which gives an advantage over conventional internal combus-

tion engines. They also have less moving parts with a simple working mechanism that make them favorable in terms of reliability and maintainability, and provide safety through redundancy.[42, 28, 27]

Another benefit is that electric motors being able to provide reasonably efficient power across a wide range of rotational shaft speeds, as opposed to combustion-based engines which are mostly efficient at a narrow range. Propellers are only efficient across a narrow range of advance ratios. Thus, when powered by combustion engines, propellers are generally designed with complicated variable pitch mechanisms to maintain the shaft speed within a small range and are twisted to maintain an efficient angle of attack over a wide range of speeds. These mechanisms bring more complexity, increase the weight and cost of the system and introduce additional reliability and maintainability penalties. On the other hand, by running efficiently over a wider range of shaft speeds, electric motors require less complex means of matching efficient angles of attack on the blade than variable pitch or constant speed mechanisms. This approach has also a secondary benefit of reducing noise.[28]

To sum up, the advantages of EP and HEP are zero or drastically reduced emissions (and thus greener aviation), less atmospheric heat release (less global warming), higher efficiency, no power lapse with altitude, scale-free efficiency and power-to-weight ratio, increased reliability and maintainability, and quieter flight. However, the substantial change in the propulsion systems also brings new challenges to the aircraft design community.

2.5.2 Challenges

The most widely known challenge is associated with the energy source characteristics of electric and hybrid electric vehicles. Specific energies of state-of-the-art (SOA) batteries are significantly below the specific energy of jet fuels. For example, jet A provides a minimum specific energy of 11.89 kWh/kg (42.80 MJ/kg), whereas today's SOA lithium-ion batteries can only hit up to about 210 Wh/kg (0.76 MJ/kg). [60, 61] However, battery

technology is aggressively advancing and there is still room to improve. Figure 2.9 shows the technological trend of the Lithium-ion battery since it was launched on the market, in terms of specific energy (mass energy density) and volumetric energy density. Scientists predict that although the current lithium-ion batteries might be approaching the practical limit, other type of lithium based batteries (such as lithium-air or lithium-oxygen with a theoretical specific energy of 3458 Wh/kg [62]) will enable higher specific energy and power values and therefore continue to play a significant role in the energy source applied research.[61, 63, 64]

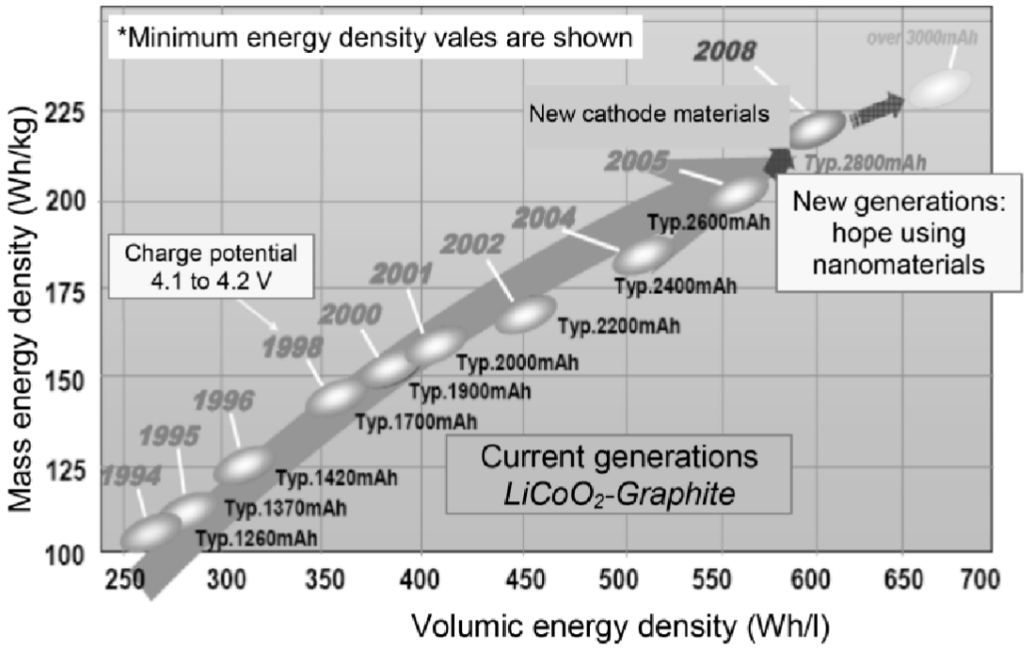

Figure 2.9: Evolution of Lithium-ion technology since its commercialization in 1991. Source: [61]

Striking advances in electric motor technology promise even better performance characteristics from lighter devices. Up until the announcement of the high performing Siemens electric motor with a power-to-weight ratio of 5 kW/kg back in 2015, the SOA electric motors which could deliver similar amounts of maximum power had power-to-weight ratios of 2-3 kW/kg. NASA set a 15-year goal to increase the electric motor power-to-weight ratio to 16 kW/kg and the power capability to 5-10 MW. [14] The same progression is also

expected from the power converter technologies. NASA's 15-year goal for the power converter is to reach a power-to-weight ratio of 19 kW/kg and a power capability of 0.25 MW from the current SOA with a power-to-weight ratio of 2.2 kW/kg and a power capability of 5-10 MW.[14, 65] Hence, the below observation can be made about EPGDS technologies:

OBSERVATION 6: EPGDS technologies rapidly improve resulting in ever-changing subsystem capabilities, which in turn can have a cumulative positive effect on vehicle design and mission performance.

Although propulsion is the first thing that comes to mind when talking about electric aircraft, one particular and important, but not yet thoroughly addressed challenge lies within the architecture design. The EA and HEA concepts pose a significant subsystem architecture challenges. The subsystems used in the electric propulsion system are responsible for providing the propulsive power. Therefore, very large amounts of power propagates through these subsystems. This creates a challenge especially in terms of generation and distribution of power. Apart from the subsystems themselves, the sizing of the distribution elements are also affected by the magnitude of the current which they carry, and hence might introduce significant amounts of weight to the system. As a result, there is a need to study these revolutionary concepts from a subsystems perspective.

Studies in literature are widely based on assumptions made on EPGDS technology levels such as a component's specific power and/or specific energy. Thus, the technological improvements are usually stated in terms of specific power/energy, without regards to other aspects (such as voltages, currents, capacities, etc.) of these subsystems. This limitation results in losing potentially valuable information due to neglecting the higher dimensionality of the problem. This leads to epistemic uncertainty, which is *"due to a lack of knowledge about the behavior of the system that is conceptually resolvable"*. [66] The following observation is made regarding this problem:

OBSERVATION 7: EPGDS are usually represented only by their specific power/energy, which leads to epistemic uncertainty due to modeling assumptions.

There also exist challenges associated with the sizing and synthesis of the EP and HEP concepts. Traditionally, the sizing of subsystem components is performed during the conceptual design stage by using empirical relationships concerning existing historical data.[67, 68] From these empirical relations, information on aircraft weight, power (or thrust) and drag polar are then estimated and fed into the sizing and synthesis process where constraint analysis (to meet point performance requirements) and mission analysis (to fly a specific design mission) are carried out through iterations, as notionally depicted in Figure 2.10.[69]

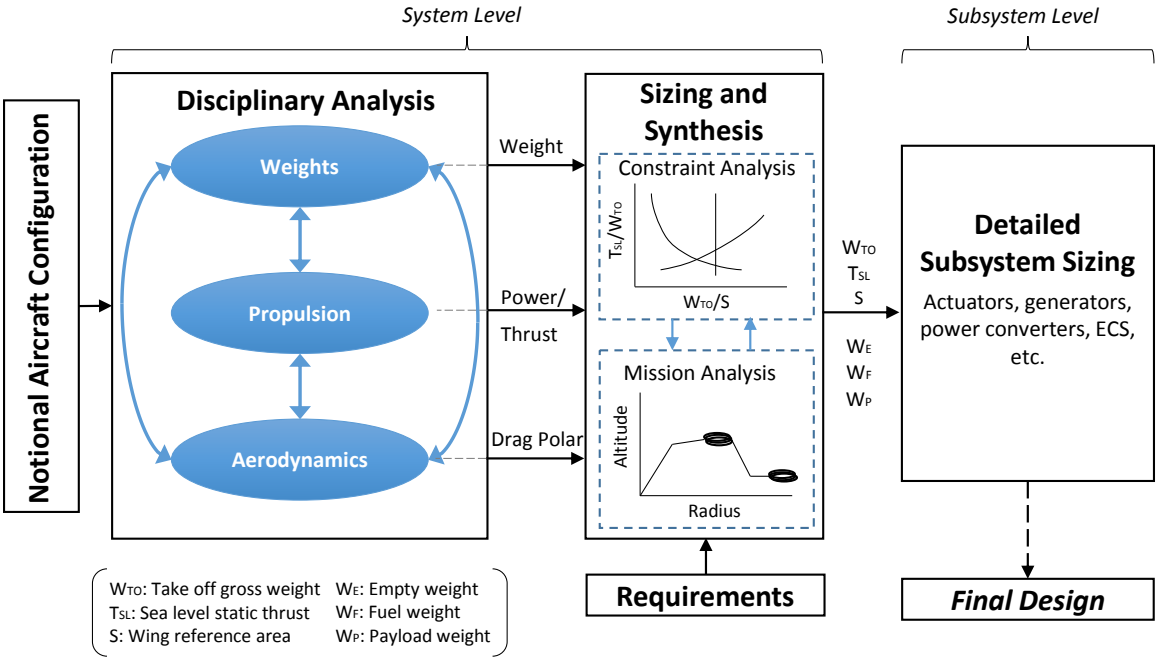

Figure 2.10: The traditional aircraft design formulation. [69]

However, there is a lack of historical data or readily available physics-based models for unconventional or more recent technologies such as ones that constitute EPGDS. Estimations on the impact of these subsystems add a significant uncertainty to the system. The flowchart in Figure 2.11b was proposed by Chakraborty and Mavris[70] for traditional

aircraft and generalized here to include EA and HEA, as shown in Figure 2.11a. The flowchart demonstrates how a generic subsystem weight, drag, and power consumption or power losses due to inefficiencies cause an increment in the required power and hence the total required energy.

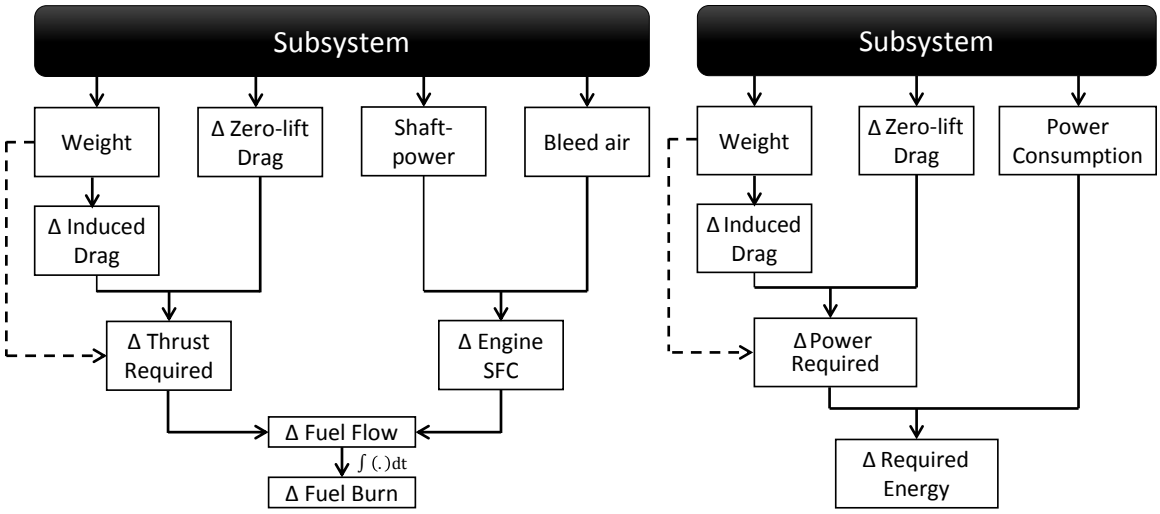

(a) Impact of subsystems on fuel consumption by Chakraborty and Mavris. [70]

(b) Effects of a generic subsystem on total energy required.

Figure 2.11: Subsystem considerations for conventional and electric propulsion.

According to Chakraborty [13], the aircraft subsystems affect the sizing process at the conceptual design stage in three ways:

1. Empty weight fraction: Subsystem components and architectures change the empty weight through changes in the fixed equipment weight

2. Engine fuel consumption: Subsystems increase the specific fuel consumption by imposing a fuel-burn penalty through the use of bleed air or shaft-power

3. Vehicle drag: Subsystems may impact the vehicle drag because of external modifications or due to the drag arising from ram air inlets

While the first and the last items in Chakraborty's list also hold true for electric propulsion, the second item needs a modification. Any additional weight imposed by the subsystems or the architecture will require additional energy to carry that component. Also, a

power consuming subsystem directly increases the overall the required power. For EP, this power is supplied solely by electricity; whereas for HEP both the specific fuel consumption and battery discharge rate is affected. Therefore, subsystems increase the required energy by increasing the required power through the use of shaft power or power off-takes.

Ultimately, the choice and sizing of aircraft subsystems has a consequential impact on the final design of a vehicle, but in the meantime subsystem level performance is limited by the system level metrics. The interrelationships, interactions and possible couplings between the subsystems and the aircraft can lead to very different results than what was anticipated for the individual subsystem performance; yielding to the following observation:

OBSERVATION 8: The level of hybridization, architecture type, performance and sizing have a bidirectional impact on the empty weight as well as the flight performance of a hybrid electric aircraft, creating an interdependence between the subsystem, aircraft and mission levels.

Moreover, the traditional sizing methods depend on the assumption that the time rate of change in aircraft weight equals the fuel flow, as used in the well-known Breguet range equation.[71] However this phenomenon does not apply for EP technology as such systems might not lose weight over the course of a mission. Modifications to these methods are also necessary for hybrid-electric aircraft. Therefore, the empirical relations and methods given by the traditional design approaches cannot be directly used for such new concepts.

To conclude, the main challenges associated with the EA and HEA and their design process can be summarized as:

- Weight and performance penalties due to the characteristics of the electrical energy source
- Significant subsystem architecture challenge due to the challenges in generation and distribution of very large amounts of power

- Lack of historical data and readily available physics-based models for EPGDS
- Interdependence among aircraft sizing, performance, subsystem sizing and architectural decisions
- The need to modify the traditional sizing methods to account for the new propulsion system

2.6 Chapter Summary

There is a growing need for a greener aviation, even better a carbon neutral one. To meet the aggressive emission goals, the aerospace industry is working on a cutting-edge aircraft concept: electric aircraft. Although electric propulsion is an enabler for the reducing CO_2 and NO_x, noise and increasing propulsive efficiency, aircraft which solely depend upon electric motors and batteries are unlikely to achieve similar flight performance of conventional propulsion systems in the near future. Hence, turbo-electric and hybrid-electric propulsion systems are envisioned as a middle step towards fully electric propulsion.

The literature survey revealed that the efforts mostly focus on the propulsion aspect of the problem alone. However, these revolutionary concepts also pose a significant architecture challenge. Throughout this chapter, the following observations about architectural considerations were made:

1. Electric aircraft research in literature does not incorporate detailed architecture analyses into sizing considerations.
2. Electric aircraft are significantly more weight sensitive than conventional ones because of the tremendous difference between the specific power/energy of conventional fuels and the specific power/energy of batteries.
3. Energy management optimization should be performed during vehicle sizing. Architectural implications of optimizing the level of hybridization have yet to be discov-

ered.

4. HEP architecture types have different benefits and drawbacks, and therefore each will perform differently. Comparisons among different vehicles and architectures only makes sense if they are operated under their optimum performance.

5. The ideal timescales at the mission level can be different than the timescales at the subsystem level, especially when battery dynamics are considered. This discrepancy might result in weight penalties due to inaccurate approximation of subsystem dynamics, or computational burden due to selecting very small time steps for an entire mission.

6. EPGDS technologies rapidly improve resulting in ever-changing subsystem capabilities, which in turn can have a cumulative positive effect on vehicle design and mission performance.

7. EPGDS are usually represented only by their specific power/energy, which leads to epistemic uncertainty.

8. The level of hybridization, architecture type, performance and sizing have a bidirectional impact on the empty weight as well as the flight performance of a hybrid electric aircraft, creating an interdependence between the subsystem, aircraft and mission levels.

CHAPTER 3
RESEARCH ARGUMENTS

The literature survey in Chapter 2 showed that the EA/HEA sizing considerations usually focus on propulsion alone, and either neglect a majority of EPGDS characteristics, or do not incorporate different architecture types. However, it was also observed that these concepts are extremely weight-sensitive, and hence the architectural choices must be made carefully. The main motivation of this dissertation is that there is a need to consider subsystem characteristics and architecture types in early stages of EA/HEA design.

The following sections of this chapter present a formulation of the research based on the observations made earlier. This formulation is depicted in Figure 3.1 and explained in detail in the upcoming sections.

The over-arching objective of the thesis was first introduced in Chapter 1 as:

Develop a methodology to perform sizing, integration and performance evaluation of electric power generation and distribution subsystems and architectures within electric and hybrid electric aircraft concepts.

The following criteria must be met for the methodology to realize the objective:

- Capture the impact of individual subsystem performance characteristics at subsystem, aircraft and mission levels
- Evaluate architectures for different types of system level requirements under varying levels of hybridization
- Subject to the constraint that the level of complexity must be suitable for rapid, low-cost analyses at the conceptual design stage

The methodology will aim to provide an analysis environment with increased dimensionality compared to the literature, reveal the interrelationships and interdependence among the

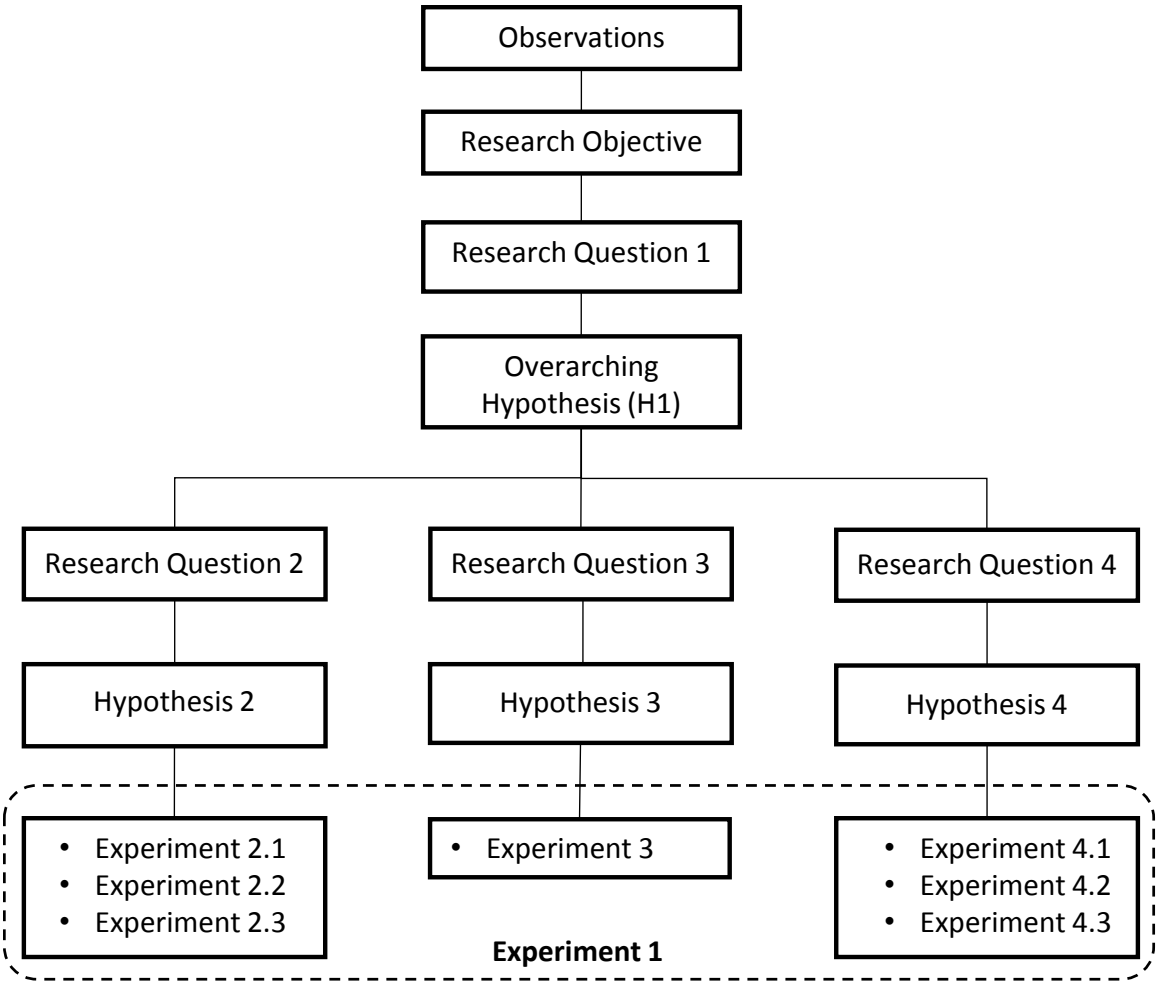

Figure 3.1: Formulation of the research arguments.

EPGDS and aircraft and mission level performance characteristics, and enable comparison of different architectures with respect to their performance at the subsystem, aircraft and mission levels.

3.1 Research Questions and Hypotheses

The following sections list the research questions to realize the research objective. A hypothesis to each question will be presented along with a set of experiments that are needed to conduct to substantiate the hypothesis.

3.1.1 Argument 1

The main research question of the thesis is recalled below:

RESEARCH QUESTION 1: How can the aircraft sizing and synthesis process be more generalized so that adequate comparisons between different types of primary power generation and distribution subsystems and candidate architectures are made available?

The literature survey conducted in Chapter 2 looked for answers to this research question. It was seen that the sizing of subsystem components is traditionally performed during conceptual aircraft design stage by using empirical relationships based on existing historical data.[67, 68] However, there is a lack of historical data and readily available physics-based models for EPGDS as they are rather new technologies. Hence, estimations on the impact of EPGDS add uncertainty to the system.

Observation 1 deducted from the literature survey showed that most research do not consider EPGDS and related architectures at the conceptual design stage, whereas observations 2 through 8 highlighted the significance of comprehensive architecture modeling during the conceptual design stage.

More specifically, Observation 2 revealed that electric aircraft are significantly more weight sensitive than conventional aircraft. This means that even small weight changes can bring significant penalties. According to Observation 3, an optimum level of hybridization should be found during the vehicle sizing process. This observation opens a door to discover any architectural trends based on optimization objectives and system level constraints. It was observed that the impacts of electrification on aircraft and mission levels vary with different architecture types (Observation 4). It was also found that inaccurate approximation of subsystem dynamics can bring additional weight penalties (Observation 5). Observations 6 and 7 showed the importance of representing the EPGDS weight and performance characteristics as well as any future technology trends to minimize the uncertainties related to architectural choices. Finally, Observation 8 revealed that the hybridization level,

architectural characteristics, aircraft sizing and performance are all interdependent.

This thesis seeks a substantiated answer to Research Question 1, as an answer could not be found in the literature. To this end, Research Question 1 is further analyzed and divided into multiple research questions (RQ):

- **RQ 1.1:** How can the sizing and synthesis process be modified so that it can be utilized for any type of aircraft, regardless of the propulsion system and its architecture?
- **RQ 1.2:** How can the dynamic EPGDS characteristics be integrated into the sizing process?
- **RQ 1.3:** How can EPGDS be represented to demonstrate various characteristics related to different types of subsystems?
- **RQ 1.4:** What capabilities are needed to enable rapid changes in the subsystem characteristics and architectures?

RQ 1.1 is related to the vehicle design and mission analysis. The "fuel burn" considerations in the mission analysis should be generalized to "energy" to account for the hybridization of the propulsion system. RQ 1.2 ties the subsystem level characteristics to the modified sizing process. This integration can be done by linking vehicle and mission level requirements to EPGDS model parameters. RQ 1.3 and 1.4 are related to the subsystem level. Different types of EPGDS can be represented by developing and/or adapting physics-based models. These models need to be parametric to enable rapid changes.

The literature review showed that in order for the architectural comparisons to be adequate, the following key aspects must be realized: (i) the architectures are sized properly, and the subsystem level impacts at the aircraft and mission levels are captured, (ii) design requirements and the dynamic behavior of the subsystems are taken into account within the aircraft sizing, and (iii) the architectures are compared based on their optimum performance.

The over-arching hypothesis given below attempts to realize these key aspects and addresses all of these questions:

HYPOTHESIS 1: *EA/HEA architectures can be adequately compared using a methodological framework which has the following capabilities:*

- *The mission performance analysis is energy-based and independent of the propulsion system type*
- *Aircraft propulsion architecture definitions are flexible enough to account for various types for architectures and their impact on the vehicle and mission levels*
- *EPGDS level performance characteristics are captured through parametric models and linked to the aircraft and mission level requirements, enabling an automated sizing process*
- *The optimum operational condition for each architecture type is acquired through integrated power management optimization*
- *The sizing process allows for the transition between high-level and detailed analyses to capture significant transients through variable step sizing*

The developed methodology must be flexible to be used for different architectures, and must be able to capture important performance variations among them. To test the flexibility and the extent of the methodology, architectural comparisons can be performed.

Since the literature review confirmed the interdependence among subsystem, aircraft and mission levels; a set of measures of performance (MoPs) can be determined to individually track the subsystem level impacts on a larger scale. For instance, assume that a series HEP architecture ends up to be heavier than a parallel one due to incorporating an additional propulsion device, when everything else is kept constant. When compared at the same operating conditions, it might be thought that either the mission performance of the aircraft with series HEP architecture would be poorer than its counterpart due to being

heavier; or the aircraft would have to be resized and require more energy overall. But this assumption might fall short unless the two architectures are compared at their optimum operating conditions or important transients at the EPGDS are taken into account.

Incorporating the optimum power management schedules and adaptive time steps can yield more reliable results when comparing the two architectures. Once these important aspects are taken into account, then the better-performing architecture can easily be differentiated by comparing the takeoff gross weight, required energy (which can be two MoPs), optimum operating conditions and subsystem dynamics of both competing configurations for the same point-performance mission requirements.

To test the validity of the overarching hypothesis, first the proposed capabilities must be developed. In the remainder of this chapter, these capabilities were divided into three hypotheses. A set of experiments were planned for each of the three hypothesis. To prove the validity and applicability of the methodological framework proposed in Hypothesis 1, all of these experiments must substantiate the associated hypotheses. Only then Experiment 1 cbe conducted to test whether the methodological framework developed according to Hypothesis 1 is capable of achieving the over-arching objective of this research.

If any one of the experiments fail, then Hypothesis 1 will be nullified.

3.1.2 Argument 2

The next argument of the thesis is related to the following observations:

Observation 2: Electric aircraft are significantly more weight sensitive than conventional ones because of the tremendous difference between the specific power/energy of conventional fuels and the specific power/energy of batteries.

Observation 6: EPGDS technologies rapidly improve resulting in ever-changing subsystem capabilities, which in turn can have a cumulative positive effect on vehicle design and mission performance.

Observation 7: EPGDS are usually represented only by their specific power/energy,

which leads to epistemic uncertainty due to modeling assumptions.

Observation 8: The level of hybridization, architecture type, performance and sizing have a bidirectional impact on the empty weight as well as the flight performance of a hybrid electric aircraft, creating an interdependence between the subsystem, aircraft and mission levels.

Observation 2 stresses the fact that uncertainty reduction in EPGDS modeling is very important because even small variations in estimating the weight of the EPGDS as well as the vehicle itself could make a snowball effect on the gross weight and the overall performance of the vehicle.

Observation 6 refers to the impacts of advances in EPGDS technologies on the vehicle design and mission performance. Although it is obvious that more advanced technologies will provide a better overall performance, the magnitude of this impact is unknown. It is important to figure out which subsystem characteristics improves the vehicle performance to what degree, so that a clear direction is given to subsystem scientists to further advance those characteristics.

Observation 7 addresses the uncertainties in EPGDS models in literature due to simplified underlying assumptions. Similar to technological uncertainty, the misleading effects of epistemic uncertainty can also be seen on the vehicle design and mission performance estimations.

Observation 8 points out to the fact that a change made at the subsystem level or in the power management strategy will have an impact on the aircraft and mission levels, which will then affect the subsystem level components and the power management strategy.

These observations emphasize the importance of the integration of EPGDS considerations into the vehicle sizing and synthesis process, leading to the next research question:

RESEARCH QUESTION 2: How can the traditional aircraft conceptual design stage be modified to make it suitable for any type of aircraft design and propulsion system?

Research Question 2 can be broken into the following sub-questions:

- **RQ 2.1:** What modifications should be done on the aircraft sizing and mission analysis process so that it is inclusive of any type of aircraft design, propulsion system, architecture and the energy storage type?
- **RQ 2.2:** How can the EPGDS characteristics be integrated into the modified sizing and mission analysis process?
- **RQ 2.3:** How can the technological sensitivities be captured?

As discussed previously, the traditional sizing and mission performance analysis process relies on fuel burn. A modification to this process is needed to make it more generic and independent of the propulsion type.

The subsystems are traditionally sized at the conceptual design stage by using empirical relationships concerning existing historical data.[67, 68] Due to the lack of historical data or readily available physics-based models, only a small portion of the electric propulsion subsystems in the chosen architecture are modeled. Moreover, the dimensionality of such models are rather low, as they are generally represented through a few design parameters, such as power-to-weight ratio, energy-to-weight ratio, rated power, maximum energy capacity, and efficiency. However, utilizing such low-dimensionality models brings an important amount of epistemic uncertainty to the results due to the modeling assumptions.

Although these parameters might be sufficient for initial sizing purposes, subsystem dynamics are completely missed until further down in the detailed design process. For instance, suppose that during the conceptual design stage, a subsystem is to be chosen among multiple state-of-the-art options that have the same functionality but the way they operate is different in principle. A selection that is made solely based on the highest power-to-weight ratio might not yield the desired dynamic response when integrated into the system. If such a case occurs later in the aircraft design process and the subsystem must be replaced

with another option, then the change in the power-to-weight ratio assumption might have a crucial impact on the overall system and weight of the vehicle.

With these thoughts in mind, the second hypothesis becomes:

HYPOTHESIS 2: *EPGDS characteristics can be integrated into the EA/HEA sizing process through a parametric sizing and synthesis framework with the following properties:*

- *A generic mission analysis approach is implemented where the required energy to fly a mission profile is tracked and budgeted between different power sources of aircraft according to preset hybridization levels*
- *A component based weight estimation technique is used*
- *Aircraft sizing and synthesis process captures the sizing of EPGDS components based on required energy and/or power*
- *EPGDS models used in the framework are parametric, physics-based and dynamic*
- *The developed EPGDS models are utilized to capture the subsystem level impacts at aircraft and mission levels*

To test the validity of Hypothesis 2, the following set of experiments will be conducted:

EXPERIMENT 2.1: Model a baseline aircraft with a conventional propulsion system within a sizing and synthesis environment built based on the proposed framework. Show that the environment is capable of producing the same design mission performance characteristics of the baseline aircraft.

- *Thought experiment:* Once the proposed framework is used to create the sizing and synthesis environment, it must be validated prior to conducting any type of analysis. Otherwise, the results cannot be deemed reliable. The validation can be performed

by comparing the output of the sizing and synthesis analysis to an existing baseline aircraft. This means that if the requirements given to the sizing and synthesis environment are the same as that of the chosen baseline aircraft, then the sizing process must converge to a design that has the same takeoff gross weight, geometric properties and mission performance characteristics. The results can be compared against manufacturer's data, literature and/or results obtained from an established aircraft sizing tool, such as FLOPS. If the environment yields a design that is acceptably accurate, then the developed framework is validated and can be used for further analysis.

EXPERIMENT 2.2: Change the baseline aircraft's propulsion system with a parallel hybrid-electric architecture using the developed EPGDS models. Use the sizing and synthesis environment to resize the hybrid-electric aircraft while matching the point-performance requirements of the baseline aircraft for a (i) 50% hybrid-electric aircraft and (ii) 100% electric aircraft. Compare the results.

- *Thought experiment:* The next step after validating the developed framework and the environment is to demonstrate that the methods used are generic enough to be used to model and size electric and hybrid electric aircraft. This requires a change in the propulsion system of the baseline aircraft with a new EPGDS architecture. Parallel hybrid-electric configuration would be a good application to test the flexibility of the analysis that can be performed, simply because a parallel configuration can be used to showcase a fully-electric, a hybrid-electric, and a conventional propulsion scenarios by changing the power management strategies. Using the same point-performance and design mission requirements as the baseline aircraft, the hybrid-electric and electric concepts should yield significantly different aircraft designs with different performance characteristics.

EXPERIMENT 2.3: Perform a parametric variation of EPGDS technology adjustment factors to determine sensitivity of aircraft and mission level measures of performance to subsystem level technology advancements.

- *Thought experiment:* The methods applied in the sizing and synthesis framework must be able to reflect technology improvements of the EPGDS. The key enablers of technology projections are the parametric property and increased dimensionality of the EPGDS models to be developed. To put these capabilities into test, for each EPGDS, a group of design metrics that will be improved with technological advancements must be identified. Then, both the individual and the combined impacts of varying technology adjustment factors (also known as technology K-factors) must be demonstrated at the aircraft and mission levels by performing tradeoff studies and sensitivity analysis.

3.1.3 Argument 3

The three observations given below form the third research question:

Observation 3: Energy management optimization should be performed during vehicle sizing. Architectural implications of optimizing the level of hybridization have yet to be discovered.

Observation 4: HEP architecture types have different benefits and drawbacks, and therefore each will perform differently. Comparisons among different vehicles and architectures only makes sense if they are operated under their optimum performance.

Observation 8: The level of hybridization, architecture type, performance and sizing have a bidirectional impact on the empty weight as well as the flight performance of a hybrid electric aircraft, creating an interdependence between the subsystem, aircraft and mission levels.

There might be more than one feasible architecture for a given set of requirements, but it is only logical to find the best performing one. Architecture comparisons might be straightforward for a given level of hybridization, but the optimum hybridization level might change for each competing architecture due to the variations in aircraft weight and energy requirement. Such architectures should be compared based on their optimal per-

formance conditions, which might imply different levels of hybridization. Moreover, hybridization level is heavily dependent on the system level requirements. It is also desired to see the architectural trends (if there are any) under varying requirements.

The optimization problem to be set up should not use parameters which are dependent on the propulsion type. For instance, if an optimization problem is solved using the "required power to sea level rated power" ratio as the control variables, the aircraft might not be able to follow the given power management schedule due to a lapsing engine. Hence, it must be ensured that the schedule determined by the optimizer is realizable.

Hence, the next research question is:

RESEARCH QUESTION 3: How can the best performing hybrid electric architecture be determined under varying levels of hybridization?

The following hypothesis aims to answer this research question:

HYPOTHESIS 3: *The optimum power management schedule for an aircraft can be obtained by implementing a segment-wise optimization technique based on a set of control points and variables which do not depend on the type of the propulsion system. The optimum schedule can then be used to determine the best performing feasible architecture among the competing architectures by comparing their associated aircraft and mission level measures of performance.*

Hypothesis 3 will be tested by the following experimental plan:

EXPERIMENT 3: Perform an aircraft sizing process where the power management schedule is obtained by solving the optimization problem for (i) minimum energy required, (ii) minimum fuel consumption, and (iii) minimum takeoff gross weight, using the same on-design mission profile. Compare the resulting architectures based on the measures of performance.

- *Thought Experiment:* If the optimum power management schedules change for a

given objective function, the resulting aircraft designs should employ different propulsion architectures. Then a mutual baseline aircraft and a design mission profile can be used to perform an aircraft resizing process where the power management schedule is determined by the optimizer. It is highly likely that the optimum power management schedule would vary with each optimization objective, which in turn should yield distinct propulsion architectures. These architectures can then be compared based on aircraft and mission level measures of performance such as takeoff gross weight, empty weight, wing area, fuel weight, energy capacity, etc. Moreover, architectural trends based on different objectives can be revealed.

3.1.4 Argument 4

The following observation forms the basis of the fourth and final research question:

Observation 5: The appropriate timescales are different at mission and subsystem levels, especially when transient regimes are concerned. This discrepancy might result in performance degradation due to inaccurate approximation of subsystem dynamics using large time steps, or computational burden due to selecting very small time steps for the entire mission in mission performance analysis.

Traditionally, a mission profile is divided into mission segments (e.g. climb, cruise, descent, etc.) which are further divided into mission legs. It is assumed that the aircraft performance characteristics and flight dynamics are frozen inside each leg. The time scale of these legs can be arranged by the desired level of accuracy, detail and the ease of computation, but it is usually in the order of minutes [68].

Conversely, transient analysis calls for much smaller time steps which can go as low as microseconds. An attempt to carry out the mission performance analysis along with the transient analysis at a scale of millionth of a second would bring enormous computational burden to otherwise high-level analysis.

If the events or conditions that would cause a transient behavior could be described in

terms of the parameters that were already computed in mission performance analysis, then one would know when to decrease the temporal step size whenever those conditions are encountered. With this knowledge, the mission performance analysis could be paused momentarily to conduct transient analysis at an appropriate timescale and for a small duration of time.

This way, the significant transients could be captured during the early levels of the design stage by changing the step size only when and where needed; and a balance between the smaller and the larger step sizes could be stroked. For this to happen, the conditions that would necessitate such a change in the step size should be evident based on the limited information derived from the mission performance analysis.

Consequently, the following question is posed:

RESEARCH QUESTION 4: How can a balance between smaller and larger time steps be found so that significant transients at the subsystem level are captured at the conceptual design stage without bringing the associated computational burden?

- **RQ 4.1:** Can the transient behavior of an electrical system be related to the mission level parameters?
- **RQ 4.2:** If they are related, how can the relationship be captured between the significant transients of a given electrical system which could occur under a wide range of inputs which are expected to be given to the electrical system during a mission?
- **RQ 4.3:** If they are related, can the relationship be generalized for the given electrical system so that the whether a significant transient occurs could be estimated with only the limited amount of information obtained from the mission performance analysis?

The following hypothesis addresses this question:

HYPOTHESIS 4: *A balanced time step size to capture the significant transients during*

the mission performance analysis can be determined within each mission leg by establishing the probability of a significant transient occurring under a certain degree of change in the mission level requirements by performing the following three-step approach:

1. *A design of experiments (DoE) concept is leveraged to intelligently sweep through the mission level parameter space to maximize the knowledge about the system response with minimal experimental effort.*

2. *The controllers of the electrical system which were tuned via gain scheduling where the schedules are determined by jointly utilizing Monte Carlo simulations and a system design optimization technique are utilized to reduce the optimization efforts and obtain a reduced number of gain sets to control the majority of the realizable cases of the DoE; whereas the cases which go beyond the physical capabilities of the system are eliminated.*

3. *The probability of a transient occurring is established by a conditional rule set determined a-priori by fitting a categorical surrogate model to the transient signal at the neighborhood of the time at which the mission level change occurred.*

To test the validity of Hypothesis 4, the following experimental plan will be employed:

- **EXPERIMENT 4.1:** Create dynamic models for an electric propulsion powertrain where power is supplied by a battery-sourced electric motor. Set a series of step inputs in terms of the required motor torque and speed of variable amplitude. Verify that (i) the results (in terms of battery SOC, subsystem voltages and currents) obtained by using large time steps differ from the results obtained by using small time steps, (ii) a significant transient behavior is missed when larger time step size is used, and (iii) not every change in the power input causes a significant transient response at the subsystem level.

- *Thought experiment:* This experiment tests (a) whether important information regarding the subsystem dynamics is really missed by performing the simulations at a relatively large time step, and (b) whether every change observed at the power requirement causes an unwanted transient response at the subsystem level. When the two simulation results are compared, the one obtained by using large time steps is expected to be flatter than the ones obtained by using smaller time steps since the sampling rate was different. The one with smaller time steps should yield results with higher resolution, and perhaps significant events occurring in the signal, such as transients, which the results from the simulation performed with larger time steps would miss. Moreover, this experiment tests whether the time step must be decreased to preform transient analysis every time a change occurs in the power drawn out of the system. If it can be shown that not all changes cause an undesired subsystem response, then the methodology proposed in Hypothesis 4 would turn out to be indeed valuable. As a result, this experiment tests (i) the impact of the change in the mission characteristics on the subsystem dynamics, and (ii) the information lost due to using a larger temporal step size than what is suitable for the system at hand.

- **EXPERIMENT 4.2:** Conduct the following steps to verify that a gain scheduling technique can be used to control a group of simulations instead of performing optimization for each case within the design space:

  1. Define the design variable space by creating a DoE with simulation input variables
  2. Create a second DoE with simulation input variables and controller gain parameters
  3. Run simulations with the second DoE cases, collect the error on the reference signal and the actual signal

4. Fit a surrogate model to the error using both the gain and input variables
5. Assess variable importance for the gain variables by performing Monte Carlo simulations to eliminate the variables which have insignificant impact on the variation of the error
6. Perform sensitivity analysis to reveal the sensitivity of the signal tracking error to the controller gains under varying model design variables and intelligently choose a case which represent the majority of the cases under a certain level of error
7. Set up a system design optimization problem where the controller gains with high importance are the optimization variables and the optimization objective is to minimize the error between the input signal and the subsystem level response
8. Run simulations for the selected case to solve the optimization problem and collect the optimum gains
9. Use the resulting gain set obtained for that particular case in all of the simulations in the first DoE and identify the cases which produced an acceptable signal tracking error
10. Return to step 5 and repeat the procedure until either acceptable gain sets are obtained for all of the cases or a saturation point is reached where the optimum gain set for one case does not yield results within the reasonable margin of error for the other cases
11. Create a schedule from the collected gain sets such that whenever a case from the first DoE is simulated the correct gain set is used to control the system

- *Thought experiment:* To be able to relate the subsystem responses to the mission level requirements given in each case of the DoE, one must make sure that the responses obtained were indeed resulted by the conditions specified in that case. This means that the electrical system must be able to track the input signal

determined from the mission level requirements. Even the least complex electric propulsion system would have multiple controllers for the electric motor, power electronics, etc. If these controllers are not tuned in advance, then the electrical subsystems might behave very differently than desired, and therefore the resulting dynamics cannot be related to the mission level inputs. To avoid such an uncertainty in the results, the controller gains must be optimized.

Finding an optimum solution for a single DoE case requires multiple simulations to be run. This contradicts the idea of utilizing the design of experiments approach because it can expand the total simulation time beyond a reasonable limit. Instead of attempting to optimize the controllers of each case, the experimental efforts can be minimized by solving an optimization problem for only a few cases randomly selected from the DoE and testing whether the solution for each case results in a tuned system for a group of cases in the DoE. If such gain sets can be found then the controllers can be scheduled to switch to the most suitable gain set for the DoE case being tested. This way, if there exists cases in the DoE which are not realizable by the electrical system due to physical limits of the designed system, they can be eliminated.

- **EXPERIMENT 4.3:** Run the simulations defined by the realizable cases of the first DoE with the appropriate timescale and the gain schedules obtained in Experiment 4.2. Define two undesirable transient behaviors for the electric motor and set a transient constraint. Examine each simulation result at the neighborhood of the moment where a change occurred in the input signal. Identify which cases violate which constraints and categorize the cases based on constraint violation separately for each transient behavior. Fit surrogate model to the response data, and determine whether there exists a clear trend between the mission level inputs and the constraint violations by evaluating variable importance and performing sensitivity analysis. If there exists a relationship between the two, set up a conditional rule set to calculate

the probability of the constraints being violated based on the mission level changes. Compare the rule sets obtained for the two transient constraints.

- *Thought Experiment:* If the likelihood of a significant transient to occur can be evaluated by only using the information available from the mission performance analysis, then a good surrogate model can be fit to the physically realizable DoE cases. Conversely, if additional information which cannot be obtained from the mission level analysis is vital to estimate the occurrence of a transient, surrogate modeling attempt would fail and disprove the hypothesis.

  When the transient constraints on the aircraft electric power characteristics defined in MIL-STD-704F by the U.S. Department of Defense were examined, it was seen that an electrical system is expected to give a transient reaction within a certain amount of time, and then return back to its steady-state characteristics. For instance, this amount of time is less than one tenth of a second for oscillations in voltage. Thus, instead of trying to fit a model on the signal considerable a long time before, during and after a change takes place, a small time interval can be defined around the neighborhood of the time of the change. The range of this neighborhood can be determined based on the expected characteristics of the transient in question.

  Then, the dynamic response can be book-kept based on two outcomes: whether the constraint is violated or not. This categorical approach would be more adequate and perhaps more suitable than trying to estimate the continuous characteristics of the transient response because it would minimize the aleatory uncertainty in the surrogate model by not incorporating the noise in the signal. Moreover, if there is a high chance of constraint violation, then the temporal step size would be adjusted accordingly and the transient analysis can be performed around the time of expected constraint violation without introducing significant amount of computational burden to the analysis, removing the need

for a surrogate model of the transient response.

Because the system is highly nonlinear, the Artificial Neural Networks (ANN) approach would be a suitable modeling technique. There are many aspects to measure the power quality of an electrical system. As a proof of concept, a major subsystem such as the electric motor and its voltage behavior can be used to demonstrate a good example, since undesired voltage transients at the motor terminals can be detrimental to the propulsion performance, and in some cases can even cause a power loss.

3.2 Chapter Summary

In this chapter, four main research arguments were determined. First, the research objective of the thesis was revisited. Then, a research question (RQ-1) which seeks a way of realizing the objective was posed. To answer this question, the over-arching hypothesis (H-1), which proposes a methodological framework to realize the research objective, was formed. To develop an in-depth formulation of the proposed framework, the over-arching hypothesis was further divided into three hypotheses which consists of the three main arguments of this dissertation.

Hypothesis 2 consists of the proposed modifications to the traditional conceptual design stage. More specifically, it lists the required steps to be taken to make the aircraft sizing and synthesis suitable for any aircraft design, independent of its propulsion type and architecture, removing the need for historical data for unconventional, recent technologies such as electric and hybrid electric aircraft propulsion subsystems.

Hypothesis 3 sets a fair ground for architecture comparisons, by providing an optimization method for the power management schedule of a hybrid electric aircraft. By utilizing the concept of control points which are strategically placed on the mission profile, this method presents flexibility in terms of the desired level of detail in analysis. Furthermore, the method makes sure that the optimized schedule can always be realized by the propulsion

system by selecting the control variables to be independent of any possible performance degradation in the propulsion system due to ambient conditions.

Hypothesis 4 integrates the computationally expensive transient analysis to relatively high-level mission performance analysis by an adaptive step sizing strategy. It describes the methodological steps to create a conditional rule set with the limited amount of information available during the mission performance evaluations to estimate when the timescale should be changed to allow for transient analysis based on the probability of a significant transient taking place. This increases the knowledge about the EPGDS design requirements at the early stages of aircraft design.

For each hypothesis, experiments were carefully planned and set up to test the validity of the arguments made. If these experiment can validate hypotheses 2, 3 and 4, then the over-arching hypothesis will be substantiated by Experiment 1 and the research objective will be realized.

The details of the proposed methodological framework were presented in the next chapter, Chapter 4. The experiment sets 2 and 3 were demonstrated in Chapter 7, along with a proof of concept. The Experiment Set 4 and finally Experiment 1 were conducted in Chapter 8. The results were integrated to substantiate the over-arching hypothesis in Chapter 9.

The formulation of the research arguments were revisited in Figure 3.2, this time with a summary of each argument.

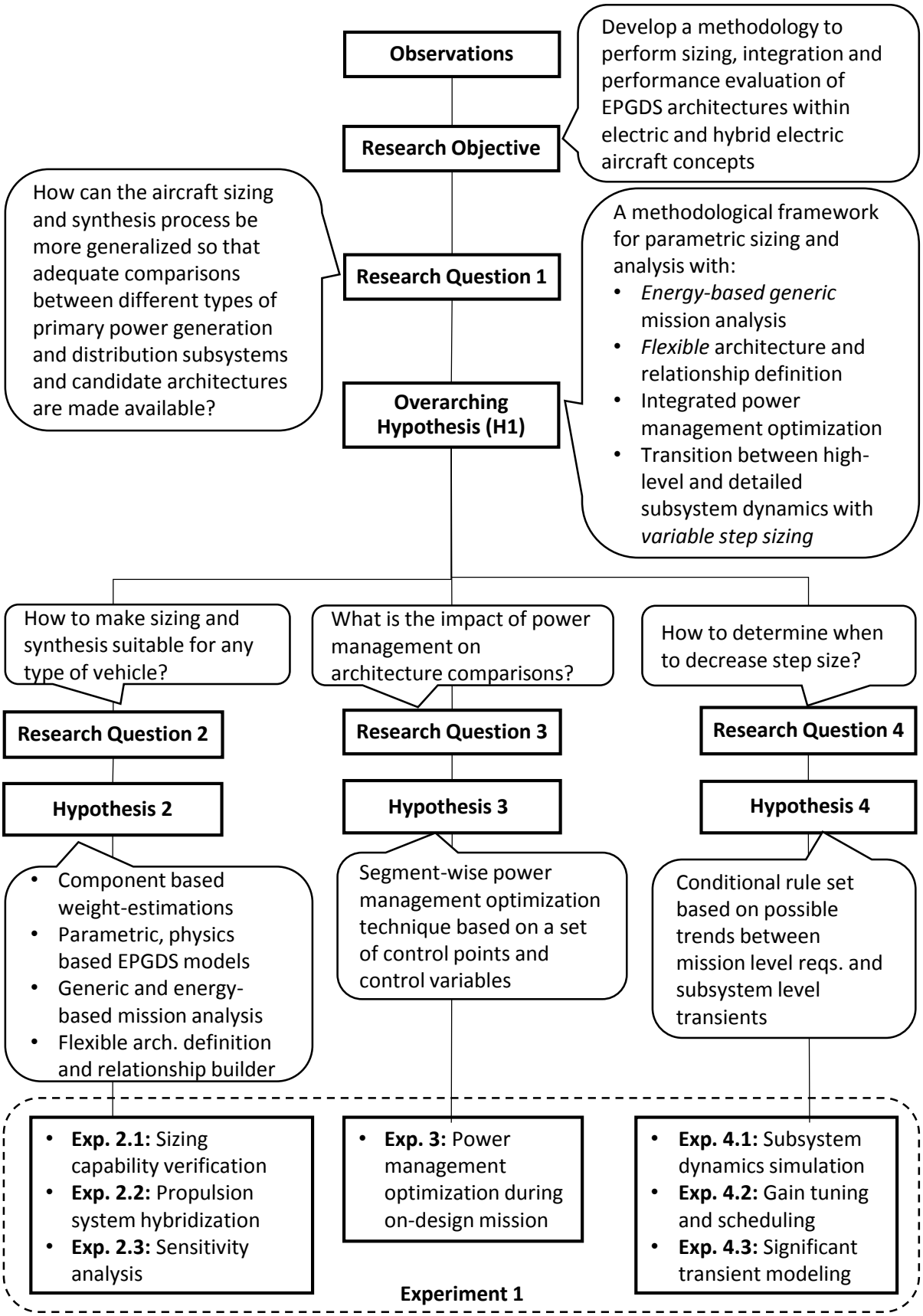

Figure 3.2: Descriptive formulation of the research arguments.

CHAPTER 4
PROPOSED METHODOLOGY

To achieve the research objective of this thesis, the proposed methodology must enable the sizing, integration and performance evaluation of electric power generation and distribution subsystems and architectures within EA/HEA concepts. To this end, a methodological framework was developed. Hypotheses 2 to 4 discussed in Chapter 3 forms the building blocks of the framework. This methodological framework supports the overarching hypothesis (Hypothesis 1) which was revisited below.

Hypothesis 1: *EA/HEA architectures can be adequately compared using a methodological framework which has the following capabilities:*

- *The mission performance analysis is energy-based and independent of the propulsion system type*
- *Aircraft propulsion architecture definitions are flexible enough to account for various types for architectures and their impact on the vehicle and mission levels*
- *EPGDS level performance characteristics are captured through parametric models and linked to the aircraft and mission level requirements, enabling an automated sizing process*
- *The optimum operational condition for each architecture type is acquired through integrated power management optimization*
- *The sizing process allows for the transition between high-level and detailed analyses to capture significant transients through variable step sizing*

Hypothesis 1 overlays the methodological framework developed in this dissertation. An overview of this framework is provided in Figure 4.1, which consists of the following

building blocks:

- A generalized sizing and synthesis approach: The sizing and synthesis approach must be suitable for sizing and analyzing flying vehicles in all categories, including advanced and/or unconventional electric or hybrid electric propulsion architectures. This block addresses Hypothesis 2.

- Power management schedule optimization: An optimizer must be set up to ensure that each architecture is sized and synthesized based on its optimum power split strategy. This strategy might change based on the architecture type, vehicle size, desired performance characteristics and the objective function. This block addresses Hypothesis 3.

- Temporal step sizer: The architectural comparisons must account for subsystem dynamics. This necessitates the subsystem level simulations to be performed with much smaller time steps than the mission level evaluations. To bridge the gap between the subsystem level dynamics and mission level performance evaluations, a temporal step sizer was developed to change the step size of computations only when necessary to account for the significant transients. This block addresses Hypothesis 4.

The process shown in Figure 4.1 starts with the selection of a notional aircraft concept. The mission and point performance requirements are applied to the notional concept within the sizing and synthesis block. Once a conceptual aircraft design which satisfies the requirements is obtained, its power management schedule is optimized based on the state of the aircraft during a given mission. For an on-design mission, an iteration takes place until the sizing and synthesis block and the optimizer converges to an optimized aircraft design. Then, the aircraft design and mission performance characteristics are fed into the temporal step sizer which determines whether transient analysis is necessary at any point in the mission. If necessary, the temporal step sizer adjusts the timescale of the analysis. If the transient analysis discloses that the subsystem dynamics violate transient constraints, then

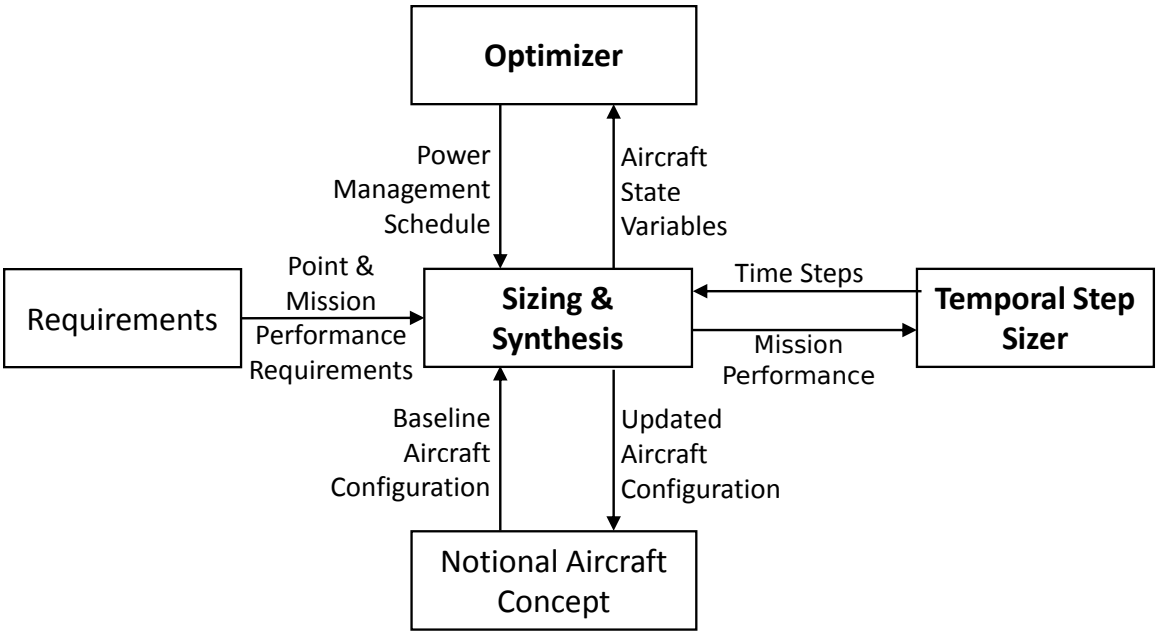

Figure 4.1: Building blocks of the methodological framework.

the subsystems are re-sized within the sizing and synthesis block in order to achieve adequate subsystem level performance. This initiates another iteration process, as the changes in the subsystem design impacts the overall vehicle design and mission performance.

The present chapter provides an overview of the methodology and introduces the building blocks, and how they come together to create the methodological framework. The next sections provide detailed information on the development of the methodological framework.

4.1 Sizing and Synthesis

At the heart of the developed methodological framework, there is aircraft sizing and synthesis. This block was modified from traditional sizing and synthesis approach to ensure that it possesses all of the capabilities discussed in Hypothesis 2, which is revisited below.

Hypothesis 2: *EPGDS characteristics can be integrated into the EA/HEA sizing process through a parametric sizing and synthesis framework with the following properties:*

- *A generic mission analysis approach is implemented where the required energy to fly*

a mission profile is tracked and budgeted between different power sources of aircraft according to preset hybridization levels

- *A component based weight estimation technique is used*
- *Aircraft sizing and synthesis process captures the sizing of EPGDS components based on required energy and/or power*
- *EPGDS models used in the framework are parametric, physics-based and dynamic*
- *The developed EPGDS models are utilized to capture the subsystem level impacts at aircraft and mission levels*

The sizing and synthesis block which is depicted in Figure 4.2, consists of generic mission analysis, constraint analysis and disciplinary analysis. This approach is similar to the traditional aircraft conceptual design approach which was demonstrated in Figure 2.10. The main difference between the proposed approach and the traditional one is that the sub-blocks within the sizing and synthesis block were modified to account for unconventional aircraft designs and propulsion systems.

The following paragraphs explain the methods used within each sub-block.

4.1.1 Disciplinary Analysis

Inside the disciplinary analysis sub-block, aerodynamics, weights, propulsion and architectural performance analyses are conducted to geometrically scale the aircraft from a baseline configuration. The baseline aircraft is a starting point for the disciplinary analysis; its aerodynamics, weights and propulsion information are taken as a first estimate to initialize the sizing process.

The traditional disciplinary analysis approach was modified to account for the impact of electric power generation and distribution subsystems (EPGDS) on the weight, aerodynamics and propulsion characteristics of the vehicle. Furthermore, performance of the

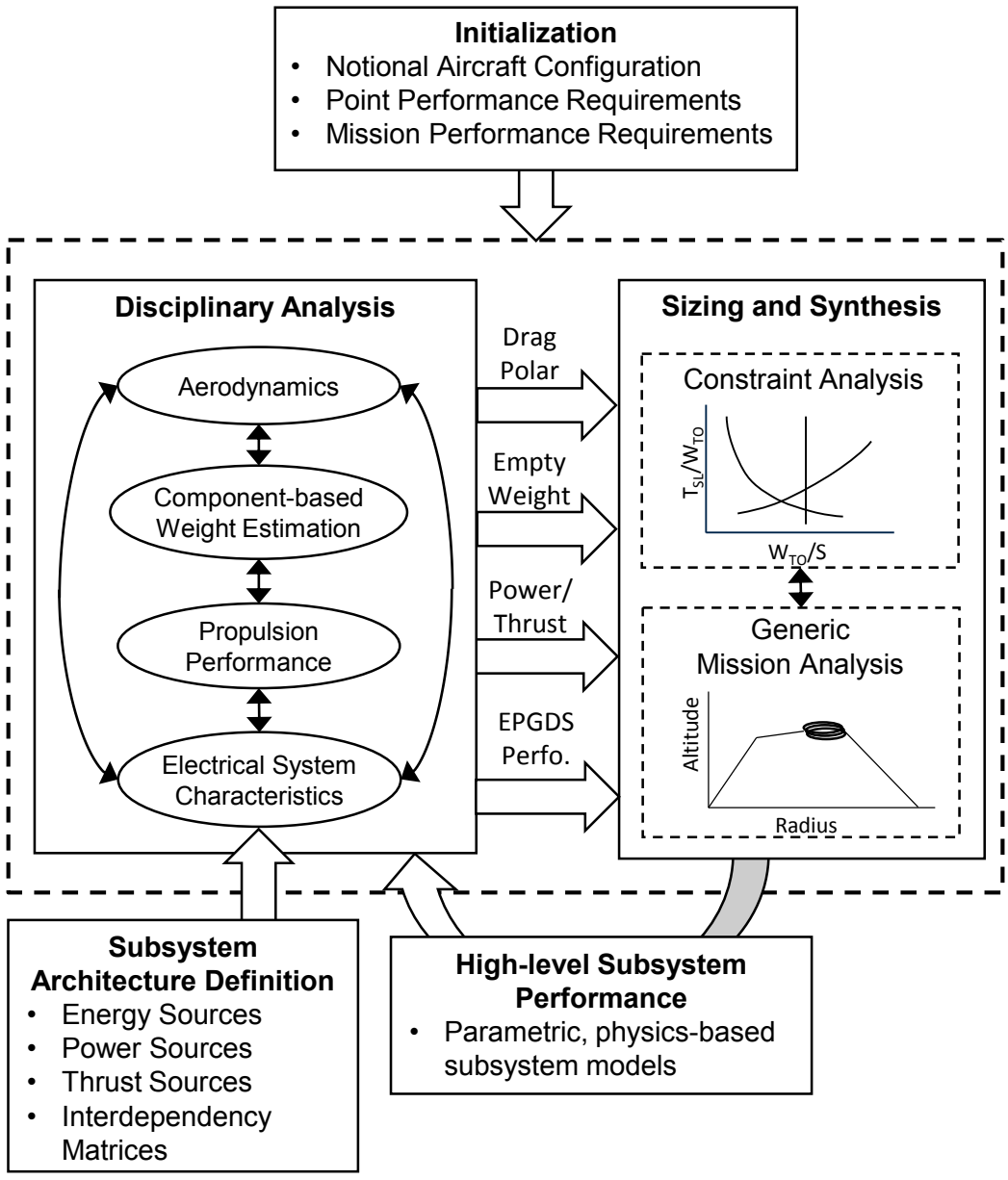

Figure 4.2: A closer look at the sizing and synthesis block.

individual subsystems and the overall architecture is captured within the "electrical system characteristics" analysis. This was accomplished by developing high-level, parametric, physics-based EPGDS models suitable for rapid analysis. The development process of the EPGDS models along with other models for the non-electrical components of hybrid-electric propulsion powertrain were explained in detail in Chapter 5.

The main subsystems in any propulsion system were categorized into three groups: (i) energy sources (such as fossil fuel, fuel cells, rechargeable battery, etc.), (ii) power sources (such as engines and electric motors), and (iii) thrust sources (such as propellers). Depending on the type of the propulsion system, the latter two categories can be combined in a single category. These categories were then used in characterization of the propulsion system, as described in Section 5.5 of Chapter 5.

The aerodynamic properties (more specifically, drag polar information) of the baseline aircraft were first obtained from literature or FLOPS and then embedded into the generic mission analysis. This process was explained in Section 6.3 of Chapter 6

Vehicle weight estimation for sizing in the early design phases has typically been done with the help of regression relationships that were developed from historical data pertaining to existing aircraft. In the most basic case, this involves representing the empty weight W_E through an empty weight fraction, which is determined based on data for existing vehicles: $(W_E/W_{TO}) = f(W_{TO})$. In a more detailed approach, the vehicle takeoff gross weight is expressed as the sum of the weights of major components which makes up the empty weight, fuel, and payload, as shown in Eqn. 4.1.

$$\mathbf{W_{TO}} = \sum_i W_{comp,i} + W_{fuel} + W_{payload} \tag{4.1}$$

The component weights themselves are expressed through relationships that typically take the form given in Eqn 4.2, where $P_1, \ldots P_n$ are parameters on which the component's

weight depends, and coefficients $A, a, x_1, \ldots, x_n$ are determined by fitting to existing data.

$$\mathbf{W_{comp,i}} = A(W_{TO})^a(P_1)^{x_1} \ldots (P_n)^{x_n} \tag{4.2}$$

Since the component weight equations typically contain the takeoff gross weight W_0 raised to some exponent, the implicit system of weight build-up equations is solved iteratively, starting with a guessed value of W_0, and iterating until the change in W_0 between iterations converges to below a suitable threshold.

The above iterative procedure to find W_0 is valid in general, however, the representation of the component weights in the form shown above requires that sufficient historical data be available to permit determination of the coefficients. This may not be the case for unconventional vehicle configurations, which do not conform to standard fixed-wing or rotary-wing vehicles configurations. In such cases, the direct applicability of standard/traditional weight estimation relationships may be questionable.

To overcome this, a weight build-up approach that comprises a combination of physics-based weight assessments (through component sizing) as well as look-ups of component weights from available product data sheets may be attempted. This is especially relevant for the case of novel concepts such as roadable flight vehicles, whose configuration may be expected to contain some aircraft elements and some automobile elements. Thus, it is clear that to evaluate novel vehicle concepts, a highly flexible and parametric weight estimation approach is required.

To this end, a database of weight estimation relationships and techniques to cover major vehicle components, including structural elements, power-train elements, and energy storage system elements were created based on methods documented by Roskam [67] and NASA [72]. Calibration factors associated with each major weight item were used to obtain reasonable agreement between the predicted weights and the aircraft's published weight breakdown, whenever available.

In some cases, no appropriate weight estimation method was found applicable to some

components, such as the air induction system and the propeller. In these cases, the empty weight margin coefficient (K_{EW}) was used to group these component weights in a single term, as defined in Eqn. 4.3, where W_e is the empty weight of the baseline aircraft, and $W_{component\,i}$ is the sum of all computable component weights within the weight estimation database, including the wing, empennage, fuselage, etc.

$$\mathbf{W_e} = (1 + K_{EW}) \sum_i W_{comp,i} \tag{4.3}$$

Once K_{EW} was determined from the baseline aircraft, its value was held constant during the sizing process to account for the weight changes of the remaining components during vehicle sizing.

The weights of some other vehicle components were directly dependent on the assumed technological state-of-the-art. Examples include weight estimation of electric motors and power electronics (based on gravimetric power densities, kW/kg), electric batteries (based on gravimetric energy density, Wh/kg), and so on. The weight estimation technique for these subsystems were provided in Chapter 5.

4.1.2 Energy Based Constraint Analysis

The main goal of the energy based constraint analysis is to obtain a proper relation between two scaling parameters, namely, required thrust loading at sea level take-off (T_{SL}/W_{TO}) and wing loading at take-off (W_{TO}/S), so that a feasible design in terms of these two scaling parameters can be found. The scaling parameters are independent of the size of the aircraft and thus, this analysis is applicable to aircraft of all sizes.

Each mission segment and corresponding key points are analyzed and a design space is obtained based on mission or performance requirements. In order to visualize the design space, a diagram which incorporates the effects of the constraints on T_{SL}/W_{TO} and W_{TO}/S -or other design variables- can be plotted, as notionally shown in Figure 4.3. A design point selected from the feasible design space ensures meeting the requirements. If there is

no feasible design space, the designer should look into other solutions, such as infusing a technology to improve a certain metric.

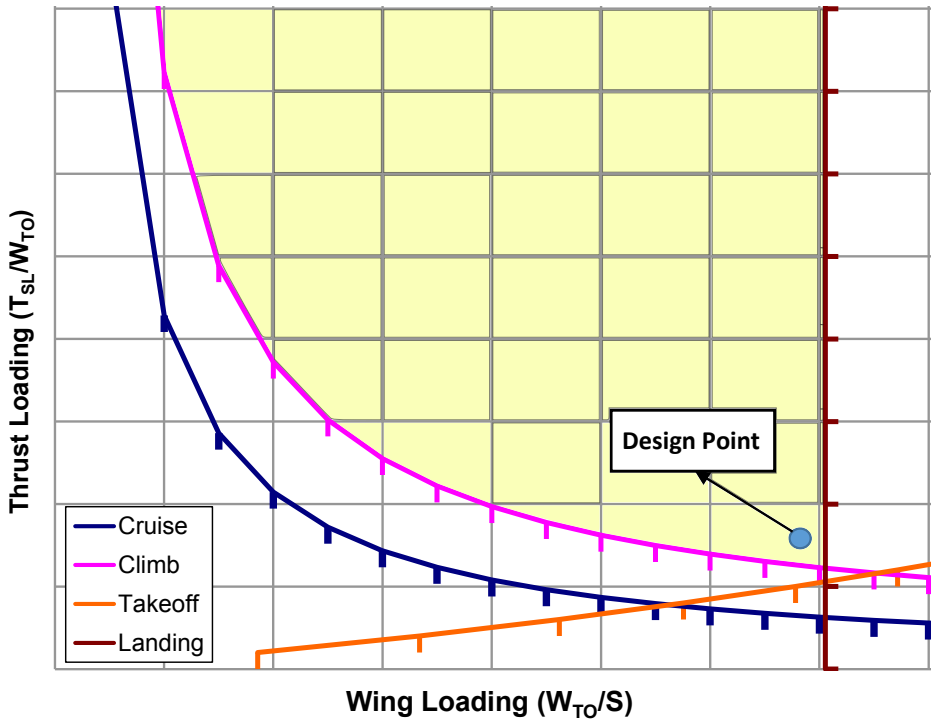

Figure 4.3: A notional constraint analysis diagram. Feasible design space is highlighted.

Mattingly [69] derives Eqn. 4.4, which is called the 'master equation' to lay out the relationship between T_{SL}/W_{TO} and W_{TO}/S. This equation is then used to find a constrained curve for each mission and point performance requirement.

$$\frac{\mathbf{T_{SL}}}{\mathbf{W_{TO}}} = \frac{\beta}{\alpha}\left\{\frac{qS}{\beta W_{TO}}\left[K_1\left(\frac{n\beta}{q}\frac{W_{TO}}{S}\right)^2 + K_2\left(\frac{n\beta}{q}\frac{W_{TO}}{S}\right) + C_{D0} + C_{DR}\right] + \frac{P_S}{V}\right\} \quad (4.4)$$

In the equation above, α is engine lapse rate, n is load factor, S is reference area and q is dynamic pressure. β depends on how much fuel has been consumed and payload delivered. Therefore, an educated guess for β is necessary to initiate the iterative design process.

In electric propulsion considerations, the variables α and β are redundant as electric motors do not have a lapse rate, and the aircraft weight remains constant as long as the

payload does not change. Hence, instead of using the master equation given in Eqn. 4.4, it would be more appropriate to start the calculations from a more generic equation, such as the principle of conservation of energy.

In fact, Eqn. 4.5 is the starting point of the master equation and hence, the energy based constraint analysis, as it is essentially based on the principle of conservation of energy:

$$\mathbf{T} - (\mathbf{D} + \mathbf{R})\mathbf{V} = W\frac{dh}{dt} + \frac{W}{g}\frac{d}{dt}\left(\frac{V^2}{2}\right) \tag{4.5}$$

where T is thrust, D is drag, R is resistive forces acting on the aircraft, V is aircraft speed, W is instantaneous aircraft weight, h is altitude and g is the gravitational acceleration.

Once a feasible space is obtained after applying all constraints, a design point can be selected and the corresponding T_{SL}/W_{TO} and W_{TO}/S values are carried on to the mission analysis to find an estimate for the takeoff gross weight.

For studies where a baseline aircraft which already meets the design requirements exists, it can be assumed that the location of this design point remains fixed. This is due to the fact that T_{SL}/W_{TO} and W_{TO}/S are scaling parameters which do not depend on aircraft size, as explained previously. For the same constraints, the values which T_{SL}/W_{TO} and W_{TO}/S take do not change by changing the propulsion system either. No matter what type of propulsion system is used, as long as it is capable of providing the sea level thrust required at the takeoff gross weight for a given reference area, the final design lands on the point selected on the constraint analysis diagram.

The only reason that might necessitate a change in the location of this point would be changes in the weight fractions and drag polar coefficients of the resized aircraft. Unless such a drastic change from the baseline aircraft occurs, the effect of minor changes in aerodynamic properties and weight fractions on the target design point can be assumed negligible.[13]

This discussion justifies the rationale of the assumption that the resized aircraft must

maintain the same design point of the selected baseline aircraft. Since the main application of the demonstrated framework will be on the comparison of aircraft with different propulsion architectures, energy-based constraint analysis is deemed to be out of scope of this thesis. Instead, the sizing process will be performed by matching the sea level thrust loading and wing loading of the baseline aircraft which electric and hybrid electric aircraft designs will be derived from and compared to.

4.1.3 Mission Analysis

Traditionally, mission analysis is performed to calculate the weight fractions of each mission segment and finally the take-off gross weight, W_{TO}. The takeoff gross weight build-up shown in Eqn. 4.1 can be rewritten in the following form given in Eqn. 4.6:

$$\begin{aligned} W_{TO} &= W_P + W_E + W_F \\ &= W_P \Bigg/ \left(1 - \frac{W_E}{W_{TO}} - \frac{W_F}{W_{TO}}\right) \end{aligned} \tag{4.6}$$

The payload weight, W_P, is set by the requirements, and W_E/W_{TO} can usually be estimated from historical trends. For electric aircraft, fuel weight W_F represents the weight of the electric energy storage which may or may not change during a mission. In case of hybrid electric aircraft, a fuel fraction can be defined for the fuel burning engine branch as a product of fuel fractions for each mission segment k as given in Eqn. 4.7.

$$\frac{W_F}{W_{TO}} = 1 - \prod_{k=1}^{n} \left(\frac{W_f}{W_i}\right)_k \tag{4.7}$$

where W_f and W_i are final and initial weights of the aircraft at the end of segment k, respectively.

There are several aircraft sizing and analysis tools that can be used for mission performance analysis for conventional fuel burning aircraft, such as the Flight Optimization System (FLOPS) tool developed by NASA. However, this is not the case for EA/HEA

concepts. Although there are some studies on HEA/EA sizing in literature (as discussed in Chapter 2), a readily available tool suitable for the scope of this thesis and developed specifically for these concepts has not been found.

In fact, FLOPS is capable of performing limited EA/HEA analysis. However, it only allows for a single propulsion type to be in use at any given point of time during the mission analysis. This means that the aircraft can only operate in electric or conventional mode, although the operation schedules are interchangeable.[73, 74] Because of this shortcoming, FLOPS is not deemed suitable as mission performance analysis tool for the type of studies proposed in this thesis.

As a result, a new sizing and synthesis tool based on energy-based sizing and generic mission analysis was built in MATLAB by applying the proposed methodological framework. The generic mission analysis is based on the principle of energy budgeting, where the energy consumption of each power source, instead of the fuel burned, is bookkept. This way, the traditional mission analysis approach was modified to account for any type of propulsion system, making it a *generic* mission analysis approach.

The energy budgeting approach was applied by first estimating a total energy capacity available at the beginning of the mission. Then, starting from the beginning of the mission, this available energy was budgeted between the employed propulsion sources based on the desired power management strategy and the required energy to fly the current mission leg. Once the end of the mission profile was reached, the energy bookkeeping revealed valuable information such as which power source used how much energy, which energy source needs to be resized, how much fuel had been burned, the final SOC of the rechargeable battery, whether the power management strategy should be modified, so on and so forth.

An in-depth and step-by-step explanation on the generic mission analysis approach is presented in Chapter 6.

4.1.4 Aircraft and Subsystem Sizing Approach

This section explains the proposed sizing method which incorporates the target design point coming from either the constraint analysis or the baseline aircraft with a generic mission analysis approach applicable to both EA and HEA concepts.

The sizing approach for vehicles with hybrid electric propulsion architectures is based on (i) matching the point performance (e.g. specified takeoff and landing field lengths, climb rate, and steady cruise speed, etc.) of either the baseline aircraft or the selected design point in the constraint analysis diagram, and (ii) an on-design mission analysis.

Point performance requirements are represented by sizing parameters such as power-to-weight ratio (P_{SL}/W_{TO}) and wing loading (W_{TO}/S). The lower limit of the former, for instance, may be driven by takeoff field length or climb gradient requirements, whereas the upper limit of the latter may be driven by an upper bound on permissible approach speed or stall speed.

As explained previously in Section 4.1.2, the sizing parameters can be set based on the chosen point on the constraint analysis diagram or based on matching the sizing parameters of the baseline aircraft. In the proof of concept study presented in Chapter 7, a general aviation aircraft with an internal combustion engine was chosen as the baseline vehicle, then its propulsion system was replaced with a hybrid electric propulsion architecture and finally the new aircraft concept was resized. In this process, the power-to-weight ratio and wing loading of sized vehicles were required to match those of the baseline vehicle, assuming that the changes in the target design point due to the changed weight fractions and drag polar coefficients of the resized aircraft were negligible, as explained previously.

Thus, in the following paragraphs, the target power-to-weight ratio and wing loading were referred to as the sizing parameters of the "baseline aircraft"; however they can be easily replaced by the same sizing parameters of the target design coming from the constraint analysis. Moreover, the power-to-weight ratio term can be changed with thrust-to-weight parameter for aircraft with jet engines.

Regardless of which method to set the sizing parameters is applied, the following conditions were set:

1. Regardless of the propulsion system architecture, the overall power-to-weight ratio of the new design must be equal to or greater than that of the baseline aircraft, as shown in Eqn. 4.8, where P_{SL} is the sea level maximum power of the aircraft at sea level, W_{TO} is the takeoff gross weight, and $P_{SL\,i}$ represents the sea level rated power of a power source i of the new aircraft.

$$\left(\frac{\mathbf{P_{SL}}}{\mathbf{W_{TO}}}\right)_{\mathbf{new}} = \left(\frac{\sum_i P_{SL\,i}}{W_{TO}}\right)_{new} \geqslant \left(\frac{P_{SL}}{W_{TO}}\right)_{baseline} \tag{4.8}$$

2. The candidate design must have the same design wing loading as the baseline, as shown in Eq. 4.9.

$$\left(\frac{\mathbf{W_{TO}}}{\mathbf{S}}\right)_{\mathbf{new}} = \left(\frac{W_{TO}}{S}\right)_{baseline} \tag{4.9}$$

The vehicle sizing is an iterative process, in which each iteration includes the recalculation of aircraft geometry, component weights, and the required energy of each energy source for the design and reserve missions. The following sections briefly describe the sizing of individual components, the overall iteration procedure, and convergence criteria.

Sizing of the Wing and Tail Geometry

In this work, the dimensions of the baseline vehicle's fuselage were maintained, but wings, horizontal tail, and vertical tails were resized. The wing was scaled through changing the wing planform area to match the baseline wing loading, as given by Eqn. 4.9. The remaining geometric properties (such as taper ratio, aspect ratio, thickness-to-chord ratio, etc.) were held constant. The empennage size was updated based on the tail volume coefficients using Eq. 4.10, where S_h and S_v are the areas of horizontal and vertical tails, c is the wing

mean aerodynamic chord, S is the wing planform area, b is the wingspan, l_h and l_v are the lengths of the moment arms of the horizontal and vertical tails with respect to the aircraft center of gravity, and V_h and V_v are the horizontal and vertical tail volume coefficients.

$$\mathbf{S_h} = \frac{Sc}{l_h} V_h, \qquad \mathbf{S_v} = \frac{Sb}{l_b} V_b \tag{4.10}$$

Sizing of the Power Sources

According to the condition described in Eqn. 4.8, the sum of sea level rated power of all the power sources on the new (resized) aircraft can be calculated for a given or previously computed takeoff gross weight. This is the total rated power required, $P_{rated\,req}$, i.e. the power which must be matched by the sea level rated power of all of the power sources of the resized aircraft combined.

The total sea level power required is distributed among the available power sources of the new propulsion architecture. To this end, a *rated power split* parameter (κ_i) was defined. This parameter describes how much of the total sea level power required the power source i must deliver (percentage-wise), as shown in Eqn. 4.11. In this equation, $P_{rated\,i}$ is the sea level rated power of the power source i, and $\sum_i \kappa_i = 1$.

$$\mathbf{P_{rated\,i}} = \kappa_i P_{rated\,req} \tag{4.11}$$

To give an example, $\kappa_{EM} = 0.7$ for the parallel hybrid-electric propulsion architecture shown in Figure 2.7b means that the electric motor delivers 70% of the required sea level power of the aircraft. To match the total rated power to that of the baseline aircraft, the fuel-burning engine must then deliver the remaining 30%, i.e. $\kappa_{EM} = 0.3$.

Once the required sea level rated powers of the power sources are determined, each power source can be sized accordingly. The details of the power source sizing process were given in Sections 5.1.4 and 5.3 of Chapter 5.

Sizing of the Propeller

The propeller sizing (along with the performance estimation) was performed by leveraging an in-house propeller model based on the blade element momentum theory. The details regarding the model and the sizing process summarized below were presented in Section 5.4 of Chapter 5.

As the takeoff gross weight of the resized vehicle changes, the thrust required and hence, the propeller size must change. The propeller was resized through its diameter and number of blades based on the rapid estimation methods presented by Gudmundsson [75] for various propeller types. The rest of the propeller characteristics were kept constant.

The permissible propeller diameter is upper-bounded by ground clearance requirements and tip speed limitations. To implement these limitations, the following approach was taken:

- Initiate the propeller sizing process with the same number of blades of the referenced propeller (i.e. propeller of the baseline aircraft)
- If the required thrust cannot be met without violating the ground proximity and/or tip speed constraints, increase the number of blades are gradually
- If the tip speed results in an unacceptably high tip Mach number, gradually reduce the RPM of the referenced propeller from that of the baseline

Sizing of the Energy Sources

In this dissertation, an energy source is defined as any type of energy stored in the aircraft and used as the primary or partial source to generate propulsive power. Two main types of energy sources are under the scope of this work: fossil fuel and rechargeable battery.

The sizing of the energy sources was performed in two steps: (i) sizing by the weight, and (ii) sizing by the volume.

Fossil fuel is a "consumable" energy source, meaning that its weight decreases as it is being burned, whereas the weight of the rechargeable battery may or may not change as energy is drawn out of it. For instance, in the case of Lithium-Ion batteries, the battery weight remains constant, whereas Lithium-Air batteries *gain* weight as they are utilized. As a result, the traditional approach presented in Eqn 4.7 cannot be used to calculate the weight of the electric or hybrid electric energy sources. Instead, a more generalized approach was taken to estimate the weight of all energy sources.

The generalized energy source weight estimation approach is based on bookkeeping the total amount of energy required from each individual energy source. This is accomplished by first calculating the energy required from each energy source to fly the given mission is calculated at each mission leg, regardless of the initial estimate on how much energy is carried on board. The amount of energy drawn out of each energy source depends on the architecture and power management strategy, and is characterized by defining the interrelationships between the energy, power and thrust sources in the given architecture. This methodology is explained in further detail in Section 5.5.

Once the required energy from each available energy sources is calculated for the given vehicle design and mission, the weight of the energy sources are computed through their individual state-of-the-art specific energy (i.e. gravimetric energy density). This approach is shown in Eqn, 4.12 where W_j is the weight of energy source j, $(E/W)_j$, $E_{req,\,j}$ is the total amount of energy required from j, and is the state-of-the-art specific energy (value obtained from literature) of j.

$$\mathbf{W_j} = \frac{E_{req,\,j}}{(E/W)_j} \tag{4.12}$$

If the required energy or the weight of the energy sources were found to be different than the initially guessed energy and weight, the aircraft is resized along with the energy sources. This is an iteration process which is carried through until the initial guesses converge to the final values found as a result of the mission performance analysis.

The second part of the energy source sizing process is based on the volume considerations. For a conventional airplane, the available volume inside the wing and/or fuselage is used to house the fuel tanks. For the hybrid propulsion system architecture, part of this volume is allocated to the batteries. For instance, the internal available volume of the wing is computed using Eqn. 4.13, based on Reference [72], where K_{wv} is a dimensionless wing internal volume coefficient, (t/c) is the wing thickness-to-chord ratio, and λ is the wing taper ratio. The value of K_{wv} was first determined such that given the baseline aircraft wing geometry, Eqn. 4.13 yields the fuel tank volume of the baseline aircraft. For a purely electric or a hybrid architecture, the volume taken up by the battery was determined by the required battery energy of the design and reserve missions and the volumetric energy density. For a hybrid architecture, the volume remaining after the placement of the battery was allocated to the fuel tanks.

$$\mathbf{V_W} = K_{wv}\frac{S^2}{b}\left(\frac{t}{c}\right)\left(1 - \frac{\lambda}{(1+\lambda)^2}\right) \tag{4.13}$$

In the case of insufficient volume left to hold the necessary fuel, the wing volume was increased by a small margin through an iteration process. Since this increase in the wing volume results in a heavier wing, the empty weight is updated iteratively.

4.1.5 The Iterative Sizing Process

Once the sizing parameters are established, the generic mission analysis approach is explained in detail in Chapter 6 is utilized to find the required energy to fly each mission leg and budget this energy between different propulsion branches. For each mission leg, the budgeting is performed based on the power management schedule which is determined by the optimizer. The percentage share of the net propulsive power supplied by each available power source is allocated by the power management schedule.

The energy based sizing of the aircraft and its propulsion subsystems is an iterative process. The iteration steps are depicted through the process flowchart of Figure 4.4, and

summarized step by step below.

1. Start with an initial guess for the takeoff gross weight and battery weight
2. Update the aircraft wing and empennage sizes
3. Size the power sources (engine(s) and/or electric motor(s))
4. Calculate the empty weight at the first iteration, update at later iterations
5. Recalculate the aircraft gross weight based on the empty weight obtained at the previous step
6. Check whether the newly calculated gross weight and the initially estimated gross weight converge to each other within a reasonable margin of error
   (a) If not converged, start the inner iteration process (iteration *i*, framed by the blue dashed line) by returning to step (2)
   (b) If converged, move on to step (7)
7. Fly the design mission to evaluate the total energy required to fly the given mission profile
8. Update the fuel and battery weights based on the individual energy requirements from each energy source
9. Recalculate the aircraft gross weight
10. Check whether the newly calculated gross weight and the gross weight obtained at the end of iteration (i) converge to each other within a reasonable margin of error
    (a) If not converged, move on to the next iteration beginning from step (2)
    (b) If converged, freeze the final vehicle design and end the iteration process

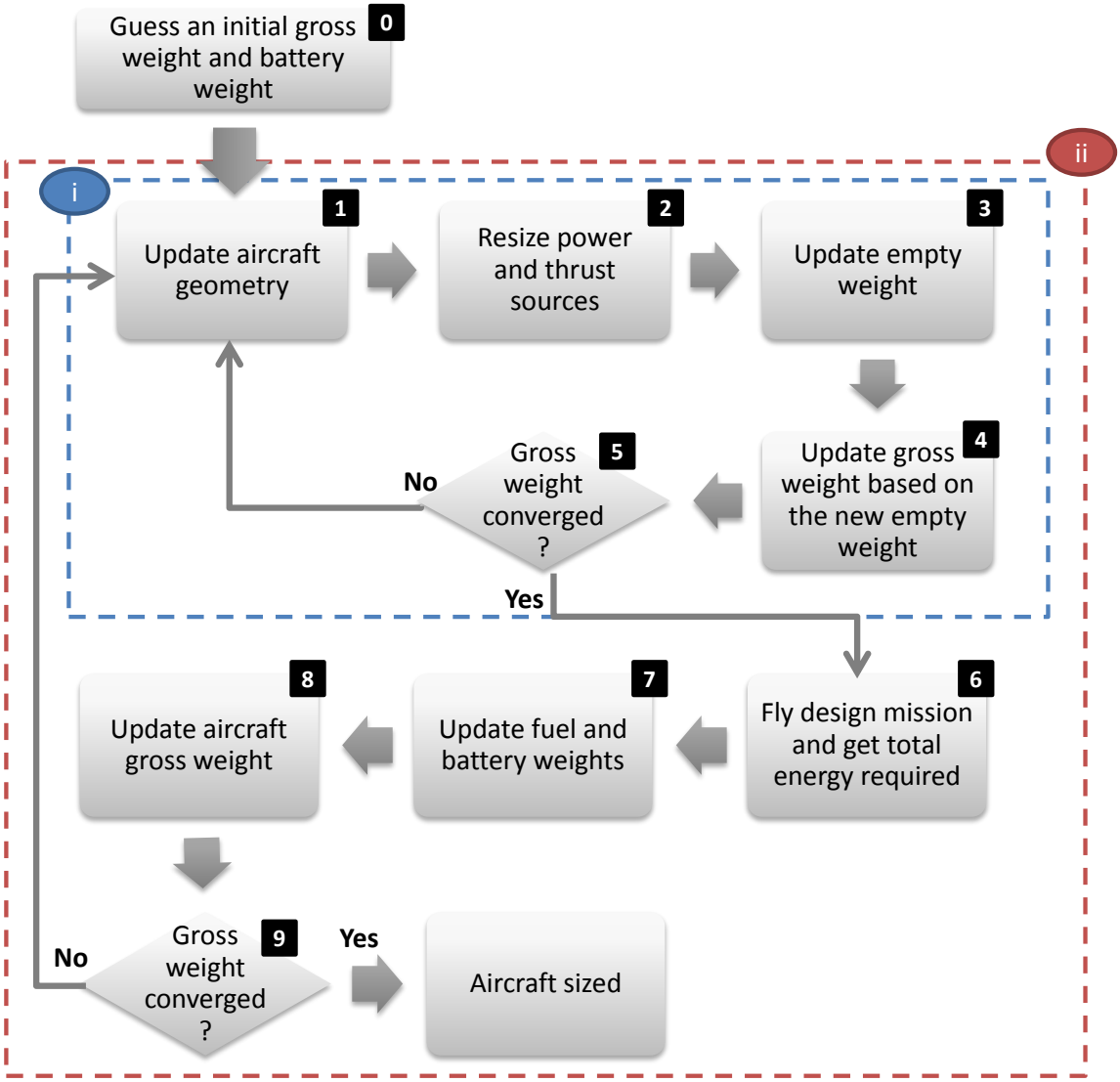

Figure 4.4: Vehicle sizing flowchart with an inner and an outer iteration process on takeoff gross weight convergence.

Once the outer iteration loop (iteration *ii*) converges, the resulting vehicle design is frozen. The performance of the sized vehicle can then be evaluated over off-design missions, where gross weight and empty weight are kept constant but tradeoffs can be made between fuel and payload weights.

4.2 Power Management Schedule Optimization

The optimal control is not only crucial for power management control but also for the optimal design of hybrid electric vehicles (including aircraft and automobiles). Comparisons among different type of hybrid electric architectures only makes sense if they are operated under their optimum performance. [76] Hypothesis 3 proposed an optimization technique to find the optimal power management strategy for each competing architecture. This technique should be suitable to be implemented within the sizing and synthesis approach proposed in Hypothesis 2.

This section describes the methodology to optimize the power management schedule of hybrid electric aircraft as proposed in Hypothesis 3, which was revisited below:

Hypothesis 3: *The optimum power management schedule for an aircraft can be obtained by implementing a segment-wise optimization technique based on a set of control points and variables which do not depend on the type of the propulsion system. The optimum schedule can then be used to determine the best performing feasible architecture among the competing architectures by comparing their associated aircraft and mission level measures of performance.*

The following paragraphs lay out a step-by-step approach on how to set up and solve the optimization problem following the methodology proposed in this hypothesis.

4.2.1 Selecting the Objective Function

An optimization problem can be written for a versatile number of objectives, such as minimum fuel burn, maximum range, minimum emissions, etc. The most common objective in hybrid electric automobile applications is to optimize for minimum fuel consumption. [77, 78, 76, 79] However, automobiles have different characteristics than aircraft, which leads to different priorities for the optimization problem. Hence, similar work in this field can be

leveraged, but it cannot be applied directly to the problem at hand.

Minimizing fuel consumption is a major concern in aerospace community, and is also the main motivation of this thesis. Interesting trade-offs are expected to come out of such a study, especially when aircraft designed for different ranges are compared. Minimization of fuel burn leads to an increase in required electrical energy. For long ranges, the required energy might be so high that an extremely heavy battery with large capacity is required. However, a heavy battery can significantly increase the power requirement, as explained previously. After some point, this might lead to even more fuel consumption compared to a lower level of hybridization, and hence, the optimizer might decide in favor of a conventional-like propulsion with low level of hybridization, if at all. On the other hand, optimizing for minimum fuel consumption for short range missions might result in high levels of hybridization or a fully electric aircraft.

As explained in Section 3.1.4, most system level requirements are tied to energy consumption. Thus, the objective function can be selected as to optimize for **minimum energy required**. However, this objective must be chosen with caution. An optimization problem solved for minimizing the required energy to fly a given mission profile can yield a different result than one solved for minimizing the required energy which must be stored in the energy sources of the aircraft. This is due to the fact that a conventional propulsion system has a very low efficiency of converting the chemical energy in the fossil fuel to mechanical energy, compared to electric propulsion. As a result, if the required energy to fly a given mission profile is to be computed by the integral of required power over the course of the flight without multiplying the required energy by an efficiency factor, it would yield a much lower value for the required energy.

Another interesting objective could be to **minimize energy expenditure per distance**. A long range mission automatically requires more energy than a short range mission, and therefore, it would not make sense to compare the two. This issue can be solved by normalizing the energy consumption by distance. This approach is similar to that of automobiles,

where "miles per gallon" is a significant factor for efficiency. This objective function is more suitable to be used in off-design mission analysis rather, as in most cases the on-design mission analysis is performed with a fixed design range requirement.

Weight is not a major concern in automobile applications, whereas it is for aircraft. It would also be interesting to solve an optimization problem for **minimum takeoff gross weight** (TOGW or W_{TO}). Optimizing for TOGW inherently deals with fuel weight, battery weight, engine weight and weight of the rest of the EPGDS. Moreover, it is also a function of how the aircraft is operated. The results can be compared with fuel optimized designs. However, due to the low specific energy of batteries, it is highly likely that the optimizer would converge on a conventional propulsion architecture rather than an electrified one.

More objectives can be populated, such as **minimum operating cost**, **minimum emissions**, and so on. The segment-wise power management optimization technique described here can be implemented regardless of the selection of an objective function. An example application is provided in Section 7.4 where the optimization problem was solved for minimum fuel burn, minimum takeoff gross weight and minimum energy.

4.2.2 Design and Control Variables

In an optimal power management solution, while the power contribution of the different sources can vary over time and over different mission segments, the variation is likely to be smooth and there is no physical reason to expect rapid and abrupt variations over short intervals of time. Therefore, the optimization problem does not have to be explicitly solved for each and every instant of time over the mission. Rather, a few strategically-chosen control points may be used to represent the overall variation of the power contributions over the course of the mission. With this in mind, two types of optimization scenarios can be addressed:

1. Optimal sizing and operation of the aircraft over a design mission
2. Optimal operation of the sized aircraft over off-design mission(s)

Table 4.1: List of design and control variables for design and off-design missions

Design and Control Variables		**Design Mission Optimization**	**Off-design Mission Optimization**
Wing planform and empennage design variables	Area, span, taper ratio, sweep, etc.	✓	✗
Propulsion system design sizing variables	Total sea level rated power; Sea level rated power split	✓	✗
Power management control variables	$u_1, u_2, \ldots, u_n$	✓	✓

Table 4.1 shows the design/control variables pertinent to these two scenarios.

The wing and empennage related variables are responsible for geometrically scaling the wing. The rated power of all fuel burning engines and electric motors are used to size the propulsion devices. These variables are kept frozen after the design mission is optimized. On the other hand, the power management strategies are mission-specific and thus applies to both on-design sizing missions and off-design performance evaluation missions.

While the goal is to find the optimum hybridization schedule, the hybridization factor may not directly be a suitable control variable, since (i) not all hybridization factors may be realizable at all flight conditions given engine power lapses and (ii) the hybridization factors for climb and cruise segments were defined differently (Eq. 6.14 and Eq. 6.25).

Instead, an alternative control variable which can be written for each power source is proposed. The *normalized power*, $u_{ps}(t)$, is defined in Eqn. 4.14, where the subscript ps stands for *power source*, $P_{ps,req}(t)$ is the instantaneous required power from the power

source ps, and $P_{ps,max\,av}$ is the maximum available power of the power source at a given flight condition. Note that for a fuel burning engine, the value of $P_{FB,max\,av}$ varies with altitude.

$$\mathbf{u_{ps}}(\mathbf{t}) = \frac{P_{ps,req}(t)}{P_{ps,max\,av}} \tag{4.14}$$

A normalized power variable must be set for each power source at each control point, yielding a total of n control variables. Then, the following invariant bounds must be applied to the control variables:

$$0 \leq u_{EM}(t) \leq 1 \tag{4.15}$$

Once $u_{ps}(t)$ is found for all power sources for an optimal design, the required power from each power source can be calculated directly from Eq. 4.14. The set of $u_{ps}(t)$ controls how each power source is utilized during the mission. The utilization is expressed by another variable, called the "hybridization factor" or "level of hybridization". Although both terms can be used to express the power split between the power sources, the hybridization factor is different than the control variable by definition.

In this dissertation, the hybridization factor term describes how the power sources are utilized within the mission in terms of and its definition varies based on the flight segment. For the flight segments which requires high power, such as climb, hybridization factor was defined similar to the power coding approach. For other segments where the aircraft operates on a specific altitude-velocity schedule, i.e. where the required power is well below the maximum power, such as the cruise segment, a required power split approach was utilized. These definitions were provided in Chapter 7 by equations 6.14 and 6.25.

The control variables, on the other hand, are utilized during the power management schedule optimization and then reported to the mission analysis block. Each control variable is then translated into a hybridization factor term for the related power source.

The main reason for using two different terms is to ensure that the aircraft can deliver the power commanded by the optimization. The hybridization factor definitions were used within the mission analysis because they simplify the calculations. However, the optimization cannot be controlled by them as the definition of the hybridization factor does not take into account engine lapsing. If an engine lapses at altitude, it might not be able to deliver the required power defined by the hybridization factor as the available power might be lower than the sea level rated power or the required power. Thus, by defining the control variable as given in Eqn. 4.14 and forcing it to be within the boundaries shown in Eqn. 4.15, it is ensured that the optimizer always asks for a realizable power.

After the optimal values of the control and design variables are found for the design mission, the wing and tail planform variables, engine power rating (and hence the engine weight), and electric motor power rating (and hence the electric motor weight) can be determined and fixed. The optimization of off-design mission performance is performed using only the control variables that determine the power split between fuel-burning and electric power paths.

Control Points

Hypothesis 3 proposes the use of a set of control points strategically placed on the mission profile. These points are different and usually more spaced out than the mission legs. This is due to the fact that there is no physical reason that would necessitate a drastic change in the power management over a small time interval, except for segment transitions. Thus, the hybridization factor variation is likely to be smooth and monotonic for the majority of the mission.

An example distribution of such control points is given in Figure 4.5 where the control points are shown with red dots and the mission points with blue dots over the mission profile. The placement of the control points depends on the nature of the mission profile. In this example, 4 control points labeled from letters a to d were placed as follows: a at the

beginning of the climb segment, b at the end of the climb segment, c at the beginning of the cruise segment, and d at the end of the cruise segment.

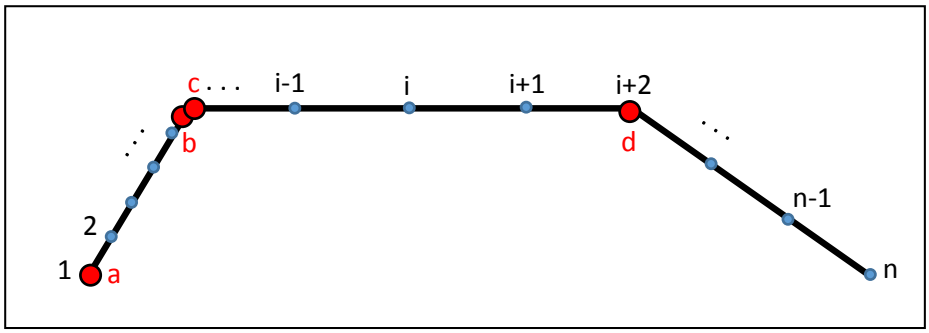

Figure 4.5: Example control points (red) and mission points (blue) on a notional mission profile.

The points b and c were placed at the same location. This is because of the anticipation that the power management strategy is likely to change during the transition between two segments. No control points were placed at the end of the descent segment assuming that it is an unpowered glide. However, if it was a powered descent, then at least one more control point should be added to this segment.

Once the control points are established, the control variables can either be held constant in between two points, or linearly interpolated. For instance, in the example given in Figure 4.5, if the control variables are to be linearly interpolated, then the power split at the mission points in between two consecutive control points is determined by the value of and the linear spacing between these consecutive control points.

Although having a large amount of control points placed on the mission profile might provide increased control over the power management, it also brings computational burden especially if the propulsion architecture consists of multiple power sources. This is because if there are n number of distinct power sources in a given architecture, then there must be n number of control variables at every control point. Even for a hybrid-electric architecture with two distinct power sources (e.g. a fuel burning engine and an electric motor), the dimensionality of the optimization problem increases rapidly as each new control point would mean two extra variables which must be optimized.

Thus, the number of control points should be determined by the number of times a significant change in the power management strategy is expected, the desired level of detail and computational resources. An example to how to place the control points was provided in the implementation of this optimization approach in Chapter 7.4.

4.2.3 Optimization Constraints

The optimization problem has to have adequate constraints on the mission and vehicle design.

First, there needs to be a minimum sea level power-to-weight ratio (P_{SL}/W_{TO}) constraint, and a maximum wing loading (W_{TO}/S) constraint. As mentioned previously, the point performance constraints were implicitly accounted for by requiring the wing loading and power-to-weight ratio of the hybrid electric aircraft to match those of the baseline.

Then, operational constraints should be defined. For the climb segment, rate of climb (ROC) cannot be chosen as a proper constraint because any airplane that has a lapsing engine on board will suffer a loss of rate of climb with altitude. Even an airplane whose engine does not lapse, propellers will make less thrust at high altitudes as air gets thinner. Hence, climb will be conducted at full power but not a constant ROC. Instead, aircraft should maintain the speed for best ROC (which might change slightly with altitude) and full available power. Then, the altitude can be integrated to find the amount of time spent to climb to the cruise altitude. As a result, minimum time to climb to a certain altitude can be set as a constraint for the climb segment, as shown in the below inequality:

$$t_{climb} \geq \zeta_{t_{climb}}$$

Next, a constraint for the cruise segment is to be set. Economy cruise for fuel burning engine means maximum distance traveled per pound of fuel burned; but that might end up being very slow. Instead, gate-to-gate block time and speed is an important utility and should not be less than a certain amount. Hence, block speed (V_{block}), which is the aver-

age speed to travel a specified distance in block time, is chosen to be another operational constraint. Block speed is chosen over block time as a constraint because block time can change drastically for short and long missions; whereas block speed might be slightly lower for shorter missions but it would not change as wildly as block time. This constraint will also dictate the cruise speed. This constraint is shown in the below inequality:

$$V_{block} \geq \zeta_{V_{block}}$$

Descent can be assumed as operated at idle power and does not necessitate a separate constraint. However, additional constraints must be set for reserve fuel and battery capacity. Landing fuel reserves and/or battery reserves in terms of SOC can be set as the following constraints:

$$W_{final\,fuel} \geq W_{req.\,reserves}$$

$$SOC_{final} \geq SOC_{req.\,reserves}$$

These two constraints do not have to be applied at the same time, as one of them might be enough.

To sum up, the operational constraints are:

- Sea level power to weight ratio
- Wing loading
- Time to climb
- Block speed
- Landing fuel reserves and/or battery reserves in terms of SOC

These operational constraints were already taken into account within the sizing and

mission analysis blocks. Since the optimization algorithm is integrated within the sizing and synthesis block, these constraints were inherently applied to the optimization problem.

Additionally, the control variable constraints shown in Eqn. 7.3 and 7.4 were applied for each power source. These constraints can be populated according to the number of power sources employed in the propulsion architecture.

4.2.4 Integration of the Power Split Optimization into the Sizing and Synthesis Framework

In a on-design mission, there is a mutual relationship between the power management schedule optimization, component sizing and mission analysis. The power management schedule optimization is an iterative process wrapped around the sizing and synthesis framework. The iteration steps are listed below:

1. Optimizer makes an initial guess on the control variables
2. Control variables are fed to the sizing and synthesis block
3. The control variables are translated into hybridization factors and used to calculate the power split throughout the flight by the mission analysis module
4. The iteration process previously shown in Figure 4.4 is performed
5. Once the iteration converges and the design is frozen, aircraft design and performance information is fed to the optimizer by the sizing and synthesis block
6. The optimizer computes the value of the objective function for the given design and performance characteristics
7. Optimizer perturbs the control variables based on the chosen optimization algorithm
8. The new control variables are fed to the sizing and synthesis block (i.e. return to Step 2)
9. The optimization continues until the desired optimization tolerance is reached

10. At the end of the on-design optimization process, the aircraft design is frozen and the optimum power management schedule is obtained

The iteration steps given above are for an on-design mission. Once the optimal values of the sizing control and design variables are found at the control points of the design mission; the wing area, engine power rating (and hence the engine weight), electric motor power rating (and hence the electric motor weight) are fixed. Battery weight (only if a modular battery is assumed) and fuel weight at takeoff are not be fixed as their values must change based on the requirements of off-design missions.

Then, the optimizer takes the control variables along with the free design variables and start the mission evaluation to find the setting that minimizes the objective function. The placement of the control points can be varied from the on-design optimization, if desired. At the end of this step, the amount of fuel and battery capacity required to fly an off-design mission is found.

This optimization approach was implemented for an on-design mission in Chapter 7.

4.3 Adaptive Step Sizing

The generic mission performance analysis approach withing the modified sizing and synthesis block described in Section 4.1 utilizes a discretized mission profile. Each segment of the mission is divided into mission legs which are enclosed by two consecutive points placed on the mission profile. The mission performance and flight dynamics computations are performed at these points, and the state of the aircraft is assumed to be frozen in between two consecutive points. Thus, the points are logically spaced out at each segment so that they are not too wide to create any abnormal discontinuity in the flight dynamics, but also not too close to increase the computational burden. Generally, the points are placed to be a couple of minutes away from each other.

As discussed earlier, a much lower timescale must be chosen for the discretization of the time-domain simulations to perform transient analysis. The enormous discrepancy

between the two timescales creates a significant problem when the two types of analysis are to be integrated. The final hypothesis of this dissertation proposed the following solution to overcome this problem:

Hypothesis 4: *A balanced time step size to capture the significant transients during the mission performance analysis can be determined within each mission leg by establishing the probability of a significant transient occurring under a certain degree of change in the mission level requirements by performing the following three-step approach:*

1. *A design of experiments (DoE) concept is leveraged to intelligently sweep through the mission level parameter space to maximize the knowledge about the system response with minimal experimental effort.*

2. *The controllers of the electrical system which were tuned via gain scheduling where the schedules are determined by jointly utilizing Monte Carlo simulations and a system design optimization technique are utilized to reduce the optimization efforts and obtain a few numbers of gain sets to control the majority of the realizable cases of the DoE; whereas the cases which go beyond the physical capabilities of the system are eliminated.*

3. *The probability of a transient occurring is established by a conditional rule set determined a-priori by fitting a categorical surrogate model to the transient signal at the neighborhood of the time at which the mission level change occurred.*

The following sections explain the approach taken for each step of Hypothesis 4.

4.3.1 Creation of the Design of Experiments

The change in the mission level variables were calculated as follows: First, the prominent mission level parameters which were expected to have an impact on the subsystem of interest were identified. Second, the change in the variables were calculated by comparing their values at the current and the previous step ($\Delta\Phi_i = \Phi_{i+1} - \Phi_i$).

Although the importance assessed to mission level parameters can change depending on the subsystem of interest, the most prominent one is the change in the power required from (or distributed via) that particular subsystem. Generally, a change in the upstream of a particular subsystem is expected to impact that subsystem as well, whether the impact might lose its intensity or get amplified. Thus, any high-level change in the required power from the electric propulsion branch of the architecture should be accounted for.

The power required from the electric propulsion branch is given by the power management schedule. Once it is calculated by the optimization method described in Section 4.2, the change can be calculated as the difference $(P_{req,e_i} - P_{req,e_{i-1}})$, or the relative difference $((P_{req,e_{i+1}} - P_{req,e_i})/P_{req,e_i})$ between the two edges of the mission leg. Although the relative difference is statistically more useful as the value gets normalized, it cannot be used if the denominator is zero, i.e. if there were no power requirements from the electric propulsion branch in the previous step. Thus, changes in the mission level function Φ_i incorporates the absolute difference, along with the initial condition to create a basis to that difference.

Any changes in the aircraft weight or dynamics can be translated into a change in the required power. This required power can be more further expanded in terms of the angular speed and torque required by the load. For instance, if the an electric motor is the first EPGDS to receive this requirement information, then it has to match the mechanical power output in terms of the shaft speed and torque output by drawing the corresponding electrical energy from the other EPGDS. The electrical power requirement of the motor is expressed as voltage and current flows within the system, and this way the required power information is propagated to each EPGDS downstream. It is also important to note that the same power might be asked from the electrical system with different torque-speed requirements; and thus, the dynamic behavior of the system can change vastly even though the same amount of power is delivered.

Thus, if the subsystem of interest is an electric motor, which is the case in the example

applications of this methodology demonstrated in Chapter 8, the mission level function Φ_i should include the change in shaft speed ($\Delta\omega_i = \omega_{i+1} - \omega_i$) and the change in load torque ($\Delta Q_i = Q_{i+1} - Q_i$), along with the initial conditions of both parameters (ω_i and Q_i).

Once the mission level function $\Delta\Phi_i$ is defined, the next step is to create a design of experiments the variables within $\Delta\Phi_i$. The goal of utilizing the design of experiments concept is to represent the variable space as much as possible while keeping the experimental efforts minimum. This step is performed before evaluating the mission performance. Thus, the design variable space should be defined keeping in mind all possible scenarios which can be encountered during the given mission.

Another example can be given for the battery state of charge, which changes throughout the mission. Depending on what the SOC is, the voltage and thus, the current characteristics of the battery and even the rest of the system would change. Since the energy flow is bookkept at the mission performance analysis, the amount of energy drawn or put into the rechargeable battery can be quickly estimated at each mission leg without the need to run a detailed battery model. Since the SOC level might impact the electrical system dynamics, it can also be included in the design variable space.

In fact, if the transient analysis is to be integrated into the sizing and synthesis process, then the design space should also include subsystem design iterations. For instance, if the battery is sized at each iteration, then the design space should include the expected total amount of energy to be carried by the battery at the beginning of the mission. In this sense, the total energy capacity is different than tracking the SOC, because it describes the size of the battery. As the total energy capacity requirement change within each design iteration, the number of cells which make up the battery vary, and thus, the voltage and current characteristics of the battery change.

An example variable space is given in Table 4.2. This design space is described by the normalized minimum and maximum limits per each variable. Hence, the minimum limit of zero only corresponds to the lowest value which can be encountered during the mission,

Table 4.2: Design variable space for the mission level function.

Design variable	Minimum Limit	Maximum Limit
Battery Energy Capacity	0	1
Battery SOC	0	1
Initial Power	0	1
Absolute Change in Power	0	1
Initial RPM	0	1
Absolute Change in RPM	0	1

not the actual value of zero. The same principle applies for the maximum limit of one. This is called "feature scaling". For instance, if the battery SOC is limited to vary between 20% and 95%, then the minimum and maximum limits of 0 and 1 represents these boundaries. Feature scaling ensures that the created DoE samples the design space is more evenly.

The list of variables shown in Table 4.2 can be modified according to what information is available at the mission level.

In Table 4.2, the term "initial" describe the initial point (i) of the mission leg, and the absolute change is the difference between the final and initial conditions at the beginning and the end of the leg. Instead of the initial condition and the absolute change, the design variable space can also be expressed by an initial and a final value. The battery energy capacity and SOC describe only the initial state, since their final values are fall-out parameters of the simulation.

In this dissertation, the EPGDS dynamics were simulated in MATLAB Simulink environment. The state variables (e.g. energy capacity and SOC) were inputs to the EPGDS models which were described in detail in Chapter 5. The changes in the mission level parameters were expressed as step function signals which were inputs to the electrical system simulations. The nature of the step inputs are demonstrated in Figure 4.6. As it can be seen

in this figure, the change in input parameters took place at the same time, the first second of the simulation. The power and motor speed inputs were interpreted as the desired motor RPM and torque.

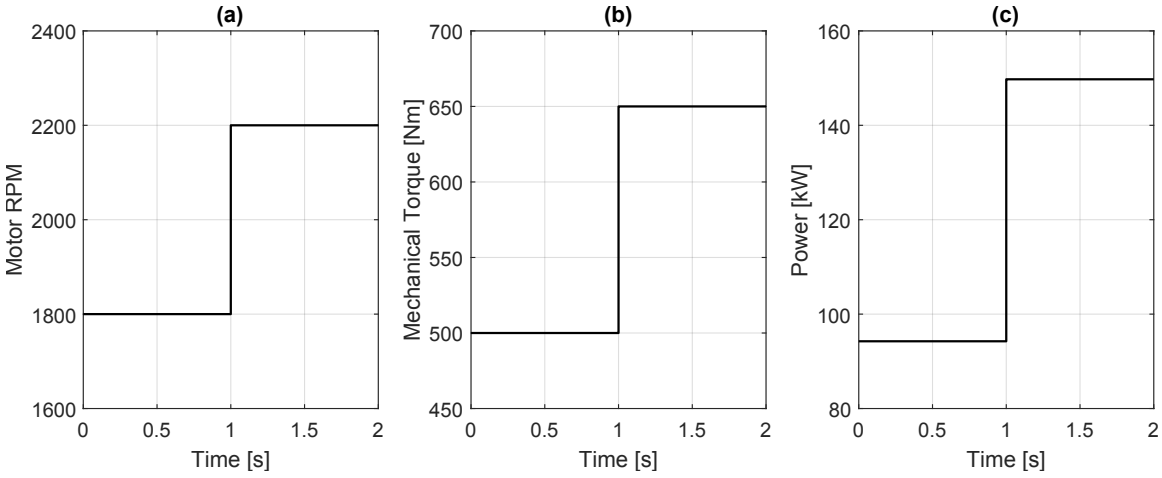

Figure 4.6: Step inputs to the electrical system in terms of (a)motor RPM, (b) mechanical torque, and the resulting power (c).

Each case defined by the DoE was simulated for 2 seconds. The duration was chosen such that there was enough amount of time before the step input is given for the oscillations due to the initialization of the subsystems to die out, and also after the step input is given so that the dynamic response to the input could be observed. This is a very short amount of time compared to the time intervals used in the mission performance analysis, but relatively long enough to capture the transients of interest.

4.3.2 Gain Tuning and Scheduling

Once the DoE is created, the next step is to tune the controllers of the electrical system, which corresponds to the second part of Hypothesis 4. The type of the controllers can vary among systems, but they all can be tuned by some control variables which shall be called gains in this dissertation. Thus, the controller gains do not have to refer to, for instance, PID gains, but can also describe the control variables in a hysteresis control approach.

As described previously, the controllers within an electrical system help the subsystems

match the desired conditions or signals. For instance, an electric motor needs a controller (or multiple ones) to vary the electrical properties (such as voltage or electromagnetic flux) of the motor to match the desired mechanical output. Power electronics also need a controller to convert the input power to the desired output characteristics. Hence, a rather simple electrical system might have multiple controllers, and each controller might have multiple gains, greatly increasing the dimensionality of the optimization problem.

If the impact of each controller gain can be estimated before setting up the optimization problem, then those variables which do not drive the system response could be eliminated in order to decrease the optimization space. The variable importance can be assessed through subject-matter expertise, trial and error, or surrogate modeling. If subject-matter expertise is not available, then a quick inspection can be done to check whether the controllers can control the subsystems with simple gains (e.g. $K_P = 1$, $K_I = 0$). If such gains can be found by trial-and-error for a randomly selected case, then the same gain set can be used to check whether reasonable results could be obtained for other randomly selected cases.

For the cases where subject matter expertise is not available and the trial-and-error approach does not yield acceptable results and becomes too cumbersome, a more systematic approach is proposed by Hypothesis 4. This approach enhances the optimization through Monte Carlo simulations.

The Monte Carlo simulations were used for two reasons. The first reason is to assess variable importance by assigning a uniform distribution to each design variable and computing the variability in the predicted response in terms of a range of variation of the variables individually. [80] Once the importance of each variable is assessed, then only the factors which has a significant impact on the response are carried forward as the control variables of the optimization. This approach can greatly reduce the dimensionality of the optimization problem.

The second reason is to enhance the optimization algorithm such that the optimum results found are not necessarily the optimum for the case at hand, but for the majority of

the system. The main enabler of this approach is sensitivity analysis through the surrogate modeling technique.

To perform the Monte Carlo simulation, first, a second DoE should be generated. The second DoE consists of not only the design variables which define the system inputs, but also the controller gains. The addition of variables into the DoE requires a much larger design space to be covered. This increases the simulation time significantly, however, saves time at the optimization step and produces rather global results for the controller gains.

The next step is to select an appropriate objective function. For instance, in a variable voltage electric motor drive, the controller varies the motor voltage to match the desired motor speed. For this case, the control variables (i.e. gains) should be optimized such that the output motor speed tracks the desired motor speed signal. Thus, the objective function was set to minimize the time averaged error between the desired motor speed signal and the output motor speed in the example implementation of this approach in Chapter 8.

The error between the reference and actual signals can be expressed with various definitions. In these simulations, the calculated error refers to a time averaged relative error, which is given in Eqn. 4.16. In this equation, y is the signal of interest, n is the total number of samples, and $y_{ref,k}$ and $y_{act,k}$ refer to the reference and actual signal values of the kth signal, respectively.

$$\epsilon = \frac{|\sum_{k=1}^{n} y_{ref,k} - y_{act,k}|/y_{ref,k}}{n} \tag{4.16}$$

Once the simulation results are obtained for the second, larger DoE, a surrogate model was fit to the data. The prediction formula obtained from this model was used to perform the Monte Carlo simulations and assess variable importance. Moreover, the prediction formula was used to conduct sensitivity analysis. More specifically, the sensitivity of the signal tracking error to the controller gains were studied *under varying model design variables*. Because both the gain variables and the simulation input variables were design factors in the created surrogate model, the sensitivity analysis revealed the relation not only between

the gains and the error, but also between the gains and the input variables.

With this capability, now the optimization problem can be set up not for any random case in the original (first) DoE, but for an intelligently selected case. This selection was made by utilizing a desirability function which minimizes or maximizes the objective based on the prediction formula established from the surrogate modeling step. The desirability function was set up to minimize the error in the tracked signal for majority of the simulation input variables. Then, the cases which yielded a reasonable amount of error (under 10% based on the error definition made in Eqn. 4.16 were identified. Next, the case which corresponded to the median error was selected and carried forward to the optimization step.

After the optimization problem was solved for the first case selected, the resulting optimum gain set (say, G1) was noted down. Then, the remaining cases in the DoE were simulated with this gain set G1. Next, the cases for which the gain set G1 gave acceptable results within a certain amount of error were assigned to be tuned with this gain set, and removed from the DoE. It was confirmed at this step that the results aligned with the trends found by the sensitivity analysis.

Then, a second case was selected among the remaining cases based on the same methodology. The steps were repeated as solving the optimization problem to find the optimum gain set G2 for that specific case, finding the cases which yielded successful results with that gain set G2, and so on. This process can be repeated a few times until a reasonable gain set for either all or most of the cases in the DoE are found. However, if the given inputs in a case are outside the physical capabilities of the electrical system, then either that case should be discarded, or the electrical system should be redesigned.

With this method, only a handful of cases in the original DoE had to be optimized, and the same gain set was used for the remainder of cases. Thus, a minimum number of gain sets were obtained for the gain scheduling.

Two example optimization results for the motor speed (in terms of revolutions per

minute, RPM) from two different cases in the DoE were depicted in Figure 4.7. In this system, there are two controllers which adjust the motor torque and speed to match the given step input. The "RPM referenced" signal is generated by the controller based on the motor speed step input and the acceleration limits of the motor (thus, the "RPM referenced" is not a step input itself). Within the first second of simulation, the motor starts up and the "RPM referenced" signal reaches to the specified initial condition with a slope defined by the motor acceleration limit. Then, at *t=1 second*, the RPM input changes and so does the reference signal.

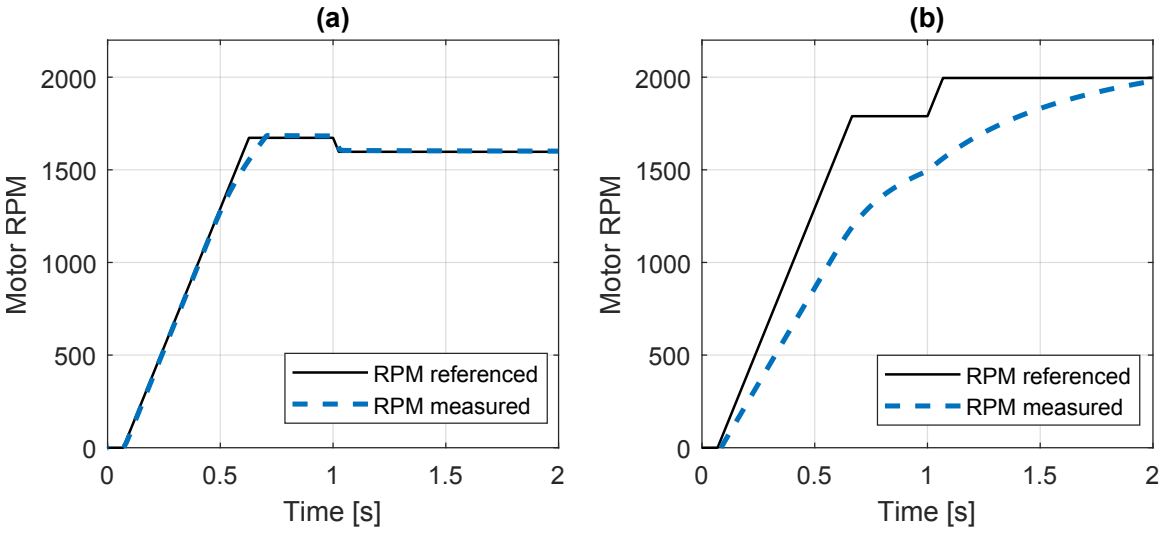

Figure 4.7: Demonstration of a (a) successful and (b) unsuccessful signal tracking for an electric motor drive.

"RPM measured" is the actual response of the motor. In scenario-(a), the controllers were able to control the motor speed such that the actual response tracked the reference signal within a reasonable margin of error. In scenario-(b), there is a significant amount of discrepancy between the reference and the actual response signals. The reason for this discrepancy might be either that (i) the controller gains were not tuned well, or (ii) the reference signal exceeds the physical limits of the motor design.

4.3.3 Defining the Conditional Rule Set

In the final step of Hypothesis 4, the simulation results obtained from the DoE and gain tuning steps are processed. The nature of the signal processing depends on the transient constraints. At this step, each signal must be checked and classified into two categories per constraint: the signals which do not violate the specific constraint, and the signals which do.

Independent of the simulation duration, this check is done in the neighborhood of the time at which the mission level changes occur. This neighborhood shall henceforth be called the reaction window. The span of the reaction window (i.e. how big a neighborhood is defined to be) depends on the nature of the transient behavior of interest. Thus, a-priori knowledge about the expected transient behavior is necessary. This knowledge can be gathered from the power quality standards in literature.

For instance, the Aircraft Power Characteristics standards given in MIL-STD-704F by the U.S. Department of Defense [58] defines the transient constraint on the normal 400 Hz and variable frequency AC voltage transient as shown in Figure 4.8.

The AC voltage transient constraint given in Figure 4.8 might not be suitable for EA/HEA applications as they are defined for secondary power generation and distribution subsystems. However, it can be seen from this figure that the amplitude of the transient is expected to attenuate within about 0.1 seconds from the onset of the transient.

Thus, although the transient constraint depicted in this figure cannot be used as it is, a reaction window can be inferred for an AC voltage transient in a normal operation. This reaction window should be no less than 0.1 seconds, and it would be good practice to add some additional time in case an unwanted transient is delayed.

For instance, during the example application of this methodology presented in Chapter 8, a quick inspection of the simulation results obtained by the DoE revealed that if the AC voltage constraint is violated due to the changes in the mission level metrics, it almost always took place within 0.5 seconds. This behavior might change based on the nature of

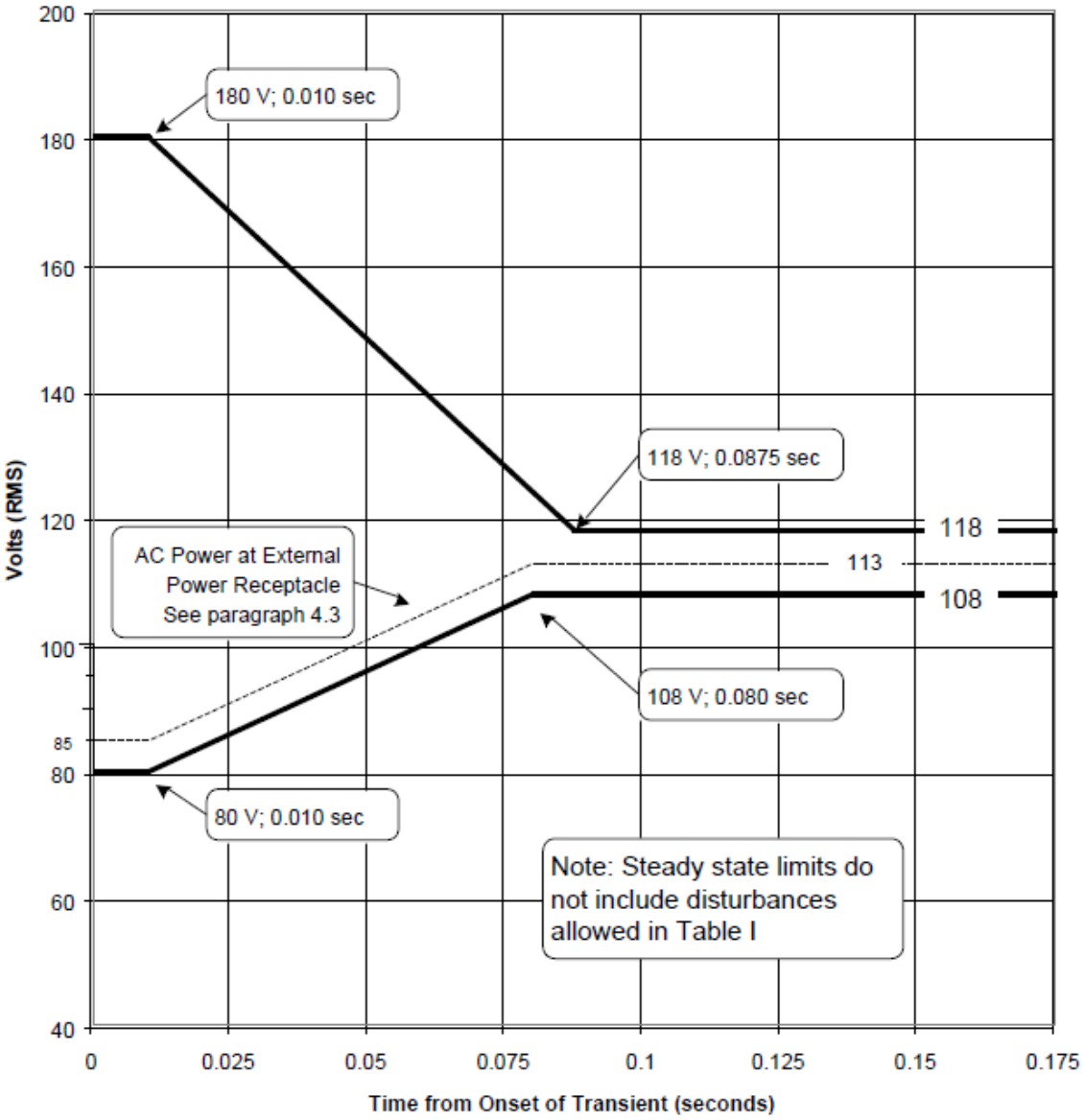

Figure 4.8: Envelope of normal 400 Hz and variable frequency AC voltage transient as given by the MIL-STD-704F. [58]

the electrical system, but a similar inspection should reveal a reasonable duration for the reaction window.

Each case which violates a given constraint within the reaction time is collected in the "constraint violation" category. Conversely, the cases which do not violate the given constraint are gathered in the "no violation" category. For the former category, transient characteristics, such as the voltage amplitude were also recorded at the time of constraint viola-

tion, and 0.5 seconds before it. For the latter category, the same information was recorded at the exact time at which the mission level changes had occurred (e.g. t=1 second), and 0.5 seconds before it. These recordings are not necessary to replicate the methodology, but the data was used to compare against the categorization method.

The design variables in the DoE are then used to fit a Artificial Neural Network model on these categorical responses, to estimate the likelihood of the same type of transient constraint violation inside the design variable space. The resulting probabilistic model can then be used to create a conditional rule set to be utilized during the mission performance analysis.

The conditional rule set obtained from the method proposed in this hypothesis corresponds to the following mathematical expression:

$$\tau = \begin{cases} \tau_j, & \text{if } P(A_j)_i > p_j \\ \tau_i, & \text{if } 0 \leq P(A_j)_i \leq p_j \end{cases}$$

where

- τ is the adaptive temporal step size to be determined
- τ_j and τ_i are the temporal step sizes appropriate for the dynamics of subsystem j and the performance evaluations of mission leg i, respectively
- p_j is a set of thresholds for the change in mission level requirements above which $P(A_j)_i$ is deemed high enough to decrease the step size from τ_i to τ_j
- $P(A_j)_i$ is the probability of a significant transient A happening for a subsystem j at the beginning of the mission leg, described by the subscript i :

$$P(A_j)_i = \zeta(\Delta\Phi_i)_j$$

- ζ_j is a conditional function of $\Delta\Phi_i$ defined for a subsystem j

- $\Delta\Phi_i$ is the change in a subset of mission level requirements between the beginning of the mission leg i and the end of the mission leg $i+1$, given by:

$$\Delta\Phi_i = \Phi_{i+1} - \Phi_i;$$

This formulation was implemented to the generic mission analysis such that the probability of a predetermined event occurring ($P(A_j)_i$) was calculated within each mission leg. If the probability was above a certain limit, say 50%, then the temporal step size was changed from the order of minutes to microseconds. Then, the first few seconds of the current mission leg were simulated using much detailed EPGDS models than those being used for the mission level analysis to inspect whether any significant transients would occur.

The action which can be taken in case of an undesired transient occurs is up to the analyst, and out of scope of this dissertation. Nevertheless, two obvious actions can be listed as follows: If the analyses are performed for subsystem design and sizing, the undesired transients can be avoided by changing the electrical system characteristics and/or the subsystem design. If the electrical system is to be kept fixed, then the mission profile can be modified to avoid the related changes in the mission level metrics so that the probability of experiencing the unwanted transient is lowered.

4.4 Chapter Summary

This section described how the proposed methodological framework can be realized to create a sizing and synthesis tool for EA/HEA concepts to conduct the experiments listed in Chapter 3. This tool is equipped with all the capabilities the framework provided. There are three main aspects to the tool:

- Sizing and synthesis capability with two different detail levels of EPGDS models and the energy-based generic mission analysis for unconventional aircraft and propulsion concepts

- A power management schedule optimizer integrated into the sizing process
- An adaptive temporal step sizing algorithm which changes the step size of the calculations from the mission analysis timescale to the transient analysis timescale where and when necessary

A top-level overview of the methodological framework was given previously in Figure 4.1. Figure 4.9 provides a more detailed look to the developed *Electric Propulsion Architecture Sizing and Synthesis* approach, or E-PASS.

The building blocks of the framework were numbered in steps as seen in Figure 4.1. The arrows between the blocks show the necessary information flow among them. The order of the calculations is not necessarily linear, as some of the steps must be performed within other steps, as explained in the previous chapters. A flow diagram explaining each step of E-PASS is given in Figure 4.10. The step numbers in Figures 4.1 and 4.10 are cross-linked.

A computational tool was created based on this methodology and the described steps. MATLAB and Simulink were chosen to be the main modeling and simulation environment. MATLAB "combines a desktop environment tuned for iterative analysis and design processes with a programming language that expresses matrix and array mathematics directly"[81]. Simulink is used for model-based design of the EPGDS, so that the dynamic properties (steady-state and transient behaviors of the signals) can be visualized and manipulated within the MATLAB environment.

All the steps described in this chapter are repeatable and does not depend on the modeling and simulation environment they are applied to.To prove that the methodological framework is indeed tool-agnostic, the capabilities described in Hypothesis 2 were also implemented within a different environment than MATLAB. Chapter 7.3 describes how Experiment 2.3 was conducted in the Pacelab SysArc, which is a system architecture design tool.

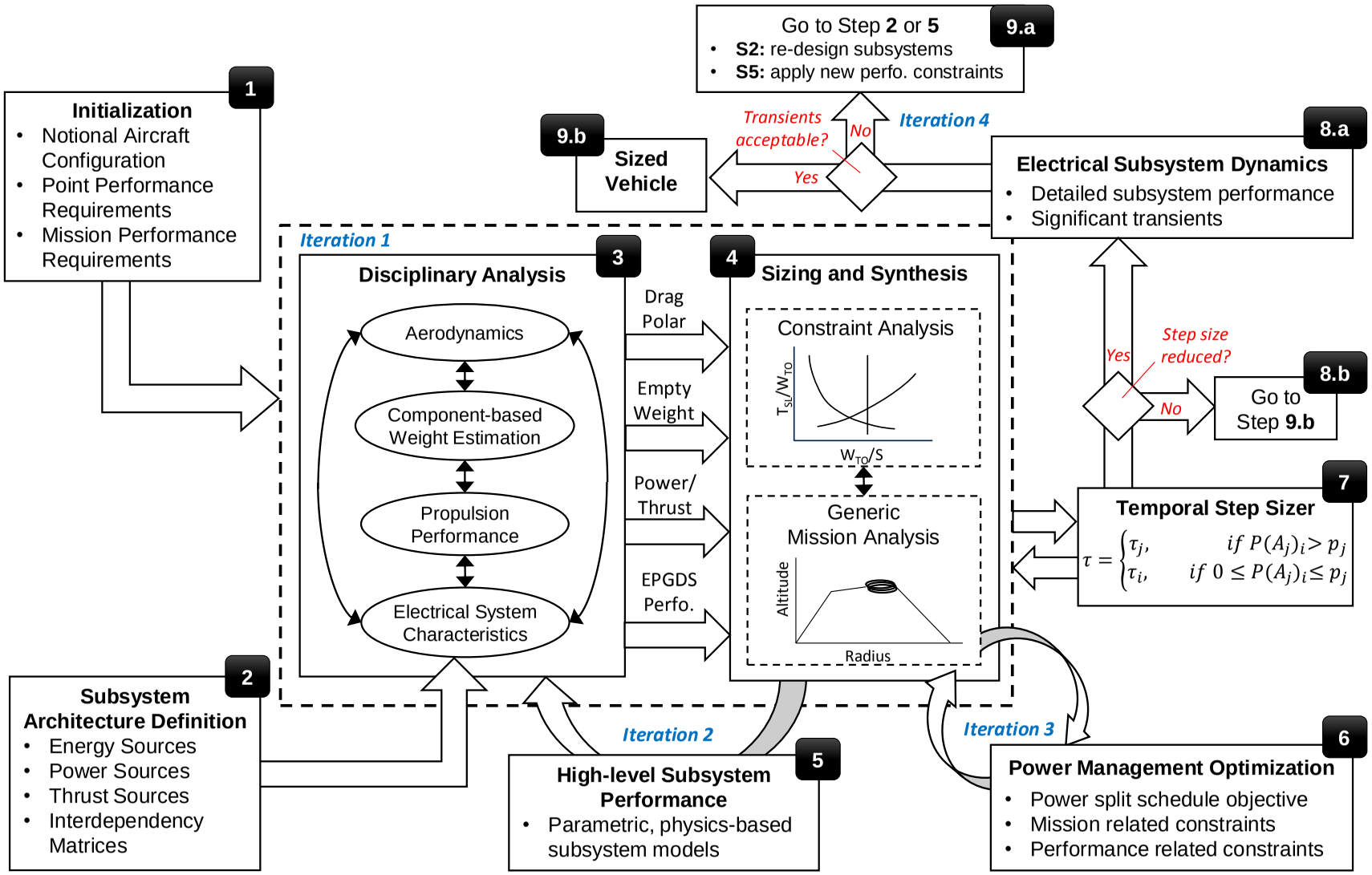

Figure 4.9: Methodological framework for Electric Propulsion Architecture Sizing and Synthesis (E-PASS).

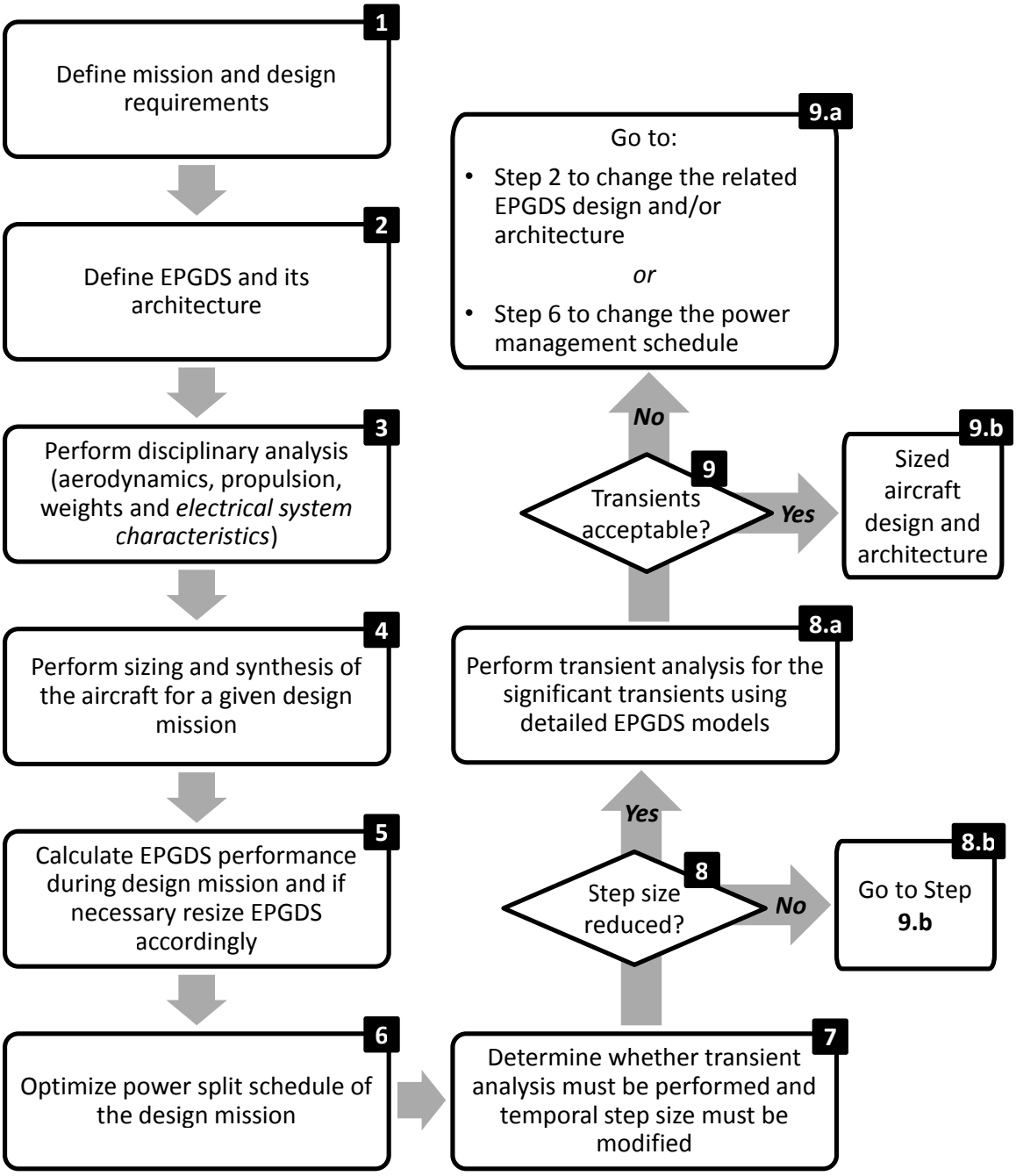

Figure 4.10: Flow diagram of E-PASS.

The upcoming two chapters, 5 and 7 demonstrate more details on how the sizing and synthesis tool was built. More specifically, Chapter 5 describes how the power generation and distribution subsystem models were chosen and developed for (i) mission performance analysis and (ii) transient analysis. Chapter 6 explains the details of the energy-based generic mission performance analysis approach.

Chapters 7 and 8 demonstrate an example application (proof of concept) for each hypothesis, and conduct the experiments planned in Chapter 3.

CHAPTER 5
DEVELOPMENT OF POWER GENERATION AND DISTRIBUTION SUBSYSTEM MODELS

This chapter describes the models developed for power generation and distribution subsystem models in electric and hybrid electric propulsion architectures. The first section deals with electric power generation and distribution subsystems, which are the main focus of this dissertation. The second section lays out the models used to simulate the traditional propulsion branch, i.e. fuel burning engine and propeller models.

5.1 Electric Power Generation and Distribution Subsystems

This section demonstrates the development of the aforementioned parametric, physics-based EPGDS models (such as battery, electric motor, power distribution and management system, etc.) to be used in the sizing and analysis environment proposed in Hypothesis 2.

There are two main parts to the models that were developed:

1. High-level models: These models do not account for the dynamic behavior of the subsystems, but rather are used for sizing purposes and rapid analysis.

2. Detailed models: These models are used to monitor the signal properties as well as the transient responses of dynamic subsystems in a time scale much smaller than that of the mission-level.

As discussed in Sections 2.4.1 and 2.4.2 of Chapter 2, transient responses are often neglected in mission performance analysis, but are critical for the design of electric power generation and distribution subsystems. The literature survey made in this domain did not reveal the impacts of neglecting the subsystem dynamics in models used to evaluate

aircraft performance for EA/HEA concepts. The impacts in EA/HEA concepts are expected to be higher as EPGDS in these concepts are responsible for generating and distributing propulsive power rather than secondary power, i.e. much higher loads than they do in traditional aircraft.

To reveal the amount of information lost by neglecting the transient analysis, comparisons between the two types of EPGDS models will be made. The high-level models will be used to simulate the rapid and low-cost sizing and analysis at the conceptual design stage. The detailed models will be used to simulate the steady-state and transient responses for the design and performance evaluation of EPGDS. The comparisons made between the two models will also help conduct the experiment set created to test Hypothesis 4.

Figure 5.1 shows a notional power train for EP, HEP connected in parallel and HEP connected in series configurations where electrical energy is delivered from a battery to an electric motor. As it can be seen from Figure 5.1, the electrical energy travels through similar subsystem components in all three concepts; including but not limited to a battery as the primary or secondary energy source, a power converter for voltage and current conversions, an electric motor, generator, and transmission system.

In order to investigate the roles of major subsystems in EP/HEP architectures, their most prominent features and working principles were studied first. Then, the two types of models were created based on the findings of this study. The most significant property of these models are being parametric, which allows for studying the uncertainty in modeling assumptions and technology advancements.

A recent study funded by the European Commission introduces these subsystems as modular elements of the propulsion system architecture. [82] The modularity covers various implementations on different HEA architectures. This study accomplishes the modularity through functional decomposition. A similar approach was taken in this thesis as a continuum of previous work done by the author. [83, 84] The main idea behind developing parametric EPGDS models is to create a library of components. Such a library would be

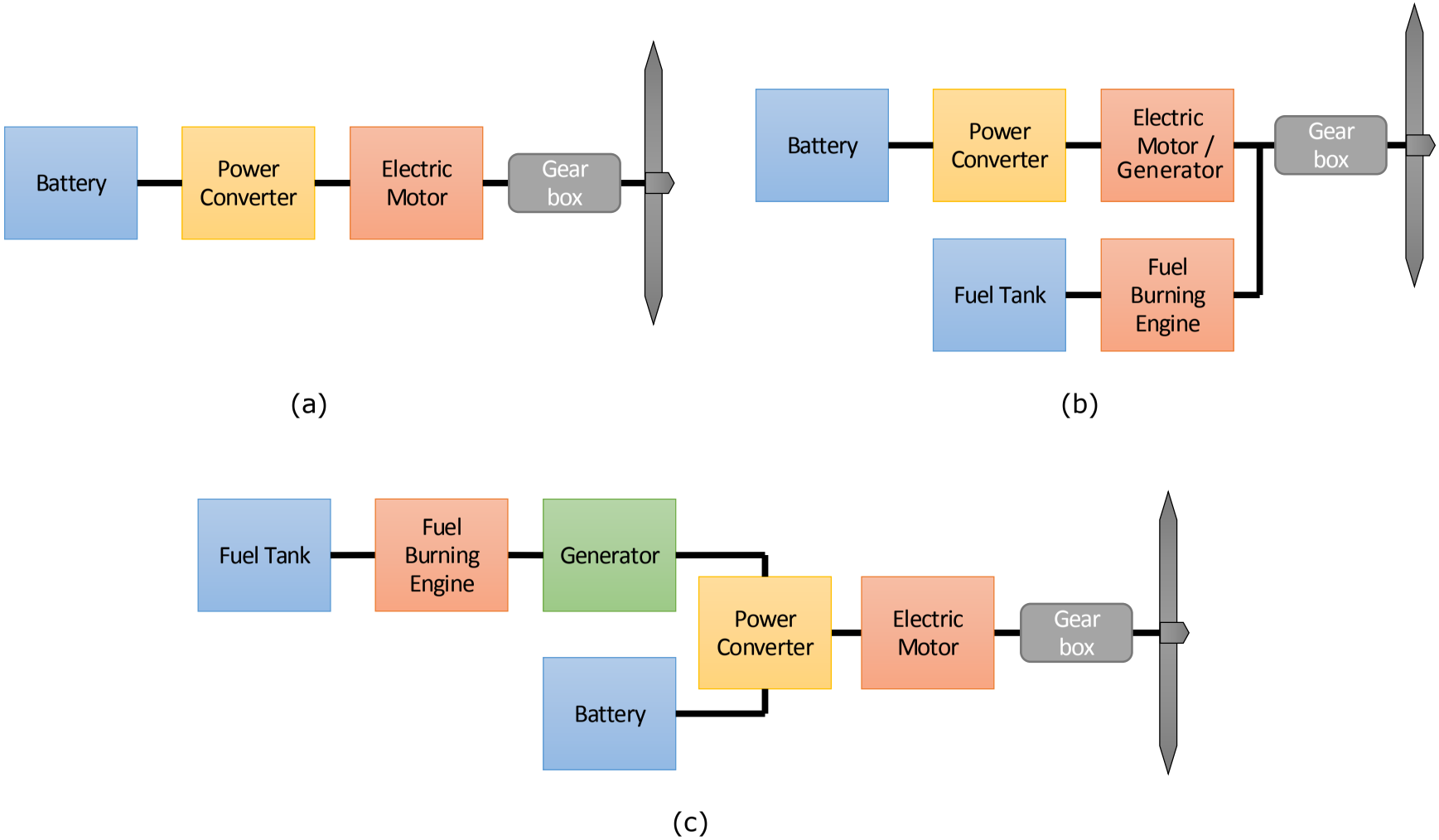

Figure 5.1: Notional subsystem components and architecture for (a) Electric propulsion, (b) Hybrid-electric propulsion connected in parallel, (c) Hybrid-electric propulsion connected in series.

useful for a wide range of EA/HEA architectures.

The EPGDS models described in the following paragraphs were developed in two environments, separately: MATLAB and Simulink. The MATLAB models are the high-level models that do not account for transient regimes, as their dynamics are computed at the mission level scale. The detailed models were built using the models and blocks available in the Simulink library. These models are require a sampling time of millionth of a second, i.e. a microsecond (μs). When more detailed, transient analysis are to be run, the parameters defined in high-level models are replaced by the corresponding parameters in the detailed models.

The model inputs and outputs are listed for both types of models for each subsystem. The outputs are grouped into "sizing outputs" which are used to determine the weight and/or volume of a subsystem, and "performance outputs" which are used in performance evaluations. The sizing outputs are the same for both model types, whereas inputs and performance outputs differ greatly, as the detailed models require considerably more inputs and as a result provide more specific and accurate information about the subsystem dynamics.

5.1.1 Rechargeable Battery

Introduction to Electric Battery Concept

Battery cells convert chemical energy to electrical energy through electrochemical reactions and generate DC electricity. This is called a "discharge" process. Rechargeable battery cells can reverse this chemical reaction when current is sent into the battery. This is called a "charge" process.[42]

Although the terms "battery" and "cell" are sometimes used interchangeably, a battery is actually made up of at least two cells connected in series configuration. Each cell has a positive terminal (cathode) and a negative terminal (anode). When the positive terminal of a cell is connected with the negative terminal of another cell, it is called a series connection.

When the positive and negative terminals of a cell are connected with the positive and negative terminals of another cell respectively, it is called a parallel connection.

Battery voltage, current and energy analyses are usually performed by building equivalent circuit models. Such a sample model is demonstrated in Figure 5.2. Here, the battery is described by an internal resistance *R* and open-circuit voltage *E*, which is the electrical potential when no load is connected to the circuit. When a current *i* flows through the battery, power is dissipated by the internal resistance as heat and therefore the terminal voltage *V* is not equal to *E*. Eqn. 5.1 gives the mathematical description of this model.

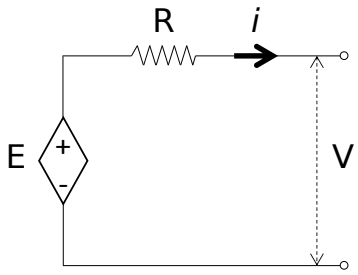

Figure 5.2: A simple equivalent circuit model of a battery [42]

$$\mathbf{V} = E - IR \tag{5.1}$$

Cells are connected in series and/or parallel in order to increase the voltage or charge capacity of the battery. When *n* number of cells are connected in series, then following Kirchhoff's voltage law, the total voltage of the battery is the sum of individual voltage values of each cell as given by Eqn. 5.2. Similarly, the sum of internal resistance of each cell gives the overall internal resistance of the battery as given by Eqn. 5.3.

$$E = \sum_{j=1}^{n} E_j \tag{5.2}$$

$$R = \sum_{j=1}^{n} R_j \tag{5.3}$$

In the case of *m* number of parallel cell connections, Kirchhoff's current law is followed

by summing up the currents flowing through each cell to find current flowing through the battery (Eqn. 5.4); and the internal resistance of the battery is given by equation Eqn. 5.5.

$$I = \sum_{j=1}^{m} I_j \tag{5.4}$$

$$R = (\sum_{j=1}^{m} \frac{1}{R_j})^{-1} \tag{5.5}$$

General Parameters

Battery package is a very important component in electric and hybrid-electric vehicle applications as it is the main or secondary energy source which, as discussed before, introduces significant weight to the system. Hence, choosing the right type and size of the battery is vital for the overall design.

There are various types of rechargeable batteries such as lead acid, nickel metal hydride, lithium polymer, etc. but their behavior and performance can be described by common parameters. These parameters will play an important role in developing the battery model. A detailed description of these parameters is given below along with their respective SI units.[42]

- **Specific Energy [Wh/kg]:** The most obvious performance parameter that is directly related to the endurance of an aircraft is battery's specific energy, as known as gravimetric energy density. It is defined as the amount of electrical energy stored for unit battery mass. Although the units are energy-to-mass units, specific energy is also referred to as energy-to-weight ratio.

- **Energy Density [Wh/m^3]:** Similar to specific energy, this is the amount of electrical energy stored for unit battery volume.

- **Specific Power [W/kg]:** This is the amount of power obtained per unit mass of the

battery. A battery which has high specific power can take in and give out energy very rapidly and therefore would be very beneficial for aircraft operations that require relatively high power. Although the units are power-to-mass units, specific power is also referred to as power-to-weight ratio.

In fact, technology comparisons between batteries are usually made by comparing their specific energy and specific power because there exists a strong trade-off between them. The capacity and energy efficiency of a battery decrease with shorter discharge time. As a result, during high power operations the battery capacity drops rapidly. Hence, if a battery has high specific energy, then it suffers from low specific power characteristics and vice versa.

- **Charge Capacity [Coulomb or Ah]:** Charge capacity, sometimes referred as charge or capacity, is the load current a battery can deliver over time. The higher charge capacity a battery has, the longer time it will run. Although the SI unit for capacity is coulomb, in battery technology Ah (ampere-hour or amphour) is a more widely used unit as it describes one ampere supplied for one hour which is a more practical description for battery applications.

  The capacity can be given numerically as, for example, "15 Ah", or "C = 15 A". Both of these notations have the same meaning: that is, the battery can provide 15 A if it is discharged for 1 hour, or 3 A if discharged for 5 hours, or 1 A if discharged for 15 hours, etc. Hence, in accordance with common sense, the higher the discharge current is, the shorter the battery will last and vice versa.

  Battery manufacturers usually provide a nominal charge capacity. Then, all other charging/discharging cases are usually based on the nominal capacity value. For example, let the nominal capacity be given as C = 20 A. Then, "discharging the battery at 40 A for half an hour" and "discharge current of 2C" (i.e. 2 times C equals 40 A current) have equivalent meanings.

Although battery capacity is a vital parameter, it does not completely describe the actual discharging behavior in practice. Discharge time and capacity are not always linearly proportional. In fact, shorter discharge time has a negative impact on capacity due to unwanted side reactions. The longer the discharge time is, the more charge capacity the battery will have. Referring to the first example, for a battery with C = 15 A, if the discharge current is 1 A the battery will most probably last more than 15 hours; whereas if the discharge current is 30 A it will last less than 30 minutes. Since discharge time can have a significant impact on capacity, it is very important not to neglect these fluctuations with various current draws during flight.

To eliminate any possible confusion with using the symbol *C*, the capacity will be given by the letter *Q* for the rest of this thesis.

- **Stored Energy [Wh]:** The energy stored in the battery is expressed by Wh (instead of the SI energy unit of Joules because Wh is a more practical unit for battery applications). It is given by Eqn. 5.6:

$$\mathbf{E} = V * Q \tag{5.6}$$

where *V* is the battery voltage, and *Q* is the capacity in Ah. However, as mentioned previously, all of these terms depend on how quickly or slowly the battery is charged or discharged. Under a high current draw, i.e. a rapid discharge process, the battery would be out of its stored energy very quickly as both *V* and *Q* would drop, and vice versa.

- **State of Charge:** State of charge, or SOC, can be defined as the ratio of the remaining capacity to the nominal capacity. This parameter is also very important as it provides information on the potential run time of the battery. Mathematically 100% SOC means a fully charged battery and 0% SOC means a fully discharged battery.

However, in some cases, batteries might be overly charged. Moreover, discharging a battery to 0% SOC can harm the battery permanently and therefore a minimum limit greater than 0% is set in practice. This limit is generally suggested to be 20% for most battery types except the lead acid one for which it is set to be 30%. Hence, when SOC hits this minimum limit, discharge process is stopped by the battery management system. The voltage value at which this limit is hit is called "the cutoff voltage".

- **Depth of Discharge:** Depth of discharge, or DOD is the ratio of the discharged capacity to the nominal capacity; also given by Eqn. 5.7:

$$\mathbf{DOD} = 1 - SOC \tag{5.7}$$

Charge and Discharge Characteristics

The dynamic battery discharge characteristics were summarized in Chapter 2. This section briefly goes through these characteristics to serve as a reminder.

Battery manufacturers usually provide a discharge curve for each battery they sell such as depicted in Figure 5.3. This curve shows the discharge behavior under a certain current draw in terms of battery voltage and capacity (or sometimes discharge time). Figure 5.3 shows an imaginary Lithium-Ion (Li-Ion) type of battery discharge characteristics. These type of batteries generally have an exponential zone at the beginning of discharge, and then the discharge curves remain almost constant for a considerable amount of battery run time. Voltage starts to drop very rapidly somewhere around the cutoff voltage, and continues to drop even more as the battery is fully discharged. The nature of these curves depend on the battery type and properties. But the main idea behind these curves is that voltage drops as battery is discharged, and increases as battery is charged.

This behavior is the main reason why the equivalent circuit model given by Figure 5.2 and Eqn. 5.1 cannot fully capture the discharge characteristics, as it assumes a constant

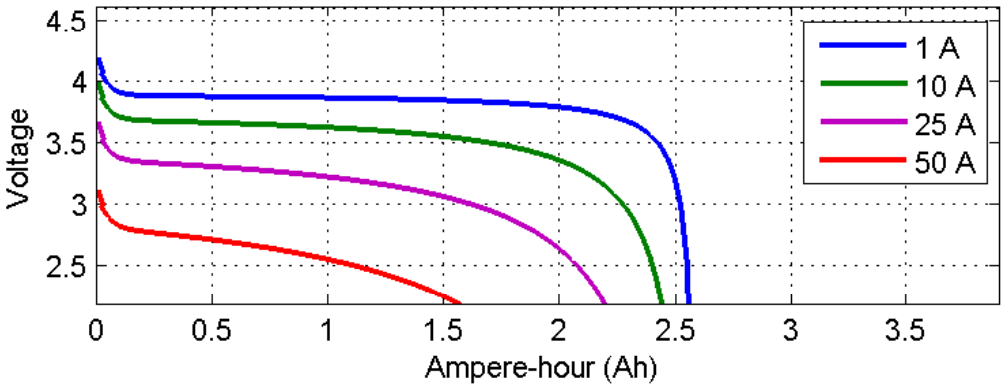

Figure 5.3: A sample discharge curve for a Lithium-Ion battery

battery voltage over time.

Furthermore, it can be seen from the different colored curves in Figure 5.3 that drawing a high amount of current (e.g. the red curve) over a short amount of time decreases the battery run time whereas drawing a low amount of current (e.g. the blue curve) over a longer time increases the run time, as described previously.

In many cases, charge characteristics can be assumed the same as discharge characteristics although they might not be exactly the same.[42]

High-level Model for the Rechargeable Battery

The high-level model for the rechargeable battery was developed with only regards to the general battery parameters, excluding the charge and discharge dynamics, to resemble most of the rechargeable battery models in literature as discussed previously in Chapter 2.

In this model, a battery pack is represented by the its specific energy, specific power, energy density, power density, efficiency and amount of energy stored in it. These are the sizing parameters used to determine how big of a rechargeable battery is needed to fly the given mission.

The technology K-factors in this model are the specific energy, specific power, energy density, power density and efficiency, as the technology level can be changed by increasing the value of these parameters. It is also possible to mimic a change in the battery type

by adjusting these parameters, but the charge/discharge characteristics are altogether neglected and hence the results would not be as accurate as the more detailed models which do account for battery dynamics.

In this battery model, the battery weight is calculated through the total energy required from the battery over the course of the design (and reserve) mission and the specific energy. The total energy required from the battery (E_{batt}) is calculated by Eqn. 5.8, where n is the number of mission legs in a given mission, η_{batt} is the battery efficiency, $\Delta P_{req,batt_i}$ is the required power from the battery during the mission leg i, and Δt_i is the time spent in the mission leg i.

$$\mathbf{E}_{\text{batt}} = \sum_{i=1}^{n} \Delta E_i = \sum_{i=1}^{n} \frac{\Delta P_{req,batt_i} \Delta t_i}{\eta_{batt}} \tag{5.8}$$

Once the total energy required to fly the given design and reserve missions is calculated, it can be scaled up to account for the reserves and the unusable energy (charge which must remain in the battery in order not to harm permanent damage).

Then, since specific energy is defined as energy-to-weight ratio ($(E/W)_{batt}$) and specific power is the power-to-weight ratio ($(P/W)_{batt}$), battery mass (M_{batt}) is given by Eqn. 5.9. [1]

$$\mathbf{W_{batt}} = max\left(\frac{\mathbf{E_{batt,req}}}{\mathbf{(E/W)_{batt}}}, \frac{\mathbf{P_{batt,peak}}}{\mathbf{(P/W)_{batt}}} \right) \tag{5.9}$$

In Eqn. 5.9, the battery mass is determined by the maximum of the following two values: (i) the battery mass dictated by the total required energy and specific energy, or (ii) the amount of peak power ($P_{batt,peak}$) drawn out of the battery and specific power.

Similarly, battery volume ($\forall_{batt}$) is calculated using Eqn. 5.10 by choosing the maxi-

[1] Specific energy and specific power definitions are actually made for energy and power per unit *mass*, respectively, not weight, as explained previously. However, the word "weight" is often used interchangeably with "mass", although the two properties are different than each other. This dissertation follows the same naming convention as literature, but utmost care was given to the calculations in order not to confuse mass with weight properties.

Table 5.1: Model parameters and sizing and performance outputs for the high-level rechargeable battery model.

Model Parameters	**Sizing Outputs**	**Performance Outputs**
Stored Energy [Wh]	Battery Weight [kg]	Energy Consumed [Wh]
Specific Energy [Wh/kg]	Battery Volume [m^3]	Energy Left [Wh]
Specific Power [W/kg]		
Energy Density [Wh/m^3]		
Power Density [W/m^3]		
Efficiency		

mum value for the battery volume obtained from (i) the total required energy and energy density ($(E/\forbidden{V})_{batt}$), (ii) the amount of peak power drawn out of the battery and power density($(P/\forbidden{V})_{batt}$).

$$\forbidden{V}_{\mathbf{batt}} = max\left(\frac{E_{batt,req}}{(E/\forbidden{V})_{batt}}, \frac{P_{batt,peak}}{(P/\forbidden{V})_{batt}}\right) \tag{5.10}$$

The modeling parameters (i.e. inputs) and the output parameters (for battery sizing and performance evaluation) of the high-level rechargeable battery model are listed in Table 5.1. As it can be seen from this table, the number of input and output parameters are acceptable for high-level analysis and a subject-matter expertise is not necessarily needed to set the model up.

Detailed Model for the Rechargeable Battery

There are various models on battery dynamics in literature, however it is important to find a suitable one that matches the level of complexity of the intended application. The objective of this thesis is to implement low-cost models that would yield reliable results for conceptual design stage. Therefore, the simple open circuit model given by Figure 5.2 and Eqn.

5.1 is not deemed suitable as it would lead to loss of critical information on the dynamic behavior of the battery.

On the other hand, a very detailed model might give results that are close to reality at the expense of a high computational cost. Since the conceptual aircraft design stage is a phase where the designer would like to analyze the impact of changing parameters on the whole vehicle design by running numerous cases, such a model could easily become impractical. Furthermore, it must be taken into account that the conceptual designer is not necessarily an expert on each of the subsystems and therefore the models should be moderately easy to use.

One approach for battery modeling is to use empirical data and create fitting equations via regression techniques. Such empirical models give computational advantage and could also produce accurate results to some extent.[85] However, generally this accuracy is limited to certain operating conditions. Hence, these models fail to project the future technology improvements which is the intent of Experiment 2.3. to test Hypothesis 2. In fact, Hypothesis 2 requires implementation of flexible models that can also be used in "what-if" kind of scenarios. That's why employing empirical models would not be a suitable approach.

Another type is electrochemical models which incorporate chemical and electrochemical kinetics and transport phenomena.[86, 87] There are a number of different approaches in this type of modeling and most of them produce more accurate results than empirical models. Employment of the physicochemical principles also allows the design of new battery chemistries or materials. However, the usage of such a model would require tremendous amount of expertise and would also be computationally costly. Thus, this type of models would not be suitable for the scope of the proposed work either.

Equivalent circuit models can produce accurate results without going into battery chemistry provided that the model is properly built up to reflect battery characteristics. Although the equivalent circuit model shown in Figure 5.2 is a simple one, it can be improved by

adding extra circuit components.[88] Hence, a trade-off can be done between the complexity and accuracy to fit the model to a specific application. One such model, presented by Tremblay and Dessaint[54] is deemed reasonable to fulfill the purpose of this work in terms of its easiness of use and level of detail. A brief summary of this model is given here along with a set of equations specifically for Li-Ion type of battery, but the interested reader can refer to Ref. [54] for further details and other battery types.

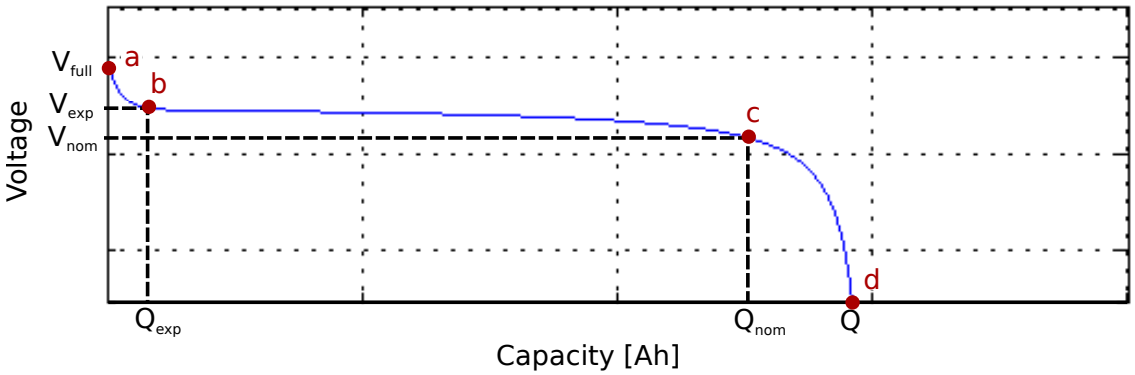

Figure 5.4: Differentiation of special zones for the battery model by Tremblay and Dessaint [54]

Tremblay and Dessaint's model [54] takes two special points along with the extremes on a typical discharge characteristics curve given at a constant current to predict the battery behavior at any other current using a set of equations. The extremes are the fully charged voltage V_{full} (point *a*) and the maximum capacity Q (point *d*). The remaining two points are namely "the end of the exponential zone" and "the end of the nominal zone" which are given by points *b* (Q_{exp}, V_{exp}) and *c* (Q_{nom}, V_{nom}) in Figure 5.4, respectively. "The end of the exponential zone" is the point at which the curve ends its exponential behavior at the beginning of discharge, whereas "the end of the nominal zone" is the point at which the voltage starts to drop abruptly. The model also use the internal resistance (R).

The discharge and charge voltages as a function of capacity for Li-Ion type of batteries are given by Eqn. 5.11 and Eqn. 5.12, respectively.

$$\mathbf{V_{batt} = E_0 - RI - K\frac{Q}{Q - Q_{act}}(Q_{act} + I^*) + A\exp(-B * Q_{exp})} \qquad (5.11)$$

$$\mathbf{V}_{\text{batt}} = \mathbf{E}_0 - \mathbf{RI} - \mathbf{K}\frac{\mathbf{Q}}{\mathbf{Q}_{\text{act}} - \mathbf{0.1Q}}\mathbf{I}^* - \mathbf{K}\frac{\mathbf{Q}}{\mathbf{Q} - \mathbf{Q}_{\text{act}}}\mathbf{Q}_{\text{act}} + \mathbf{A}\exp(-\mathbf{B} * \mathbf{Q}_{\text{exp}}) \quad (5.12)$$

where V_{batt} is battery voltage [V] , E_0 is battery constant voltage [V], Q_{act} is actual battery charge [Ah], and I^* is filtered current [A]. The terms K (polarization constant [V/Ah] or polarization resistance [Ω]), A (exponential zone amplitude [V]) and B (exponential zone time constant inverse [$(Ah)^{-1}$] are calculated using the previously chosen points on the typical discharge curve and Equations 5.13, 5.14 and 5.15 as follows:

$$\mathbf{K} = \frac{-\mathbf{E}_{\text{nom}} + \mathbf{E}_0 + \mathbf{A}\exp(-\mathbf{B}\mathbf{Q}_{\text{nom}})(\mathbf{Q} - \mathbf{Q}_{\text{nom}})}{\mathbf{Q}(\mathbf{Q}_{\text{nom}} + \mathbf{I})} \quad (5.13)$$

$$\mathbf{A} = \mathbf{E}_{\text{full}} + \mathbf{E}_{\text{exp}} \quad (5.14)$$

$$\mathbf{B} = \frac{\mathbf{3}}{\mathbf{Q}_{\text{exp}}} \quad (5.15)$$

In this model, the internal resistance R is assumed to remain constant all the time. Moreover, temperature effects and self-discharge of the battery are neglected.

In this model, battery weight is computed based on the same criteria used in the high-level model, i.e. through its specific energy and total energy capacity or its specific power and the peak power requirement; whichever is greater. However, the method used to calculate the battery energy required differs from the high-level model, since battery current and voltage at a given time are known values and the power can be calculated with this information.

The total energy requirement $E_{batt,req}$ is calculated by Eqn. 5.16 over the course of a

mission as a function of time, where the mission lasts for t_f amount of time.

$$\mathbf{E_{batt,req}} = \int_0^{\mathbf{t_f}} \mathbf{P_{batt,req}(t)tdt} = \int_0^{\mathbf{t_f}} \mathbf{V_{batt}(t)Q_{batt}(t)dt} \tag{5.16}$$

The battery weight and volume properties are then calculated using Equations 5.9 and 5.10, respectively.

Tremblay and Dessaint's rechargeable battery model [54] exists in Simulink's model library under "Electric Drives/Extra Sources". This model does not differentiate between cell-level and battery level. However, cell level characteristics can be translated into battery level characteristics thanks to the parametric nature of the inputs. The following arguments (using the Kirchoff's law) and assumption are used to build up battery packs using cell-level characteristics:

- Nominal voltage of the battery is equal to the nominal voltage of cell times the number of cells connected in series.
- Rated capacity of the battery is equal to the rated capacity of cell times the number of cells connected in parallel.
- It is assumed that every cell in the battery is discharged at the same rate, and have the same SOC at any given time.

On top of the sizing parameters listed in Table 5.1, the additional input and output parameters for the detailed rechargeable battery model are given in Table 5.2.

5.1.2 Battery Management System (BMS)

Battery Management System (BMS) monitors and controls the status of the battery to ensure that it is operating within safe operating conditions. [89] It has been discussed previously in detail that the battery performance has a vital impact on the overall performance of the flight due to the continuously changing discharge behavior under different power

Table 5.2: Model parameters and performance outputs for the detailed rechargeable battery model.

Model Parameters	**Performance Outputs**
Battery Type	Battery Voltage [V]
Nominal Voltage [V]	Battery Current [I]
Rated Capacity [Ah]	State of Charge [%]
Initial State of Charge [%]	Battery Capacity [Ah]
Battery Response Time [s]	

needs. Hence, it is important to have control over the battery run time at each point of the flight. This can be done by checking the battery SOC at certain time steps throughout the mission.

BMS estimates the battery SOC and makes sure that SOC does not exceed a predefined maximum and a minimum limit. This is a necessary step to avoid overcharging and overdischarging for a longer battery life and safe operation. [89]

The detailed model for the BMS applies the following constraint during the mission analysis:

$$SOC_{min} \leq SOC(t) \leq SOC_{max}$$

In the case of a discharge process, the battery tries to match the power requirement by changing the amount of current. To do so, it has to have enough capacity throughout a time interval in which the power demand is assumed to be constant.[2] The battery SOC at the end of a mission leg is then calculated by the power drawn out of the battery for a given time interval. BMS then checks whether the SOC value at the end of each mission leg is above or below the minimum limit, as shown above. If SOC hits the minimum limit, the

[2]This time interval is the time step that will be strategically determined by the Temporal Step Sizer, as discussed previously in Chapter 4.

discharge process is immediately terminated.

SOC at the end of *each time interval* Δt (referred to as SOC_j for a time step between $j-1$ and j) and is calculated as follows: For each Δt interval, the capacity discharged out of the battery (Q_{disch}) is given by the amount of current drawn (I_{disch}) during the interval Δt as shown in Eqn. 5.17.

$$\mathbf{Q_{disch_j}} = I_{disch_j} * \Delta t \tag{5.17}$$

Then, the battery voltage V_{batt} can be calculated for each time interval Δt using equations 5.11 through 5.15. Finally, the capacity left in the battery at the end of the time interval Δt is determined, and SOC_j can be calculated by Eqn. 5.18, where SOC_{j-1} is the initial SOC value *at the beginning of the time interval*, and the beginning of *the mission* is designated by $n = 1$:

$$\mathbf{SOC_j} = SOC_{j-1} - \frac{\sum_{n=1}^{j} Q_{disch_n}}{Q} * SOC_{j-1} \tag{5.18}$$

This SOC_j value is checked to see whether it is above the pre-specified minimum SOC limit. If it is, then the final battery voltage after the discharge process is calculated before moving to the next time interval. In the case that SOC drops under the minimum limit, the discharge process must be terminated.

The detailed rechargeable battery model used in Simulink already keeps track of the battery SOC. Hence, there is no need to have another model to carry out this task.

BMS is also responsible for estimating the battery state-of-health, thermal management and circuit protection to increase the battery efficiency. [90] In this thesis, it is assumed that the BMS has a perfect control over these issues, as the scope of this thesis does not include battery management strategies.

Another responsibility of BMS is voltage regulation through power converters embedded in it. As explained in the previous section, battery voltage changes as the battery

is charged or discharged during flight. However, the battery supplies energy to the electric motor or other non-propulsive subsystems which might work under different voltage demand. A power system should be able to provide voltage stability such that steady acceptable voltages at all buses in the system are maintained under both normal operating conditions and after being subjected to a disturbance.[91] Hence, a nominal system voltage must be set independent of the battery voltage to keep consistency between other subsystem voltage requirements. [92] This task is carried out by a DC-DC voltage converter model, which is explained in detail in Section 5.1.3.

There is not a separate high-level model for the BMS, because BMS is responsible for monitoring the battery dynamics and such dynamics are not a part of the high-level models. Instead, the high-level model for the rechargeable battery is assumed to account for it by keeping track of the energy consumed and the energy left in the battery.

5.1.3 DC-DC Voltage Converter

Voltage of any electrical power source varies with time, especially with current. [42] This phenomenon can be seen in the discharge curves demonstrated in Figures 2.8, 5.3, and 5.4 for rechargeable batteries. Although battery voltage is relatively well regulated compared to fuel cells, voltage regulation is still necessary to keep it within allowable boundaries. Moreover, voltage regulation is required to control the speed of an electric motor. [42]

Power electronics control the flow of electrical energy from a source to a load by changing input voltage to a desired output voltage.[43, 93] Eqns. 5.19, 5.20 and 5.21 show this conversion, where P_{pc} is power, I_{pc} is current, V_{pc} is voltage and η_{pc} is the efficiency of the power converter. Subscripts *in* and *out* designates the input and output ports.

$$\mathbf{P_{pc,in}} = \mathbf{I_{pc,in}}\mathbf{V_{pc,in}} \tag{5.19}$$

$$\mathbf{P_{pc,out}} = \mathbf{I_{pc,out}}\mathbf{V_{pc,out}} \tag{5.20}$$

Table 5.3: Model parameters and sizing and performance outputs for the high-level power converter model.

Model Parameters	**Sizing Outputs**	**Performance Outputs**
Specific Power [W/kg] Efficiency	Converter Weight [kg]	Output Power [W]

$$\mathbf{P_{pc,in}} = \frac{\mathbf{P_{pc,out}}}{\eta_{\mathbf{pc}}} \tag{5.21}$$

The DC-DC voltage converter converts the DC input voltage into a DC output voltage. There are two main types of DC-DC converters: (i) hard-switching pulse width modulated (PWM) converters, and (ii) resonant and soft-switching converters. [93]

PWM converters are more widely used as they consist of a small amount of components, are highly efficient, are relatively easy to control, operate at constant frequencies, and can achieve high conversion ratios. [93]

High-level Model for the DC Bus

A generic power converter model is used to represent a DC bus connected to the battery. This black-box converter model converts input power to output power according to Eqn. 5.21. It has a constant efficiency factor (η_{PC}) and a power-to-weight ratio.

The weight of the converter (W_{PC}) is calculated by its power-to-weight ratio ($(P/W)_{PC}$) and peak power ($P_{PC,peak}$) required or encountered in a design mission as given by Eqn. 5.22:

$$\mathbf{W_{PC}} = \frac{P_{PC,peak}}{(W/M)_{PC}} \tag{5.22}$$

The modeling parameters and the output parameters of the high-level power converter model are listed in Table 5.3.

Detailed Model for the DC Bus

The detailed model for the DC bus consists of two parts: a DC-DC converter and a controller. Figure 5.5 shows how the controller model communicates with the DC bus model to regulate the output voltage. The converter takes the input voltage, which is the battery voltage, and converts it to the desired voltage, which is the system voltage. The desired system voltage ("Ubus Ref" block in Figure 5.5) is a constant, user-defined input to the system. A controller determines how the switching devices operate to achieve the target output voltage through PWM pulses.

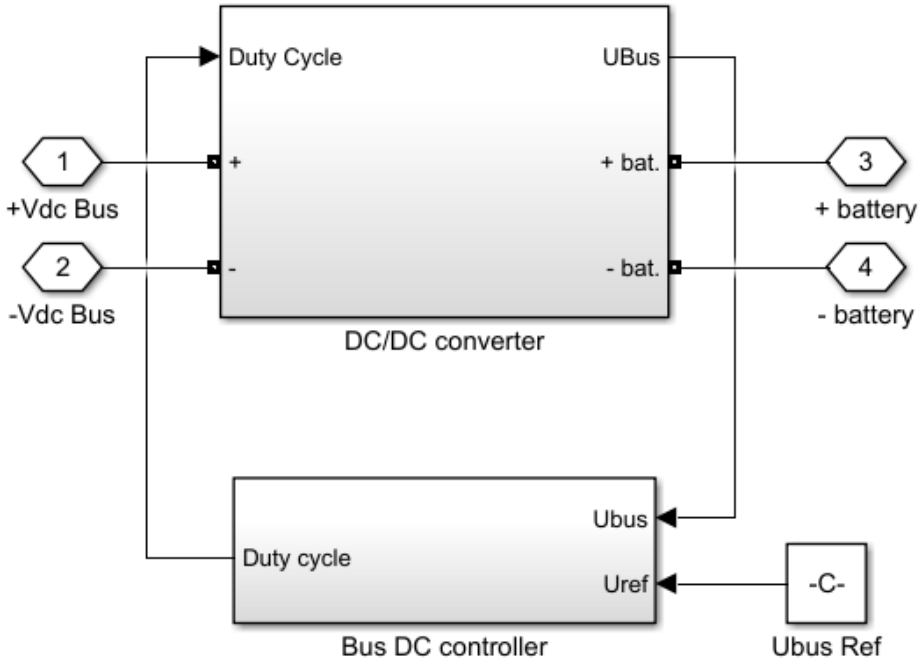

Figure 5.5: Integration of DC bus and its controller in Simulink

The detailed model for DC bus is a two-quadrant DC-DC power converter which can be found under Fundamental Blocks/Power Electronics library in Simulink. The converter is used in switching devices mode which is modeled with Insulated Gate Bipolar Transistor (IGBT) and diode pairs.

On top of the sizing parameters listed in Table 5.3, the additional input and output

Table 5.4: Model parameters and performance outputs for the detailed DC-DC converter model.

Model Parameters	**Performance Outputs**
Sample time [s]	Output Voltage [V]
Reference Voltage [V]	Output Current [A]
Device on-state resistance (Ohms)	
Snubber resistance (Ohms)	
Snubber capacitance (F)	

parameters for the detailed DC-DC converter model are given in Table 5.4.

5.1.4 Electric Motor

Introduction and General Parameters

Electric motors convert electrical power to mechanical (shaft) power. They can operate at very high efficiency and have high reliability. Electric motor efficiency is independent of operational altitude which gives an advantage over conventional internal combustion engines.[42] Furthermore, recent advances in electric motors enabled higher power-to-weight ratios (i.e. specific power), such as Siemens' electric motor for aircraft which has a state-of-the-art power-to-weight ratio of 5 kW/kg and delivers a continuous output of about 260 kW.[41]

Mechanical performance of an electric motor is determined by its torque (T) and rotational speed (ω) characteristics. Shaft power (i.e. mechanical power, P_{mech}) is given by Eqn. 5.23, whereas electric power (P_{el}) is given by Eqn. 5.24. An ideal electric motor would convert electrical power into mechanical power with 100% efficiency, and therefore the two expressions in Equations 5.23 and 5.24 would be equal to each other. However, real life motors suffer from losses due to some magnetic effects, heat dissipation caused

by friction, etc. Hence, the electrical (input) power is related to the mechanical (output) power via an efficiency factor as shown in Eqn. 5.25, where η_{EM} is the electric motor efficiency. [42]

$$\mathbf{P_{mech}} = \mathbf{T_{EM}}\omega_{\mathbf{EM}} \tag{5.23}$$

$$\mathbf{P_{el}} = \mathbf{I_{EM}}\mathbf{V_{EM}} \tag{5.24}$$

$$\eta_{\mathbf{EM}} = \frac{\mathbf{P_{mech}}}{\mathbf{P_{el}}} \tag{5.25}$$

In parallel hybrid electric propulsion systems, electric motor torque is additive to engine torque. In series hybrid electric propulsion systems, electric motor(s) provides all the torque required to propel the vehicle. Hence, the electric motor torque and power requirements in a series hybrid configuration are roughly the same as that of an electric motor in a fully electric propulsion.[94]

There are mainly two types of electric motors which are mostly used in electric vehicles: brushed DC motors and brushless motors. Brushed DC motors are widely used as traction motors in electric cars. These types of motors are easier to control. Torque of a brushed DC motor is directly proportional to the current traveling through its wires (also known as rotor or armature current). This relation is given by 5.26 where k_T is the torque constant in [Nm/A] and I_A is the armature current in [A]. Value of the torque constant depends on the motor design. [42]

$$\mathbf{T_{EM}} = \mathbf{k_T}\mathbf{I_{EM}} \tag{5.26}$$

In case the torque-current relationship of a motor is more complex or completely unknown, current going into the motor can still be found by Eqn. 5.26 to simplify the cal-

culations. [42] Moreover, it can be seen by comparing Equations 5.23, 5.24, 5.25 and 5.26 that a similar relationship also exists between the motor speed and voltage as given by Eqn. 5.27:

$$\omega_{\mathbf{EM}} = \mathbf{k}_{\omega}\mathbf{V}_{\mathbf{EM}} \tag{5.27}$$

High-level Loss-based Electric Motor Model

Similar to the previous subsystems, the high-level electric motor model does not account for electrical performance and dynamics, but utilizes the Equations 5.23 and 5.25 to relate motor torque to speed and input power to output power through the motor efficiency. The electric motor efficiency η_{EM} varies based on how the motor is used during an operation. It is possible to estimate this variable efficiency by looking at the current motor torque and speed settings. Thus, instead of assuming a constant efficiency for this subsystem, a loss-based motor model was adapted from literature.

Inefficiencies in an electric motor can be caused by various factors depending on the motor design, torque and speed. If these losses can be calculated, then the motor efficiency for different operation conditions can be approximated and an efficiency map can be created. Efficiency maps consist of efficiency islands for each allowable torque-speed combination and are useful to determine the optimum torque and speed settings. An example efficiency map is shown in Figure 5.6.

In order to develop an electric motor model, the major sources of loss must first be identified. Lowry and Larminie [42] divides the major sources of loss into four main sections which are generally the same in all motor types, as follows:

- **Copper Losses:** caused by energy dissipation into heating due to the electrical resistance of wires. It is proportional to the second power of armature current and therefore to the torque as shown in Eqn. 5.28 where k_c is a constant that depends on brush resistance and magnetic flux. This type of loss can be the largest cause of

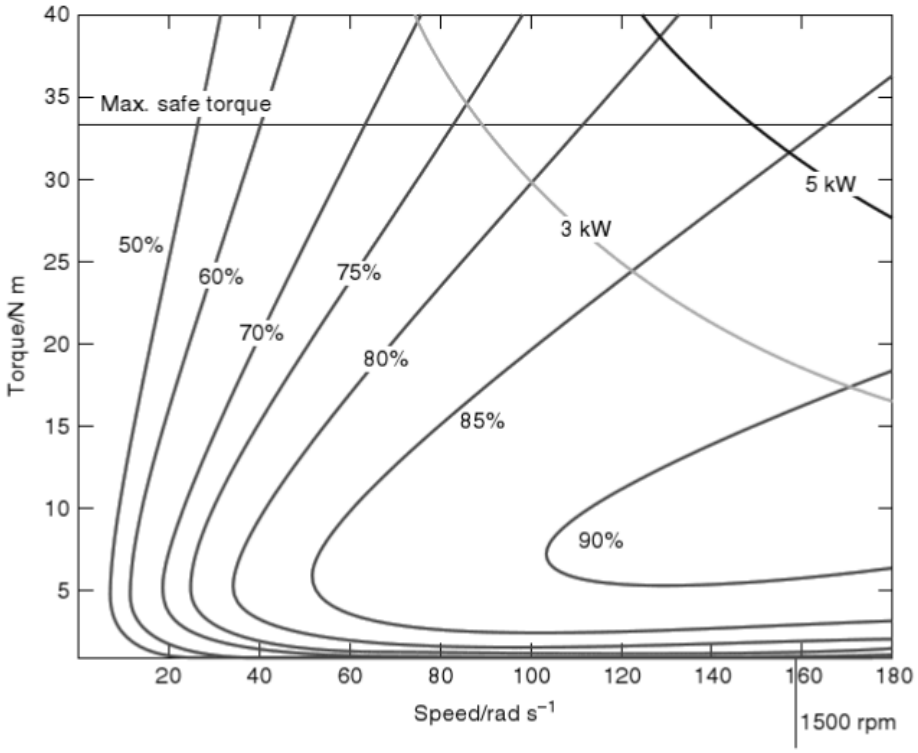

Figure 5.6: Efficiency map for a typical permanent magnet DC motor with brushes. Source: [42]

inefficiency especially for small motors.

$$\mathbf{Copper\ Loss} = \mathbf{k_c T^2} \tag{5.28}$$

- **Iron Losses:** caused by the ever-changing magnetic field effects in the iron of the motor. It is proportional to motor speed as given by Eqn. 5.29 where k_i changes with variations in the magnetic field strength but can be assumed constant.

$$\mathbf{Iron\ Loss} = \mathbf{k_i \omega_{EM}} \tag{5.29}$$

- **Friction and Windage Losses:** caused by a friction torque in the bearings of the motor and the wind resistance. Relevant power terms for friction and windage losses are given respectively in Eqn. 5.30 and Eqn. 5.31, where T_f is the friction torque and

k_ω is a constant which depends on the size and shape of the motor and whether it has a cooling fan.

$$\textbf{Friction Power} = \mathbf{T_f \omega_{EM}} \tag{5.30}$$

$$\textbf{Windage Power} = \mathbf{k_w \omega_{EM}^3} \tag{5.31}$$

- **Other Losses:** occurs regardless of the torque and speed of the motor, even when the motor is stationary. It is shown with the letter C.

The total loss is given as the sum of all these losses as shown in Eqn. 5.32 and can be assumed true for all motor types.

$$\textbf{Total Losses} = \mathbf{k_c T_{EM}^2 + k_i \omega_{EM} + k_w \omega_{EM}^3 + C} \tag{5.32}$$

Since the efficiency is given by the ratio of output power to the input power (which is the output power combined with total losses), efficiency η_{EM} can be calculated by Eqn. 5.33.

$$\eta_{\mathbf{EM}} = \frac{\mathbf{T_{EM} \omega_{EM}}}{\mathbf{T_{EM} \omega_{EM} + k_c T_{EM}^2 + k_i \omega_{EM} + k_w \omega_{EM}^3 + C}} \tag{5.33}$$

The constants given in these equations can be found based on experimentation or regression of a known torque-speed envelope with efficiency maps.

Although electrical dynamics are neglected in the high-level model, once the motor losses are found electrical power can still be computed. A comparison between Eqn. 5.25 and 5.33 gives the electrical power P_{el} in terms of the motor losses as given in Eqn 5.34. If the loss constants and operating conditions are known in terms of motor torque and rotational speed, then supply voltage and current can easily be calculated using equations

Table 5.5: Model parameters and sizing and performance outputs for the high-level electric motor model.

Model Parameters	Sizing Outputs	Performance Outputs
Specific Power [kW/kg]	Motor Weight [kg]	Mechanical Power [kW]
Mechanical torque [Nm]		Electrical Power [kW]
Motor speed [rad/s]		Total losses
Loss constants or torque-speed envelope		Efficiency
Rated Power Required [kW]		

5.26 and 5.34.

$$\mathbf{P_{el}} = \mathbf{T_{EM}}\omega_{\mathbf{EM}} + \mathbf{k_c}\mathbf{T_{EM}^2} + \mathbf{k_i}\omega_{\mathbf{EM}} + \mathbf{k_w}\omega_{\mathbf{EM}}^{\mathbf{3}} \tag{5.34}$$

This loss-based motor model is a good approximation for all types of motors. [42] Hence, no specific motor type is assumed for the high-level model.

Similar to the other subsystem models, the weight of the electric motor is calculated from its specific power (i.e. power-to-weight ratio, $(P/W)_{EM}$) and the rated power required ($P_{EM,rated}$), as shown in Eqn. 5.35:

$$\mathbf{W_{EM}} = \frac{P_{EM,rated}}{(P/W)_{EM}} \tag{5.35}$$

The modeling parameters and the output parameters of the high-level electric motor model are listed in Table 5.5.

Detailed Model for the Electric Motor

Unlike the high-level loss-based motor model, the detailed motor model has to be more specific as the motor dynamics vary among different types.

A literature survey revealed that most of the motors specifically designed (or being

designed) by Siemens for EA/HEA applications are AC motors. [21, 95] DC motors are brushed motors and suffers the extra friction and heat generation inside the motor (rather than the outer stator) associated with the brushes. [42]

AC motors can be categorized into three types:

- **Permanent Magnet Synchronous Motor (PMSM):** PMSM is a variable frequency motor whose torque/speed characteristics are very similar to that of DC motors. It employs a permanent magnet on its rotor. The field rotates It is also known as "brushless DC motor" (although it is an AC motor), "self-synchronous AC motor", "variable frequency synchronous motor", and "electronically commuted motor". PMSM is very efficient and has a greater torque density (torque-to-volume ratio) compared to induction motors. [42, 96] However, they suffer from short constant power range because of its limited field weakening capability. [47]

- **Switched Reluctance Motor (SRM):** In this motor, the magnetized rotor is not in-line with the magnetic field, and hence creates "reluctance" by producing a torque is in order to minimize the gap between the rotor and the magnetic field. SRM maintain its efficiency for a greater range of torque-speed configurations compared to other motor types, allowing it to operate at extremely high speeds. However, its peak efficiency is lower than that of PMSM. [42, 96, 47]

- **Induction Motor:** Induction motors are widely used, and very reliable due to their well matured technology, simplicity, robustness and wide speed range. [47] When used with DC energy sources such as batteries, it requires an inverter to convert DC power to AC power. When all else equal, the efficiency of an induction motor is usually 1% or 2% smaller than that of PMSM. [42, 96]

All of these motor types need a converter and controller to adjust the speed and/or torque of the motor by varying its voltage and/or current. A power converter, or more specifically an inverter, is needed to provide controlled AC voltage or current from the DC

energy source, which is in this case, the battery. A controller is needed to adjust the motor characteristics so that it matches with what the load requires. [97]

Although all three motor types could be used in EA/HEA applications (as they are currently in use in electric/hybrid-electric cars [42]), an induction motor model with field oriented control (FOC) was used as the detailed model. This is because Simulink has useful and readily-available information on the modeling parameters for the induction motor which is of the suitable size for the proof of concept. Even though some modeling parameters would change based on the selection of the motor type and its controller, the approach is the same.

The detailed motor drive model applies the following relationship between the electromagnetic torque (T_e), mechanical torque (T_m) and speed of the motor (ω_r):

$$\mathbf{T_e} = J\frac{d}{dt}\omega_r + F\omega_r + T_m \tag{5.36}$$

In Eqn. 5.36, J is the combined rotor and load inertia coefficient, and F is the combined rotor and load viscous friction coefficient.

The motor drive tries to match the mechanical torque and speed requirement coming from the aircraft mission level. These requirements are translated into flux and torque references for the FOC controller. The motor speed is controlled by a PI controller to produced the referenced motor torque and flux. The torque and flux references are then translated into three reference motor line currents by the FOC controller. The FOC controller then a three-phase current regulator and feeds the reference motor line currents into the motor to match the desired torque and flux. [98] The control strategy is further explained in Chapter 8.

Voltage variations from low to high values are usually necessary to control the speed of the motor. By regulating the motor voltage, power electronics (converters) control the electric motor to operate at any allowable torque-speed combination. [92, 94] As it can be seen from Figure A.4, there are two power electronics used in this model. The DC voltage

coming from the supply is first regulated by a braking chopper. Then, the DC current is inverted to an AC current by a three-phase inverter.

The braking chopper model works with the detailed DC-DC voltage converter (bus) model described in Section 5.1.3 to maintain the desired system voltage at the bus, while the motor voltage is varied. It is a capacitive DC bus with proportional control, and can be found in Electric Drives/Fundamental Drives Library of Simulink. The DC voltage is controlled with a PWM control to keep it within a determined boundary. The boundary (i.e. hysteresis band) is determined by an upper and lower voltage limit. A braking chopper (i.e. braking resistance) is enabled when the bus voltage reaches the upper limit (called as activation voltage), and shut down when the bus voltage reaches a lower limit called as (shutdown voltage). The frequency at which the braking resistance is switched on and off is also an input to the model. [98]

The three-phase inverter model converts the DC voltage to AC voltage. It is a three-leg, two-level model which can be found under Electric Drives/Fundamental Drive Blocks library in Simulink. It consists of a total of three controlled current sources: one on the DC side, two on the AC side. It also has three controlled voltage sources, all of them on the AC side. The relationship between the DC power ($P_{inv,DC}$) and the AC power ($P_{inv,AC}$) is given in Eqn. 5.37, where $I_{inv,DC}$ and $V_{inv,DC}$ are the input DC current and voltage, respectively. This equation comes from the more generic equations 5.19 through 5.21 derived for power electronics.

$$\begin{aligned} \mathbf{P_{inv,DC}} &= I_{inv,DC} V_{inv,DC} \\ &= P_{inv,AC} + P_{losses} \end{aligned} \tag{5.37}$$

The detailed model shares the same sizing parameters used in the weight estimation technique with the high-level electric motor model: power-to-weight ratio (specific power) and rated power required. The rest of the input and output parameters of the detailed electric motor model components are given in Tables 5.6, 5.7 and 5.8. Since this model

represents not only the induction motor but the complete AC drive, Tables 5.6, 5.7 and 5.8 list inputs each component of the drive: induction motor, power converters (braking chopper and inverter) and controllers (speed controller and FOC).

As it can be seen from Tables 5.6, 5.7 and 5.8, some components have sampling time as a separate input from the induction motor. The controllers has two sampling time input for each controller type to simulate a digital controller device. [98]. Simulink suggests a base sample time (i.e.simulation time step) of 2 μs, and an FOC sampling time of 20 μs.

5.1.5 Generator

A generator transforms the kinetic energy into electricity. In series hybrid electric propulsion, engine drives the generator which in turn powers the electric motor and/or charges the batteries. [43]

There are various types of generator models in literature. The interested reader can refer to the IEEE Guide [91] for different types of available models and their working principles.

In many cases, electric motors can be used as generators. [42] Hence, for the high-level generator model, Equations 5.23 and 5.24 can be repeated for the mechanical (input) power $P_{G,mech}$ and electrical (output) power $P_{G,el}$ of the generator, respectively, where the generator efficiency (η_G) is given by Eqn. 5.38:

$$\eta_{\mathbf{G}} = \frac{\mathbf{P_{G,el}}}{\mathbf{P_{G,mech}}} \tag{5.38}$$

Similarly, the same AC drive can be used as the detailed-model of the generator. The differentiation between motoring mode and generator mode is made through the sign of mechanical torque input: if mechanical torque is positive, the induction machine acts as a motor, whereas if mechanical torque is negative, it acts as a generator.

Table 5.6: Model parameters and performance outputs for the induction motor component of the AC motor drive

	Model Parameters	**Performance Outputs**
Induction Motor	Base sample time [s]	Electromagnetic torque [Nm]
	Reference mechanical torque [Nm]	Actual mechanical tourque [V]
	Reference rotor speed [rad/s]	Actual rotor speed [rad/s]
	Nominal Power [VA]	Rotor angle [ra]
	RMS Voltage [Vrms]	Rotor 3-phase (a,b,c) currents
	Frequency [Hz]	Rotor (q,d) currents
	Main winding stator resistance [ohm]	Rotor (q,d axes) flux [Vs]
	Main winding stator leakage inductance [H]	Rotor (q,d axes) voltage [V]
	Main winding stator mutual inductance [H]	Stator 3-phase (a,b,c) currents
	Main winding rotor resistance [ohm]	Stator (q,d axes) currents
	Main winding rotor leakage inductance [H]	Stator (q,d axes) flux [Vs]
	Inertia [kg m^2]	Stator (q,d axes) voltage [V]
	Friction factor [N m s]	Motor Line Voltages (ab, bc, ca)
	Pole pairs	Magnetizing inductance [H]
	Initial slip	
	Initial angle [deg]	

Table 5.7: Model parameters and performance outputs for the power converter components of the AC motor drive components in the detailed electric motor model

	Model Parameters	**Performance Outputs**
Braking Chopper	Sample time [s]	Output Voltage [V]
	Bus capacitance [F]	Output Current [A]
	Resistance [Ohms]	
	Frequency [Hz]	
	Activation Voltage [V]	
	Shutdown Voltage [V]	
Inverter	On-state resistance [ohm]	Output Voltage [V]
	IGBT forward voltage [V]	Output Current [A]
	Diode forward voltage [V]	
	Nominal Power [VA]	
	Fall time [s]	
	Tail time [s]	
	Snubber resistance [ohm]	
	Snubber capacitance [F]	

Table 5.8: Model parameters and performance outputs for the controller components of the AC motor drive in the detailed electric motor model

	Model Parameters	**Performance Outputs**
Speed Controller	Speed controller sampling time [s]	Speed reference error
	Acceleration ramp [rpm/s]	
	Deceleration ramp [rpm/s]	
	Proportional gain	
	Integral gain	
	Speed cutoff frequency [Hz]	
	Negative torque output limit [Nm]	
	Positive torque output limit [Nm]	
	Initial machine flux [Wb]	
	Nominal machine flux [Wb]	
FOC with SVM Controller	FOC sampling time [s]	Flux Reference [Wb]
	Flux proportional gain	Torque reference [Nm]
	Flux integral gain	Flux reference error
	Low-pass filter cutoff frequency	Torque reference error
	Negative flux output limit [Wb]	
	Positive flux output limit [Wb]	
	d-axis current regulator proportional gain	
	d-axis current integral proportional gain	
	q-axis current regulator proportional gain	
	q-axis current integral proportional gain	
	DC bus voltage sensor cutoff frequency [Hz]	
	SVM switching frequency [Hz]	

5.2 Transmission Subsystems

Gearbox is a mechanical subsystem in the powertrain which establishes the power transmission between the power sources and propellers. Essentially, a gearbox transfers the rotational motion at the output shaft of a mechanical power source. [99]

A gear unit called propeller speed reduction unit is used in single power source-propeller architectures to allow the power source (engine or motor) to run at a different speed than the propeller. For hybrid electric propulsion architectures, a gear unit called a power split device must be used to apply different amount of power to the same shaft.

In this dissertation, the models used for the transmission components are simplified, generic models represented by an efficiency factor. Although the need for these complex mechanical subsystems is acknowledged, their design and performance characteristics are not in the scope of this research. They will be represented only by the capabilities they bring to the system.

5.2.1 Propeller Speed Reduction Unit

Generally, engines and electric motors run at higher efficiency at higher rotational speeds relative to propellers which are more efficient at lower speeds due to tip speed and structural restrictions. In such cases, a propeller speed reduction unit (PSRU), which is essentially a gearbox, is employed to run the engines at a higher rotational speed than the propeller. [99]

In case of a single gear ratio transmission operation, PSRU can be modeled by defining the relationship between the electric motor rotational speed (ω_{EM}) and the propeller rotational speed (ω_{prop}) through a predefined gearbox ratio (R_g) as given in Eqn. 5.39. If the maximum motor speed is higher than the vehicle speed, then a higher gear ratio and a larger gear size is needed. [94]

$$\mathbf{R_g} = \frac{\omega_{\mathbf{EM}}}{\omega_{\mathbf{prop}}} \tag{5.39}$$

While most electric motors also require a PSRU, newest technology motors can drive the propeller at low speeds with high efficiency. [21] These motors are called direct-drive motors, such as the SP260D electric motor for aircraft designed and manufactured by Siemens. [41] The proof of concept later demonstrated in Chapter 7 assumes that all the utilized power sources are direct-drive.

5.2.2 Power Split Device

Power split devices allow hybrid electric vehicles to employ various power management strategies for the optimum efficiency and performance. They adjust the power flow among the power sources (engines and motors), generator and the battery. [47] When a power-split device is used in a hybrid electric architecture, the power sources can be used as if they were connected in series *and* parallel. The motor can drive the propeller with the energy coming from the battery and/or fuel-burning engine, just like the case in a series configuration; or the power sources can drive the propeller directly, just like the case in a parallel configuration. Hence, the power split device brings the advantages of both the parallel and series configurations, without having most of the disadvantages[100]

One of the most widely used power split devices in hybrid electric vehicles is the planetary gear set. [47, 101] Planetary gear sets employ a ring gear, a sun gear, a carrier gear and pinion gears. It splits the total required power between the power sources based on the desired power split schedule. [102, 100]

The power split schedule management discussed in Chapter 4.2 and later in Chapter 7 assumes that a power split device which is capable of realizing the desired splits is utilized in the hybrid-electric architectures considered.

5.3 Fuel-Burning Engine

As discussed previously, the literature survey conducted on HEA concepts revealed that there is a lot of effort on the propulsion aspect of the problem, but incorporation of de-

tailed architecture analyses into sizing considerations is missing. Hence, detailed propulsion analysis (such as engine cycle analysis) is not in the scope of this thesis. Accordingly, the engine modeling approach should be at a similar complexity of EPGDS models so that the sizing and analysis approach does not become propulsion-centric.

The performance parameters of an engine to be used in the sizing and analysis block can be obtained by generating an engine deck, or by digitizing the performance curves (fuel flow and thrust or power as a function of altitude, velocity and temperature) manufacturer's manual.

The developed framework can be used with all propulsion types, provided that the integration of the employed propulsion devices is accurately represented. The use of jet engines with electric propulsion requires in-depth engine analysis to reveal the impacts of the integration of motor. [34, 103] Such analysis can be performed offline using advanced multidisciplinary analysis environment for aerospace propulsion systems such as the one developed by NASA for conventional propulsion systems, or GT-HEAT developed by Georgia Tech's ASDL for hybrid electric propulsion. [104, 34] Then, the integrated performance can be represented by a modified engine deck which contains information regarding electric energy flow as a function of level of hybridization.

One way to generate a conventional engine deck is to utilize the Numerical Propulsion System Simulation (NPSS) tool, which is an advanced multidisciplinary analysis environment for aerospace propulsion systems developed by NASA.[104] Correlation between break specific fuel consumption (BSFC) trends, shaft horse power and engine weight will also be obtained by running NPSS offline for a range of engine sizes. This correlation can be used to size the engine during aircraft mission analysis, such that if the rated shaft power is scaled, then a corresponding new engine weight is assigned. This weight change can create new power targets, and therefore the process has to be repeated until the engine scaling is no longer necessary.

If the fuel-burning engine is a reciprocating or turboshaft engine, then the engine and

the motor are connected through a shaft. As explained in Chapter 2, in series configuration, the engine drives the motor by applying torque on the shaft; and in parallel configuration the engine and the motor both apply torque on the same propeller shaft. For more complex configurations, a power split device is used to adjust the power contribution from the connected power sources. Hence, for reciprocating or turboshaft engines, the performance of each power source model can be isolated from the others by differentiating the individual torque contributions on the shaft.

The fuel-burning engine model used in the proof of concept in Chapter 7 represents an internal combustion engine (ICE) for general aviation aircraft. The model was generated based on manufacturer's data sheets on engine performance in terms of break horse power and fuel consumption as a function of pressure altitude, manifold pressure, engine RPM, and ISA deviation. Performance data was collected to create a repository of existing general aviation aircraft engines of different sizes and similar power-to-weight ratios.

The engine sizing is performed based on the sea level rated power required from the engine. An algorithm was developed to check the rated power of all the engines in the engine repository and compare their rated power with the required rated power, and automatically select the baseline engine which has the closest rated power compared to the required rated power. The baseline engine is then sized to meet the desired rated power. An engine scaling factor (k_{engine}) is defined as a ratio of the rated power to the new engine ($P_{rated,new}$) to the rated power of the baseline engine ($P_{rated,baseline}$), as shown in Eqn. 5.40.

$$\mathbf{k_{engine}} = \frac{P_{rated,new}}{P_{rated,baseline}} \tag{5.40}$$

This scaling factor k_{engine} is then used to scale the baseline engine's fuel consumption and power characteristics. As the engine gets scaled up or down, the algorithm selects a new baseline engine from the repository, and the new engine inherits its scaled characteristics. Better results are achieved by adding a variety of engines of different sizes, so that excessive scaling is avoided.

Table 5.9: Model parameters and sizing and performance outputs of the fuel-burning engine model.

Model Parameters	Sizing Outputs	Performance Outputs
Power-to-weight ratio [kW/kg]	Engine weight [kg]	Shaft Power Realized [kW]
Sea level rated power [kW]	Sizing factor	Fuel Flow [kg/s]
ISA Deviation [°C]		Energy Flow [Wh/s]
Altitude [m]		
Mach Number		
Hybridization factor [%]		
Shaft Power Required [kW]		

Engine weight is determined by the power-to-weight ratio of the baseline engine and the required rated power, as shown in Eqn. 5.41. Although the repository consists of engines with mostly similar power-to-weight ratios, they are not the same. Thus, as the engine is being sized, there might be a jump in its power-to-weight ratio.

$$\mathbf{W_{engine}} = \frac{P_{rated}}{(P/W)_{baseline}} \tag{5.41}$$

The modeling input and output parameters of the reciprocating/turboshaft engine are listed in Table 5.9. If the analyses are performed for a jet engine instead, then the required shaft power parameter can be replaced with required thrust.

5.4 Propeller

An in-house propeller model was utilized to be used with the reciprocating and turboshaft engines. The propeller model predicts the performance of a propeller from its geometry. The geometric input consists of the blade chord lengths and pitch angles at several stations throughout the blade span. XFOIL [105], which is an open-source 2-D aerodynamic

prediction software is used to predict the aerodynamic properties of the propeller. This information is then combined with the geometric properties to estimate the 3-D performance of the full propeller using blade element momentum theory. [106]

The propeller performance is given by the torque coefficient C_Q and thrust coefficient C_T at a list of propeller pitch angles, β and advance ratios, J. The corresponding power coefficient C_P and propeller efficiency $\eta_{propeller}$ are then calculated as shown in Equations. 5.42 and 5.43, respectively.

$$\mathbf{C_P} = 2\pi C_Q \tag{5.42}$$

$$\eta_{\mathbf{propeller}} = J\frac{C_T}{C_P} \tag{5.43}$$

The advance ratio, J is obtained by Eqn. 5.44, where V_∞ is the free stream velocity, n is revolutions per second, and D is the propeller diameter.

$$\mathbf{J} = \frac{V_\infty}{nD} \tag{5.44}$$

To calculate the thrust output of the propeller model at any given flight state, an interpolant was created for each of the following parameters: C_T as a function of J and β, C_Q as a function of J and β, and β as a function of J and C_T. These interpolants are queried during the mission performance evaluations which is explained in detail in Chapter 6.

Propeller thrust and torque are computed from the coefficients as shown in Equations 5.45 and 5.46, respectively.

$$\mathbf{T} = C_T \rho_\infty n^2 D^4 \tag{5.45}$$

$$\mathbf{Q} = C_Q \rho_\infty n^2 D^5 \tag{5.46}$$

There are three types of propellers that the model can be used for:

- **Constant speed propeller:** If the propeller model is to be used for a constant speed propeller, then for a given propeller speed (n), the propeller efficiency $\eta_{propeller}$ corresponding to a vector of realizable propeller pitch angles are calculated. Then, available thrust values for the same speed and the vector of pitch angles are computed. The pitch angle which produces a thrust equal to or more than the required thrust at maximum efficiency is carried forward as the pitch angle setting for the given state of flight.

- **Fixed pitch propeller:** If the propeller model is used for a fixed pitch propeller, similar calculations are performed by this time varying the propeller speed at a constant propeller pitch angle to find the best configuration which gives the desired propeller efficiency and thrust.

- **Variable pitch propeller:** In this case, the pilot varies the propeller pitch angle and as a result, propeller speed changes. The propeller model finds the propeller speed and pitch angle combination which yields the maximum propeller efficiency at a realizable shaft power.

The propeller model was combined with the engine and motor models to compute the thrust output. As explained earlier, one propeller can be driven by multiple power sources. Hence, the available thrust is predicted through architecture-specific calculations. The logic behind how the propeller model is integrated automatically with all of the connected power sources within different architectures is explained in Section 5.5.

The propeller sizing is performed based on the propeller diameter and number of blades. Similar to the engine deck repository, a propeller repository was created. This is done by first selecting a suitable baseline propeller model. Then, 2-bladed, 3-bladed and 4-bladed propeller derivatives of this propeller are generated.

Table 5.10: Factor K_p for typical metal propeller types based on Reference [75]

Type of propeller	K_p
Two-bladed	22
Three-bladed	18
Four-bladed	16

The baseline propeller is first tested to produce the thrust required by the given design mission profile. During each step of the mission legs, two properties related to the performance of the propeller were tracked: available thrust (when the propeller is combined with the related power sources), and propeller tip speed.

If the available thrust is less than the required thrust, then there are two sizing options: (i) increase the diameter, (ii) increase the number of blades.

The initial choice is to increase the size of the diameter so that the resized propeller can produce the thrust required. This is to avoid an increase in weight due to the increase in number of blades, which can be higher than using a 2-bladed propeller with greater diameter. [75] Gudmundsson [75] provides rapid estimation of required propeller diameter techniques for wooden and metal propellers suitable for general aviation applications.

The technique used in this propeller model to estimate the required diameter is given in Eqn. 5.47 for metal propellers, where P_{BHP} is the break horse power, K_p is a factor varying with the number of blades, and propeller diameter D is given in inches. The values which K_p takes based on the number of blades are listed in Table 5.10.

$$\mathbf{D} = K_p \sqrt[4]{P_{BHP}} \tag{5.47}$$

There are to caveats to increasing the propeller diameter. The first one is that the resized propeller might experience increased noise and shock formation at the tips due to very high tip speeds, which reduces efficiency. The second one is that the larger diameter might

Table 5.11: Model parameters and sizing and performance outputs for propeller model.

Model Parameters	Sizing Outputs	Performance Outputs
Blade chord lengths along span	Diameter	Thrust coefficient
Pitch angles along span	Number of blades	Torque Coefficient
Advance ratio		Power Coefficient
Rotational speed		Efficiency
Brake horse power		Thrust

cause ground proximity problems. [75] For these reasons, the resized propeller diameter is checked against the following two criteria:

- Does the rotational tip speed exceed a predefined tip speed limit? [3]
- Does the propeller diameter exceed the allowed size limit due to ground proximity?

If the answer to any of the above questions is yes, then the diameter can not be increased for the given propeller design. But instead, the number of blades can be increased. By increasing the number of blades by 1 (i.e. if the baseline propeller is 2-bladed, the new design is 3-bladed; if the baseline propeller is 3-bladed, then the new design becomes 4-bladed, and so on), greater thrust can be obtained with smaller diameters.

Each time the propeller is resized (i.e. every time diameter or number of blades changes), the new design is checked against these two criteria. The sizing is performed until a propeller design, which can provide the thrust required when combined with the related power sources, is obtained.

The modeling parameters and the output parameters of the propeller model are listed in Table 5.11.

[3] According to Gudmundsson [75], rotational tip speeds are in the 0.6 Mach range for wooden propellers and are in the 0.75 Mach - 0.8 Mach range for metal and aluminum propellers. The tip speed limit must be set accordingly.

5.5 Characterization of Propulsion Architecture

The next step after defining the modeling parameters and sizing and performance outputs of each EPGDS is to integrate them within the desired architecture. In order to make rapid architecture comparisons, the integration process must be made as simple as possible to the architect. This necessitates the development of a methodology that will be the basis of building diverse architectures by *logically* connecting the necessary subsystems.

To this end, a methodology was developed to establish the relationship between the main subsystems in a propulsion architecture. This methodology enables rapid analyses and comparisons between architectures, without requiring manual interference. The resulting logical connections, which describe the information flow between subsystems, are used to develop the necessary relationships within the propulsion system characterization function described in Chapter 6.2 for the propulsion system architectures of interest.

First, a set of definitions to reveal the relationship between the main electric power generation and distribution subsystems must be established. In this work, the propulsion system architecture operates through interactions among components falling into three main categories:

1. **Power source (PS):** includes any subsystem that generates primary (propulsive) power, such as an electric motor, internal combustion engine, turboprop engine, etc.

2. **Thrust source (TS):** includes any subsystem that generates thrust, such as a propeller.[4]

3. **Energy source (ES):** includes any subsystem that stores energy to be used by the primary power sources, such as batteries, fossil fuel, fuel cells, etc.

Next, each distinctive source is given an identification number to ensure convenience and traceability. An example to this is given in Figure 5.7 for a series hybrid-electric

[4]The power and thrust source categories can be combined under a single category for some systems, such as jet engines.

configuration. In this architecture, the fuel inside the fuel tank was labeled as ES 1 , battery as ES 2, fuel burning engine as PS 1, electric motor as PS 2, and propeller as TS 1.

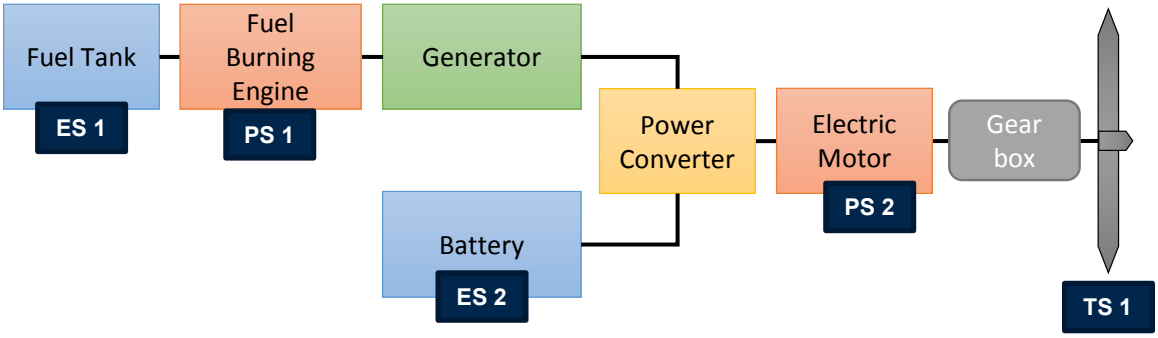

Figure 5.7: A notional series hybrid-electric configuration where its energy, power and thrust sources are coded by source identification numbers.

Once the components are distributed under these three categories, their effects on the system can be represented by *n-by-1* matrices (i.e. column arrays) where n is the number of sources in the propulsion system. The ES, PS and TS matrices for the series HE example in Figure 5.7 are given in part a, b and c of Equation 5.48, respectively.

$$A_{ES} = \begin{bmatrix} ES_1 \\ ES_2 \end{bmatrix} \tag{5.48a}$$

$$A_{PS} = \begin{bmatrix} PS_1 \\ PS_2 \end{bmatrix} \tag{5.48b}$$

$$A_{TS} = \begin{bmatrix} TS_1 \end{bmatrix} \tag{5.48c}$$

The next step is to define any applicable inter-relationships between the same-type and different-type sources. This is performed by a set of matrices which contain information regarding component dependencies. These matrices are:

1. **Energy Source - Power Source Matrix** (B_{ESPS})**:** This matrix lays out which power source draws its energy from which energy source by logical comparisons.

2. **Thrust Source - Power Source Matrix** (B_{TSPS})**:** This matrix includes information

on which power source is connected to which thrust source.

Each element b_{ij} of matrix B is a logical true-or-false (1 or 0) value. Matrix B describes the relationship of the power source matrix with the energy and thrust source matrices in terms of dependencies. The form of this description for the relationship between the energy sources and the power sources is given in Eqn. 5.49. through Equations 5.49 and 5.52.

$$B_{ESPS}A_{PS} = A_{ES} \tag{5.49}$$

The elements of matrix B_{ESPS} consist of logical values of 1 (true) and 0 (false). This means that if $a_{i,j}$ takes the logical value of 1, then the *i*th element of the energy source matrix A_{ES} (i.e. ES *i*) is linked to the *j*th element of the power source matrix A_{PS} (i.e. PS *j*). On the contrary, if it takes the logical value of 0 (false), then these two sources are not related.

For the series configuration depicted in Figure 5.7, the ES-PS matrix (B_{ESPS}) is therefore a two-by-two identity matrix, and the Eqn.5.49 becomes Eqn.5.50.

$$\begin{aligned} \begin{bmatrix} 1 & 0 \\ 0 & 1 \end{bmatrix} \begin{bmatrix} PS_1 \\ PS_2 \end{bmatrix} &= \begin{bmatrix} ES_1 \\ ES_2 \end{bmatrix} \\ &= \begin{bmatrix} PS_1 \\ PS_2 \end{bmatrix} \end{aligned} \tag{5.50}$$

The right-hand-side of Eqn.5.50 is a logical equation, relating ES_1 to PS_1 and ES_2 to PS_2.

Unlike matrix B_{ESPS}, matrix B_{TSPS} must capture not only the direct logical relationship of a power source with any other source, but also the indirect ones. Here it should be reminded that "direct" and "indirect" connections do not refer to physical connections, but to logical ones. Although there may be other subsystems in between a two sources

physically, Matrix B is created only to define the impact of the power sources on other sources, whether directly or indirectly. For instance, in the series configuration shown in Figure 5.7, electric motor "directly drives" the propeller. Since the electric motor can also be fully or partially driven by the mechanical power transmitted from the fuel burning engine through the generator, the two power sources are related. Furthermore, fuel burning engine has a part in driving the same propeller as well, through the electric motor. The relationship between the fuel burning engine and the propeller is then regarded as an "indirect relationship".

Such relationships must be explicitly defined by matrix B_{TSPS} so that there remains no ambiguity in the architecture definition, especially when any two power sources are connected in series, series-parallel, or complex HE configurations, or when any thrust source is run by more than one power source. Therefore, matrix B_{TSPS} must include not only the relation between a power source and a thrust source, but also among the other power sources. But first, matrix A_{PS} must be modified to include the indirect effects, so that it becomes an $(n+m) - by - 1$ matrix where n is the number of power sources and m is the total number of possible combinations of any two power sources.

The modified PS matrix (A^*_{PS}) for the series configuration shown in Figure 5.7 is given in Eqn. 5.51.

$$A^*_{PS} = \begin{bmatrix} PS_1 \\ PS_2 \\ PS_{1-2} \end{bmatrix} \tag{5.51}$$

The third element PS_{1-2} builds a bridge between power sources 1 and 2, so that the combined impact of these two sources can be captured in the TSPS matrix (B_{TSPS}). This approach not only clears the ambiguity in which power sources are decoupled from the thrust sources, but also clarifies which power sources can be driven by which other power sources.

The TSPS matrix B_{TSPS} then takes the form given in Eqn. 5.52

$$B_{TSPS}A^*_{PS} = A_{TS} \tag{5.52}$$

Just like B_{ESPS}, B_{TSPS} takes logical values of 1 (true) and 0 (false). Continuing with the series configuration example, B_{TSPS} takes the values given in Eqn. 5.53, so that when multiplied by the modified PS matrix A^*_{PS}, the resultant matrix clearly lays out the dependencies in this architecture, as shown in Eqn. 5.54.

$$B_{TSPS} = \begin{bmatrix} 1 & 0 & 1 \end{bmatrix} \tag{5.53}$$

$$\begin{aligned} \begin{bmatrix} 1 & 0 & 1 \end{bmatrix} \begin{bmatrix} PS_1 \\ PS_2 \\ PS_{1-2} \end{bmatrix} &= \begin{bmatrix} TS_1 \end{bmatrix} \\ &= \begin{bmatrix} PS_1 + PS_{1-2} \end{bmatrix} \end{aligned} \tag{5.54}$$

The resultant matrix shown in the right-hand-side of Eqn. 5.54 equates TS_1 to $[PS_1 + PS_{1-2}]$, meaning that Thrust Source 1 (propeller) is directly connected (logically) to Power Source 1 (electric motor), but also is indirectly linked to Power Source 2 (fuel burning engine) through Power Source 1.

It should be noted one more time there is no need to define any "indirect relationships" between the power sources and energy sources for the ESPS matrix, B_{ESPS}. This is due to the fact that even though a power source might be coupled with another power source, the amount of energy transferred from one power source to the other is dictated only by the energy that the directly-connected power source draws. Hence, for the series example in Figure 5.7, the only power source drawing energy from ES 1 is PS 1, and from ES 2 is PS 2 as shown in Eqn.5.50.

The matrices defined here can easily be expanded to represent more complex configurations or architectures with multiple power sources. A few examples for the notional configurations introduced in Figure 2.7 are provided below.

5.5.1 Parallel Configuration

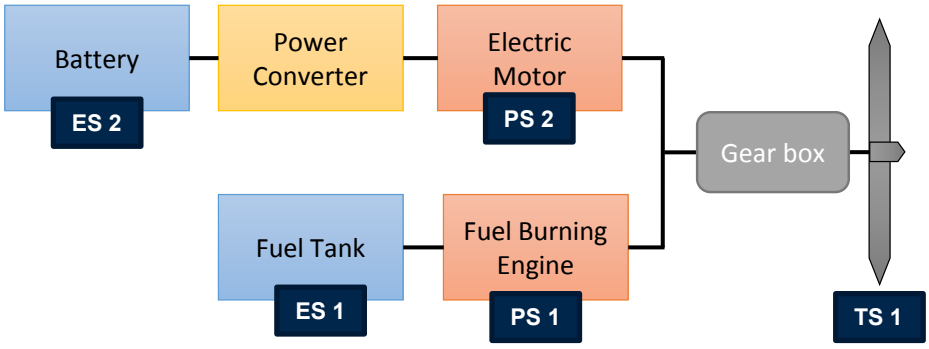

Figure 5.8: A notional parallel hybrid-electric configuration where its energy, power and thrust sources are coded by source identification numbers.

For the parallel configuration shown in Figure 5.8, the source matrices are the same as the ones defined for the series configuration in Eqn. 5.48. This is because there are same number of sources in this configuration as in the series one. Similarly, the ES-PS matrix (B_{ESPS}) is a two-by-two identity matrix where rows represent the energy sources and columns represent the power sources. Again, ES 1 (fuel) supplies energy only to PS 1 (fuel burning engine) and therefore is logically connected to PS 1, as shown in the first element of the ESPS matrix, (A_{ESPS}). Similarly, ES 2 (battery) supplies energy to PS 2 (electric motor), not to PS 1, as shown in the second row of (A_{ESPS}). Hence, Eqn. 5.49 for

this configuration becomes:

$$\begin{bmatrix} 1 & 0 \\ 0 & 1 \end{bmatrix} \begin{bmatrix} PS_1 \\ PS_2 \end{bmatrix} = \begin{bmatrix} ES_1 \\ ES_2 \end{bmatrix} = \begin{bmatrix} PS_1 \\ PS_2 \end{bmatrix} \tag{5.55}$$

In the parallel configuration, the two power sources are decoupled from each other, but individually coupled with the same thrust source. Hence, the inter-relationship matrices for the parallel HE configuration in Figure 5.8 become:

$$\begin{bmatrix} 1 & 1 & 0 \end{bmatrix} \begin{bmatrix} PS_1 \\ PS_2 \\ PS_{1-2} \end{bmatrix} = \begin{bmatrix} TS_1 \end{bmatrix} = \begin{bmatrix} PS_1 + PS_2 \end{bmatrix} \tag{5.56}$$

It can easily be inferred from matrix B_{TSPS} that PS 1 (fuel burning engine) and PS 2 (electric motor) are connected to TS 1 (propeller) through $b_{1,1} = 1$ and $b_{1,2} = 1$, respectively, but are independent of each other since $b_{1,3} = 0$.

5.5.2 Series-Parallel Configuration

In the series-parallel configuration depicted in Figure 5.9, the ESPS matrix is the same as the ones written for the series and parallel configurations, given in Equations 5.50 and 5.55, respectively.

However, the TSPS matrix B_{TSPS} differs from them as this time both power sources are directly connected to the thrust source, but also the fuel burning engine has an indirect

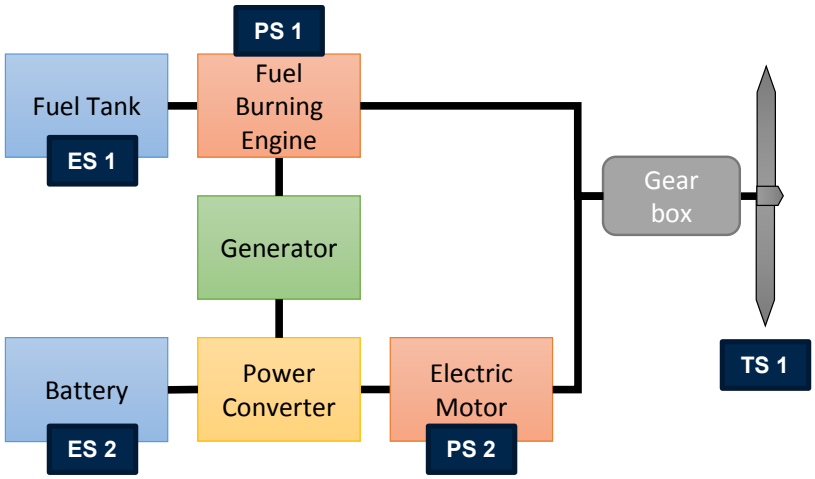

Figure 5.9: A notional series-parallel hybrid-electric configuration where its energy, power and thrust sources are coded by source identification numbers.

connection through its link to the electric motor. Hence, Eqn. 5.52 for this configuration becomes:

$$\begin{bmatrix} 1 & 1 & 1 \end{bmatrix} \begin{bmatrix} PS_1 \\ PS_2 \\ PS_{1-2} \end{bmatrix} = \begin{bmatrix} TS_1 \end{bmatrix} \\ = \begin{bmatrix} PS_1 + PS_2 + PS_{1-2} \end{bmatrix} \tag{5.57}$$

5.5.3 Complex Configuration

As discussed in 2.2.4, the complex configuration shown again in Figure 5.10 is different than the series-parallel one in that (i) there are three power sources, and (ii) the power flow of the electric motor (labeled as PS 2) is bidirectional as it also acts as a generator to recharge the battery. But when operating as an electric motor, PS 2 can either be driven by the fuel burning engine (PS 1) or draw energy from the battery (ES 2). Hence, Eqn. 5.49 for this configuration takes the form shown in Eqn. 5.58.

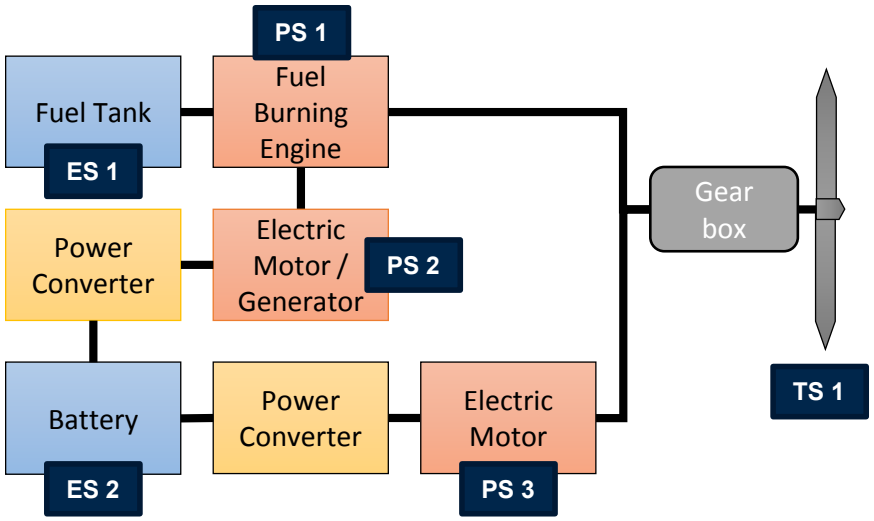

Figure 5.10: A notional complex hybrid-electric configuration where its energy, power and thrust sources are coded by source identification numbers.

$$\begin{bmatrix} 1 & 0 & 0 \\ 0 & 1 & 1 \end{bmatrix} \begin{bmatrix} PS_1 \\ PS_2 \\ PS_3 \end{bmatrix} = \begin{bmatrix} ES_1 \\ ES_2 \end{bmatrix} = \begin{bmatrix} PS_1 \\ PS_2 + PS_3 \end{bmatrix} \tag{5.58}$$

As it can be seen from the second row of the resultant matrix given in Eqn. 5.58, ES 2 (battery) feeds two power sources, PS 2 and PS 3.

The TSPS matrix written for the complex configuration given in Eqn. 5.59 captures all of the following relationships:

- PS 1 and PS 3 are directly connected to TS 1,
- PS 1 can drive PS 2,
- PS 2 can drive TS 1 indirectly through PS 1
- PS 1 and PS 3 are in parallel

- PS 1 do not drive PS 3

$$\begin{bmatrix} 1 & 0 & 1 & 1 & 0 & 0 \end{bmatrix} \begin{bmatrix} PS_1 \\ PS_2 \\ PS_3 \\ PS_{1-2} \\ PS_{1-3} \\ PS_{2-3} \end{bmatrix} = \begin{bmatrix} TS_1 \end{bmatrix} \tag{5.59}$$

$$= \begin{bmatrix} PS_1 + PS_3 + PS_{1-2} \end{bmatrix}$$

As it can be seen from the four examples given in this section for series, parallel, series-parallel and complex configurations, the method of categorizing the main power generation components into three sources and creating the related ESPS and TSPS matrices can be easily used for other configurations that were not covered here. This method brings convenience to describing any propulsion system architecture and using them within the propulsion system performance function to distribute the required power, thrust, and energy from each existing source. Defining the relations between different sources with the logical B_{ESPS} and B_{TSPS} matrices is convenient as the power, thrust, or energy from each source can be easily computed by multiplying the power, thrust, or energy in the powertrain by the matrix itself. This method is also very useful in rapidly changing architectures within mission performance analysis.

5.6 Chapter Summary

Traditionally, the sizing of the subsystem components is performed during the conceptual aircraft design stage by using empirical relationships based on existing historical data. [67, 68] From these empirical relations, information on aircraft weight, power (or thrust) and drag polar are then estimated and fed into the sizing and synthesis process where constraint analysis (to meet point performance requirements) and mission analysis (to fly a specific

design mission) are carried out through iterations. [69] However, there is a lack of historical data and readily available physics-based models for unconventional or more recent technologies such as EPGDS. Hence, estimations on the design, performance and system-level impact of such subsystems introduce epistemic uncertainty to the conceptual design analysis.

This chapter described the development and integration of parametric, physics-based models for the most prominent power generation and distribution subsystems in hybrid-electric propulsion architectures. Due to the absence of historical data, the models were created from first-order analysis. The need for creating these subsystem models came from Hypothesis 2, which is repeated below. The parts necessitating the development of the EPGDS models were emphasized with bold characters.

HYPOTHESIS 2: EPGDS characteristics can be integrated into the EA/HEA sizing process through a parametric sizing and synthesis framework with the following properties:

- A generic mission analysis approach is implemented where the required energy to fly a mission profile is tracked and budgeted between different power sources of aircraft according to preset hybridization levels
- Aircraft sizing and synthesis process captures the sizing of EPGDS components based on required energy and/or power, simultaneously with aircraft sizing
- **EPGDS models used in the framework are parametric, physics-based and dynamic**
- **The developed EPGDS models are utilized to capture the subsystem level impacts at aircraft and mission levels**
- **The parametric property of the developed models enable technology projections**

The first part of this chapter dealt with electric power generation and distribution subsystems. Two types of were developed or adapted from literature for EPGDS: high-level models which are more suitable for rapid analysis, and detailed models which represent the subsystem level dynamics more accurately. Both types of models are parametric, physics-based and dynamic, in accordance with Hypothesis 2.

Modeling parameters were given for both types of EPGDS models. The main difference between the two types of models can easily be seen by comparing the modeling parameters and outputs for each subsystem. The high-level EPGDS models do not require subject-matter expertise and hence can be modeled with only a basic understanding of the subsystem. The modeling inputs for the high-level models generally consist of sizing parameters for weight estimation through power-to-weight or energy-to-weight ratios, whichever is more limiting; and performance parameters to estimate the subsystem efficiency. The efficiency estimation is either done by back-of-the-envelope type calculations, or estimated through constant efficiency values found from commercial-off-the-shelf components.

Although such models enable rapid analysis, there still exists uncertainty due to modeling assumptions. Moreover, the high-level models do not provide much resolution on the subsystem dynamics and hence cannot be used for transient analysis. The literature review in Chapter 2 revealed that the transient regimes in EPGDS dynamics might cause major problems as they are expected to generate and carry much greater amounts of power compared to the electric subsystems used as secondary power systems in conventional aircraft architectures. Hence, transient analysis must be accounted for in the design of EPGDS.

Combined with the lack of historical data, the uncertainty in the design and performance estimation of these subsystems can have a cascading impact on the vehicle design and mission performance. Another observation *(Observation 2)* made during the literature review in Chapter 2 was that EA/HEA concepts are more weight sensitive compared to their traditional counterparts. Thus, inaccurate subsystem weight and performance estimations made at the conceptual design stage can bring greater weight penalties to the aircraft

design and overshadow more suitable architectures.

This drawback of high-level EPGDS models necessitated the development of more detailed models which offers higher resolution on subsystem dynamics at the expense of higher computational resources and increased amount of initial knowledge and expertise about the subsystems. The detailed models enable time-domain simulations suitable for steady-state and transient analysis. They also reduce the uncertainty due to modeling assumptions as the modeling inputs require much detailed information and even subject-matter expertise. However, the sample time steps to run these simulations are in the order of microseconds - more than a 10^6 times smaller than mission level analysis. Hence, rapid simulations suitable for the aircraft conceptual design stage cannot be performed with these detailed models.

The comparison between the two types of models supports the argument that a new way of incorporating the subsystem design and performance evaluation to the early stages of design must be found. This discussion is continued in Chapter 8 where a methodology is proposed to utilize these two types of models cooperatively so that maximum knowledge about the design can be achieved without exhausting computational resources.

Apart from the EPGDS models, parametric engine and propeller models were also developed to be used in hybrid-electric architecture studies. The level of detail of these models were carefully chosen to balance the electric and non-electric subsystems to focus on architectural considerations.

Finally, a methodology to systematically categorize and logically connect the main EP/HEP subsystems was proposed. The main subsystems were categorized by their functionality under three sources: energy sources, power sources, and thrust sources. The interrelationships among these sources were established by interrelationship matrices. Any EP/HEP architecture can be defined with the help of these matrices, effortlessly.

This feature of the proposed methodological framework enables rapid architectural comparisons, a trait which was missing before. The matrices are directly used in mis-

sion performance analysis to calculate the energy and power flow from and to each source. As explained in Chapter 6, these matrices were combined with the generic mission analysis approach in order to remove the necessity of modifying the performance calculations based on architecture-specific requirements. This means that the same codes can be used to define and evaluate the performance of various architectures, as long as the codes were generated following the proposed framework.

The interrelationship matrices presented here represent only the "main subsystems". This is in accordance with the level of detail of the models used for rapid conceptual design stage analysis found in literature. As discussed previously, such studies do not account for the remaining subsystems. However, implementation-specific heuristics (e.g. for fault-tree analysis) can be implemented to create subsystem architectures with increased dimensionality. Although such considerations are out of the scope of this dissertation, the proposed methodology provides the means to automate architectural comparisons with the flexibility to increase the level of detail and dimensionality of the studied architectures.

CHAPTER 6

GENERIC MISSION PERFORMANCE ANALYSIS

As briefly described in Section 4.1.3 of Chapter 4, mission analysis is performed in traditional conceptual design stage to establish the scale of the aircraft via the estimation of takeoff gross weight (W_{TO}). This is accomplished by defining a mission profile, i.e. an operational scenario, and flying the aircraft through this entire mission on paper. [69]

As Mattingly [69] lays out, the takeoff gross weight consists of three main weights in the traditional design approach. These are, namely, the payload weight (W_P), the empty weight (W_E) and the required fuel weight (W_F). The takeoff gross weight is then given by Eqn. 4.6, as shown in Chapter 4.

$$\begin{aligned} W_{TO} &= W_P + W_E + W_F \\ &= W_P \Big/ \left(1 - \frac{W_E}{W_{TO}} - \frac{W_F}{W_{TO}}\right) \end{aligned} \tag{4.6}$$

While the payload weight is specified in the Request for Proposal and the empty weight accounts for the basic aircraft structure and permanent equipment, the fuel weight has to be calculated through fuel consumption analysis. The key enabler in fuel consumption analysis is thrust specific fuel consumption ($TSFC$) which depends on engine cycle, flight conditions and throttle setting. The performance of any mission leg is then evaluated for minimum fuel usage. This is a very advantageous approach in terms of simplicity since the rate of fuel consumption also means the rate of the decrease in aircraft weight (excluding instantaneous release of any payload), as previously shown in Eqn. 4.7.

When the sole energy source flying the aircraft is conventional *consumable* fuel, the performance of such a source can be based on its weight rather than a required energy capacity. However, for unconventional energy sources, such as rechargeable batteries, this

approach is inadequate.

Hence, a different mission analysis approach is required in cases where the performance of at least one of the energy sources cannot be measured by its weight reduction. Such an analysis must also be capable of tracking and reporting the key instances during the mission, similar to the traditional analysis which yields fuel fractions at the beginning and the end of each mission leg within a mission.

The common measure of performance for all types of energy sources is simply the energy expenditure. Hence, an alternative method to bookkeeping the amount of fuel burn during mission analysis is bookkeeping the rate of change of energy for each and all of the energy sources. This way, the amount of energy consumption and performance of each energy source can be tracked, regardless of the type. This approach requires modifications to some of the traditional mission analysis equations. More specifically, equations must be rewritten to account for the rate of change of energy rather along with rate of change of aircraft weight.

As discussed previously, there are several aircraft sizing and analysis tools in literature that can be used for mission performance analysis for conventional fuel burning aircraft, such as the Flight Optimization System (FLOPS) tool developed by NASA [73]. While FLOPS is capable of performing limited EA/HEA analysis, it only allows for a single propulsion type to be in use at any given point of time during the mission analysis. This means that the aircraft can only operate in full-electric or conventional mode (but not hybrid-electric), although the operation schedules are interchangeable [73, 74]. While some cumbersome workarounds (involving performing additional calculations outside FLOPS) have been reported in literature, the FLOPS tool in current form is not ideally suited for the analysis of hybrid-electric propulsion systems. The current chapter lays out an approach to generalize mission performance analysis, so that it can be utilized regardless of the aircraft or propulsion type.

The following sections of this chapter describes the approach taken and the code written

to analyze mission performance of a generic vehicle. The code tracks down the required and available energy throughout each given mission leg by evaluating the state of the vehicle. In this context, a mission leg is defined by the flight interval between two consecutive user-defined points within a segment, as depicted on a notional mission profile in Figure 6.1. The state of the vehicle is evaluated at each point by utilizing some general performance characteristics functions for the propulsion system and aerodynamics.

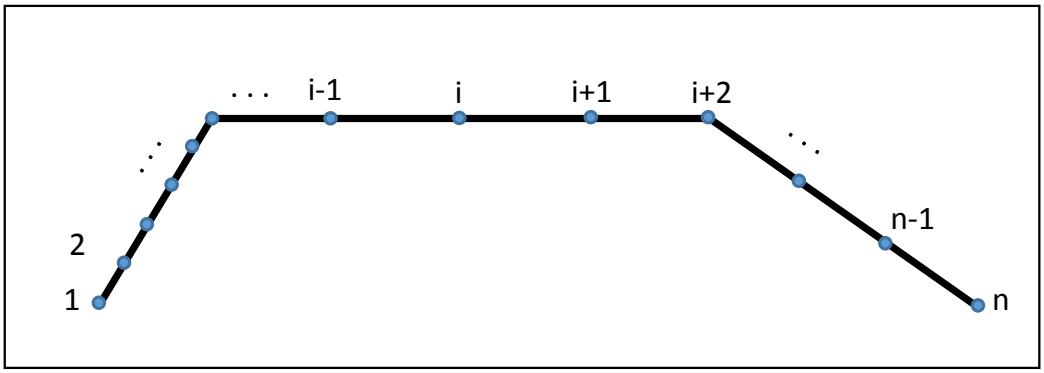

Figure 6.1: A notional mission profile divided into several mission legs.

Note that the mission segment points do not have to be evenly distributed throughout the segment. Moreover, the number of mission legs at each segment and the distance between two successive points can be modified by the temporal step sizer if and when necessary. Further discussions related to the temporal step sizer are provided in Chapter 8.

The next sections explain the main idea behind the approach, the performance characteristics functions and three main flight segments, namely, climb, cruise and descent. The resulting mission performance analysis approach is applicable to any type of propulsion device and energy source.

6.1 An Energy-based Approach

The basis of the mission performance analysis approach derives from energy methods, more specifically what is referred to as the *energy reservoir analogy* [107, 108]: the fact that the rates at which the propulsion system and aerodynamic drag respectively supply

and remove energy from the vehicle system yields the rate of change of its total mechanical energy (sum of kinetic and gravitational potential energies), as shown in Eqn. 6.1.

$$\vec{T} \cdot \vec{V} + \vec{D} \cdot \vec{V} = \frac{d}{dt}\left(Wh + \frac{1}{2}\frac{W}{g}V^2\right) \tag{6.1}$$

In Eqn. 6.1, the dot product of thrust T and velocity V is referred to as the propulsive power. For the case where the thrust vector is exactly or closely aligned with the velocity vector, the simplification $\vec{T} \cdot \vec{V} = TV$ occurs. Henceforth, these two terms are shown as grouped (TV). Since the drag force, by definition, is aligned opposite to the velocity vector, the simplification $\vec{D} \cdot \vec{V} = -DV$ occurs. The rate of energy dissipation to drag is henceforth expressed as the product of drag and velocity, (DV).

The difference between (TV) and (DV) is called the *excess power* (P_s), and can be modulated through the vehicle's control effectors to change the energy state of the aircraft, through a change of kinetic and/or gravitational potential energy. Depending on the flight phase and the intended manner in which it is to be flown, the excess power can be suitably apportioned to kinetic and potential energy rates, thus allowing computation of vehicle acceleration (dV/dt) and rate of climb (dh/dt). The numerical integration of these time derivatives along with time derivatives of vehicle mass and energy consumption rate (described subsequently) form the core of the mission performance analysis method.

6.2 Characterization of Propulsion System Performance

The modeling of the propulsion system performance is embedded within a function Φ_{psp}, which is responsible for computing the propulsive power (TV), the rate of change of vehicle mass (dm/dt), the rate of change of vehicle energy content (dE/dt), and the actual power split between power sources (λ_{act}).

$$\left[(TV), \frac{dm}{dt}, \frac{dE}{dt}, \lambda_{act}\right] = \Phi_{psp}\left[(TV)_{req}, h, M, P_{off}, Engine\ Deck\right] \tag{6.2}$$

It should be noted that if the propulsion system architecture or operation mode is such that no mass change occurs, then $dm/dt = 0$. Moreover, if the vehicle contains multiple energy sources, then the energy E comprises multiple elements: $E = \{E_1, \ldots, E_n\}$. To compute these output quantities, evaluation of the function Φ_{psp} requires the required propulsive power $(TV)_{req}$, the flight condition (altitude h, Mach number M), the non-propulsive (secondary) power off-take P_{off}, engine deck information of all engines and motors on the vehicle.

Power split among the power sources at each mission leg λ is obtained within the propulsion system performance function from the power split optimizer which was described in Chapter 4.2. The propulsion system performance function distributes the amount of required propulsive power $(TV)_{req}$ among all power sources (designated by the subscript j) according to the related power split λ_j for each mission leg. There are three logical conditions against which demanded power from every power source $(TV)_{req,j}$ is checked:

1. If the available power at a given flight condition or any other operational constraints have not been reached, then the propulsive power is nominally equal to the demanded propulsive power: $(TV)_j = (TV)_{req,j}$

2. If the demanded propulsive power exceeds the available power $(TV)_{av,j}$, then the propulsive power is set to be the available power: $(TV_j) = (TV)_{av,j}$

3. If the demanded power or power split is null, then this is interpreted as engine idle condition and the propulsive power is equal to the engine idle power at given flight condition: $(P)_j = (P)_{idle,j}$

The manner in which the flight condition ($h,\ M$) affects the propulsion system performance is highly dependent on the nature of the propulsion system architecture, i.e., the nature of power lapse (if present) and the impact of flight condition on propulsion system performance (which may affect both dm/dt and dE/dt).

Non-propulsive (secondary) power off-takes, the extraction of power from the propulsion system to satisfy vehicle power requirements other than that required for propulsion, always degrade propulsion system performance (affecting dE/dt and dm/dt for a given (TV)). If maximum available power is already demanded, then secondary power off-takes result in a reduction of the effective propulsive power output, and thus degradation in the point performance (dh/dt and/or dV/dt).

It should also be noted that the above formulation can be used to model any propulsion system, including fuel-burning internal combustion and gas turbine engines, electrically powered systems, as well as hybrid systems (through varying relationships contained within Φ_{psp}).

6.3 Characterization of Aerodynamic Drag

The aerodynamic performance calculations are embedded within a function Φ_{aero}, which is responsible for computing the vehicle drag (D), lift (L), non-dimentional drag and lift coefficients (C_D and C_L respectively), lift-to-drag ratio (L/D) and the rate of energy dissipation due to aerodynamic drag (DV).

$$\left[(DV), D, L, C_D, C_D, \frac{L}{D}\right] = \Phi_{aero}\left[W, h, M, \frac{dh}{dt}, Drag\ Polar\right] \tag{6.3}$$

The rate of energy dissipation due to aerodynamic drag (DV) is modeled using the drag characteristics of the vehicle in question. The general approach (also followed in this work) is to model the aerodynamic efficiency of the vehicle through a *drag polar* which expresses the non-dimensional drag coefficient C_D as a function of the non-dimensional lift coefficient C_L, i.e., $C_D = f(C_L, \ldots)$.

First, the lift coefficient C_L is computed from Eqn. 6.4:

$$\mathbf{C_L} = \frac{W\cos(\gamma)}{\frac{1}{2}\rho V^2 S_{ref}} \tag{6.4}$$

where ρ is air density, S_{ref} the reference area based on which the lift coefficient C_L is defined and the flight path angle γ is given by Eqn. 6.5:

$$\gamma = \arcsin\left(V\frac{dh}{dt}\right) \tag{6.5}$$

Once C_L is known, the corresponding C_D is found from the drag polar information of the vehicle in question. Finally, (DV) product is then given by Eqn. 6.6:

$$(DV) = \frac{1}{2}\rho V^3 S_{ref}\ C_D, \tag{6.6}$$

6.4 Mission Segment Functions

The mission segment functions are used to calculate the vehicle performance for climb, cruise and descent segments. For each of these segment, the segment profiles can scheduled by specifying velocity and altitude at various points within the segment, or a suitable segment profile can be chosen as discussed in the following sections.

As briefly explained in the beginning of this chapter, each segment is discretized by a number of control points. These points will be henceforth referred as segment points. The vehicle state and performance are calculated at each one of these points. This information is carried on to the final output as the mission history. Unless the number of segment points (np) are specified by the user, each segment is set to have 50 segment points by default, arbitrarily.

The following paragraphs describe the calculation methods used in each mission segment.

6.4.1 Climb Segment

The climb segment can be initiated by specifying the starting altitude, starting velocity, end altitude, and a power split schedule among the propulsion devices. The end altitude can be

a specified numerical value, the best cruise altitude or the best endurance altitude.

There are three climb strategies embedded in the code: the climb profile can be (i) optimized to fly at "minimum time to climb" conditions, (ii) optimized to fly at "minimum energy (fuel) to climb" conditions, or (iii) specified in terms of airspeed.

Minimum Time and Minimum Energy to Climb

Unless an airspeed profile is specified, the climb profile can be solved for minimum time or energy to climb to a certain altitude. The minimum time to climb case corresponds to the maximum rate of climb, and hence the fastest way to climb to a given altitude. Minimum energy to climb (which is the generalized form of minimum fuel to climb in the conventional sense) represents the most economic way to climb to a given altitude in terms of source allocation.

The climb segment deals with the general case of equilibrium or accelerated rate of climb at any climb angle. For this purpose, energy methods have been utilized.

The climb segment is discretized by energy height. Energy height is the weight specific energy of the aircraft and given by Eqn. 6.7. Some contours of constant energy height H_e are generated on an altitude-Mach number map illustrated in Fig. 6.2.

$$\mathbf{H_e} = h + \frac{V_\infty^2}{2g} \tag{6.7}$$

Since the altitude-Mach number map consists of constant energy height curves, the curves can be discretized by picking constant energy height increments (i.e. equal distance curves) where the increments (ΔH_e) are given by Eqn. 6.8:

$$\mathbf{\Delta H_e} = \frac{h_{final} - h_{initial}}{np_{climb}} \tag{6.8}$$

where h_{final} and $h_{initial}$ are the initial and final altitudes at the beginning of the segment respectively, and np_{climb} is the number of climb segment points.

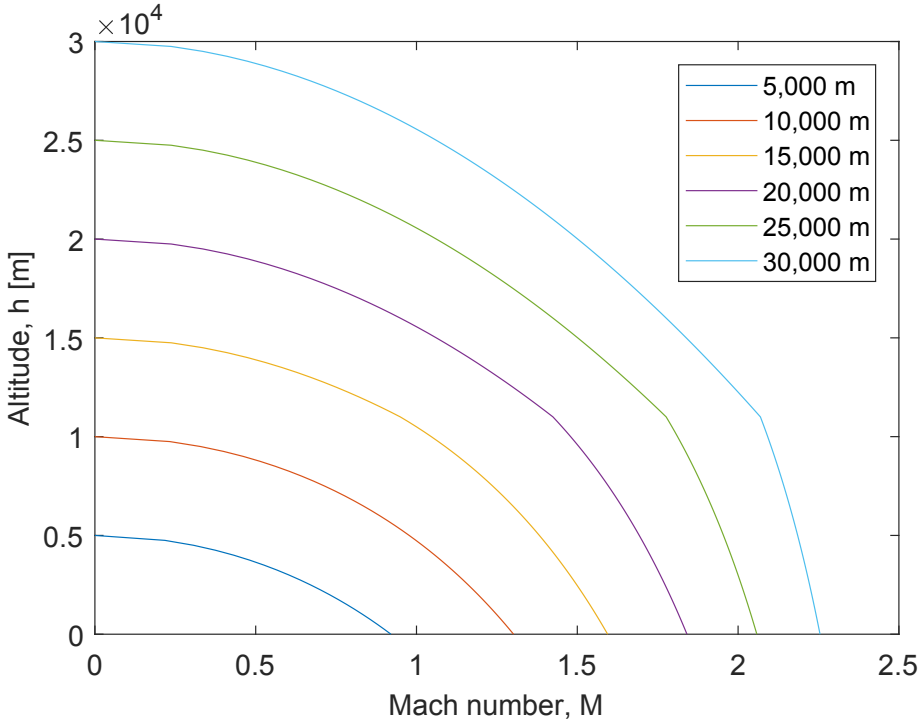

Figure 6.2: Contours of constant energy height on an Altitude-Mach number map.

The minimum time to climb can be found by selecting a path where the excess power P_s is maximized at each point of the energy height map, as given in Eqn. 6.9. The minimum energy to climb profile can be obtained by maximizing the energy function given in Eqn. 6.10.

$$\mathbf{f_{min\ time}} = P_s \tag{6.9}$$

$$\mathbf{f_{min\ energy}} = -\frac{P_s}{\left(\frac{dE}{dt}\right)_{avg}} \tag{6.10}$$

where the denominator in Eqn. 6.10 is the average rate of change of energy at the end and beginning of a mission leg (i.e. two consecutive points in the mission).

The optimization can be done using any suitable optimization method of choice. One simple and fast yet accurate way to find the flight conditions which maximizes the objective

functions is the following approach.

The maximum change in velocity from one constant energy height curve to another is generally not expected to be drastic. Similarly, there exists a minimum velocity limit at each altitude which aircraft is not allowed to fly under. Hence, searching for the optimum altitude-Mach number combination at every point of a given constant energy height curve is unnecessary. Instead, the optimization problem can be solved within a cone of altitude-Mach number combinations where the edges of the cone are defined by the minimum and maximum velocity values determined by a pre-specified scaling factor. This approach is illustrated in Fig. 6.3.

On Fig. 6.3, assume that the an aircraft is to fly from an energy height of 10,000 m to 15,000 m. The initial conditions are known (shown with a red dot on the 10,000 m energy height curve), and the final conditions that maximizes the objective function are to be found. The minimum and maximum velocities allowed at the next energy height level of 15,000 m are obtained through the scaling factor. Then, a cone is created by drawing two lines which represent the velocity limits (shown by black dashed lines) from the red point to the next energy height. Any altitude-Mach number combination within this cone is a candidate solution for the optimization problem. Once the solution is found (depicted as a yellow dot on the energy height curve of 15,000 m), new limits on the velocity are obtained to search for the solution at the next energy height curve. This operation continues until the final altitude is reached.

The velocity scaling factor can be adjusted depending on the type of the vehicle. For a conventional commuter, a drastic change in velocity is not expected to happen and hence the factor can be set small (e.g. a maximum of 20% increase from the current value); whereas for a jet fighter a large factor might be needed due to possible instantaneous acceleration and deceleration maneuvers.

The optimization is executed by creating a vector of equally spaced velocity testing points within the cone. The reason for vectoring lies within the selection of the modeling

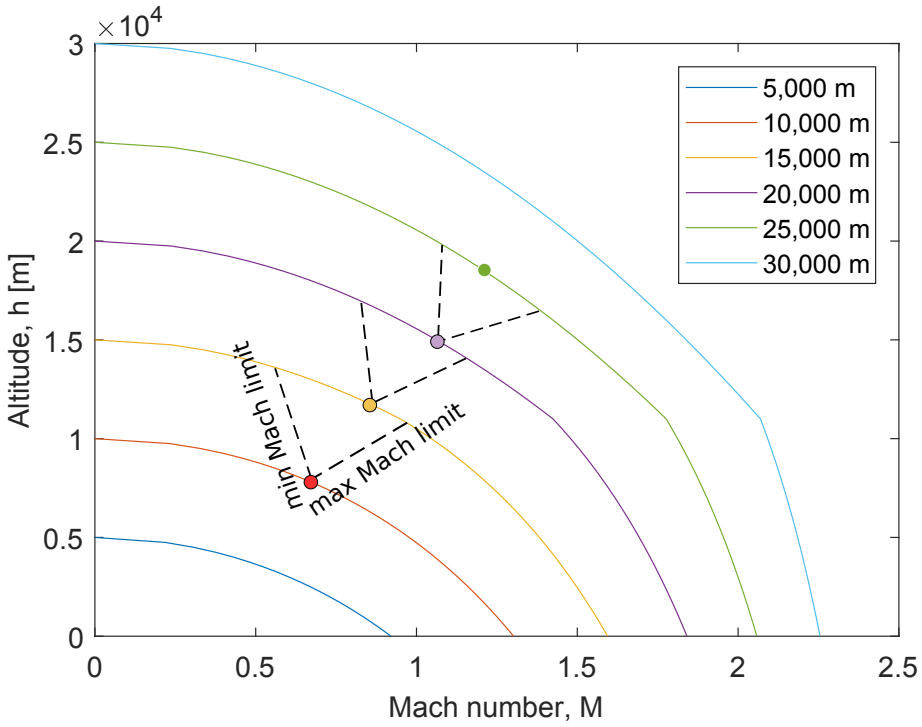

Figure 6.3: Search for the altitude-Mach number combination that maximizes the objective function at a constant energy height curve. Points are selected arbitrarily for demonstration purposes.

tool. Matlab handles vector quantities very efficiently, and the author found that this approach works much faster than Matlab's widely-used nonlinear programming solver code *fmincon* while producing accurate results to a significant degree.

The vector of velocity testing points are then used to calculate the corresponding altitude at the next energy height by solving Eqn. 6.7 for altitude h. Once the velocity testing points and the corresponding altitudes which represent the velocity and altitude at the end of the current mission leg are known, aerodynamic properties (including drag and hence demanded power DV), propulsion system performance (including available power TV and time rate of change of mass dm/dt) can be obtained. The excess power at the next energy height is given by Eqn. 6.11:

$$\mathbf{P_s} = \frac{TV - DV}{W} \tag{6.11}$$

Then, mean excess power which is assumed to be effective between the old and the new energy heights is computed. Since the mean excess power is equal to the time rate of change of energy height (see Eqn. 6.12), time needed to jump between old and new energy heights (dt) is obtained.

$$\mathbf{P_s} = \frac{dH_e}{dt} \tag{6.12}$$

Finally, the rate-of-climb (dh/dt) between the old and the new energy heights is calculated. The calculated rate-of-climb must be greater than a specified service ceiling. A convergence criterion is defined to confine the relative error between the initially guessed and the calculated rate-of-climb values to a desired percentage. Once the calculated value converges to the guessed value, the velocity testing point and the corresponding change in altitude which maximize the objective function in equations 6.9 or 6.10 among the other testing points are selected to be the optimum velocity and altitude at the end of the mission leg. This procedure is followed for each mission leg within the climb segment, until the final altitude is reached.

Specified Airspeed Profile

If the climb profile is specified in terms of airspeed, and the final altitude is given, then the segment can be linearly discretized by picking constant altitude increments (Δh) from the initial to the final altitude, as shown in Eqn. 6.13:

$$\mathbf{\Delta h} = \frac{h_{final} - h_{initial}}{np_{climb}} \tag{6.13}$$

Then, the corresponding energy height at each point in the segment is calculated from Eqn. 6.7. The change in energy height from one mission leg to another is computed using Eqn. 6.8. The propulsion system performance (including available power TV and time rate of change of mass dm/dt) is obtained from the Φ_{psp} function.

Similar to the previous climb conditions, the rate-of-climb (dh/dt) is unknown at this

point. Hence, an initial guess is made assuming that the rate-of-climb remains constant throughout a given mission leg. Using this guessed value and the known initial velocity at the beginning of a mission leg, current aerodynamic properties (including the drag and hence demanded power DV) are calculated. The specific excess power at every point in the segment is calculated from Eqn. 6.11.

Next, Eqn. 6.12 is solved for the time spent climbing from one mission point to another. Finally, the rate-of-climb (dh/dt) for each point in the segment is calculated. The procedure is iterated until the calculated rate-of-climb converges to the guessed value within a chosen margin of error. The climb ends when the end altitude or a previously defined service ceiling is reached.

Hybridization Factor Definition

In the climb segment, the hybridization factor λ_i for a power source i is defined as the ratio of the desired output power (P_i) to its respective sea level rated power ($P_{SL,\,rated}$), as described in Eqn. 6.14. In that sense, each λ_i is independent of the utilization of the remaining power sources.

$$\lambda_{i,\,climb} = \frac{P_i}{P_{SL,\,rated}} \tag{6.14}$$

Note that the actual available power for a setting of $\lambda_{i,climb}$ depends on the lapse characteristics of the power source in question. Thus, for an IC engine, there will be a power lapse with altitude. However, this will not be the case for an electric motor.

6.4.2 Cruise

The cruise segment is initiated by specifying the starting altitude, starting velocity (both of which can be fed from the end point of the previous segment, if applicable), and a power split schedule among the propulsion devices.

If a desired cruise velocity which is not equal to the segment's initial velocity is specified, then the vehicle needs to accelerate or decelerate to the desired velocity to begin

cruising.

The cruise segment can be defined either by providing a velocity-altitude schedule, or by choosing a desired optimization objective: (i) best specific air range, or (ii) best endurance.

Best Specific Air Range

A general relation to calculate specific air range (SAR) can be obtained as follows. For an airplane in steady, level flight, the time rate of change of the horizontal distance covered over the ground (ds) is given by the velocity of that airplane, assuming stationary atmospheric conditions. Hence, ds is given by Eqn. 6.15.

$$\mathbf{ds} = V dt \tag{6.15}$$

Specific air range is defined for traditional fuel consuming aircraft as the ratio of the distance flown per unit of fuel consumed (i.e., ds/dW_f).[109] Expanding this definition by substituting Eqn. 6.15 results in the following relation, as given in Eqn. 6.16:

$$\frac{\mathbf{ds}}{\mathbf{dW_f}} = \frac{ds/dt}{dW_f/dt} = \frac{V}{dW_f/dt} \tag{6.16}$$

where dW_f is the change in fuel weight.

Eqn. 6.16 can be integrated and solved for the distance s by substituting thrust specific fuel consumption definition where thrust T is equal to aircraft drag D and aircraft weight W equals to lift L (due to the steady level flight condition). This approach yields the well-known *Breguet range equation*, which is shown in Eqn. 6.17 [110].

$$\mathbf{R} = \frac{V}{c_t}\frac{L}{D}\ln\frac{W_0}{W_1} \tag{6.17}$$

However, the Breguet range equation does not apply to aircraft which does not burn fuel. Hence, one needs to modify the SAR definition and the relation given in Eqn. 6.16 to

include any type of propulsion system and energy source, regardless of fuel consumption. Since energy is the common measure of performance for both fuel burning and electric propulsion systems, the SAR definition can be modified as:

*Specific air range (SAR) is the ratio of the distance flown per unit **energy** consumption.*

$$\mathbf{SAR} = \frac{ds}{dE} = \frac{V}{dE/dt} \tag{6.18}$$

The energy term E in Eqn. 6.18 represents the total amount of energy, including chemical energy (e.g. conventional fuel) and electrical energy (e.g. rechargeable batteries).

When it is desired to maximize the aircraft range in the most efficient way possible, the optimum flight conditions (in terms of altitude and velocity) can be found by maximizing the right-hand-side of Eqn. 6.18. Then the objective function becomes:

$$\text{maximize } \mathbf{f_{SAR}} = \frac{V}{dE/dt} \tag{6.19}$$

Best Endurance

For aircraft with conventional propulsion systems, endurance is defined as the amount of time that an airplane can stay in the air on one load of fuel.[110] Similar to the previous discussion about SAR, this definition can be generalized as:

*Endurance is the amount of time that an airplane can stay in the air limited by the total amount of **energy** on-board to spend.*

Thus, this relation can be interpreted as the following differential equation:

$$\mathbf{dt} = \frac{dE}{dE/dt} \tag{6.20}$$

where E represents the total energy. In Eqn. 6.20, the total amount of available energy at any given time is fixed. Hence, the best endurance, i.e. maximum dt can be found by the

following objective function:

$$\text{maximize } \mathbf{f_t} = \frac{1}{dE/dt} \tag{6.21}$$

A Table Look up for the Cruise Performance

Prior to starting the mission analysis, a look-up table for the cruise segment is generated. This lookup table consists of optimum velocity and altitude values over a wide range of aircraft weights for all objective functions. This way, any kind of velocity or altitude optimization is avoided during the flight.

If the weight of the aircraft changes by burning fuel or by any other means, then the aircraft might need to change its speed and/or altitude to maximize any of the objective functions given in Eqns. 6.19 or 6.21. Since the lookup table provides a range of different aircraft weights that might occur during cruise, the target velocity and/or altitude can be easily found by its matching weight.

There are three types of lookup tables generated for each of the objectives, making a total of six tables. This means that the target values for best SAR ensures that Eqn. 6.19 is maximized for the given given conditions. Similarly, the target values for best endurance ensures that Eqn. 6.21 is maximized for the given given conditions. The given conditions vary among the three types of tables as:

- Optimum altitude and velocity as a function of mass:

  This table lists the target velocity V_{target} and target altitude h_{target} as a function of aircraft mass, as shown in Eqn. 6.22. The table is generated by testing a range of realizable velocity and altitude combinations for each aircraft mass condition (V_{test}, h_{test}), and picking those combinations which optimize the associated objective function as

the target values for the related aircraft mass.

$$(\mathbf{V_{target}}, \mathbf{h_{target}}) = f(Mass) \tag{6.22}$$

The steps taken in between to obtain the target values from the testing values are depicted in Fig. 6.4. First, the required power (DV) is computed by the aerodynamics function Φ_{aero} for all tested altitude and velocity values at each mass condition. Then, the resulting required power (DV) information is fed to the propulsion system performance function Φ_{psp} to obtain the rate of change of energy dE/dt information. The results are then compared and the two velocity-altitude combinations which separately maximizes the objective functions at a given aircraft mass are listed in the lookup tables.

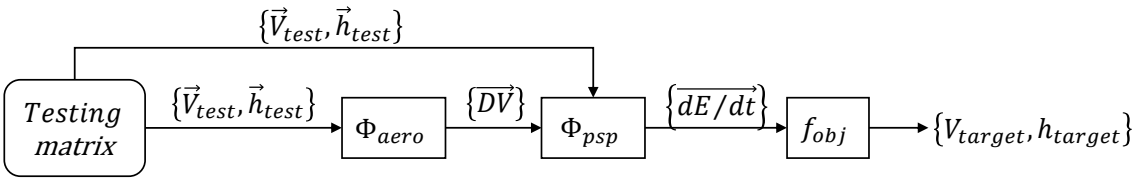

Figure 6.4: Illustration of the computation steps to create a velocity-altitude lookup table for a given aircraft mass. The testing values are shown as a vector of velocity and altitude, and form a velocity-altitude matrix where each row is a realizable velocity-altitude combination and represents a candidate velocity and altitude target.[1]

- Only the end altitude is specified:

  This table is created when an altitude schedule for the cruise segment is given by the user. The table lists the target velocity V_{target} as a function of aircraft mass and altitude, as shown in Eqn. 6.23.

$$\mathbf{V_{target}} = f(Mass, h) \tag{6.23}$$

[1]Although each row of the testing matrix can be tested one by one instead of in a vector format (i.e. sequentially), this format was favored here due to Matlab's efficiency in handling vectors and matrices.

The computation steps are the same as the previous case, except this time altitude is a given and the testing matrix shown in Fig. 6.4 is actually a vector of candidate velocity values.

- Only end velocity is specified:

  Similar to the previous case, this table is created when a velocity schedule for the cruise segment is given. The table lists the target altitude h_{target} as a function of aircraft mass and velocity, as shown in Eqn. 6.24.

$$\mathbf{h_{target}} = f(Mass, V) \tag{6.24}$$

  Again, computation steps are the same as the previous case, except this time velocity is a given and the testing matrix shown in Fig. 6.4 is actually a vector of candidate altitude values.

The lookup tables are used with three options based on what information about velocity and altitude are available. These options are:

- Neither the end altitude nor the end speed is specified:

  In this case, there are two degrees of freedom. Both the velocity and altitude is chosen from the first lookup table to optimize the objective functions at each point in the segment.

- Only the end altitude is specified:

  Since the initial and final altitude of the segment are known, the segment is discretized by np_{cruise} number of linearly spaced altitude points. The target velocity is then obtained from the second lookup table by matching both the altitude and aircraft mass information at every point.

- Only end velocity is specified:

Similar to the previous case, the segment is discretized by np_{cruise} number of linearly spaced velocity points. The optimum altitude distribution which optimizes the objective function is obtained from the third lookup table at the given velocity and weight values is found. It should be noted that if the end velocity is specified in terms of Mach number or equivalent air speed, then the corresponding true air speed is calculated within a velocity update function which is called at each new altitude the vehicle climbs or descents to.

To be able to use the lookup tables, the weight of the aircraft at each point in the cruise segment must be known. This initiates an iteration process, since the aircraft weight may or may not change from one mission leg to another, and hence the optimum cruise velocity and/or altitude.

The iteration process begins with guessing the aircraft weight at each point in the segment. Then, the velocity and altitude profiles are obtained from the user-specified schedules or from lookup tables based on the chosen cruise profile, as explained previously.

The initial guesses for the aircraft weight are used to calculate aerodynamic and propulsion system performance embedded within the aforementioned Φ_{aero} and Φ_{prop} functions, respectively. The propulsion system performance outputs the actual time rate of change of mass (dm/dt) at the beginning and the end of each mission leg for the given flight conditions. Hence, the average change in weight at each mission leg is easily computed. The velocity and altitude profiles are then updated with the ones corresponding to the new aircraft weight information.

Three convergence criteria are defined to confine the relative error between the initially guessed and the calculated values of aircraft weight, velocity and altitude. The iteration process is continued until all three calculated values converge to the guessed values for each point in the segment.

Hybridization Factor Definition

The cruise segment definition of the hybridization factor differs from the one defined in the climb segment. In this segment, λ_i for each power source i is defined as a percentage of the required power (TV_{req}), as shown in Eq. 6.25. Therefore, the sum of λ_i must be equal to 1 for unaccelerated level flight at a given altitude and velocity.

$$\lambda_{i,\,cruise} = \frac{P_i}{TV_{req}} \tag{6.25}$$

6.4.3 Descent

The descent segment can be initiated by specifying the starting altitude, starting velocity (both of which can be fed from the end point of the previous segment, if applicable), end altitude, and power split of the propulsion devices.

The segment is first discretized within the specified initial and final altitudes according to the number of segment points. Then a descent profile is chosen to calculate or optimize the vehicle state at each one of these points.

If the chosen profile starts with a specified initial speed other than the initial velocity at the beginning of the segment, the vehicle needs to match that speed before first. If the specified descent velocity is less than the current segment's initial velocity, then the vehicle will be decelerated at constant altitude until the desired descent velocity is reached. If the specified descent velocity is greater than the current segment's initial velocity, then the vehicle must dive to gain the necessary airspeed. The descent will commence only after the specified initial speed is reached.

There are four profile options for this segment: (i) a given rate of descent, (ii) a given velocity, (iii) minimum equilibrium glide angle, (iv) minimum rate of descent.

Specified Rate of Descent

The rate of descent (also known as the sink rate; shown as dh/dt with a negative value) can be specified as a varying or a constant ratio throughout the segment. In this case, the aerodynamic and propulsion system performance are simply calculated one segment point at a time, each time using the state of the flight information from the previous point.

Specified Descent Velocity

In this case, the segment is flown with a constant specified velocity. First, the energy height at each point of the segment is calculated from Eqn. 6.7. Then, an iteration takes place to converge on the rate of descent.

The iteration process begins with guessing the rate of descent at every segment point and then calculating the aerodynamic and propulsion system performance throughout the segment. The instantaneous specific excess power (P_s) for each point is computed from Eqn. 6.11. Then, the mean excess power is obtained by averaging between pairs of consecutive points. The mean excess power is used to calculate the time needed to jump between old and new energy heights by solving Eqn. 6.12 for dt. Finally, the actual dh/dt for each segment point is calculated from the altitude difference and the time interval between each consecutive points. The iteration continues until the guessed rate of descent value converges to the computed value.

Minimum Equilibrium Glide Angle

For an unpowered aircraft in descending flight , the equilibrium glide angle (θ) is strictly a function of lift-to-drag ratio, as shown in Eqn. 6.26. [110].

$$\tan\theta = \frac{1}{L/D} \tag{6.26}$$

Observing Eqn. 6.26, it is obvious that the minimum equilibrium glide angle is obtained

at maximum lift-to-drag ratio, $(L/D)_{max}$. As discussed previously, the lift-to-drag ratio for a given state of flight can be obtained from the drag polar of the vehicle using the aerodynamic performance function, Φ_{aero}. Hence, the maximum lift-to-drag ratio can be found by testing a range of vehicle speed at the given flight conditions.

To fly at $(L/D)_{max}$, the vehicle must fly at a specified velocity called the equilibrium glide velocity V_∞ [110]. This means that the velocity corresponding to the target (i.e. maximum) lift-to-drag ratio should be the descent velocity. Although the equilibrium glide angle does not depend on altitude or wing loading, the equilibrium glide velocity does, as it can be seen from Eqn. 6.27.

$$\mathbf{V}_\infty = \sqrt{\frac{2\cos\theta}{\rho_\infty}\frac{W}{S}} \tag{6.27}$$

Since the target (L/D) is kept constant, the corresponding C_L remains constant along the gliding path. However, the wing loading and altitude (thus the air density ρ_∞) changes during descent, and so does the equilibrium glide velocity. Therefore, at every point of the mission segment, V_∞ must be updated such that the target C_L is achieved.

The next step after obtaining the initial target airspeed is to iterate and converge on the rate of descent that will result in the minimum gliding angle at every point of the segment. The iteration process begins with guessing the aircraft weight and velocity at each point. Then, the same iteration steps described in *Specified Descent Velocity* are followed to obtain the actual rate of descent, dh/dt. The only difference is that at the end of each iteration, the descent speed V_∞ is updated to keep C_L constant at the targeted value.

Minimum Rate of Descent

The rate of descent is proportional to the power required for steady, level flight (DV), as given in Eqn. 6.28. Therefore, the minimum rate of descent occurs at minimum (DV).

$$\frac{\mathbf{dh}}{\mathbf{dt}} = \frac{DV}{W} \tag{6.28}$$

The minimum (DV) is obtained when $L^{3/2}/D$ is maximum. Similar to the previous case, the C_L value which makes $L^{3/2}/D$ maximum is selected as the target C_L. The target C_L value does not depend on aircraft weight or altitude, and hence remains constant; whereas the corresponding airspeed does. Therefore, the aircraft velocity is updated to give the target C_L at each point in the segment. The rest of the calculations (and iterations) are the same as the previous case. The resulting dh/dt is the minimum rate of descent.

Hybridization Factor Definition

The hybridization factor λ definition for the descent segment can be the same as the cruise segment λ definition. This means that for an unpowered descent, λ would be zero.

6.4.4 Convergence on Mission Range or Endurance

If the cruise distance is provided in the mission definition rather than a cumulative mission distance or total time, then an iteration over the mission segments is not necessary. However, if a mission range or endurance requirement is to be fulfilled and the cruise distance is unknown, then an iteration over the cruise distance is necessary.

As this is a forward marching approach, any target mission range or endurance criterion is applied only after all segment analyses within the mission are performed. For the initial analysis only, a cruise distance is guessed. Once all the mission segments are flown, the cumulative distance flown or total time spent is calculated and compared with the target range or endurance. The difference between the calculated and the target value is interpreted into cruise distance for the next iteration process. Iteration continues until the calculated value converges to the target mission range or endurance.

6.5 Chapter Summary

This chapter provided the details of an energy-based mission performance analysis. The main idea was to keep the mission analysis calculations as generic as possible, so that the

mission performance any kind of flying vehicle with any power and energy source could be analyzed.

Thus, an energy-based approach was deemed suitable rather than the traditional weight-based approach due to the unconventional energy sources. Energy expenditure is the common measure of performance for all energy sources, regardless of whether the weight of an energy source changes or not. Hence, all analyses were boiled down to the rate of change of energy for all energy sources on the vehicle.

Another important aspect of this energy-based approach is that there is no configuration-specific assumption. For instance, no small angle approximation is made in any of the calculations. The small angle approximation is generally made for steady, unaccelerated climbing flight, by assuming that the cosine term in the drag expression equals to 1. Anderson [110] discusses that this assumption yields very accurate results for climb performance for climb angles up to 50° degrees. However, the energy-based method provides accurate results for any climb angle (even 90° angle, i.e. vertical flight). This provides flexibility in terms of vehicle definition as even a vehicle which is not limited to wing-borne lift, such as helicopters or VTOL vehicles.

This generic mission analysis method provides flexibility in terms of hybridization, i.e. number of different power and energy sources. Various configurations can easily be handled within the mission performance analysis through the source categorization and inter-relationship matrices defined in Section 5.5 of this chapter. Any type of sources can be mixed and used together or separately. This is the main capability that could not be obtained from FLOPS.

It should be noted that any optimization made within the flight segments are done only on kinematics. Vehicle sizing and power split optimization are done outside the mission performance analysis block.

Numerous mission metrics are book-kept at each point in the mission and reported altogether as a mission history. These metrics include (but not limited to) time stamp,

altitude, velocity (in terms of TAS, EAS, Mach number and ground speed), energy height, distance, acceleration or deceleration (dV/dt), rate of climb or descent (dh/dt), flight path angle, required power and thrust, available power and thrust, specific power, aerodynamic data (L, D, C_L, C_D, etc.), aircraft weight, mass change (dm) and time rate of change of mass (dm/dt) for *each* fuel-burning energy source, total energy (E) and time rate of change of energy (dE/dt) for *each* energy source, and realized power split.

CHAPTER 7
ELECTRIC AND HYBRID ELECTRIC VEHICLE SIZING AND SYNTHESIS

This chapter demonstrates an example application of the methodological framework to serve as a proof of concept and substantiate the hypotheses 2 and 3 set in Chapter 3. To this end, a modeling and simulation tool was built in MATLAB and Simulink environments based on the proposed framework. It comprises of the approach explained in Chapter 4, subsystem models presented in Chapter 5, and the algorithms described in Chapter 6.

In the remaining chapters of this dissertation, it was demonstrated that this tool:

- Has all of the capabilities listed in the overarching hypothesis
- Enables the integration of EPGDS architectures into the aircraft sizing and synthesis process
- Allows for transient regime analysis at early design stages
- Evaluates and compares EPGDS architectures

7.1 Verification of the Sizing Capability (Experiment 2.1)

This section addresses the second research question (more specifically, question 2.1) and the validity of Hypothesis 2, both of which are revisited below:

Research Question 2: How can the EPGDS considerations be integrated into the electric and hybrid electric aircraft sizing process?

- **RQ 2.1:** How can the traditional mission performance analysis approach be modified to work with any type of propulsion system, regardless of the architecture and the energy storage type?

- **RQ 2.2:** How can the EPGDS characteristics be integrated into the modified sizing process?

- **RQ 2.3:** How can the technological sensitivities be captured?

Hypothesis 2: *EPGDS characteristics can be integrated into the EA/HEA sizing process through a parametric sizing and synthesis framework with the following properties:*

- *A generic mission analysis approach is implemented where the required energy to fly a mission profile is tracked and budgeted between different power sources of aircraft according to preset hybridization levels*

- *A component based weight estimation technique is used*

- *Aircraft sizing and synthesis process captures the sizing of EPGDS components based on required energy and/or power*

- *EPGDS models used in the framework are parametric, physics-based and dynamic*

- *The developed EPGDS models are utilized to capture the subsystem level impacts at aircraft and mission levels*

To test the validity of Hypothesis 2, a set of experiments were prepared. First, it must be proven that the sizing and synthesis tool built based on the proposed framework is capable of sizing a conventional aircraft and meeting its mission performance capabilities within a reasonable margin of error. To test this, the following experiment was conducted:

Experiment 2.1: *Model a baseline aircraft with a conventional propulsion system within a sizing and synthesis environment built based on the proposed framework. Show that the environment is capable of producing the same design mission performance characteristics of the baseline aircraft.*

Literature review conducted in Chapter 2 suggested that the initial receivers of the electric propulsion technology are the general aviation (GA) and urban air mobility (UAM)

type vehicles due to their low passenger capacity and light weight compared to other sizes of transport aircraft. Hence, the baseline aircraft to be used as a proof of concept was chosen to be a low-speed four-seater GA aircraft powered by a single piston engine, similar to the Cessna Model 172R [111]. The main reason behind imitating the Cessna 172 rather than any other GA type aircraft is publicly available data.

Table 7.1 lists the major specifications and performance parameters of Cessna 172R normal category. This model employs the Textron Lycoming IO-360-L2A engine, which is a 160 BHP internal combustion engine. It can carry up to 4 passengers (including the pilot), and the design range is 580 nautical miles with 53 gallons of usable fuel and at 80% power and a cruise speed of 122 knots. The reserve mission is 45 minutes long. [111]

Data pertaining to the baseline aircraft was first used to validate the developed sizing and weight estimation framework (Experiment 2.1). First, the specifications listed in Table 7.1 and the geometric properties of the aircraft were fed into the sizing and synthesis tool built based on the methodological framework.

Second, appropriate weight estimation techniques to estimate the weight of major vehicle components were chosen from the database which was created based on methods documented by Roskam [67] and NASA [72], as previously explained in Section 4.1.1. [1] Table 7.2 lists the methods used in estimating empty weight breakdown of the baseline aircraft. Calibration factors associated with each major weight item were used to obtain reasonable agreement between the predicted weights and the aircraft's published weight breakdown given in Reference 7.1.

In Table 7.2, the first column lists the major components corresponding to Table A2.1a in Reference [67]. The method used for each component is shown in the second column, where the Cessna method is given in Reference [67], and the FLOPS method in Reference [72].

Next, the power, thrust and energy sources of the baseline aircraft were modeled fol-

[1]The creation of this database was a joint effort with the co-authors of the paper cited in Reference [112].

Table 7.1: Cessna 172R performance and specifications [111]

Specification	**Value in British Units**	**Value in SI Units**
Maximum speed at sea level	123 kts	63.3 m/s
Cruise speed at 8000 ft, 80% power	122 kts	65.8 m/s
Range at specified cruise conditions	580 nmi	1074 km
Sea level rate of climb	720 ft/min	219.5 m/min
Service ceiling	13,500 ft	4,115 m
Stall speed (flaps up)	51 KCAS	26.24 m/s (CAS)
Stall speed (flaps down)	47 KCAS	24.18 m/s (CAS)
Max ramp weight	2457 lbs	1114.5 kg
Max takeoff weight	2450 lbs	1111.3 kg
Max landing weight	2450 lbs	1111.3 kg
Standard empty weight	1639 lbs	743.4 kg
Max useful load	818 lbs	371.0 kg
Wing loading	14.1 lbs/ft^2	68.7 kg/m^2
Power loading	15.3 lbs/hp	9.3 kg/kW
Fuel capacity	56 gal	0.22 m^3
Usable fuel capacity	53 gal	0.20 m^3
Engine power at 2400 RPM	160 BHP	119.3 kW
Propeller diameter (2-bladed)	75 in	1.9 m

Table 7.2: Methods used in estimating the aircraft empty weight breakdown

Component	**Method**	**Primary Equations in Reference**
Wing	Cessna	(5.2), (5.3)
Empennage	FLOPS	(48), (52)
Fuselage	Cessna	(5.23), (5.24)
Landing gears	Cessna	(5.38), (5.39)
Nacelle	N/A	N/A
Engine	FLOPS (modified)	(75)
Air induction system	N/A	N/A
Fuel system	FLOPS	(152)
Propeller	N/A	N/A
Engine installation	N/A	N/A
Flight control system	Cessna	(7.1)
Avionics and electrical systems	Cessna	(7.12)
Hydraulics	N/A	N/A
Furnishing	Cessna	(7.41)
Air conditioning	N/A	N/A
Anti-icing system	N/A	N/A

lowing the techniques explained in Chapter 5. For the power source model, the Lycoming IO-360-L2A engine data was gathered from the Operator's Manual [113]. The rated power of this engine is 134.2 kW (160 BHP) at sea level, and its power-to-weight ratio is 1.13 kW/kg. The performance of the internal combustion engine was modeled based on the part throttle fuel consumption (Figure 3-9 in Reference [113]) and sea level and altitude performance (Figure 3-25 in Reference [113]), as described in Section 5.3 of Chapter 5.

For the thust source, a propeller model similar to that of the baseline engine was generated using the in-house propeller modeling tool and techniques described in Section 5.4. The efficiency, torque constant and thrust constant curves as a function of advance ratio are shown in Figure 7.1. The main difference is that the actual aircraft utilizes a fixed-pitch, 2-bladed propeller [111], whereas the modeled aircraft utilizes a constant-speed one.

The energy source is 100LL Grade Aviation Fuel (Avgas). Avgas was modeled with a specific energy of 44 MJ/kg (12.2 kWh/kg) and a volumetric energy density of 0.718 kg/L. [114] The fuel tank is housed inside the wing. The internal available volume of the wingwas computed using Eq. 4.13.

Then, the interrelationship matrices for power, thrust and energy sources were established, as described in Section 5.5. The propulsion architecture of the baseline aircraft is a simple one, where one energy source (fuel) feeds a single power source (ICE) which drives a single thrust source (propeller). Hence, the energy source-power source matrix becomes: $B_{ESPS} = [1]$, and the thrust source-power source matrix becomes: $B_{TSPS} = [1]$.

The vehicle sizing was performed to meet the point performance characteristics of the baseline aircraft. Thus, the power-to-weight ratio and wing loading of the sized vehicles were required to match those of the baseline vehicle. These values are listed in Table 7.1.

Finally, the design mission was defined to reproduce the payload-range diagram of the Cessna 172R. Figure 5-9 in Reference [111] demonstrates the range profile of a 2450 lbs (fully loaded) Cessna 172R for various altitudes, velocities, and throttle settings with a 45 minutes reserve mission and 53 gallons usable fuel at standard temperature and zero

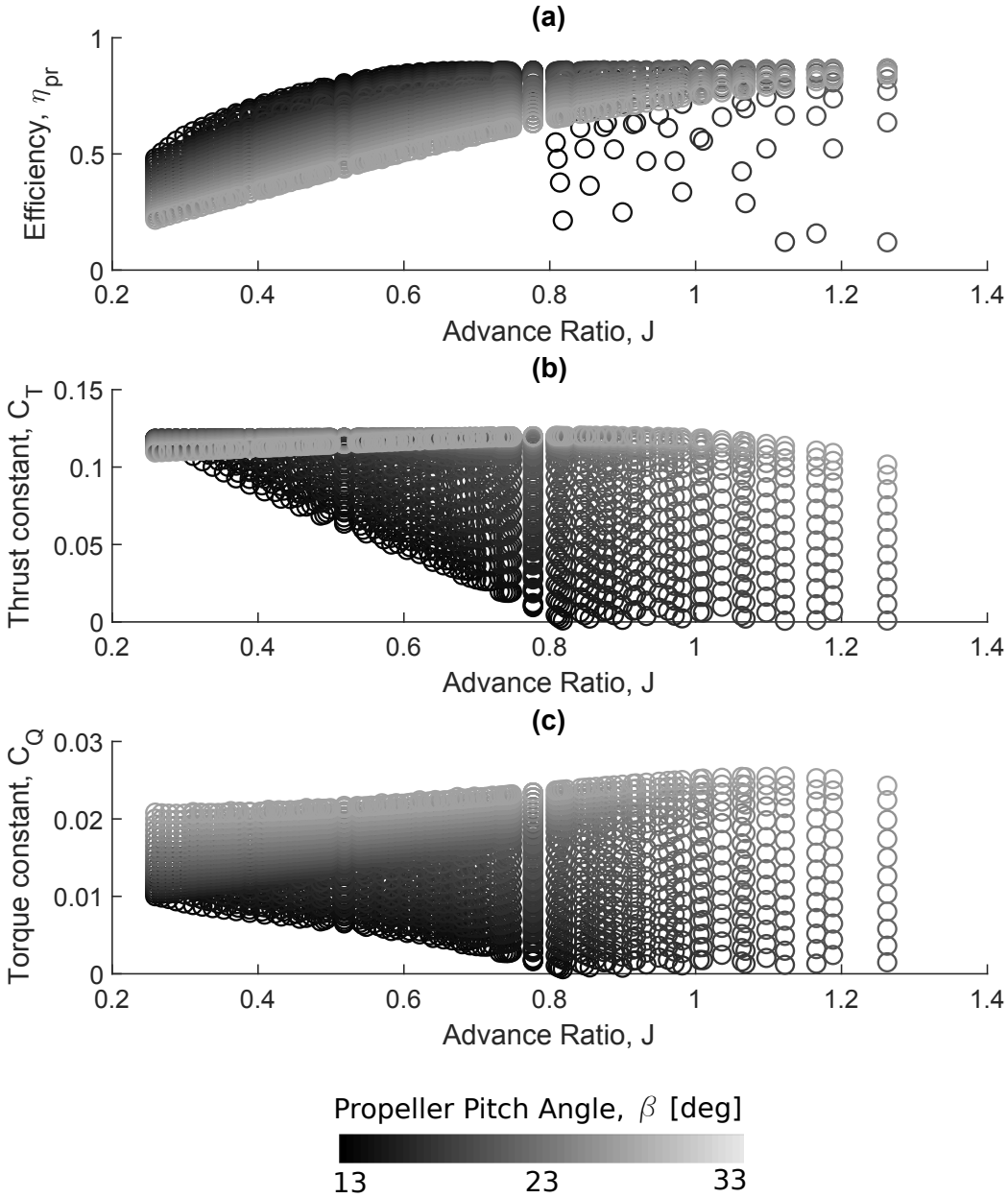

Figure 7.1: (a) Efficiency, (b) torque constant and (c) thrust constant curves of the 2-bladed propeller model plotted as a function of advance ratio and pitch angle. The change with pitch angle is demonstrated with the gray color scale.

wind conditions. The point which corresponds to 580 nautical miles (1074 km) of range at a cruise altitude of 8000 ft (2438 m) and a cruise speed of 122 knots (62.8 m/s, true air speed) at 80% power was selected as the cruise specifications of the design mission. The design and reserve mission profiles used to achieve an aircraft design similar to Cessna 172R is described by the parameters listed in Table 7.3.

There are three segments listed for each mission in Table 7.3: climb, cruise and descent. The mission performance evaluation methods and techniques used in these segments were previously explained in Section 6.4. There is no special consideration for takeoff and landing; but an additional 5% fuel burn was added in the required fuel calculations to represent the remaining fuel-demanding procedures, such as engine start, taxi, takeoff and landing.

As discussed previously, the hybridization factor stands for the power split schedule between the power sources. Since this mission is defined for the baseline aircraft with a single internal combustion engine, the hybridization factor was set to zero at all times. This setting means that the required power is solely provided by the internal combustion engine.

The “start velocity” and “end velocity” entries represent the scheduled initial and final velocities of the relevant segments, but not necessarily the actual ones. This is because of the fact that there cannot be a discontinuity between two consecutive segments as they share the same space and time point in the mission profile. Hence, the final velocity at the end of the previous mission segment naturally becomes the initial velocity at the very beginning of the next segment.

However, the scheduled values can be different than the actual values. For example, the final velocity at the end of the climb segment becomes the initial velocity of the cruise segment. If this initial velocity is less than the scheduled ”start velocity”, then the aircraft dives to reach to the higher scheduled velocity. Conversely, if the initial velocity is greater than the start velocity, the aircraft slows down.

If velocity or altitude does not take any value, which is shown as “not specified” in Table 7.3, then the start altitude or velocity of the current segment takes the value of the

Table 7.3: The design and reserve missions definitions for Cessna 172R.

	Parameter	**Design Mission**	**Reserve Mission**
Climb Segment	Profile	Min time to climb	Min energy to climb
	ISA temperature deviation [°C]	0	0
	Hybridization factor	0	0
	Start altitude [m]	0	0
	Start velocity [m/s]	41.15 (TAS)	41.15 (TAS)
	End altitude [m]	2438	Max SAR altitude
	End velocity [m/s]	not specified	not specified
Cruise Segment	Profile	Scheduled	Max SAR
	ISA temperature deviation [°C]	0	0
	Hybridization factor	0	0
	Start altitude [m]	not specified	not specified
	Start velocity [m/s]	62.8 (TAS)	not specified
	End altitude [m]	2438	1000
	End velocity [m/s]	62.8 (TAS)	not specified
Descent Segment	Profile	Min equil. glide angle	Min equil. glide angle
	ISA temperature deviation [°C]	0	0
	Hybridization factor	0	0
	Start altitude [m]	not specified	not specified
	Start velocity [m/s]	not specified	not specified
	End altitude [m]	0	0
	End velocity [m/s]	not specified	not specified
	Cumulative Target:	1074 km (580 nmi)	45 minutes

final altitude or velocity of the previous one, provided that a previous segment has been defined.

If the altitude and/or velocity entry is a profile-specific entry, (e.g. in Table 7.3, the end altitude of the climb segment of the reserve mission is specified as "max SAR altitude"), then the cruise performance segment is utilized. This means that if a profile has been set for the cruise segment, then the end altitude and/or velocity of the segment previous to the cruise segment takes the *best value* for the given profile from the cruise performance lookup table. This case was explained in detail in Section 6.4.2. Similarly, whenever a profile is set without specifying start and/or end altitude and/or velocity, the missing values are automatically read from the cruise performance lookup table. This property of the mission analysis module not only optimizes the mission segments in advance, but also enables performance projections before even flying the whole mission. This way, the best altitude-velocity combinations for various profiles can be studied in advance.

The cruise segment of the design mission profile described in Table 7.3 was scheduled to be flown at a constant true air speed (TAS) of 62.8 m/s and an altitude of 2438 m. This corresponds to the design mission point selected from the range profile chart of Reference [111]. Although a full velocity-altitude schedule is given for the cruise segment, the cruise segment profile was set to maximum specific air range so that the end velocity of the climb segment is automatically set from the lookup table.

On the other hand, the reserve mission profile was set to achieve maximum specific air range at an end altitude of 1000 m. Because no velocity schedule was given in the reserve mission case, the velocity schedule which achieves the maximum specific air range at the current aircraft weight (which varies throughout the segment) and the given altitude automatically came from the lookup table.

The descent segment was set to fly at minimum equilibrium glide angle. The start altitude and velocity were not defined so that the unpowered gliding starts from the end of the cruise segment. The end velocity was also not specified, but is a fall-out parameter of

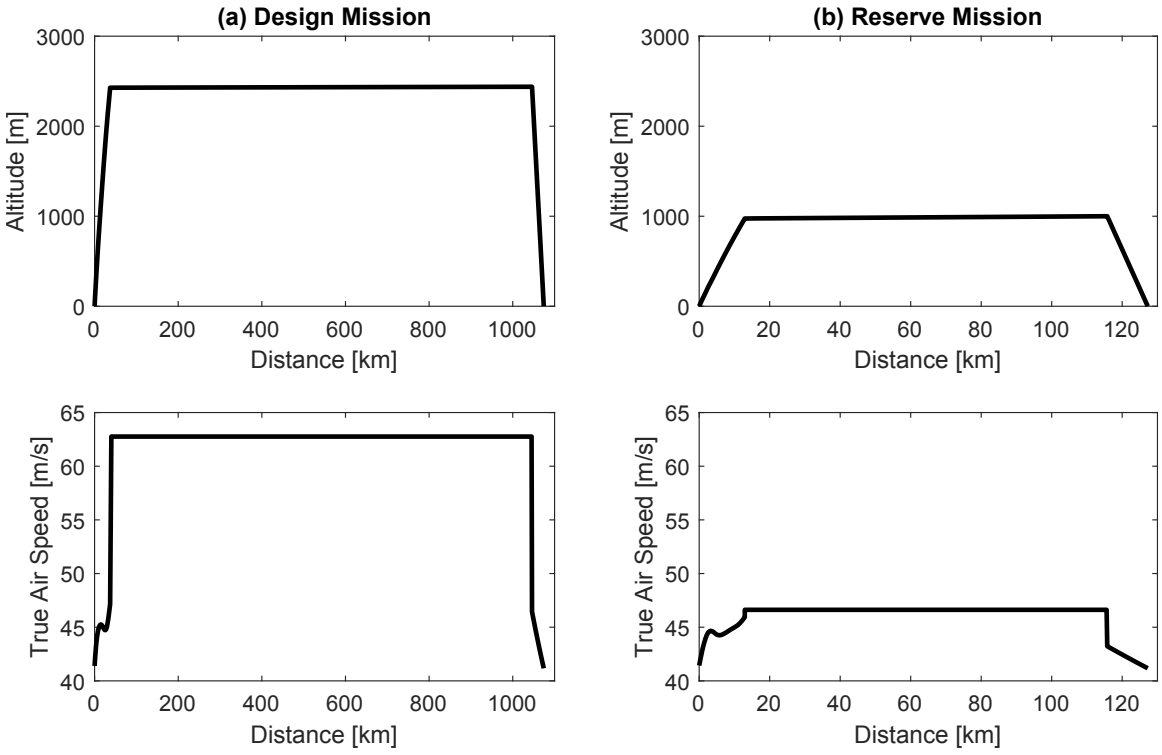

Figure 7.2: Flight trajectory for (a) the design mission, (b) the reserve mission.

the selected profile.

The cumulative target was the design range of 1074 km (580 nmi) at the given conditions for the design mission; and 45 minutes of trip time for the reserve mission. The iterations were performed until the final range and trip time converged to the required values within a relative error margin of $5x10^{-3}$.

Apart from the mission profile parameters shown in Table 7.3, the following limits were set within the mission performance module based on the Cessna 172R data [111]: sea level maximum velocity, sea level stall velocity, maximum rate of climb as a function of altitude.

Figure 7.2 shows the resulting mission profiles for the design and reserve missions. It can be seen from the design mission profile that the velocity and altitude values were kept constant at the chosen design range mission point. On the other hand, a cruise-climb is observed in the reserve mission profile where the end altitude was set to 1000 meters; and the best velocity to accompany this altitude schedule was automatically selected from the cruise performance look-up table by the algorithm.

Table 7.4: Sized aircraft specifications and deviation from Cessna 172R (normal category).

Specification	**Sized Aircraft**	**Deviation from Cessna 172R**
Wing loading	68.7 kg/m^2	0%
Power loading	9.3 kg/kW	0%
Design range	1074 km	0%
Payload	218.8 kg	0%
Takeoff gross weight	1100.6 kg	-0.93%
Empty weight	741.8 kg	-0.21%
Maximum fuel capacity	0.21 m^3	-1.07%
Fuel weight	140 kg	-8.02%
Engine rated power	118.4 kW	-0.75%
Propeller diameter (2-bladed)	1.9 m	0%

The main performance parameters and weight specifications of the resulting vehicle design is presented and compared against the published data (previously shown in Table 7.1) of Cessna 172R (normal category) in Table 7.4.

It can be seen from Table 7.4 that the sized aircraft is in a reasonable agreement with the baseline data. The first four rows of Table 7.4 represent the main design parameters which were matched with the baseline Cessna 172R. The sizing and synthesis tool estimated the takeoff gross weight and empty weight of the sized aircraft within only 1% error compared to the baseline aircraft. This was accomplished by an empty weight calibration factor of only 2.5%, which shows that the component-based weight estimation methods used for this aircraft returned successful results.

The maximum fuel capacity represents the maximum available volume which can be occupied by the fuel tanks inside the wing. Table 7.4 shows that this maximum available volume also only about 1% less than the actual total fuel capacity. The total fuel weight

(which consists of the fuel weight required to fly the design and reserve missions as well as the trapped fuel weight) turned out to be around 8% less than the actual amount of fuel carried on board. This might have been caused by the combination of the following facots: difference in mission profile for the reserve mission, utilization of a constant speed propeller instead of a fixed pitch one, differences in climb and descent segment optimization objectives (i.e. profiles).

Apart from the parameters listed in Table 7.4, climb performance was also compared to the published data given in Figure 5-7 of Reference [111]. This figure consists of time, fuel and distance to climb as a function of altitude. The results were a good match. For instance, the time it took to climb to the cruising altitude of 2438 m (8000 ft) was found as 14.8 minutes; which is only 12 seconds shorter than the published value of 15 minutes. Similarly, the distance to climb was calculated by the generic mission analysis tool as 40 km, which is only 1 km less than the published value of 39 km.

The relatively small deviations seen in Table 7.4 proves that the vehicle sizing and generic mission analysis tool built based on the sizing and synthesis block of the developed framework produces acceptable results. The sized aircraft is indeed almost identical to the actual aircraft in terms of its takeoff gross weight and empty weight, with an error margin of only 1%. The 8% discrepancy in fuel weight was expected and deemed reasonable due to the aforementioned differences.

7.1.1 Summary of the Results of Experiment 2.1

In this section, it was shown that when the same set of design and mission requirements were given to the sizing and synthesis tool which was created based on the methodological framework, the sizing process converged to an aircraft design which matched with the takeoff gross weight, geometric properties, and mission performance characteristics of the baseline aircraft within a small margin of error.

Thus, the results of Experiment 2.1 proved that:

1. It is possible to build an aircraft sizing and synthesis environment based on the proposed methodological framework

2. The modular weight estimation approach yielded an empty weight value within a 0.2% percent error relative to the baseline with an empty weight calibration factor of only 2.5%

3. The generic mission analysis approach yielded a very similar mission performance to that of the actual aircraft, which means that the energy-based methodology of the approach is capable of simulating the mission performance of a conventional aircraft with a fuel-burning engine

4. The comparisons made between the sized aircraft and the manufacturer's data showed that all of the major design and mission performance specifications were in reasonable agreement

Experiment 2.1 validates the sizing and synthesis capabilities of the developed framework for a conventional aircraft and hence the related arguments of Hypothesis 2.

7.2 Electrification of the Propulsion System (Experiment 2.2)

This section addresses the second research question (more specifically, question 2.2) which is related to Hypothesis 2 and revisited below:

- **RQ 2.2:** How can the EPGDS characteristics be integrated into the modified sizing process?

Hypothesis 2 proposes that the sizing and synthesis process should capture the sizing of EPGDS components based on the required energy and/or power, while the aircraft is being sized. It also argues that the EPGDS components must be represented by parametric, physics-based, dynamic models, and interrelationships among the subsystem, system and mission levels must captured.

The following experiment was conducted to test whether the proposed framework is capable of representing the major EPGDS characteristics in an electric or hybrid-electric propulsion architecture and simultaneously sizing them within the aircraft sizing and synthesis block:

Experiment 2.2: *Change the baseline aircraft's propulsion system with a parallel hybrid-electric architecture using the developed EPGDS models. Use the sizing and synthesis environment to resize the hybrid-electric aircraft while matching the point-performance requirements of the baseline aircraft for a (i) 50% hybrid-electric aircraft and (ii) 100% electric aircraft. Compare the results.*

In this experiment, a parallel hybrid electric propulsion architecture replaces the conventional propulsion architecture of the baseline aircraft. The reason why a parallel configuration was selected above others is that this configuration allows for the demonstration of a fully-electric application on the same architectural. This can be done by changing the power management strategy to favor the electric propulsion branch of the parallel architecture.

The flexibility of the sizing and synthesis tool in terms of varying architectural decisions enables rapid analysis on different architectures. The methodology behind selecting the main subsystems in the desired architecture and defining the interrelationships among them makes it very easy to change the propulsion system from a conventional, to a hybrid, and to a fully electric.

7.2.1 Case 1: 50% Hybridization

In the previous section, the baseline aircraft was already defined and verified against data based on the literature. The next step to change the propulsion architecture of the baseline aircraft is to *logically define the architecture*. The details of this method was given previously in Section 5.5. A short summary of the method is provided below.

The main subsystems of the propulsion architecture are first grouped into three cate-

gories: energy source, power source and thrust source. Then, the impact of each source among the same type as well as the different type of sources are captured via *interrelationship matrices*. These matrices determine how the sources interact with each other by setting *logical relations*. The algorithm within the sizing and synthesis tool then converts these logical relations into *energy and power flows* within the architecture. The distribution of the energy and power is also done based on these logical relations. Thus, in a sense, the algorithm converts the logical relations into physical ones by automatically finding or forming the correct equations for different element and configurations. This property of the sizing and synthesis tool and thus the methodological framework behind it is the main enabler in rapid architecture comparisons.

A notional parallel hybrid-electric configuration was depicted in Figure 2.7b. The interrelationship matrices defined for this architecture in Equations 5.55 and 5.56 given in Section 5.5 and revisited below were used to define the parallel hybrid electric architecture which replaced the conventional propulsion architecture of the baseline aircraft. Eqn. 5.55 establishes the relationship between the power and the energy sources, whereas Eqn. 5.56 establishes the relationship between the power sources and the thrust source.

$$\begin{bmatrix} 1 & 0 \\ 0 & 1 \end{bmatrix} \begin{bmatrix} PS_1 \\ PS_2 \end{bmatrix} = \begin{bmatrix} ES_1 \\ ES_2 \end{bmatrix} = \begin{bmatrix} PS_1 \\ PS_2 \end{bmatrix} \tag{5.55 revisited}$$

$$\begin{bmatrix} 1 & 1 & 0 \end{bmatrix} \begin{bmatrix} PS_1 \\ PS_2 \\ PS_{1-2} \end{bmatrix} = \begin{bmatrix} TS_1 \end{bmatrix} \qquad \text{(5.56 revisited)}$$
$$= \begin{bmatrix} PS_1 + PS_2 \end{bmatrix}$$

The notations used in Equations 5.55 and 5.56 are as follows:

- The fuel-burning engine branch: PS_1 represents the internal combustion engine, ES_1 the fossil-fuel (Avgas)
- The electric motor branch: PS_2 represents the electric motor, ES_2 the rechargeable battery (Lithium-ion)
- TS_1 represents the propeller

Eqn. 5.55 suggests that PS_1 draws energy only from ES_1, and PS_2 draws energy only from ES_2. Eqn. 5.56 shows that the propeller shaft (TS_1) is driven by both of the power sources (PS_1 and PS_2) *in parallel*, because there exists no direct relation between PS_1 and PS_2.

The architecture definition algorithm within the sizing and synthesis tool uses these relationship matrices to ensure that the required power to fly any given mission leg (or secondary power requirements) is split between the two power sources based on the given hybridization factors, and the amount of energy drawn out of each energy source only goes to the connected power sources.

After defining the logical relations within the propulsion architecture, the power split among the power sources were determined. Experiment 2.2 consists of two architectures: a 50% hybrid electric and a 100% electric propulsion. For this example, the 50% hybrid electric was interpreted as following:

1. The power sources must sized such that the sea level rated power of each source equals to 50% of the required sea level rated power.

2. The required thrust power within the mission is shared equally between the power sources, as long as the power sources are able to provide their share of the power demand. If a power source fails to provide the required power to fly the given mission profile, the other power source must make up for that.

The first bullet point sizes the power sources such that they have the same sea level rated power, and when combined, they produce the required rated power at sea level. This ensures a 50% hybridization of the propulsion system in terms of the engine and motor rated performance at sea level static conditions.

In this work, the required sea level rated power was determined from the power loading of the baseline aircraft. This means that regardless of the type of the propulsion system architecture, the overall power loading of the new design must be equal to that of the baseline aircraft. This relation was shown previously in Eqn. 4.8 which was revisited below. In Eqn. 4.8, P_{SL} is the sea level maximum power of the aircraft at sea level, W_{TO} is the takeoff gross weight, and $P_{SL\,i}$ represents the sea level rated power of a power source i of the new aircraft.

$$\left(\frac{\mathbf{P_{SL}}}{\mathbf{W_{TO}}}\right)_{\mathbf{new}} = \left(\frac{\sum_i P_{SL\,i}}{W_{TO}}\right)_{new} \geqslant \left(\frac{P_{SL}}{W_{TO}}\right)_{baseline} \qquad \text{(4.8 revisited)}$$

The second bullet point arranges the power split during flight. Although the electric motor does not lapse, the internal combustion engine lapses with altitude. Hence, there might be times during flight where the power demand exceeds the maximum power available of the lapsed engine. In such cases, the power split automatically varies from 50% in favor of the electric propulsion as the remaining power required from the lapsed engine must be supplied by the electric motor. If the motor cannot provide the amount of power required to make up for the lapsed engine, then the aircraft cannot maintain its altitude

and/or speed, in which case the mission fails and the power sources must be resized.

Once the required sea level rated powers of the power sources were determined from the rated power split factor, each power source was sized accordingly.

The input and output parameters of the engine were listed in Table 5.9. The baseline engine (Lycoming IO-360-L2A) was kept during the initialization of the sizing process. However, as the propulsion system changes and the aircraft is resized, the sea level rated power requirement for the IC engine will change. It was explained in Section 5.3 that a repository of fuel-burning engines was built to avoid excessive scaling-up or scaling-down of a single engine's performance curves.

Hence, the Lycoming IO-360-L2A engine model is only one of the many models in the engine deck repository. The engine sizing algorithm scales the rated power of the engine along with its weight, power characteristics and fuel consumption curves up to a certain limit. If a scaling beyond this limit is required, a more suitable engine of the same type (i.e. ICE for general aviation purposes) is chosen from the repository. For instance, if the baseline engine IO-360-L2A, which has a sea level rated power of 119 kW (160 BHP) at 2400 RPM is to be down-scaled to a rated power of around 90 kW, then the smaller IO-235-K2C engine which has a rated power of 88 kW (118 BHP) at 2800 RPM would be more suitable. Conversely, if it is to be up-scaled up to about 160 kW, then the bigger IO-360-C1A6D engine with a rated power of 157 kW (210 BHP) at 2575 RPM is chosen by the algorithm.

As the engine model changes throughout the sizing iterations, the performance characteristics of the engine changes based on the curves found in the manufacturer's data sheets. Hence, once the engine is resized such that the baseline engine changes, the same performance cannot be expected. Another important parameter that changes with changing baseline engines is power-to-weight ratio. The Lycoming IO-360-L2A engine has a power-to-weight ratio of 1.134 kW/kg (0.658 HP/lb), whereas the less powerful IO-235-K2C engine has a much smaller power-to-weight ratio of 0.608 kW/kg (0.370 HP/lb); and

the more powerful IO-360-C1A6D engine has a greater power-to-weight ratio of 1.081 kW/kg (0.658 HP/lb). Thus, discontinuities in engine weight is expected as the engine is scaled beyond its own capabilities.

The electric motor was represented by the high-level loss-based electric motor model which was explained previously in Section 5.1.4. The input and output parameters were listed in Table 5.5. A "rubberized" motor approach was taken: the torque-speed curves of the motor were re-plotted every time the motor was resized, such that the motor delivers the required rated power, and its maximum efficiency (which was taken to be 95%, similar to the SP260D [21]) occurred at the power required during cruise (the most dominant segment of the mission) from the previous iteration.

To size the electric motor, first, the motor weight was calculated from the rated power and power-to-weight ratio information. In this work, a power-to-weight ratio of 5 kW/kg was chosen for the electric motor, similar to the state-of-the-art Siemens SP260D [21] motor. Then, the maximum efficiency was set to 95%, which is, again, equal to the maximum efficiency of the SP260D [21] motor. The initial motor loss constants were also chosen to mimic the performance of such an electric motor based on manufacturer's data.

In order to generate efficiency maps on the motor torque-speed curves, first the maximum efficiency must be mapped to a certain torque-speed setting. The first iteration was initialized by a guessed setting. Then, after the first and each iteration the sizing algorithm inspected the most occurring power requirement at the cruise segment. This required power was chosen as the "reference power setting", i.e. the torque-speed setting that should correspond to the maximum efficiency. Before the next iteration started, a new torque-speed profile was calculated for the sized motor and the reference torque-speed setting from the previous mission was mapped as the most efficient setting.

This approach ensures that the "rubberized" electric motor is *specifically* sized for the given design mission by assigning its maximum efficiency to the torque-speed region which the motor is responsible for providing most of the time during its design mission.

In the baseline aircraft, the fuel tanks were housed inside the wing. For the fully-electric propulsion architecture, all of this volume was allocated to the batteries, whereas for the hybrid electric propulsion system architecture, the volume remaining after the placement of the battery was allocated to the fuel tanks. In the case of insufficient volume left to hold the necessary fuel, the wing volume was increased by a small margin through an iteration process. The change in the wing volume and hence the wing weight was taken into account by updating the empty weight as well.

The high-level battery model presented in Section 5.1.1 was utilized for the Lithium-Ion rechargeable battery. The input and output parameters of this model were listed in Table 5.1. The battery was sized based on the total required energy for the design and reserve missions and the specific energy and volumetric density of the battery. At the beginning of the sizing process, a guess value was set as the total required energy. Then, before starting the next iterations, it was updated by the amount of energy required to fly the design and reserve missions of the previous iterations. A 5% safety limit was also added to the energy capacity. Based on the literature survey made on Lithium-Ion rechargeable batteries (Section 2.4.1), a state-of-the-art specific energy of 250 Wh/kg, a density of 2500 kg/m^3, and an efficiency factor of 95% (including the battery management system) were selected. [82]

For the 50% hybrid-electric architecture, the power split schedule was determined based on the 50% hybridization strategy as follows: maximum available power from both power sources (full throttle climb) and 50% hybrid cruise. This schedule was kept constant throughout the climb and cruise segments. However, the realized schedule can be different than the desired schedule if the engine lapses beyond the expected power requirements, as explained previously.

As a result, the hybridization factors for each power source at climb and cruise segments become:

- $\lambda_{climb,\,ICE} = 1, \quad \lambda_{climb,\,EM} = 1$

- $\lambda_{cruise,\,ICE} = 0.5, \quad \lambda_{cruise,\,EM} = 0.5$

The descent segment was assumed to be an unpowered glide, and therefore a hybridization factor was not defined for descent.

Lastly, along with matching the power loading, the design wing loading was also matched with the baseline aircraft, as explained previously in Eqn. 4.9 which was revisited below.

$$\left(\frac{\mathbf{W_{TO}}}{\mathbf{S}}\right)_{\mathbf{new}} = \left(\frac{W_{TO}}{S}\right)_{baseline} \tag{4.9 revisited}$$

7.2.2 Case 2: 100% Electrification

In the fully electric architecture case, the same approaches and modeling techniques were utilized for the electric motor and the rechargeable battery. The engine branch of the propulsion architecture was completely removed by simply setting the required sea level rated power of the engine to zero, and deleting the related sources from the interrelationship matrices. In this case, the interrelationship matrices took the exact same form as the one that would be written for a conventional propulsion architecture with a single power, energy and thrust source, although the power and energy source types were completely different.

Everything else was set the same as Case 1. There was no longer a power split schedule, as the sole power source of this design was the electric motor which was responsible for providing all of the required power.

7.2.3 Comparison of Case 1, Case 2 and the Baseline

The sizing process for the two cases was first attempted with the same design mission profile defined in Section 7.1 which was defined for the Cessna 172R. However, neither of the electrified designs converged to a solution. This was expected as the assumed battery technology level (which represented an optimistic specific energy for current state-of-the-art)

would not allow for fully or mostly electric flights for the same design range of conventional GA-type aircraft.

To set a more appropriate design range target for such vehicles, a literature study on on-demand electric aviation was made. It was found that there is a potential for such vehicles to disrupt short-range trips in the future, as around 30% of all U.S. travel is made between 100 to 300 nautical miles, where by ground transportation (automobiles) currently dominates [115, 116]. Moreover, urban air mobility concepts are envisioned to fly a typical trip distance of around 25 nautical miles, and sized to a maximum range of 50 nautical miles [117].

Since the main goal of this experiment is not to compare the electric propulsion technology with the conventional one, but to demonstrate the capability of building different types of propulsion architectures with the developed framework, the design mission range target was lowered down to 50 nautical miles (92.6 km) so that the sizing process can converge on an electric aircraft design. Accordingly, the reserve mission duration was lowered down to 30 minutes. Furthermore, the design payload was lowered down to 163 kg (360 lb). This is in accordance with the *maximum useful load* capacity of Cessna 172R *utility category*. [118] Note that the useful load consists of both the payload and the fuel weight.

Apart from the design range and the duration of the reserve mission, the design and reserve mission profiles were kept the same. With the reductions in range, reserve mission time and payload, both of the electrified designs converged to a feasible solution. To compare with new the electrified propulsion system, the baseline aircraft with a conventional propulsion system was also sized for the modified mission profile and payload requirement. The results are shown in Table 7.5. Note that the empty weight does not account for the battery weight for the electrified designs.

The results presented in Table 7.5 shows that there is a significant difference between the three aircraft designs, especially in terms of vehicle size. Although drastic changes were made to the design mission and payload requirements so that the electrified designs could

Table 7.5: The main design and mission characteristics of resized aircraft designs with (i) conventional, (ii) 50% hybrid-electric parallel, (iii) fully electric propulsion systems.

Specification	**Conventional**	**50% Hybrid**	**100% Electric**
Wing loading	68.7 kg/m^2	68.7 kg/m^2	68.7 kg/m^2
Power loading kg/kW	9.3	9.3	9.3
Design range [km]	92.6	92.6	92.6
Payload [kg]	163.3	163.3	163.3
Takeoff gross weight [kg]	889.9	1147.6	1536.8
Empty weight [kg]	713.3	684.2	855.2
Fuel weight [kg]	13.3	148.3	N/A
Battery weight [kg]	N/A	151.8	462.8
Engine	IO-360-L2A	IO-235-K2C	N/A
Engine rated power [kW]	97.5	67.4	N/A
Engine weight [kg]	86.0	110.9	N/A
Motor rated power [kW]	N/A	67.4	160.5
Motor weight [kg]	N/A	13.5	32.1
Propeller diameter [m]	1.55 (3-bladed)	1.68 (3-bladed)	1.75 (3-bladed)

converge to a feasible solution with the current EPGDS technology levels, the hybridization of the propulsion system did not reduce the fuel burn. This is mainly due to the fact that at each iteration the rechargeable battery was so heavy that more fuel was required to carry the increased takeoff gross weight, which also added up.

Because the design mission range was reduced from around 580 nautical miles to 50 nautical miles, the resized conventional design ended up to be much lighter than the baseline aircraft, and the fuel weight carried on board drastically dropped to 13 kg. When this design is compared to the fully electric one, a savings of 13 kg of fuel comes with a penalty

of about 73% increased takeoff gross weight.

It should also be noted that a quick comparison between the three designs reveals the necessity of a better power split management strategy for the hybrid-electric one. This supports the observations made: architectural comparisons can only be made fairly if each design is compared at its best performance. This problem was tackled by Hypothesis 4 by adding an optimization strategy to the sizing and synthesis process, as previously explained in Section 4.2.

7.2.4 Summary of the Results of Experiment 2.2

As it can be seen from Table 7.5, the sizing and synthesis tool successfully sized three different vehicle designs with distinct propulsion architectures. Hence, this experiment proves that the proposed methodology is generic enough to size aircraft with unconventional propulsion systems. The main enablers behind the methodology is are (i) the energy-based approach used in the mission performance analysis sub-block as it does not depend on fuel burn calculations, and (ii) flexibility in defining various architectures thanks to the interrelationship matrices which can be used to define any type of propulsion architecture regardless.

The EPGDS modeling techniques explained in Chapter 5 were used to model the electric branch of the propulsion system. More specifically, the high-level models were utilized in this applications to focus on the integrated sizing approach and the architecture definition methodology rather than the subsystem level dynamics. The models were used to represent state-of-the-art products found in literature. The parametric capability of the models were used to perform "rubberized" sizing.

Better architectural comparisons can be made by further improving the modeling assumption, level of detail of the EPGDS, the power management strategy, and even the design mission profile as only the trip distance was altered from the original profile. However, the goal of this experiment was not to compare architecture and present definite results, but

to demonstrate the capability of the developed framework.

The Experiment 2.2 proved that:

1. The proposed interrelationship matrix technique provides a very useful capability in terms of rapidly defining and evaluating distinct propulsion architectures such as the fully conventional, fully electric, and hybrid-electric ones

2. The energy-based mission analysis approach is agnostic to the propulsion type, as it does not rely on fuel burn, but depends only on the law of conservation of energy

3. The developed EPGDS models were sized simultaneously with the aircraft, and their impact on the aircraft design and mission performance were captured in the results

Experiment 2.2 demonstrates that the developed methodological framework is generic and flexible enough to be used for unconventional aircraft designs, such as electric and hybrid-electric aircraft.

7.3 Sensitivity Analysis (Experiment 2.3)

This section addresses the second research question (more specifically, question 2.3) which is related to Hypothesis 2 and revisited below:

- **RQ 2.3:** How can the technological sensitivities be captured?

Hypothesis 2 claims that the parametric property of the developed EPGDS models enable technology projections. To test this claim, the following experiment was conducted:

Experiment 2.3: *Perform a parametric variation of EPGDS technology adjustment factors to determine sensitivity of aircraft and mission level measures of performance to subsystem level technology advancements.*

As it was shown in the previous section, the battery technology, more specifically the low specific energy of the battery, did not allow for a comparison between the Cessna

172R-like aircraft and an electric one, because when the conventional propulsion system was replaced with the electric one, the sizing iterations did not converge to a feasible design.

The literature review showed that the battery technology is indeed the bottleneck of electric aircraft. The drastically low specific energy of rechargeable batteries relative to the fossil fuels prevents the application of electric propulsion systems on majority of the aircraft classes. However, EPGDS technologies rapidly advance as the need for a greener aviation grows. Hence, performing the technology projections such as the sensitivity analysis demonstrating the level of technology which must be reached for desired capabilities show how much improvement is needed.

The key enabler of the technological sensitivity studies is the parametric capability of the framework. To demonstrate demonstrate this capability on this time a bigger size aircraft, the methodological framework was used to model the Dornier 328 Turboprop, which is a regional turboprop commuter plane.

The detailed technical data of this aircraft was provided by 328 Design GmbH. [119] A summary of the aircraft specifications are shown in Table 7.6.

The Dornier 328 Turboprop was modeled using the same methodological framework proposed presented in this dissertation, but in a different modeling environment than MATLAB. At the time of this study, Pacelab SysArc environment, which is a system architecture design tool, was chosen as the main modeling and simulation environment for system and subsystem level design and analysis.

The EPGDS models used in this experiment were built by the author within Pacelab SysArc using the same modeling approach described in Chapter 5. The sizing and mission performance analysis techniques used in this study were also the same. As it can be seen from this example application, the proposed methodological framework has a wide range of applicability in terms of modeling environments.

In this study, the baseline aircraft was modeled by matching geometry and performance of the Dornier 328. Next, it was retrofitted with a parallel hybrid-electric architecture

Table 7.6: Dornier 328 General Specifications [119].

Crew	3
Passengers	31
Engines	Pratt & Whitney Canada - PW 119B
Takeoff Power	2 x 2180 SHP
Takeoff gross weight	13990 kg
Typical OEW (incl. crew)	8900 kg
Max. Fuel	3416 kg
Max. Payload	3671 kg
Power Loading	4.30 kg/kW
Wing Loading	349.8 kg/m^2
Max Cruise Speed (at 95% TOGW)	620 km/h

by integrating the EPGDS models. Then, sensitivity analysis were conducted to study the sensitivity of important subsystem characteristics to mission level measures of performance (MoPs).

Because this is a retrofit study, the baseline aircraft was not be re-sized. Hence, the maximum takeoff weight remained fixed along with the vehicle geometry. Moreover, the equipment weight fractions were also kept constant. However, because the propulsion system was changed with a hybrid-electric one, the equipment and structural weight changed due to the additional weight coming from the new subsystems, and hence the operating empty weight.

To balance this change in weight, the amount of fuel carried on board was varied such that the resulting weight of the new aircraft was always equal to the takeoff gross weight of the baseline aircraft. It would be the ideal case if the weight of the new subsystems could simply correspond to the extracted fuel weight for the given mission range. However, if the

new subsystems weigh more than the maximum amount of fuel that can be replaced, then the aircraft cannot fly the same range anymore.

Figure 7.3 shows the mission profile defined for the baseline aircraft along with some prominent characteristics of each mission segment. The range of the baseline aircraft for the mission payload of 2790 kg is 1140 NM, with a cruise segment of 958 NM. This mission profile is very similar to that of the actual Dornier 328. However, the range of retrofitted designs will vary due to keeping MTOW fixed, as explained previously. Finally, 5% of the trip fuel was set as the contingency fuel.

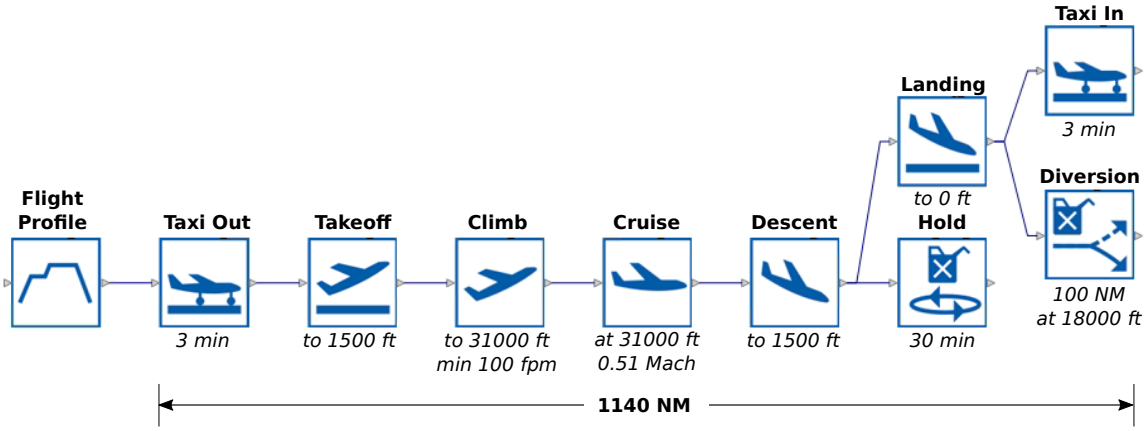

Figure 7.3: The design mission profile for the Dornier 328 retrofit study.

The relevant EPGDS models were placed into the vehicle and the hybrid electric propulsion architecture was created as demonstrated in Figure 7.4. In this architecture, there are two electric motors connected to each propeller in parallel and fed by a single battery pack. The nominal voltage of the system was set to 270 V. Two sample secondary subsystems per motor and per engine were also connected via generators. These are arbitrarily placed dummy subsystems with negligible effect on the overall power requirement, but connected to the system to illustrate power off-takes.

After the subsystems were positioned inside the baseline aircraft, the logical connections were then physically connected (i.e. physically wired) by Pacelab SysArc. Electrical wiring was automatically performed by the tool which uses an automatic routing algorithm to find the shortest possible route between two system components along the previously

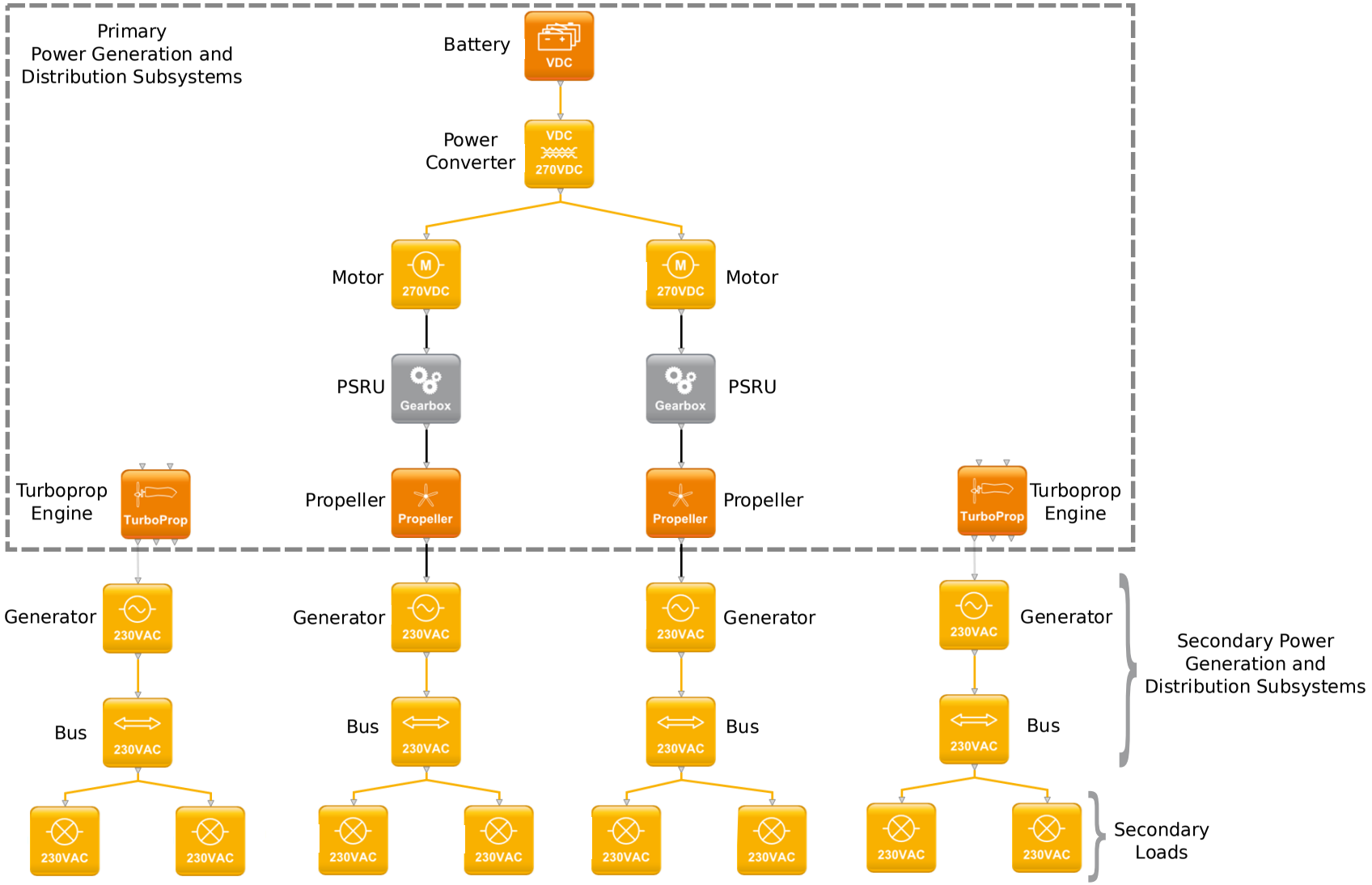

Figure 7.4: The parallel hybrid electric architecture for the Dornier 328 retrofit study.

defined pathways. Figure 7.5 depicts the Dornier 328-like aircraft with the EPGDS right after the routing algorithm was performed. The electrical cables are shown as green lines traveling between the subsystem components in Figure 7.5.

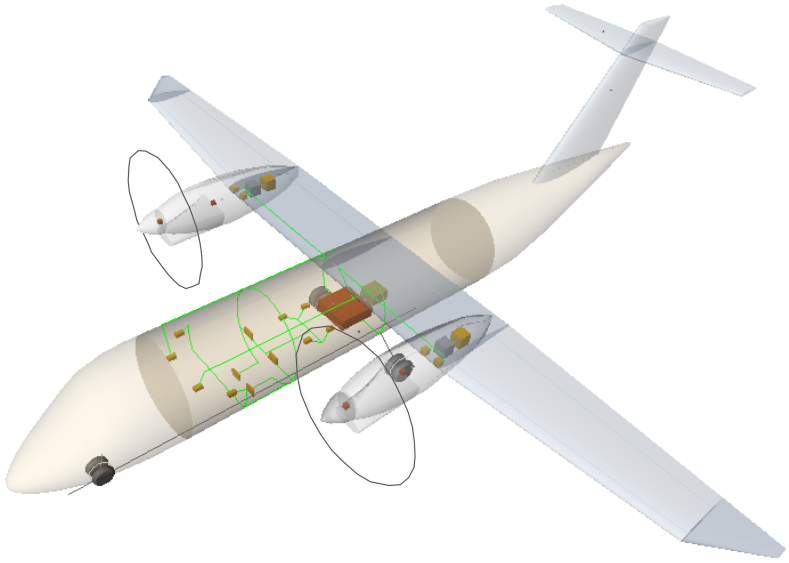

Figure 7.5: EPGDS placed into the baseline aircraft and physically connected through electrical wiring.

Because this baseline aircraft is a larger size aircraft than the Cessna 172R used in the previous experiments, the power management strategy was selected such that the hybridization only occurs during the cruise segment. In order to demonstrate the effects of changing subsystem technology along with more electrification of the cruise segment, the hybridization factor was also included in the sensitivity analysis.

Three main technology K-factors were identified and utilized in the sensitivity analysis: the battery specific energy, electric motor power-to-weight ratio, and power converter power-to-weight ratio.

The design variable space created for the selected parameters are listed in Table 7.7.

The minimum limits of the battery specific energy, motor specific power and converter specific power reflect the current state-of-the-art technology levels for these components.[14] As a matter of fact, recent advances in electric motors enabled higher power-to-weight ratios, such as Siemens' electric motor for aircraft which has a state-of-the-art

Table 7.7: The design variable space for the technological sensitivity analysis.

Design Variable	**Minimum**	**Maximum**	**Units**
Hybridization Factor	0	50	%
Battery Specific Energy	200	5000	Wh/kg
Electric Motor P/W	2.2	16	kW/kg
Power Converter P/W	2.2	19	kW/kg

power-to-weight ratio of 5 kW/kg. [41] However, most of the other electric motors still can not deliver as much power at a similar specific power, and hence the minimum limit was set to be 2.2 kW/kg to be more representative.

The maximum specific power limits for the motor and power converter were chosen based on NASA 15-year goals.[120, 14] The converter inside the motor model was also taken into account along with the power converter (DC bus) shown in Figure 7.4. Since it was expected that the battery would turn out to be the heaviest component among the considered EPGDS, the maximum limit of battery specific energy was set to a rather aggressive, and even unrealistic value for the near-future. The main reason behind this unrealistically high value was to reveal where the battery technology should be to achieve the same design range as the baseline conventional aircraft.

The minimum level of hybridization of 0% in this context means that although EPGDS were placed inside the baseline aircraft, the propulsive power is solely supplied by the turboprops. Therefore, when the hybridization factor is 0%, the EPGDS were sized based on the power required by the secondary subsystems. Due to the nature of mission performance calculations in Pacelab SysArc, the maximum value of the hybridization factor was limited to 50% rather than 100% (fully electric cruise).

The sizing of the subsystem components except for the battery were done based on user-specified power-to-weight ratios and rated powers, as discussed previously. However, in order to automate the sizing process for sensitivity analysis, an additional iteration was

performed such that the rated power of these subsystems were chosen automatically to be 5% greater than the maximum power required from the subsystems during cruise. The determination of the maximum required power from each subsystem and the weight of the overall system are interdependent, and hence an iteration was necessary.

In order to alleviate the computational burden of simulating the response to every combination of design metrics, surrogate modeling approach was used. To this end, a custom-made space-filling design of experiments (DoE) was generated within the design variable space shown in Table 7.7. This DoE was fed to Pacelab SysArc and the response data of various response metrics were collected. Then, a prediction formula for each response metric was obtained using the Gaussian process. These prediction formulas were tested for goodness of the fit and validated with data which was not used to create the formulas. Then, prediction profilers were created to study the sensitivity of the vehicle and mission level measures of performance to changing subsystem characteristics and level of hybridization. The results are given in the prediction profiler in Figure 7.6.

In Figure 7.6, the prediction profiler with prediction traces for each variable gives the predicted response as one design variable is changed while the others are kept constant at their current values and therefore makes it possible to see the effect of each variable separately. The values shown in red on the horizontal axis are the median values within the limits of each design variable; and similarly, the values shown in red on the vertical axis are corresponding predicted responses.

To show how the EPGDS weight effect the structural weight, the operating empty weight (OEW) shown in Figure 7.6 does not include the EPGDS weight, which is shown separately in the same figure. It can be seen in Figure 7.6 that total EPGDS weight (sum of all electric motors, converters, gearboxes, and battery) increases with increasing level of hybridization, as greater power is drawn from these subsystems. The overall weight changes increase the operating empty weight. Since the takeoff gross weight was kept constant, less fuel had to be taken on board. Hence, both the trip fuel weight and total fuel

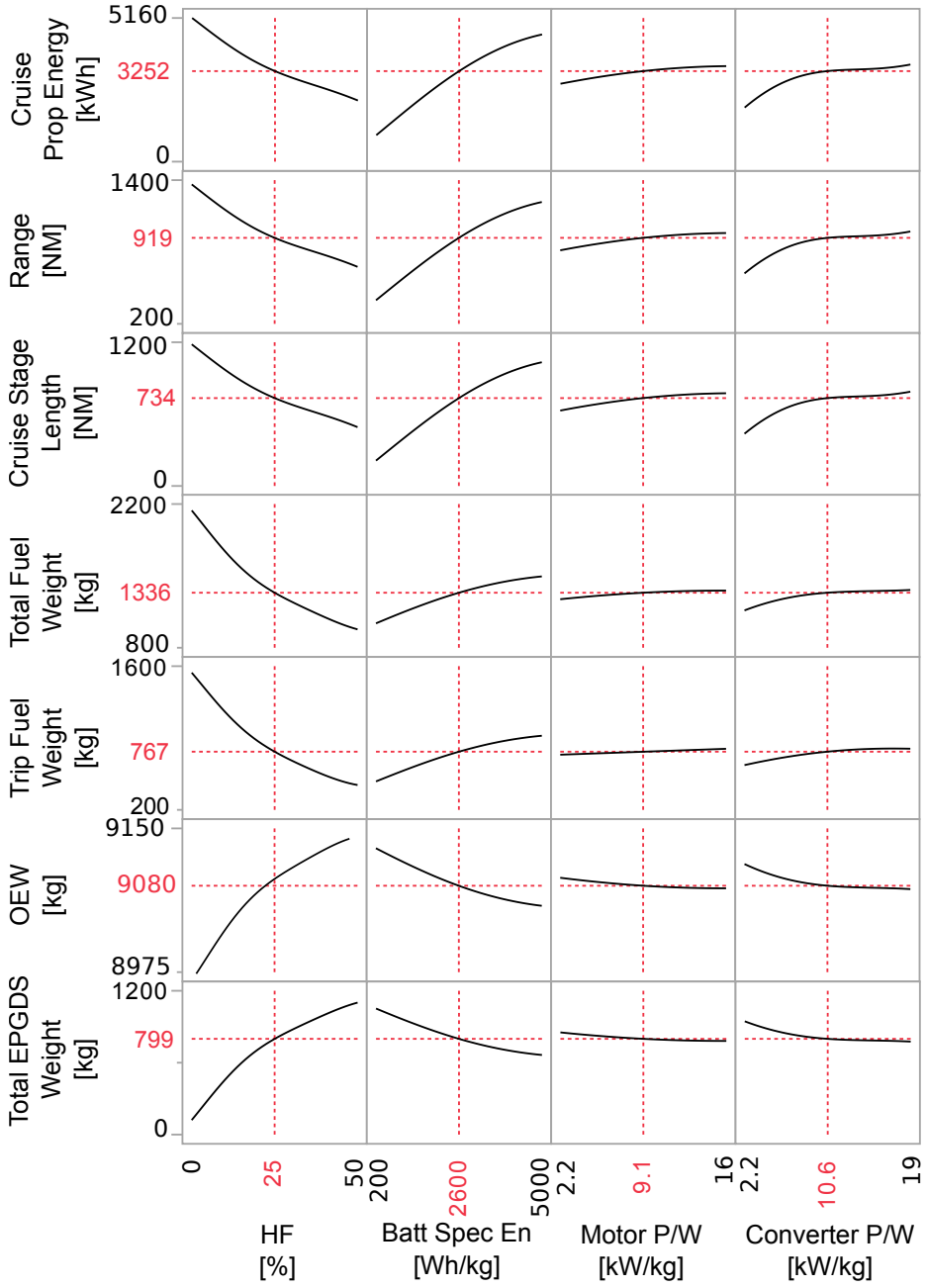

Figure 7.6: The prediction profiler showing predicted response at system and mission levels for changing design variables ("HF" stands for "hybridization factor")

weight dropped. As a result, cruise stage length and mission range reduced significantly, and therefore less propulsive energy was required during cruise.

An obvious result is seen on the battery specific energy column. Aircraft range increases as battery technology advances in terms of specific energy, as expected. Since the

battery weighs less for increasing specific energy and the equipment weight factors were kept fixed, OEW also drops in a similar trend as seen in the total EPGDS weight. The extended range is not only due to having a greater battery capacity, but also carrying more fuel on board thanks to the lighter battery pack.

Advances in motor and converter technology in terms of higher power-to-weight ratios benefits longer range by reducing total EPGDS weight and OEW. In the chosen architecture shown in Figure 7.4, there are three converters (two of which are inside the motors) and two motors. Only less than half of the power drawn from the converter connected to the battery is drawn individually from the electric motors as a result of the chosen architecture. Since the rated power of these components were determined by the maximum required power, the power converter weight exceeded the motor weight. Therefore, the effect of the converter power-to-weight ratio ended up to be greater than that of the electric motor.

The effect of the converter power-to-weight ratio on the response metrics fades out after a certain value (about 9 kW/kg for the conditions given in red in Figure 7.6) as the weight of the converters become negligible. A similar phenomenon can be seen in the electric motor power-to-weight ratio, where the effect on the response metrics diminishes after about 8 kW/kg for the conditions given in red in Figure 7.6.

Figure 7.6 demonstrates the sensitivities to the design metrics at mission level in terms of required energy, range and fuel weight; aircraft level in terms of OEW; and subsystem level in terms of total EPGDS weight. A closer look at the subsystem level is provided in Figure 7.7 where the sensitivities of the individual subsystem components to the same design metrics can be inspected. In this figure, PMAD stands for "power management and distribution" unit, which represents the converter within the electric motor model.

When the EPGDS are compared individually, the heaviest component is the battery regardless of the hybridization factor and subsystem technology levels. The effect of the battery specific energy on the motor, converter and PMAD weights are negligible. On the other hand, changing the motor and converter power-to-weight ratios seem to affect

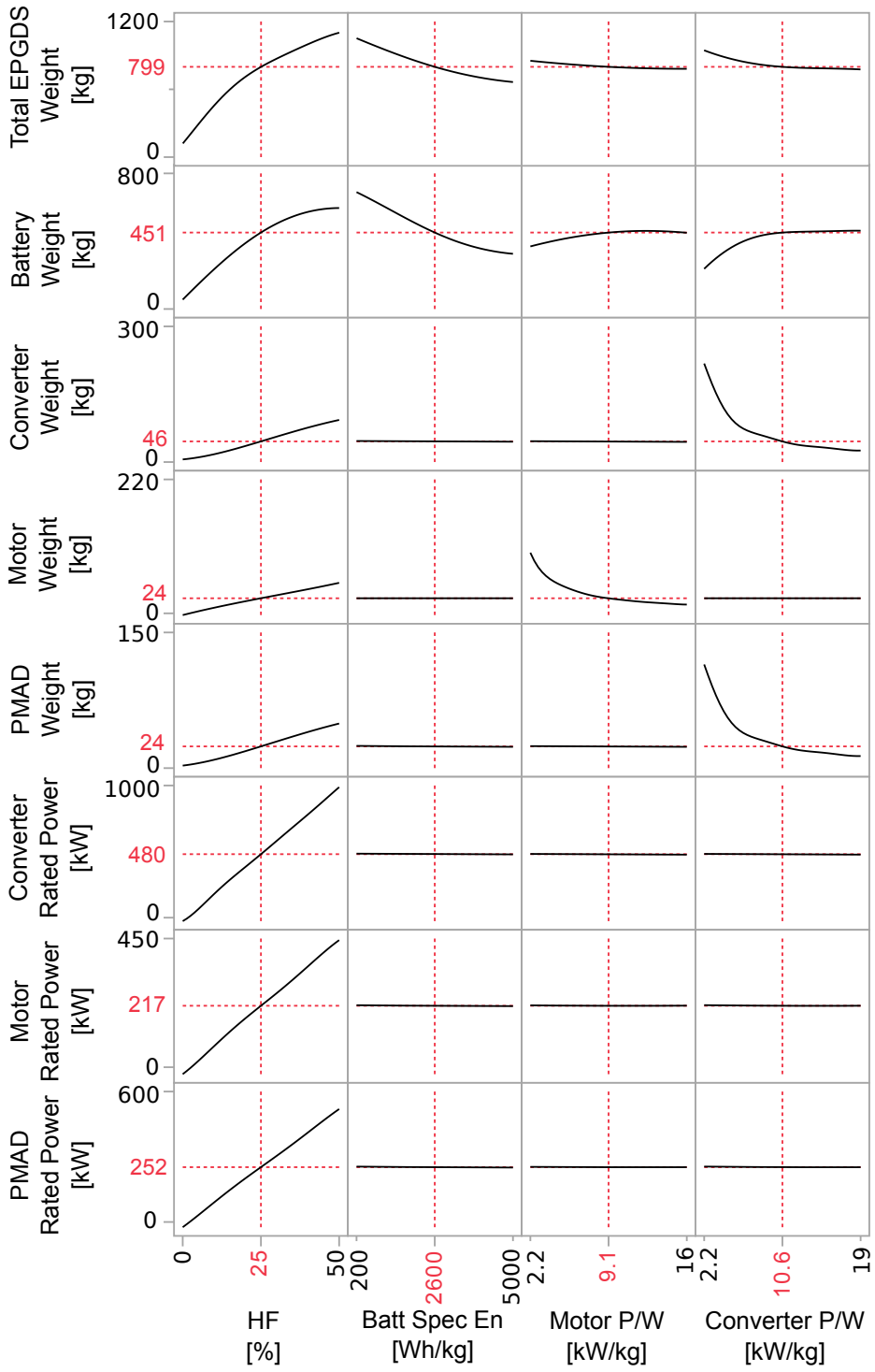

Figure 7.7: The prediction profiler showing predicted response at the subsystem level for changing design variables

the battery weight. The main reason behind the battery weight reduction at lower motor and converter power-to-weight ratios is that because the motors and the converters become

heavier while the takeoff gross weight is kept fixed, the range of the aircraft reduces, as previously shown in Figure 7.6. Thus, to balance the required energy provided by the battery, the battery size had to get smaller.

Figure 7.7 shows that the hybridization factor and the required rated powers of the converter, motor and PMAD are *almost* directly proportional. This means that although the technology levels of the battery, motor and converter change the weight of the total EPGDS weight, this weight change is negligible compared to overall weight of the aircraft; and therefore, does not impact the maximum power required from the power converter, motor and PMAD.

7.3.1 Summary of the Results of Experiment 2.3

The sensitivity analysis made in Experiment 2.3 demonstrated that the subsystem level impacts were not only captured at the subsystem level, but also the aircraft and mission levels. The parametric nature of the EPGDS models in addition to the increased dimensionality of the propulsion architecture were the key enablers of this capability.

Experiment 2.3 proves that the methodological framework has the necessary capabilities to capture technological sensitivities.

7.4 Power Management Optimization (Experiment 3)

This section addresses the third research question and the validity of Hypothesis 3, both of which are revisited below:

Research Question 3: How can the best performing hybrid electric architecture be determined under varying levels of hybridization?

Hypothesis 3: *The optimum power management schedule for an aircraft can be obtained by implementing a segment-wise optimization technique based on a set of control points and variables which do not depend on the type of the propulsion system. The optimum schedule can then be used to determine the best performing feasible architecture*

among the competing architectures by comparing their associated aircraft and mission level measures of performance.

The validity of Hypothesis 3 tested by the following experiment:

Experiment 3: *Perform an aircraft sizing process where the power management schedule is obtained by solving the optimization problem for (i) minimum energy required, (ii) minimum fuel consumption, and (iii) minimum takeoff gross weight, using the same on-design mission profile. Compare the resulting architectures based on the measures of performance.*

Experiment 3 combines the previously developed sizing capability with the power management optimization approach explained in Section 4.2. As discussed previously, comparison of different hybrid electric architectures are meaningful provided that the candidates are evaluated under their optimal power management strategy.

In this section, the proposed optimization approach was implemented on the same parallel hybrid-electric architecture derived from the baseline general aviation aircraft which was introduced and used in Experiment 2.2. The objective functions, constraints and design and control variables of the optimization problem were described in Section 4.2.

An optimization problem for the three objective functions selected in the experiment was solved separately. Thee following constraints were applied for the hybridization factor of each power source:

$$0 \leq \lambda_i \leq 1, \qquad \forall \lambda_{climb} \ \& \ \forall \lambda_{cruise}$$

$$\sum_i \lambda_{cruise,\,i} = 1$$

where, λ_i is the hybridization factor for mission leg i. Similar to $u_{EM}(t)$ and $u_{FB}(t)$, the minimum limit (0) indicates zero power, and the maximum limit (1) indicates maximum available power for the electric motor and the internal combustion engine at the relevant flight condition.

Th control variables that were employed are electric motor normalized power, $u_{EM}(t)$, and fuel burning engine normalized power, $u_{FB}(t)$, as defined in Eqn. 7.1 and Eqn. 7.2, respectively.

$$\mathbf{u_{EM}}(\mathbf{t}) = \frac{P_{EM,req}(t)}{P_{EM,max\,av}} \tag{7.1}$$

$$\mathbf{u_{FB}}(\mathbf{t}) = \frac{P_{FB,req}(t)}{P_{FB,max\,av}} \tag{7.2}$$

In Eq. 7.1 and Eq. 7.2, $P_{EM,req}(t)$ and $P_{FB,req}(t)$ are instantaneous required power from the electric motor and IC engine, and $P_{EM,max\,av}$ and $P_{FB,max\,av}$ are the maximum available power of the electric motor and the IC engine at a given flight condition, respectively. Note that the value of $P_{FB,max\,av}$ varies with altitude.

The following invariant bounds were applied to the control variables:

$$0 \leq u_{EM}(t) \leq 1 \tag{7.3}$$

$$0 \leq u_{FB}(t) \leq 1 \tag{7.4}$$

Once $u_{EM}(t)$ and $u_{FB}(t)$ were found (for all power sources) for an optimal design, required electric motor and fuel-burning engine power were calculated directly from Eq. 7.1 and Eq. 7.2. Thereafter, hybridization factor for each power source at each control point was computed from Eq. 6.14 and Eq. 6.25.

For this analysis, four control points were selected and each was placed on the mission profile as follows: at the beginning and end of the climb, and at the beginning and end of the cruise segments. Then, a pattern search based optimizer was provided an initial design with guessed values for the control variables. This optimizer calls the mission analysis which evaluates the value of the objective function at the given control points. The

optimizer perturbs the control variables at the control points until the objective function is minimized. The control variable values in between the control points were obtained by linear interpolation. The remaining K-factors and mission profile parameters were selected as follows:

- The rechargeable battery has a specific energy of 0.25 kWh/kg
- The electric motor rated power split is set to different values for different architectures as: 60% for hybrid-electric, 0% for fully conventional, and 100% for fully electric designs
- Payload weight, wing loading, and power loading values match those of the baseline aircraft (utility category as given in Section 7.2)
- Design mission range is 100 nautical miles (in addition to a 15 minutes long reserve mission)
  - Climb segment objective is minimum time to climb for the main mission; minimum energy to climb for the reserve mission
  - Cruise segment objective is best specific air range
  - Descent segment objective is minimum equilibrium glide angle

An IC engine powered baseline aircraft was sized based on the same baseline aircraft properties for a 100 nautical miles of design range to compare the resulting optimized vehicles for each objective function in terms of a list of design properties shown in Table 7.8. The associated optimized control variables are presented in Figure 7.8 throughout the mission profile.

The designs corresponding to the minimum takeoff gross weight and minimum energy objectives were not explicitly shown in Table 7.8 because of the fact that the resulting optimized vehicles ended up almost identical with the baseline aircraft, that is, the electric propulsion branch was not utilized to avoid the increase in battery weight. This result

Table 7.8: Comparison of the baseline aircraft to the new HEA design optimized for minimum fuel consumption to fly the 100 nautical miles design mission and 15 minutes long reserve mission.

Design Variable	Baseline 1	Design 1
TOGW [kg]	693.7	991.8
Change over baseline	-	*+43.0%*
Fuel Weight [kg]	11.8	10.1
Change over baseline	-	*-14.4%*
Battery Weight [kg]	N/A	226.3
Energy Stored [kWh]	144.2	180.0
Change over baseline	-	*+24.9%*
IC Engine Rated Power [kW]	84.0	72.0
Change over baseline	-	*-14.3%*
Electric Motor Rated Power [kW]	N/A	61
Propeller diameter [m]	1.3 (2-bladed)	1.5 (2-bladed)
Change over baseline	-	*+15.4%*
Wing Area [m^2]	11.3	16.1
Change over baseline	-	*+42.5%*
Wing loading [N/m^2]	605.6	605.6
Power loading [kW/kg]	0.12	0.12
Payload [kg]	163.3	163.3

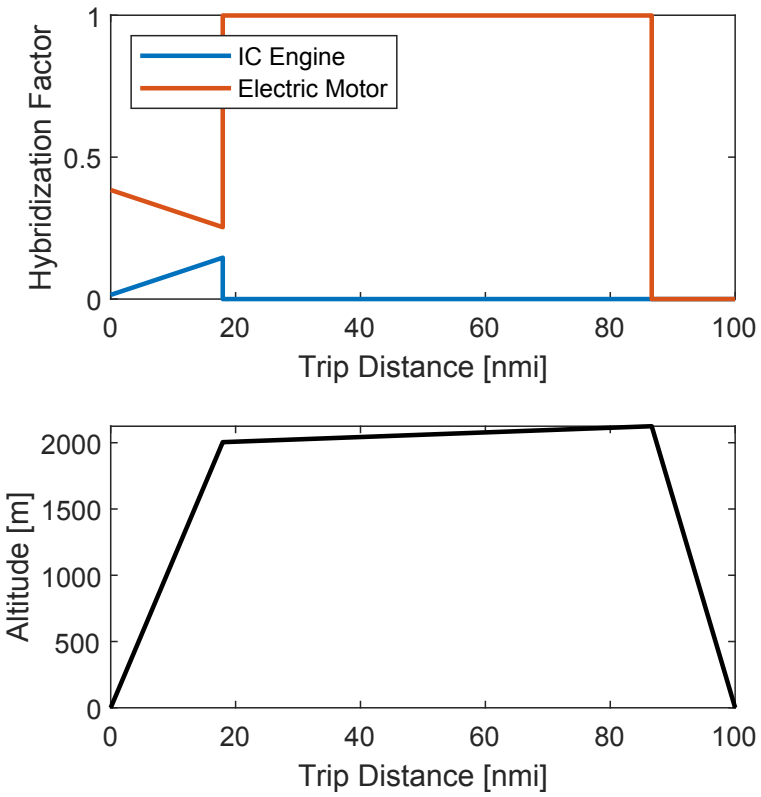

Figure 7.8: Variation of the optimized power management schedules for Design 1 with altitude and trip distance for the 100 nautical miles design mission. Refer to Eqn. 6.14 and Eqn. 6.25 for the hybridization factor definitions, as the definitions are different for climb and cruise segments.

implies that that the minimum takeoff gross weight and minimum energy objectives are obtained (separately) when the aircraft does not run on electric energy.

In fact, none of the optimized designs showed significant advantage over the baseline aircraft in terms of the listed design variables. On the contrary, the baseline aircraft with conventional propulsion is the lightest, smallest design that requires only slightly more fuel than the hybrid electric Design 1 which was optimized for minimum fuel consumption.

Although a hybrid electric propulsion system turned out to be disadvantageous for a range of 100 nautical miles with the current battery technology level, its advantages can be seen when the design range is dropped to 50 nautical miles and the cruise altitude to 1000 meters, similar to the aforementioned urban air mobility type concepts [117]. The results are given in Table 7.9. The associated optimized control variables are presented in

Figures 7.9 throughout the mission profile.

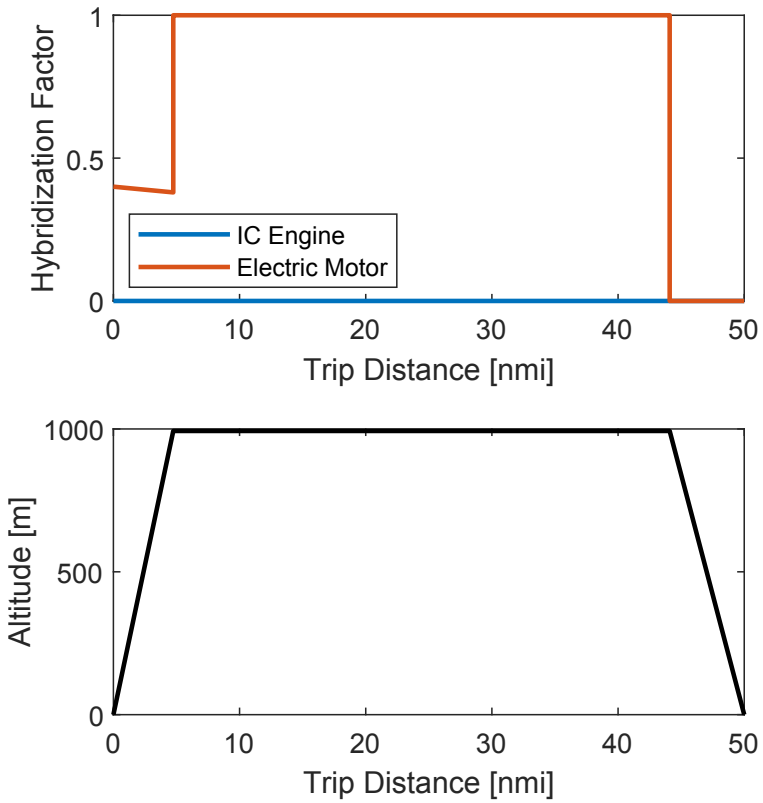

Figure 7.9: Variation of the optimized power management schedules for Design 1 with altitude and trip distance for the 50 nautical miles design mission. Refer to Eqn. 6.14 and Eqn. 6.25 for the hybridization factor definitions, as the definitions are different for climb and cruise segments.

Similar to the previous case, the power split optimizer favored the internal combustion engine throughout the mission profile when the optimization problem was solved for the minimum takeoff gross weight. However, interesting results were obtained by solving the optimization problem for minimum fuel and minimum energy required. The optimizer converged on a power management schedule which carried almost no fuel and favored the electric propulsion branch of the parallel hybrid electric architecture, as shown in Figure 7.9.

To demonstrate the impact in a more dramatic way, the internal combustion engine was removed from the design and thus the aircraft weight along with the required battery weight was further reduced, making the propulsion architecture completely electric. The

Table 7.9: Comparison of the baseline aircraft to the new HEA design optimized for minimum fuel consumption to fly the 50 nautical miles design mission and 15 minutes long reserve mission.

Design Variable	Baseline 2	Design 2
TOGW [kg]	684.8	866.2
Change over baseline	-	*+26.5%*
Fuel Weight [kg]	7.1	0
Change over baseline	-	*-100.0%*
Battery Weight [kg]	N/A	161.5
Energy Stored [kWh]	86.8	40.4
Change over baseline	-	*-53.5%*
IC Engine Rated Power [kW]	82.6	0
Change over baseline	-	*-100.0%*
Electric Motor Rated Power [kW]	N/A	103.9
Propeller diameter [m]	1.3 (2-bladed)	1.4 (4-bladed)
Change over baseline	-	*+7.7%*
Wing Area [m^2]	11.1	14.0
Change over baseline	-	*+26.1%*
Wing loading [N/m^2]	605.6	605.6
Power loading [kW/kg]	0.12	0.12

resulting takeoff gross weight was still higher than the baseline aircraft. However, this time the energy required to fly the same design mission was much less in the electric design than the conventional one. This is due to the drastically higher inefficiency of the powertrain in the conventional propulsion architecture.

Note that Design 2 is a different electric aircraft design than the one previously shown in Case 2 of Experiment 2.2 in Section 7.2, because different mission requirements were applied. The electric aircraft design shown in Experiment 2.2 had the same design range requirement, but the reserve mission lasted 30 minutes as opposed to 15 minutes, and the cruise altitude was set to 2438 meters instead of 1000 meters. That's why Design 2 presented in this section was lighter.

7.4.1 Summary of the Results of Experiment 3

In this section, an experiment was conduct to test the optimization approach described in Hypothesis 3. A parallel hybrid-electric architecture was compared with its conventional counterpart under three different objectives and two separate mission profiles.

A parallel architecture was chosen as the primary hybrid-electric example because of its ability to perform as a purely electric, purely conventional (fuel-burning) and hybrid electric propulsion system. In fact, of all the six aircraft designs optimized for each objective-mission profile combination, three of them converged to a conventional design, two converged to an electric design, and one converged to a hybrid-electric design. Consequently, the importance of power management optimization during the sizing of the aircraft manifested itself.

Some architectural trends were also obtained by the optimization. It was seen that for the example application (in terms of design and mission requirements), the minimum takeoff gross weight objective always favored the conventional propulsion system. On the other hand, minimum fuel burn converged to a more electrified propulsion system as the design range decreased. This is due to the reduction in the required energy capacity of the

battery and thus the battery weight. Similarly, the minimum energy requirement objective yielded a conventional design for the higher mission range, but then favored an electric one as the higher efficiency of the electric propulsion powertrain prevailed the low specific energy of the battery.

Experiment 3 validates that the optimum power management schedule for an aircraft can be obtained by implementing a segment-wise optimization technique based on a set of control points and variables which do not depend on the type of the propulsion system, and the optimum schedule can then be used to determine the best performing feasible architecture among the competing architectures by comparing their associated aircraft and mission level measures of performance.

7.5 Chapter Summary

This chapter provided a proof of concept for hypotheses 2 and 3 which addressed the sizing and synthesis of novel architectures with an integrated optimization capability for power management strategy for hybrid electric aircraft.

First, three experiments were conducted to test the validity of Hypothesis 2. This hypothesis argued that the EPGDS characteristics could be integrated into the sizing and synthesis process by developing the following set of capabilities: (i) generic mission analysis based on conservation of energy laws instead of the traditional weight fraction estimation techniques, (ii) parametric, physics-based EPGDS models to enable simultaneous sizing based on the maximum required energy and/or power from each individual subsystem as well as technology projections, (iii) component based weight estimation techniques, and (iv) relationship establishments among the primary subsystems as well as the aircraft and mission levels.

A sizing and synthesis tool was built based on the developed framework. This tool was first validated by Experiment 2.1, where the Cessna 172R which is a general aviation type aircraft with a conventional propulsion system was replicated. The tool was given

the same design and mission requirements as the Cessna 172R. The design mission profile also mimicked the actual design mission of the baseline aircraft. At the end of the sizing process, the converged aircraft design was in a reasonable agreement with the baseline aircraft in terms of both the weight characteristics and mission performance.

A second experiment was conducted to replace the conventional propulsion architecture of the baseline aircraft with a hybrid-electric and then an electric one. Because of the drastically low specific energy of rechargeable batteries compared to fossil fuel, the design range had to be reduced to 50 nautical miles so that the EA/HEA designs could converge to a feasible solution. Even then, the electrified designs did not demonstrate remarkable advantages over their conventional counterpart. In fact, these designs ended up to be much heavier than the conventional one.

Moreover, because the design range was dropped to 50 nautical miles, the corresponding fuel weight of the conventional aircraft dropped so much that the electrification of the propulsion system did not seem to bring significant fuel savings. In fact, the 50% hybrid-electric aircraft ended up to require about 10 times more fuel than the conventional one due to the additional battery weight and thus the increased takeoff gross weight. The non-optimum power management strategy was also a cause of this failed design.

Although the electrified aircraft designs were not very promising, Experiment 2.2 verified the applicability of the new mission analysis approach to unconventional aircraft concepts such as EA/HEA. Furthermore, the proposed interrelationship matrices were proven to be very useful to define and evaluate distinct propulsion architectures.

The final experiment conducted to verify Hypothesis 2 was Experiment 2.3. This experiment aimed to test and demonstrate how the parametric nature of the EPGDS models could be utilized to perform sensitivity analysis. Moreover, a different analysis platform was used to apply the methodological framework, demonstrating that the proposed framework was indeed tool-agnostic.

In this experiment, the baseline aircraft was selected to be a turboprop commuter which

is larger than the general aviation aircraft baseline used in the previous experiments. A parallel hybrid-electric architecture was employed while keeping the aircraft takeoff gross weight constant, so that this time the impact of hybridization of the propulsion system could be studied on the mission design range. Then, a design variable space for the technology K-factors was defined for the EPGDS utilized in this architecture, and then a set of design of experiments was generated.

The mission performance analysis and the subsystem sizing process was performed for each case in the DoE. Various response metrics at both the aircraft and mission levels were tracked, such as the design range, the required energy to fly the hybridized cruise segment, required fuel weight, operating empty weight, total EPGDS weight, and so on.

Finally, a Gaussian surrogate model was fit to the data. The surrogate modeling approach alleviated the computational burden of simulating the response at each point of the design space and made sensitivity analysis available. The sensitivity of the aircraft and mission level measures of performance to the changes in EPGDS technology levels was demonstrated for a range of hybridization factors.

This experiment showed that of all the EPGDS components of the hybrid electric architecture, the mission performance was most sensitive to the varying technology levels of the battery specific energy. However, even an unrealistically high battery specific energy assumption of 5 kWh/kg was not enough to yield the same design range as the baseline aircraft.

Consequently, experiments 2.1, 2.2 and 2.3 tested the arguments made in Hypothesis 2. It was shown that the sizing and synthesis block of the proposed methodological framework enabled the sizing, integration and performance evaluation of electric power generation and distribution subsystems within the aircraft conceptual design phase.

Once the sizing and synthesis block was verified, an optimization algorithm was set up to find the optimum power management schedule of hybrid electric architectures. To this end, a control variable was defined for each power source.

If an optimization problem was attempted to be solved at each mission leg, it would require an immense amount of function calls and thus computational time. Because the main objective is to enable rapid architecture comparisons, a different, more practical approach had to be taken. To this end, the optimization problem was set up to be solved at certain strategic points at the mission profile rather than all of the mission legs. This is due to the fact that there is no physical reason that would necessitate a drastic change in the power management strategy over a small time interval, especially within a mission segment. As a result, four control points were selected based on the expected changes in the power requirement which in turn would necessitate changes in the power split schedule.

Two studies were conducted for this experiment. First, a parallel hybrid-electric aircraft was sized for a given design mission profile while simultaneously being optimized for (i) minimum energy expenditure, (ii) minimum fuel burn, and (iii) minimum takeoff gross weight, separately. The resulting designs were then compared with the baseline aircraft. In this study, it was seen that the minimum energy and takeoff gross weight objectives yielded a design where electric energy was not being utilized at all. Although minimum fuel burn objective did converge to a parallel hybrid electric architecture, the resulting takeoff gross weight was so high that the required fuel weight for this hybrid architecture was not much different than the fuel weight of the baseline aircraft.

These results were expected due to the low specific energy of the battery. In fact, many UAM concepts assume a much higher battery specific energy (e.g. Uber Elevate Common Reference Models assume a battery specific energy of 0.4 kWh/kg [117]) and shorter range to see the benefits of electric propulsion and converge to a feasible design. To demonstrate when the electric propulsion could be beneficial, the optimization study was repeated for a reduced design range and cruise altitude.

The results of the second study demonstrated that with the current battery technology, electric and hybrid electric architectures are advantageous only for short flight profiles. When the design range and cruise altitude of the initial mission profile were halved to 50

nautical miles and 1000 meters, the optimizer favored the use of electric propulsion for the entire course of the mission for the minimum fuel burn and energy objectives. The final design was still heavier than the baseline, and the result of the optimization problem solved for the minimum takeoff gross weight objective did not change. However, when the two studies were compared, it was seen that the electric design could fly the same mission while storing less energy thanks to the considerably higher efficiency of the electric propulsion powertrain.

To summarize, Experiment 3 tested the applicability of the optimization technique proposed in Hypothesis 3. It was shown that this optimization approach was suitable to be used with the sizing and synthesis block developed in Hypothesis 2 to compare competing architectures at their best performance. Furthermore, architectural trends for different architectures and mission requirements were revealed.

CHAPTER 8
TRANSIENT ANALYSIS

This chapter provides a proof of concept to demonstrate its adaptive step sizing capability and the increased dimensionality of the subsystem level considerations. More specifically, this chapter focuses on the final research questions, hypothesis, and the experiments which were set up back in Section 3.1.4 and revisited below:

Research Question 4: How can a balance between smaller and larger time steps be found so that significant transients at the subsystem level are captured at the conceptual design stage without bringing the associated computational burden?

- **RQ 4.1:** Can the transient behavior of an electrical system be related to the mission level parameters?
- **RQ 4.2:** If they are related, how can the relationship be captured between the significant transients of a given electrical system which could occur under a wide range of inputs which are expected to be given to the electrical system during a mission?
- **RQ 4.3:** If they are related, can the relationship be generalized for the given electrical system so that the whether a significant transient occurs could be estimated with only the limited amount of information obtained from the mission performance analysis?

Hypothesis 4: *A balanced time step size to capture the significant transients during the mission performance analysis can be determined within each mission leg by establishing the probability of a significant transient occurring under a certain degree of change in the mission level requirements by performing the following three-step approach:*

1. *A design of experiments (DoE) concept is leveraged to intelligently sweep through the mission level parameter space to maximize the knowledge about the system response with minimal experimental effort.*

2. *The controllers of the electrical system which were tuned via gain scheduling where the schedules are determined by jointly utilizing Monte Carlo simulations and a system design optimization technique are utilized to reduce the optimization efforts and obtain a few numbers of gain sets to control the majority of the realizable cases of the DoE; whereas the cases which go beyond the physical capabilities of the system are eliminated.*

3. *The probability of a transient occurring is established by a conditional rule set determined a-priori by fitting a categorical surrogate model to the transient signal at the neighborhood of the time at which the mission level change occurred.*

The following sections of this chapter answers the three-part research question by conducting the experiments set up for each part. The methodological steps followed in these sections were explained in Section 4.3. This methodological framework was applied in Simulink for an example electric propulsion system architecture. Then, two significant voltage transients were defined for the electric motor; and a conditional rule set was generated for each transient by following the proposed methodology.

8.1 Electric Propulsion System Architecture

This section describes the electric propulsion system architecture which was used in the upcoming experiments.

In the previous chapter, the propulsion system architecture was represented using the high-level models developed in Chapter 5. These models were suitable for rapid, high-level analysis and did not require much knowledge about the design of the subsystems. However, due to the limited level of detail, they cannot be used to simulate the dynamic response of

the electrical system. Thus, along with these high-level models, detailed EPGDS models with increased dimensionality were developed in Chapter 5 and were used to build the electric propulsion system architecture for the transient analysis.

These detailed models can be used to create a variety of propulsion architectures. However, the most general case shall be given here. If a control volume is enclosing the electric propulsion branch of the architectures previously shown (e.g. Figure 2.7), it can be seen that the information flow into and from the control volume can be expressed with a similar term: power P as a function of shaft speed ω, torque Q, and time t. Two such control volumes are depicted in Figure 8.1.

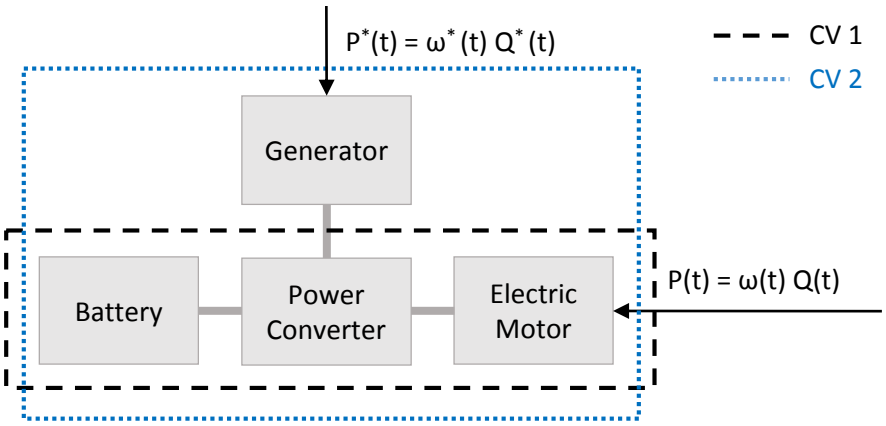

Figure 8.1: Information flow into the electric propulsion branch enclosed by a control volume.

In Figure 8.1, the variables $P(t)$, $\omega(t)$ and $Q(t)$ indicate the time-dependent values required by the mission performance and set by the power management schedule. The direction of the arrows carrying these variables indicate *the direction of the information flow* coming into the control volumes from the other non-electrical subsystems outside the perimeter, and not the physical direction of power distribution. The first control volume, CV 1, receives information through the electric motor only. This control volume corresponds to, for instance, a purely electric propulsion architecture, or the electric propulsion branch of a parallel hybrid electric architecture. The second control volume, CV 2, receives information through both the electric motor and generator, and corresponds to, for

example, series, series-parallel and complex architectures.

Since the working principles of the electric motor and generator are similar, and can be represented using the same models operating at different directions as explained in Chapter 5, the control volume denoted by CV 1 was chosen as the electrical system architecture in the following example applications.

Note that the power, speed and torque requirements are requirements from the particular electric propulsion branch only, and not the entire propulsion system of the aircraft. In the remaining of this chapter, the required or realized power, speed and torque terms indicate the required or realized power, speed and torque of the electric motor.

The approach of isolating the electric propulsion branch by the control volume becomes useful when the analysis are to be performed in different environments or at different timescales. This approach was used in the upcoming application of Hypothesis 4, where the mission performance analysis calculations were carried out in MATLAB at its own appropriate timescale (in the order of minutes), and the transient analyses were performed in Simulink with a microsecond timescale.

The electrical system architecture consists of a Lithium-Ion rechargeable battery, DC/DC converter (which serves as a DC bus), and a field-oriented control induction motor drive. The individual components of each model were explained in Chapter 5.

8.2 Simulation of the Subsystem Dynamics (Experiment 4.1)

This section addresses Experiment 4.1, which is revisited below:

Experiment 4.1: *Create dynamic models for an electric propulsion powertrain where power is supplied by a battery-sourced electric motor. Set a series of step inputs in terms of the required motor torque and speed of variable amplitude. Verify that (i) the results (in terms of battery SOC, subsystem voltages and currents) obtained by using large time steps differ from the results obtained by using small time steps, (ii) a significant transient behavior is missed when larger time step size is used, and (iii) not every change in the*

power input causes a significant transient response at the subsystem level.

Two simulations were run with the same input and modeling variables for 10 seconds. The electric propulsion architecture created in the previous section takes the required power input in terms of the required motor speed and torque. Figure 8.2 shows the input signal schedule used for the Experiment 4.1 simulations.

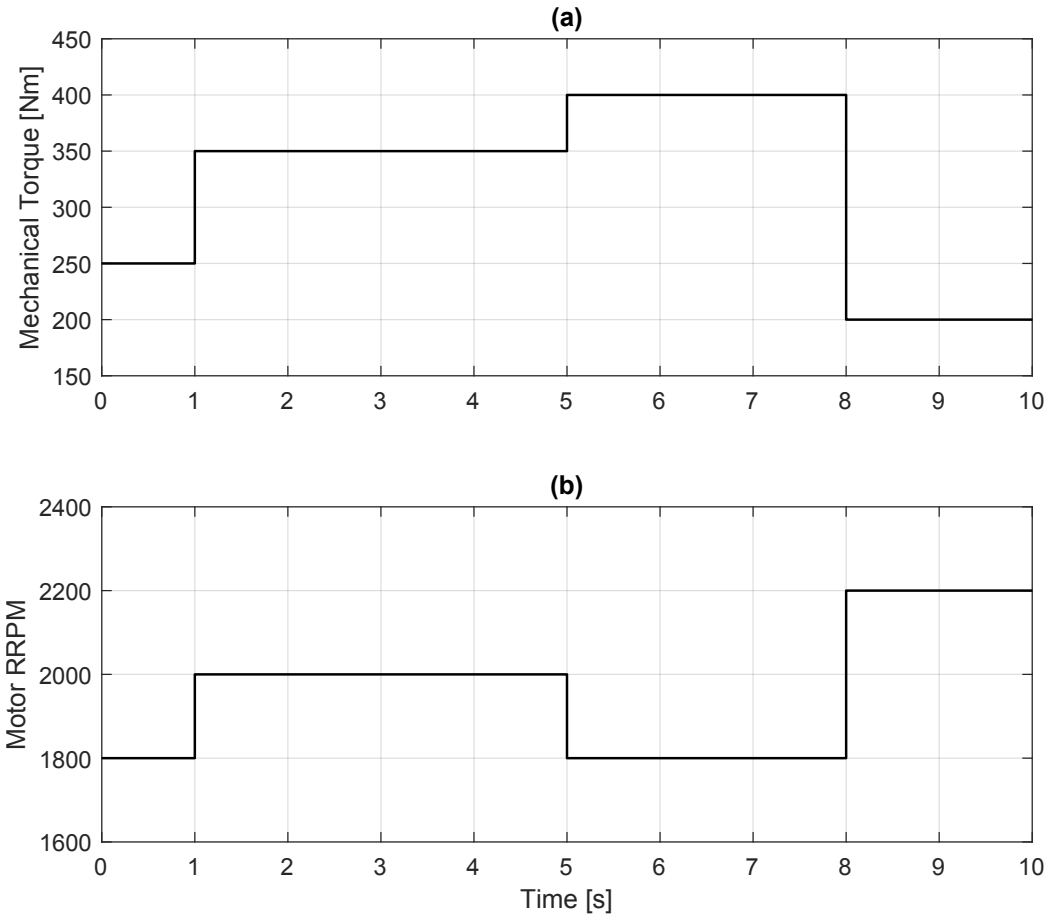

Figure 8.2: (a) Mechanical torque, and (b) motor RPM input signal schedules for Experiment 4.1

Two different time steps were used for comparison:

- **Sim-1:** sampling time of 2 microseconds
- **Sim-2:** sampling time of 2 seconds

The sampling time of $2\mu s$ used in Sim-1 is the recommended time for the induction motor drive model. The time step used in Sim-2 is still not as high as the step sizes generally

Table 8.1: The list of recorded EPGDS signals.

Battery	**DC/DC Converter**	**Electric Motor Drive**
Voltage	Reference Voltage	RMS Voltage
Current	Output Voltage	Line to Line Voltages (ab, ca, bc)
State of Charge	Output Current	Phase Currents (A, B, C)
Power	Power	DC Current
		Reference RPM
		Measured RPM
		Mechanical Torque
		Reference Electromagnetic Torque
		Measured Electromagnetic Torque
		Mechanical Power
		Electrical Power

used in mission level analysis, but high enough to prove that important information about the subsystem transients gets lost when the appropriate timescale is not used.

Table 8.1 provides the list of variables which were recorded during both of the simulation runs.

8.2.1 Sim-1 Results

The outputs of the Sim-1 are shown in Figures 8.3 and 8.4.

The top two plots of Figure 8.3 show how the system tracked the input signals after the controllers were tuned (the controllers used in the motor drive were explained in Chapter 5 and were revisited in the next section, Section 8.4). The system was able to track the motor RPM reference very well.

In this system, the electromagnetic torque reference gets adjusted by the controllers to

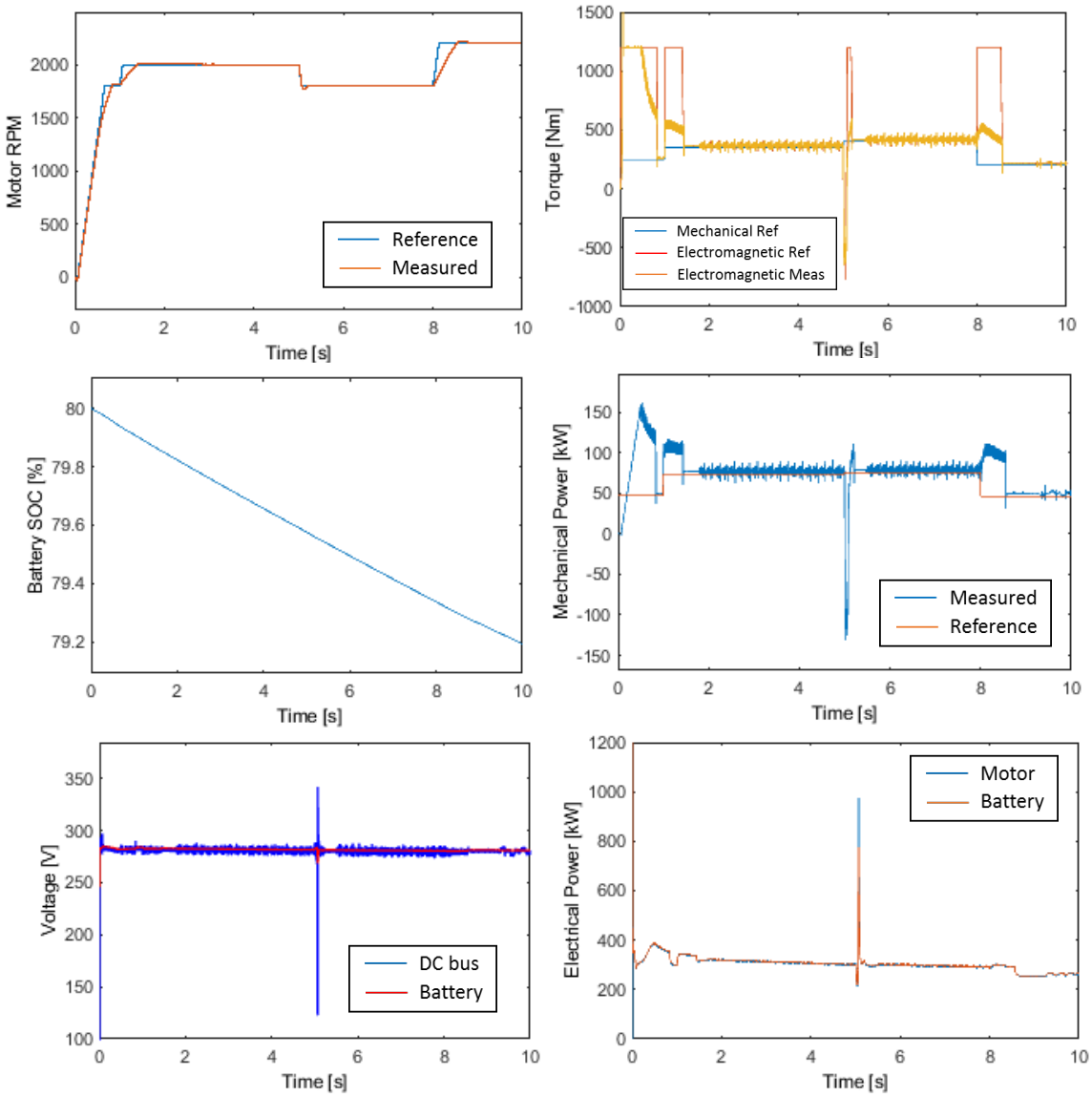

Figure 8.3: Dynamic response of the electrical system with a simulation time step of 2 microseconds (Sim-1)

accelerate or decelerate the motor speed. This trend can be seen in the top-right torque plot in Figure 8.3. Electromagnetic torque rises in the beginning of the simulation in order to start the motor and accelerate the RPM to the initial reference motor speed of 1800 RPM while producing the reference mechanical torque of 250 Nm. Then, at t=1s, the motor speed and mechanical torque requirements were increased to 2000 RPM and 350 Nm, respectively. As a result, the electromagnetic torque reference rises up, and so does the measured electromagnetic torque, until the measured motor speed catches up with the

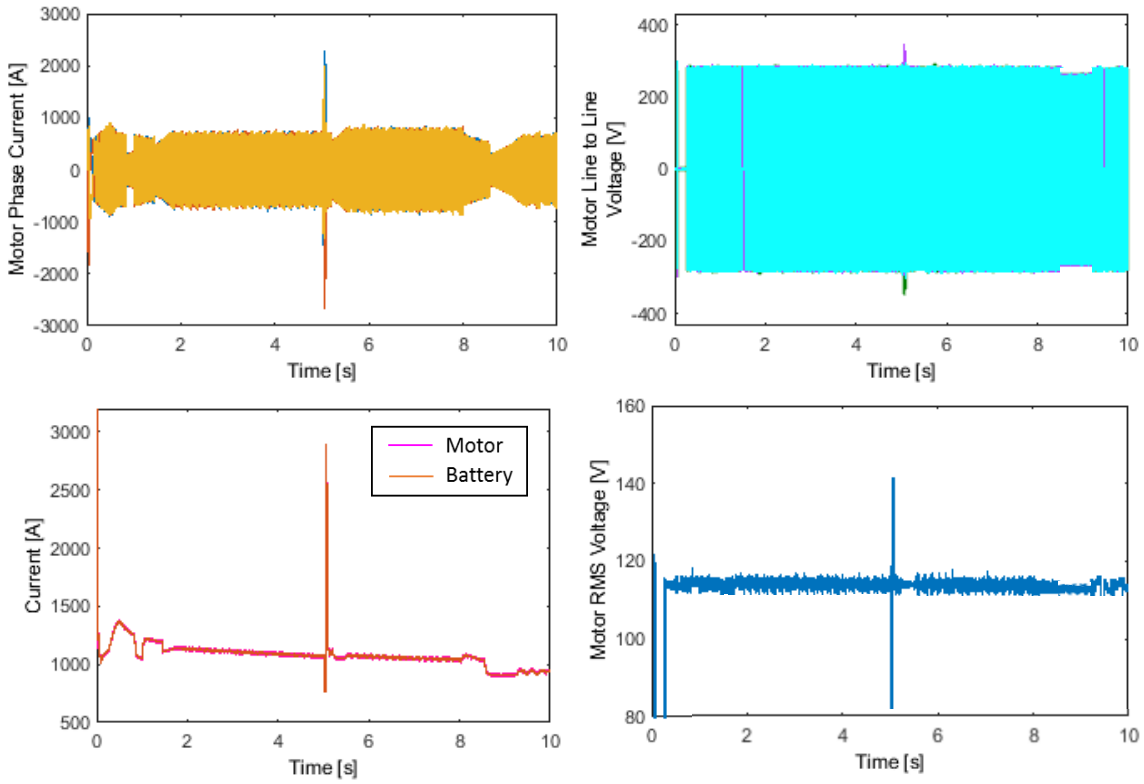

Figure 8.4: Dynamic response of the electrical system with a simulation time step of 2 microseconds (Sim-1), continued

reference motor speed.

The fluctuations in voltage and current readings of the system seen at the beginning of the simulations (between t=0s and t=1s) were expected due to the motor start up. At t=1s, the subsystem current and voltage characteristics change to adapt to match the motor torque and speed to the reference signals, again as expected. For instance, the motor RMS (root mean square) voltage increases slightly a few microseconds after the change in input at t=1s. However, this fluctuation is not a significant transient. Although the electrical power quality standards shown in MIL-Std-704F (Ref. [58]) is not a suitable reference for the EA/HEA applications due to the high subsystem voltages and the use of a variable voltage motor, as explained previously, this particular experiment was conducted with suitable inputs so that the RMS voltage of the electric motor falls inside the allowed voltage envelope given in this standard. This is demonstrated in Figure 8.5, where the neighborhood

of the input signal (i.e. reaction window for t=1s) is magnified and the motor RMS voltage response is compared to the constraint envelope given in MIL-Std-704F (which was previously shown in Figure 4.8).

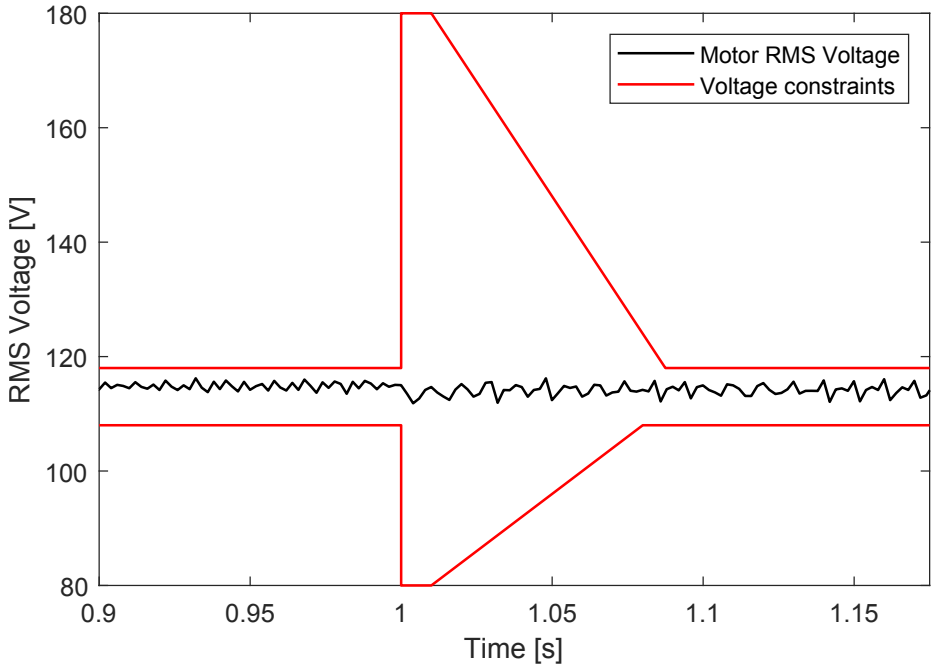

Figure 8.5: RMS Voltage constraint on the motor voltage signal at the neighborhood of t=1s in Sim-1.

At t=5s, the input motor speed signal falls down back to 1800 RPM, whereas the mechanical torque rises up to 400 Nm. As a result, the reference electromagnetic torque momentarily spikes, but the measured electromagnetic torque dives down before rising up. This causes a greater oscillation in the system compared to the first input at t=1s. As a result, the motor RMS voltage violates the constraint, by spiking up and down, as shown ini Figure 8.6.

Finally, at t=8s, the final change in the input signals occur. This time, the mechanical torque drops to 200 Nm and the motor speed rises up to 2200 RPM, as can be seen from Figure 8.2. As a result, although the reference mechanical torque input drops, the electromagnetic torque briefly increases to speed up the motor, and then falls down to the reference torque. This change causes a fluctuation in the system, especially seen in the cur-

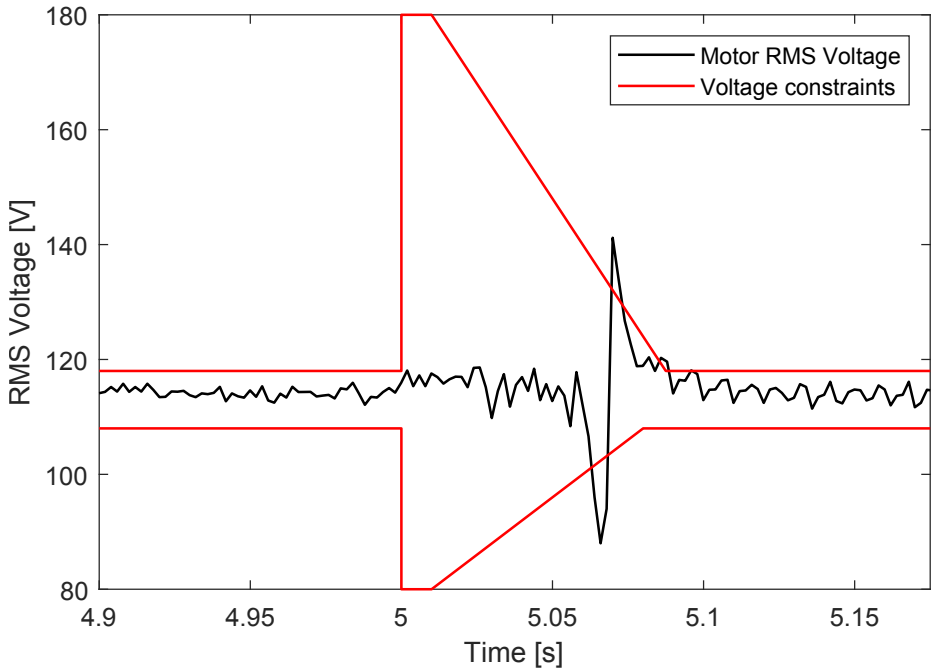

Figure 8.6: RMS Voltage constraint on the motor voltage signal at the neighborhood of t=5s in Sim-1.

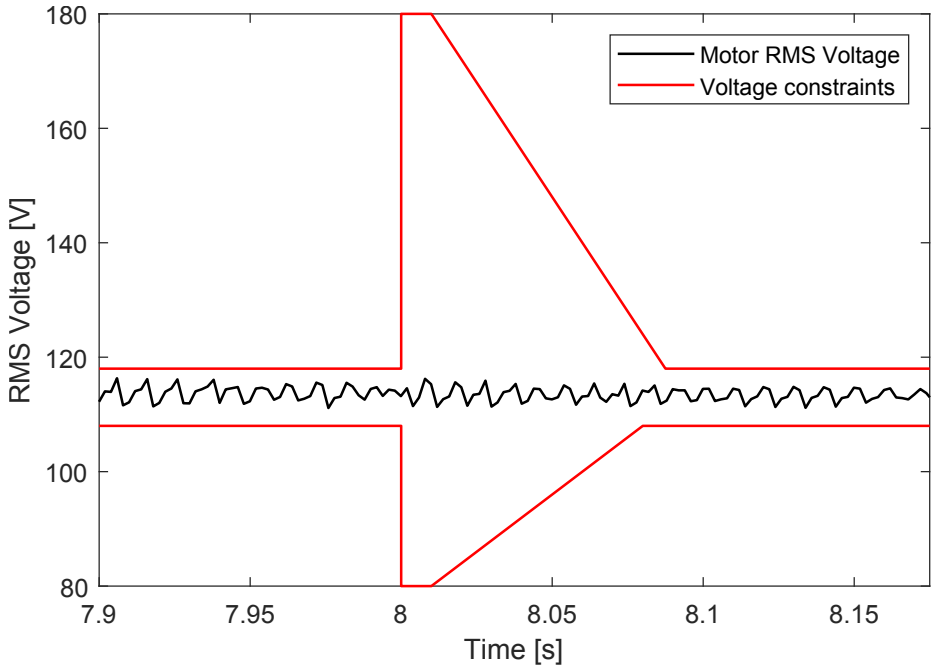

Figure 8.7: RMS Voltage constraint on the motor voltage signal at the neighborhood of t=8s in Sim-1.

rent graphs of Figure 8.4. The motor RMS voltage does not exceed the voltage envelope shown in Figure 8.7. However, the voltage oscillation changes its shape, resulting in what

looks like a voltage sag.

8.2.2 Sim-2 Results

The results of the second simulation are given in Figures 8.8 and 8.9. A drastic change is observed in the results when compared to the response of the same simulation under the same inputs shown in Figures 8.3 and 8.4. The sole reason for this drastic change is the increase in the temporal step size of the simulation.

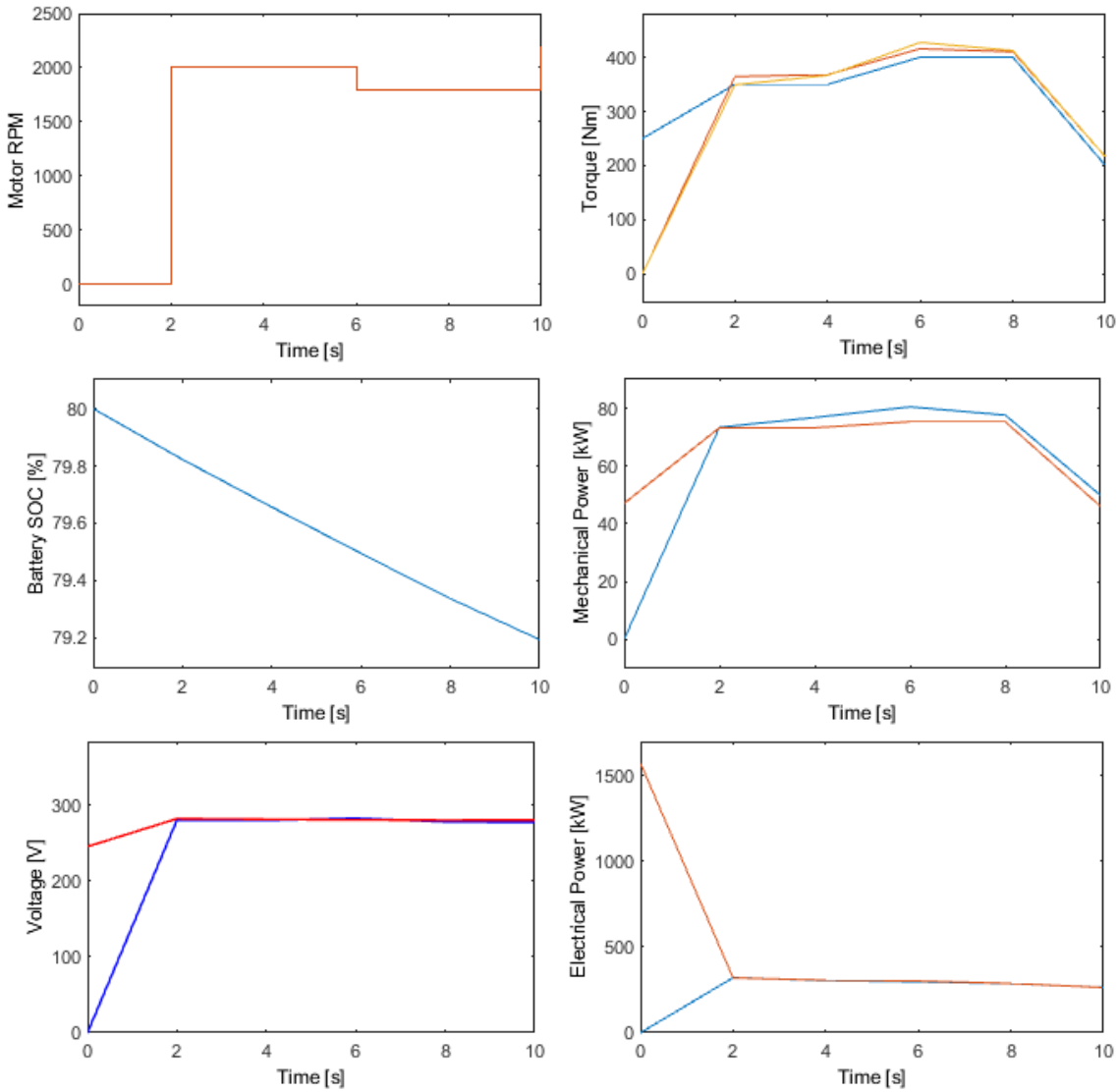

Figure 8.8: Dynamic response of the electrical system with a simulation time step of 2 seconds (Sim-2).

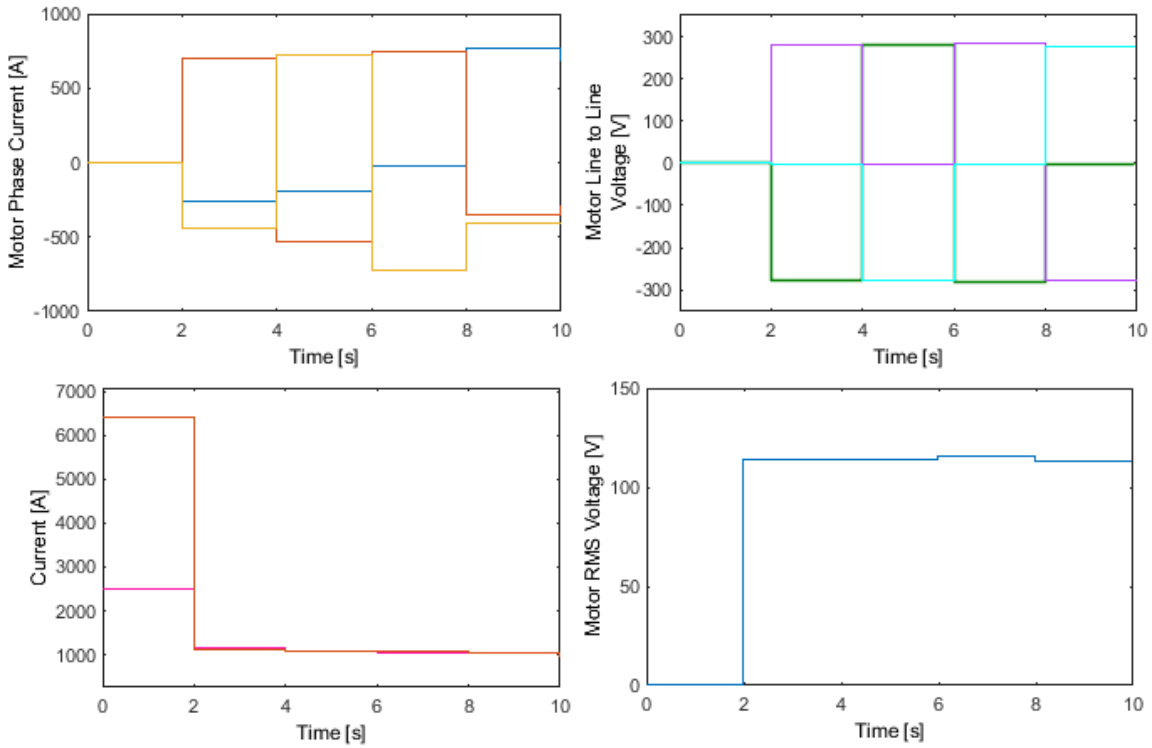

Figure 8.9: Dynamic response of the electrical system with a simulation time step of 2 seconds (Sim-2).

A step size of 2 seconds was used in Sim-2. 2 seconds is still rather small compared to the mission analysis timescale which is in the order of minutes. However, the amount of information lost can already by observed by comparing Sim-1 and Sim-2. The voltage spikes seen at t=5s were flatted out by the low sampling rate. Thus, a misleading result emerged: the electric motor RMS voltage seems to be not violating the constraint, as shown in Figure 8.10.

On the contrary, the high step size gave a false constraint violation result at the early seconds of the simulation. Because the subsystem dynamics were much faster (almost a million times faster!) than the step size, Sim-2 missed the motor voltage values between t=0s and t=2s. The resulting interpolation among the two values gives the false impression of a violated constraint, as shown in Figure 8.11.

Thus, as the results of Sim-2 showed, the results obtained with mission level time steps cannot be trusted to perform transient analysis.

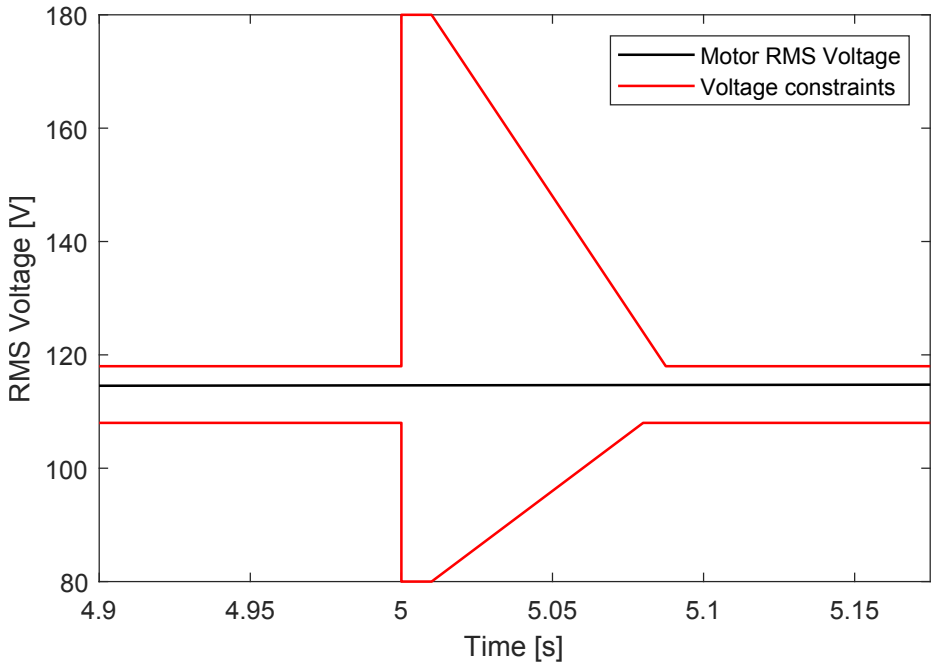

Figure 8.10: RMS Voltage constraint on the motor voltage signal at the neighborhood of t=2s in Sim-2.

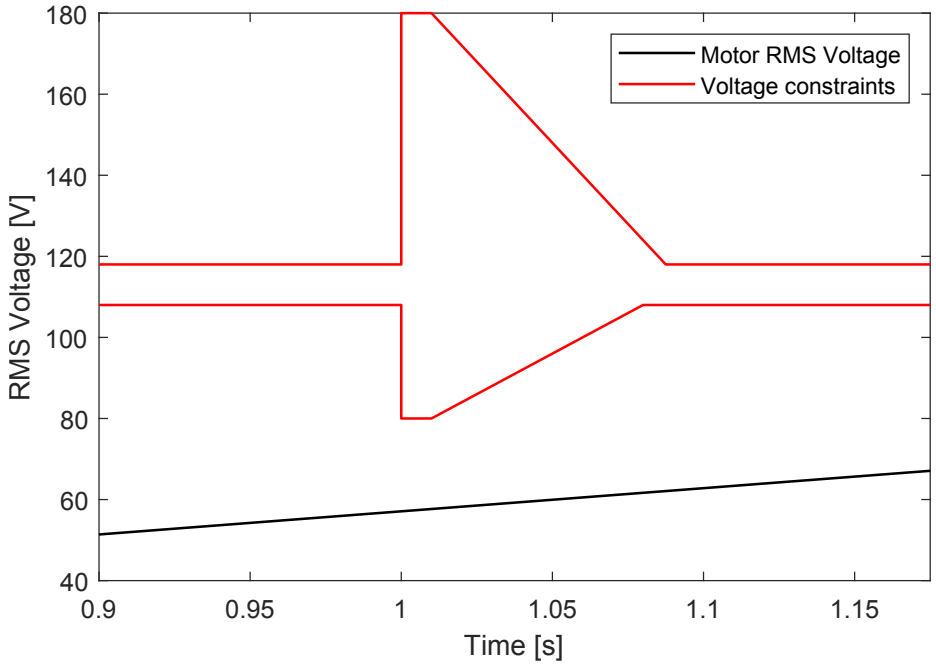

Figure 8.11: RMS Voltage constraint on the motor voltage signal at the neighborhood of t=1s in Sim-2.

8.2.3 Summary of the Results of Experiment 4.1

Both simulation results of Sim-1 and Sim-2 provided increased dimensionality compared to the high-level EPGDS models used in the previous chapter. However, the oscillations in the resulted of Sim-2 are much smoother than the results of Sim-1. This was due to the low sampling rate (i.e. higher time step) used in Sim-2.

In fact, a significant transient, i.e. a transient which violated the constraint of interest, was observed at t=5s in the higher-resolution simulation results of Sim-1. This constraint violation was altogether missed in the results of Sim-2.

Although the first and the last changes in the input at time $t = 1s$ and $t = 8s$ also changed the voltage and current behaviors, they were within the boundaries of the voltage envelope, and thus were relatively insignificant. Note that the concept of significance can change based on which constraint the signal is compared against.

Moreover, when the time of the voltage transient seen in Sim-1 at $t = 5s$ was inspected, it was seen that it took place a few microseconds after the change in the input signals had occurred. This observation is in agreement with the reaction window assumption made in Hypothesis 4.

There are two lessons that can be inferred from this experiment. First, Sim-1 yielded more accurate and reliable results than Sim-2 due to using the appropriate timescale. Second, although the power input was changed three times through the course of the simulation, a significant transient occurred only once.

The latter argument supports the idea that it is not always necessary to perform the transient analysis every time a change occurs at the mission level. Doing so would bring enormous amount of computational burden to the analyses and thus would not be suitable at the aircraft conceptual design stage. Increasing the size of the time steps is also not an option as proven by the comparison between the two simulations of this experiment. That's why, estimating which actions taken at the mission level are more likely to cause the undesired transients is a very valuable capability which allows the transient analysis to be

performed at early design stages.

Thus, Experiment 4.1 proved that:

1. Transient analysis simulations should be performed with small time steps (in the order of microseconds for this example) as important information about the transients can be missed with the large time steps (in the order of seconds for this example)

2. Not all the changes made in the mission level cause a significant transient

3. For a balanced system, a transient response caused by the mission level changes can be captured within a small reaction window

Experiment 4.1 verifies that (i) the results obtained by using large time steps differ from the results obtained by using small time steps, (ii) a significant transient behavior is missed when larger time step size is used, and (iii) not every change in the power input causes a significant transient response at the subsystem level.

8.3 Design of Experiments

The first step of the methodology proposed in Hypothesis 4 is to generate a subset of simulation cases which can represent the design space as well as possible without exhausting the computational resources. To this end, the design of experiments approach was utilized as previously explain in Section 4.3.1.

First, the design variable space was defined as shown in Table 8.2. The minimum and maximum limits shown in this table were normalized through feature scaling before the DoE was created, as previously explained in Section 4.3.1. These values were chosen in accordance with the requirements for and capabilities of the baseline general aviation aircraft modeled in Chapter 7, so that the results can be integrated into the mission analysis performed for this aircraft and its derivatives.

A custom DoE design was created by augmenting a full-factorial design on the edges (64 cases + 1 case at the center point) and a space filling design for the interior design space

Table 8.2: Design variable space used in Experiments 4.2 and 4.3.

Design variable	**Minimum Limit**	**Maximum Limit**
Battery Energy Capacity [kWh]	10	100
Battery SOC [%]	25	100
Initial Power [kW]	0	100
Absolute Change in Power [kW]	0	100
Initial RPM	1500	2400
Absolute Change in RPM	0	900

(1000 cases). As a result, 1065 cases were generated where each case consists of the inputs for a 2 second long simulation with 2 microsecond time steps.

A system voltage of 270 V was set. The battery energy capacity designated the number of cells connected in parallel and series. The initial battery SOC designated the SOC value at the beginning of the simulation. The battery capacity and SOC were included in the design space to check whether the changing battery voltage throughout the flight (as the battery is charged or discharged) would have any impact on the simulation results.

The power and motor RPM inputs were translated into motor mechanical torque and RPM inputs. Each change in the torque and RPM was applied at precisely t=1 second. This way, the system fluctuations due to the start-up period of the motor were avoided.

Although this DoE created set to represent the design space as much as possible, some cases were not suitable for the electrical system created in Section 8.1 due to the physical limits. Thus, all of the cases in this DoE were first tested to check whether the electrical system could simulate the given inputs within the physical limits set by the design parameters of the EPGDS models in the architecture.

8.4 Gain Tuning and Scheduling (Experiment 4.2)

The gain tuning and scheduling approach utilized in this methodological framework was previously described in Section 4.3.2. This section demonstrates how this approach was followed for the electrical system at hand in more detail, and how Experiment 4.2 was performed. Experiment 4.2 is revisited below:

Experiment 4.2: *Conduct the following steps to verify that a gain scheduling technique can be used to control a group of simulations instead of performing optimization for each case determined by the DoE:*

1. *Define the design variable space by creating a DoE with simulation input variables*
2. *Create a second DoE with simulation input variables and controller gain parameters*
3. *Run simulations with the second DoE cases, collect the error on the reference signal and the actual signal*
4. *Fit a surrogate model to the error using both the gain and input variables*
5. *Assess variable importance for the gain variables by performing Monte Carlo simulations to eliminate the variables which have insignificant impact on the variation of the error*
6. *Perform sensitivity analysis to reveal the sensitivity of the signal tracking error to the controller gains under varying model design variables and intelligently choose a case which represent the majority of the cases under a certain level of error*
7. *Set up a system design optimization problem where the controller gains with high importance are the optimization variables and the optimization objective is to minimize the error between the input signal and the subsystem level response*
8. *Run simulations for the selected case to solve the optimization problem and collect the optimum gains*

9. *Use the resulting gain set obtained for that particular case in all of the simulations in the first DoE and identify the cases which produced an acceptable signal tracking error*

10. *Return to step 5 and repeat the procedure until either acceptable gain sets are obtained for all of the cases or a saturation point is reached where the optimum gain set for one case does not yield results within the reasonable margin of error for the other cases*

11. *Create a schedule from the collected gain sets such that whenever a case from the first DoE is simulated the correct gain set is used to control the system*

Before implementing these experimental steps, first a brief description regarding the controllers used in the electrical system shall be given. In this system, there are three main controllers. A PI controller is used in the DC/DC converter (DC bus) to regulate the system voltage. The remaining two controllers, field-oriented control (FOC) and speed controller are a part of the induction motor drive.

The motor drive tries to match the torque and speed requirement coming from the aircraft mission level. These requirements are translated into flux and torque references for the FOC controller. The motor speed is controlled by a PI controller to produced the referenced motor torque and flux. The torque and flux references are then translated into three reference motor line currents by the FOC controller. The FOC controller then a three-phase current regulator and feeds the reference motor line currents into the motor to match the desired torque and flux. [98]

The output of the closed-loop speed control is the reference electromagnetic torque and rotor flux of the induction motor. The controller schematic for the speed control is provided in Figure A.5 in the Appendix.

An indirect vector control strategy is used to derive direct and quadrature components of the stator current (dq) based on the flux and torque references. These components are then

used to produce the necessary gate signals for the inverter by a PWM current controller. The controller schematic for the field-oriented control with space vector modulation (SVM) is provided in Figure A.6 in the Appendix.

For the electrical system at hand, there are a total of 10 gains (5 PI controllers) to tune, as listed below:

- DC bus controller ($K_{P,conv}$, $K_{I,conv}$)
- Motor speed controller ($K_{P,speed}$, $K_{I,speed}$)
- Motor field-oriented control with space vector modulation
  - Flux controller ($K_{P,flux}$, $K_{I,flux}$)
  - SVM d-axis regulator ($K_{P,svm,d}$, $K_{I,svm,d}$)
  - SVM q-axis regulator ($K_{P,svm,q}$, $K_{I,svm,q}$)

8.4.1 System Design Optimization Enhanced by Monte Carlo Simulations

As it can be seen from the controller gain list given in the previous section, even a rather simple system with a single electric motor drive and a DC/DC converter require such a high number of controller gains to be tuned. This adds on top of the computational burden already existed due to the high sampling rate necessary for the transient analysis. Thus, the optimization effort could be significantly reduced if the variable importance is first evaluated to reveal whether some gains can be quickly estimated and/or whether their variance has a negligible effect on the outcome.

The variable importance can be assessed through subject-matter expertise, trial and error, or surrogate modeling. If subject-matter expertise is not available, then a quick inspection can be done to check whether the controllers can control the subsystems with simple gains (e.g. $K_P = 1$, $K_I = 0$). If such gains can be found by trial-and-error for a randomly selected case, then the same gain set can be used to check whether reasonable results could be obtained for other randomly selected cases.

In this electrical system, trial-and-error approach quickly yielded acceptable results for the DC bus controller. The selected gain set returned simulation good results for various cases. This was expected as the voltage on the battery-DC bus side did not change much and the controller was able to maintain the system voltage at the output port of the bus with the selected gains.

For the cases where subject matter expertise is not available and the trial-and-error approach does not yield acceptable results and becomes too cumbersome, a more systematic approach is proposed.

For the remaining gains, i.e. the motor drive gains, a more systematic approach which was proposed by Hypothesis 4 (see Section 4.3.2) was taken.

The trial-and-error approach only yielded good results for the DC bus controller gains. For the motor controllers, the surrogate modeling approach was used to perform sensitivity analysis to determine which variables have a greater impact on the system response. To this end, a second DoE was created. An additional design space of the motor gain variables were added on top of the design variables shown in Table 8.2, making the new design space consist of 11 design variables. The second DoE was created with the same augmented design approach, but the number of cases were increased to 10,000 due to the increased number of variables.

Same 2-second long simulations were run for the 10,000 cases in the DoE. Note that such high number of simulations were able to be done thanks to parallel computing. For each simulation, the root mean squared error between the tracked signal (reference motor RPM) and the response (actual motor RPM) was recorded.

Then, an Artificial Neural Network (ANN) model was fit to the relative mean error in the signal using the 11 design variables and 10,000 cases which made up the DoE. A two layer ANN model with 20 nodes each gave good results. The model fit to the training data which made up 2/3 of the DoE cases produced an R-square of 0.99, and the validation data which was made up by the remaining cases produced an R-square value of 0.98. The actual

by predicted and the residual by predicted plots are also shown in Figure 8.12 for both the training and the validation points.

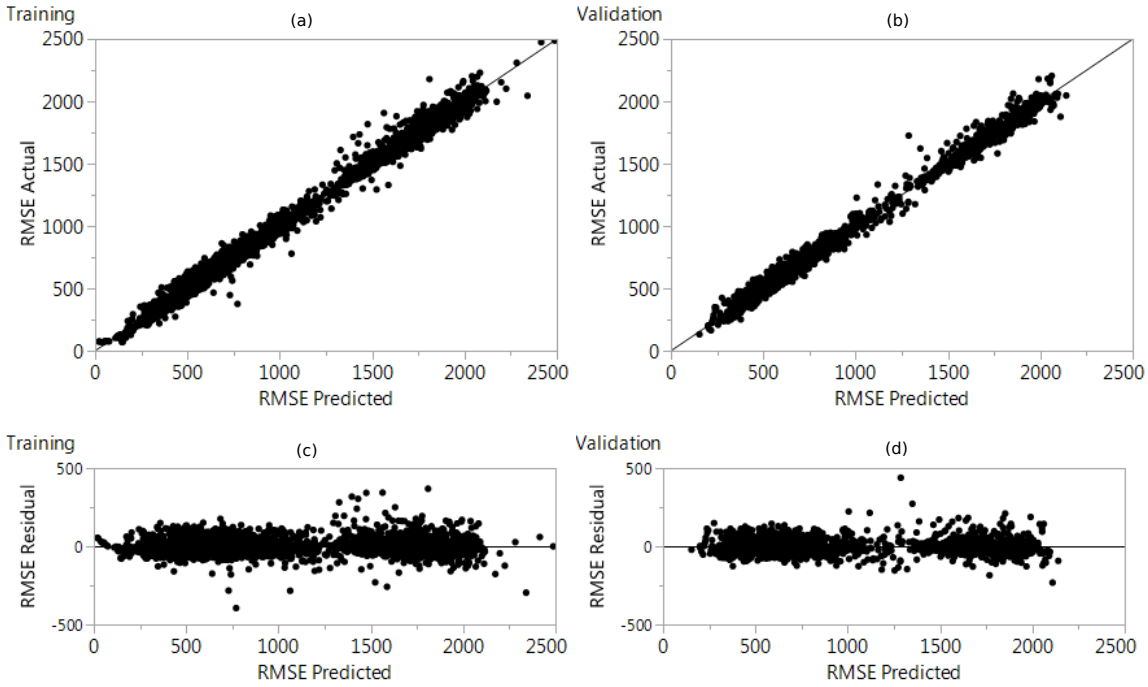

Figure 8.12: Goodness of the fit tests for the ANN model: (a) and (b) shows the actual by predicted results for training and validation points; (c) and (d) shows the residual by predicted results for training and validation points, respectively.

The prediction formula which was published using the ANN model was then used in the variable importance assessment in JMP, which is a statistical data analysis software. This assessment is independent of the model type and fitting method, but the predicted values are calculated by the prediction formula. This assessments computes the variability in the predicted response in terms of a range of variation for each factor by using the Monte Carlo technique with uniform distribution. [121]

The variable importance assessment showed that mainly the proportional gains of the SVM d-axis and q-axis regulators (i.e. $K_{P,svm,d}$ and $K_{P,svm,q}$) drove the root mean square error of the signal. The next gain which made the third-most impact on the response was the proportional gain of the speed controller ($K_{P,speed}$). The integral gains of the SVM d-axis and q-axis regulators (i.e. $K_{I,svm,d}$ and $K_{I,svm,q}$) had little to no impact on the response.

Next, the ANN model was used to perform sensitivity analysis to reveal the sensitivity of the signal tracking error to the controller gains were studied under varying model design variables. The desirability function was set up to minimize the error in the tracked signal for majority of the simulation input variables. Then, the cases which yielded a relative mean error under 10% were identified, and the which corresponded to the median error was selected and carried forward to the optimization step.

The optimization problem was set up with the *important* controller gains as the control variables. The Nelder-Mead simplex direct search method was utilized for the unconstrained optimization. Although this algorithm does not guarantee to converge to a local minimum, this potential problem was avoided by setting the initial guess to be the gain set obtained from the sensitivity analysis.

Since the initial conditions were set with the knowledge of the design space, the simplex method converged to a local minimum within only a few iterations. The resulting gain set was tested with the original cases in the first DoE set. Out of 1065 cases, 410 cases were deemed successful with the given gain set as they returned a signal tracking error under 10%.

Then, a second case was selected to tune the controller gains for the majority of the remaining realizable cases and the optimization problem was solved once more for this case. Out of the remaining 645 cases, 238 cases yielded a signal tracking error under 10% with the second gain set.

This process was repeated for a few more times, but the gain sets found for for the remaining 417 cases did not result in an accepted margin of error. This was expected as the sensitivity analysis already revealed that the remaining region in the design space would return a signal tracking error greater than 10%. Thus, these failed cases were eliminated from the original DoE, and only 648 cases along with two gain sets were carried forward for to be used in the next experiment.

8.4.2 Summary of the Results of Experiment 4.2

The integration of the surrogate modeling technique and Monte Carlo simulations to the system design optimization problem provided a-priori knowledge about the design space in terms of both the controller gains and the simulation input variables.

Experiment 4.2 proved that:

1. There is no need to try to optimize each case in the design space represented by the DoE

2. A handful of gain sets which tune the controllers for majority of the system applications can be obtained by utilizing the system design optimization enhanced by the Monte Carlo simulations method

Experiment 4.2 verifies the second argument of Hypothesis 4, which is that the controllers of the electrical system which can be tuned via gain scheduling where the schedules are determined by jointly utilizing Monte Carlo simulations and a system design optimization technique can be utilized to reduce the optimization efforts and obtain a few numbers of gain sets to control the majority of the realizable cases of the DoE.

8.5 Surrogate Modeling of Transient Constraint Violations (Experiment 4.3)

In the previous sections of this chapter, the necessary experimental apparatus was prepared to finally conduct the final experiment of Hypothesis 4. This section addresses Experiment 4.3 which is revisited below:

Experiment 4.3: *Run the simulations defined by the realizable cases of the first DoE with the appropriate timescale and the gain schedules obtained in Experiment 4.2. Define two undesirable transient behaviors for the electric motor and set a transient constraint. Examine each simulation result at the neighborhood of the moment where a change occurred in the input signal. Identify which cases violate which constraints and categorize*

the cases based on constraint violation separately for each transient behavior. Fit surrogate model to the response data, and determine whether there exists a clear trend between the mission level inputs and the constraint violations by evaluating variable importance and performing sensitivity analysis. If there exists a relationship between the two, set up a conditional rule set to calculate the probability of the constraints being violated based on the mission level changes. Compare the rule sets obtained for the two transient constraints.

8.5.1 Constraint Definitions for the Significant Transients

There are many aspects to measure the power quality of an electrical system. For instance, the aircraft electric power characteristics are defined in MIL-STD-704F by the U.S. Department of Defense. [58] However, as discussed previously, these standards are not specifically for EA/HEA concepts and thus cannot be used directly. The EPGDS used in ES/HEA applications experience dramatically higher loads than the secondary power EPGDS, and as a result, the electrical system characteristics differ.

For instance, the RMS voltage constraint applied in Section 8.2 cannot be applied to all of the cases of the DoE, simply because the electric motor used in this electric architecture is a variable voltage motor. Because the motor voltage is varied by the controllers to match the required motor speed, the constraints given for the 115 VAC systems could not be utilized.

Due to the absence of established standards for EA/HEA, some studies in literature use the MIL-STD-704F as basis to propose modified limits on the steady state and transient electrical system characteristics. [122] In the following implementation, a similar approach was taken.

The methodology proposed in Hypothesis 4 does not depend on the definition of the constraint. It can be utilized for both steady-state and transient constraints for a given electrical system. The resulting conditional rule set would differ for different constraint definitions, but the methodology to generate the rule set remains the same.

In this dissertation, the definition made by MIL-STD-704F was used for the term "transient" which is quoted directly from MIL-STD-704F (Ref. [58]) below:

"A transient is a changing value of a characteristic that usually occurs as a result of normal disturbances such as electric load change and engine speed change. A transient may also occur as a result of a momentary power interruption or an abnormal disturbance such as fault clearing.

(a) *Transients that do not exceed the steady state limits are defined as lesser transients.*

(b) Transients that exceed the steady state limits but remain within the specified normal transients limits are defined as normal transients.

(c) Transients that exceed normal transients limits as a result of an abnormal disturbance and eventually return to steady state limits are defined as abnormal transients."

As explained previously, the significance of a transient is determined by constraint violation. Thus, the constraint definition can be made liberally to address any of the transient categories (a,b, or c) given above. In the following application, two separate constraints and thus two "significant transients" were identified to serve as an example implementation of the methodology on the electrical system given in Section 8.1.

1. **Voltage Sag:** momentary decrease in the voltage outside the normal tolerance. [57] The normal tolerance was chosen as to be a decrease in the AC voltage which is no greater than 20% of the steady-state voltage.

2. **Voltage Swell:** momentary increase in the voltage outside the normal tolerance. [57] The normal tolerance was chosen as to be an increase in the AC voltage which is no greater than 20% of the steady-state voltage.

8.5.2 Time Domain Signal Processing

Section 8.4 described how the controller gains of the system at hand were tuned sing DoE. Good signal tracking results were obtained for 648 cases out of 1065 cases of the DoE within a 10% relative error margin. These 648 cases were carried forward to process various signals gathered for the EPGDS in the architecture.

Each simulation was run for 2 seconds with a sampling time step of 2 microseconds. During each 2-second long simulation, 1,000,035 samples were gathered for each signal, making up 648,022,680 samples in total per signal.

Since the transient constraints were defined for the AC voltage, the subsystem of interest became the induction motor drive as the sole AC subsystem in the given electric propulsion system. Out of the recorded signals previously listed in Table 8.1, the RMS voltage response of the electric motor drive was carried forward for the signal processing stage.

In each simulation, a mission level input was changed at precisely t=1 second. The reaction window was set to be 0.1 seconds within a mission level change had occurred. Then, the minimum and maximum values of the RMS voltage within t=1 s and t=1.1 s were compared against the average RMS voltage in the neighborhood of t=0.8 s and t = 0.99 s, i.e. the steady-state RMS voltage before the system was triggered. The cases where the RMS voltage dropped beyond 80% of the steady-state value violated the previously set voltage sag constraint, and were tagged as such. Similarly, the cases where the RMS voltage rose beyond 80% of the steady-state value violated the previously set voltage swell constraint, and were tagged as such.

An example constraint violation where both the voltage oscillated beyond both the minimum and maximum tolerances is demonstrated in Figure 8.13, along with the system dynamics before, during and after the violation.

The simulation inputs and the electric motor dynamics before and at the time of the constraint violation were also recorded for each case. In some cases, the tolerance was

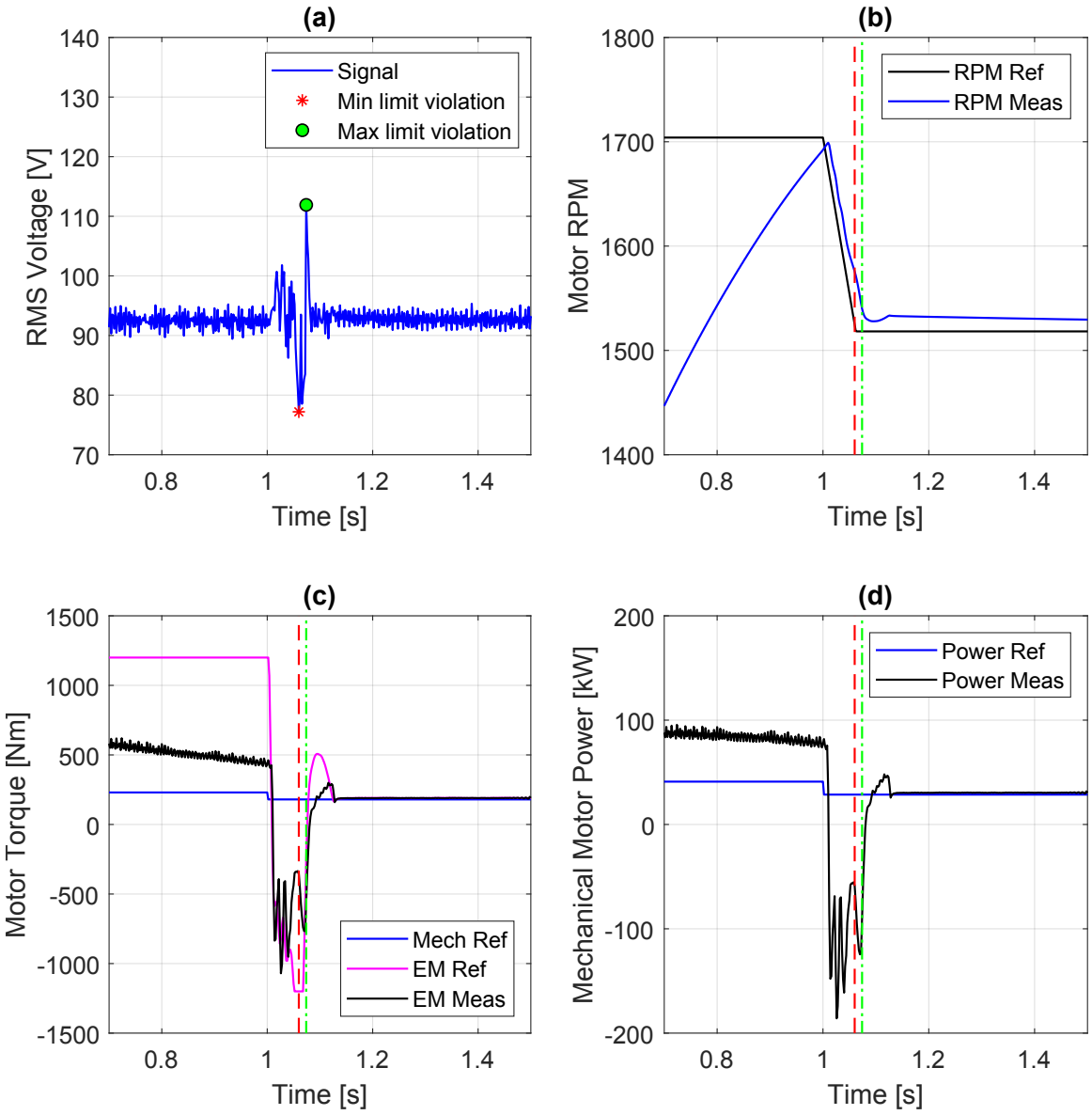

Figure 8.13: An example case where voltage exceeds minimum and maximum limits within the reaction window. The moment of the minimum constraint violation is shown with a red star on figure (a), and vertical red lines on figures (b), (c), and (d). The moment of the maximum constraint violation is shown with a green dot on figure (a), and vertical green lines on figures (b), (c), and (d).

exceeded multiple times for a given constraint. These violations were recorded separately at each instance. The cases where no constraint violation occurred were also recorded in a similar manner, but the time of constraint violation was changed with 1.05 seconds, that is, 0.05 s after the mission level changes had occurred.

Table 8.3: Number of cases and instances of constraint violation per constraint type.

Event Count	Sag	Swell
Number of cases without violation:	603	617
Number of cases with violation:	45	31
Number of instances with violation:	117	45

The number of instances recorded were shown in Table 8.3 by case and instance. These instances

8.5.3 Modeling the Constraint Violations

The instances recorded in the previous step were grouped into two categories based on constraint violation per constraint type:

- **Category 0:** consists of the instances which did not violate the constraint
- **Category 1:** consists of the instances which did violate the constraint

The distribution of the number of occurrences of each category are shown Figure 8.14 by constraint type.

It can be seen from Figure 8.14 that most cases of the DoE did not violate either one of the constraints. Compared to the swell constraint, there were 117 more instances recorded which violated the voltage sag constraint. Moreover, it can be seen that the voltage sag constraint violation category makes up the 21% of all the instances recorded for this constraint type. Whereas the voltage swell constraint violation category makes up only 7% of all the instances recorded for the swell constraint.

A more even distribution is usually preferred in model creation so that neither of the categories would be underrepresented. However, since the Category 1 represents an undesired

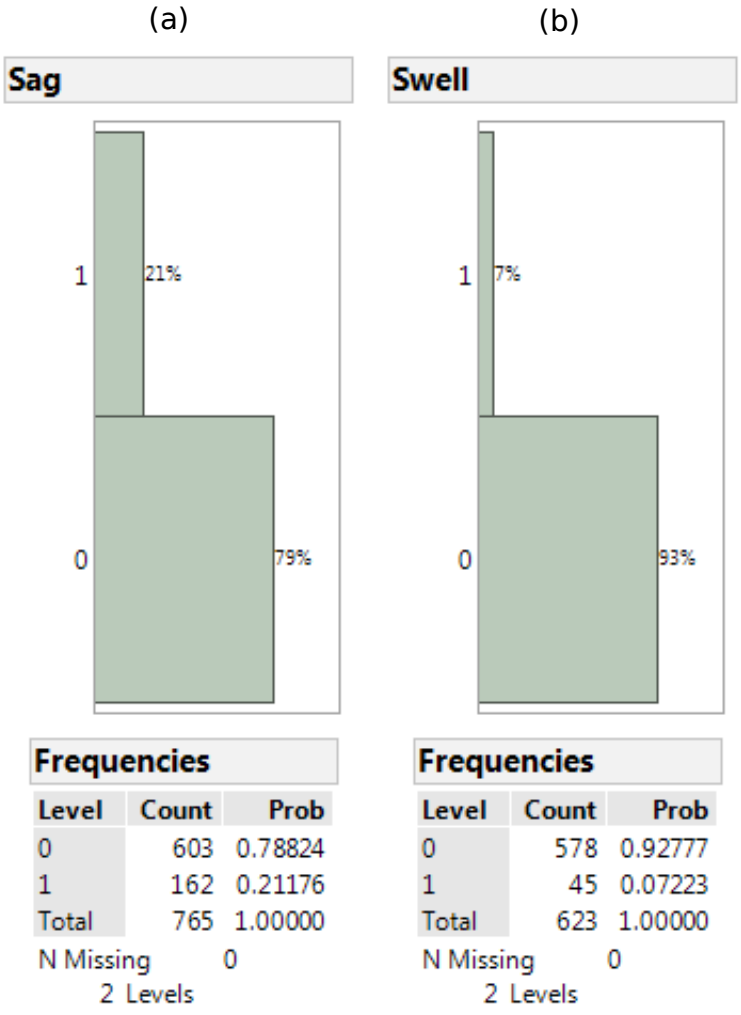

Figure 8.14: Distribution of constraint violation for (a) Sag constraint, and (b) Swell constraint. Category "1" means constraint violated, Category "0" means no violation.

event, such an uneven distribution was expected as it is a demonstration that the developed electrical system is in most cases capable of delivering the desired power quality.

Once the categories are established, a categorical surrogate model for each constraint type was fit to the data. The design factors used in these models were chosen based on the mission level changes and the state of the system *before* the time of the incident. The changes in the simulation inputs were expressed in terms of the initial motor RPM reference, absolute change in the motor RPM input, initial mechanical torque input, absolute change in the mechanical torque input, and battery state of charge.

Table 8.4: Confusion matrix and rate for the categorical voltage sag constraint model.

Training			*Validation*		
Actual	**Predicted Count**		**Actual**	**Predicted Count**	
Sag	**0**	**1**	**Sag**	**0**	**1**
0	400	2	0	197	4
1	9	99	1	3	51
Actual	**Predicted Rate**		**Actual**	**Predicted Rate**	
Sag	**0**	**1**	**Sag**	**0**	**1**
0	0.995	0.005	0	0.980	0.020
1	0.083	0.917	1	0.056	0.944

The main reason behind selecting the design factors as these variables was to test whether a good surrogate model could be fit to estimate the constraint violation with only the variables calculated at the mission level. That's why the current state of the motor was expressed by the *initial* state, i.e. the values which correspond to the mission leg *i*, instead of the values recorded at the instance of a constraint violation.

Due to the high complexity of the system, the Artificial Neural Network approach was chosen as the surrogate model type. Two thirds of the data was used to train a categorical ANN model, and the remaining one thirds was used to validate the model. As a result, two categorical ANN models for each constraint type were obtained.

The goodness of the fit was first evaluated by the confusion matrices obtained for the training and the validation data. The matrices are shown in Table 8.4 and Table 8.5 for the sag and swell constraint models, respectively.

The confusion matrix displays the results in terms of true positive, false positive, true negative and false negatives. It can be seen from Table 8.4 that the model was able to predict the actual response with more than 90% accuracy for both the training and the validation

Table 8.5: Confusion matrix and rate for the categorical voltage swell constraint model.

Training			*Validation*		
Actual	**Predicted Count**		**Actual**	**Predicted Count**	
Swell	**0**	**1**	**Swell**	**0**	**1**
0	379	0	0	180	5
1	0	27	1	1	17
Actual	**Predicted Rate**		**Actual**	**Predicted Rate**	
Swell	**0**	**1**	**Swell**	**0**	**1**
0	1.000	0.000	0	0.973	0.027
1	0.000	1.000	1	0.056	0.944

data. It was able to correctly predicted 99 cases out of 108 cases in the constraint violation category (category 1), which corresponds to a success rate of 91.7%. The success rate for the category 0 (no violation) was even higher, where the model was able to predict 400 cases out of 402; which is a success rate of 99.5%.

A similar success is seen when the model was used to predict the validation data. Validation data consisted of the cases which were not used to train the model. This step was necessary as one problem which can be faced when dealing with ANN is over-fitting the data. This problem can be avoided by validating the model against data which was not used in training. If the model was an over-fit, then the validation results would be poor. As it can be seen from the *Validation* column of Table 8.4, this was not the case for this model. The model correctly predicted the no-violation cases (category 1) with a 98% success rate by missing only 4 cases out of 201. Similarly, it correctly predicted the cases which violated the sag constraint (category 1) with a success rate of 94.4% by missing only 3 cases out of 54.

The swell constraint model was also successful in predicting both the training and validation data with a success rate over 94%, as shown in Table 8.5. In fact, the model fit on the training data was so good that it did not miss any case in neither of the two categories. Fortunately, this was not an over-fit as validated by the success of the predictions made on the validation data. The model was able to correctly predict 180 Category-0 cases out of 185 data points, which resulted in a success rate of 97.3%. In spite of the low number of data points in Category-1 with respect to Category-0, the model provided very good results in predicted 17 of the 18 Category-1 cases correctly.

The high success rates are strong indicators that the models are able to predict either of the two categories not by chance, but by the goodness of the fit. Nevertheless, the predicted assignments were also tested by Matthews correlation coefficient (MCC), which is a technique to measure the quality of binary classifications in biology and machine learning. [123] MCC returns a value between -1 and 1, where -1 means that the predicted and the observed cases are in total disagreement, 0 means there is no correlation between the predictions and the observation, and 1 means a perfect prediction. [124]

For binary classifications, MCC is given by Eqn. 8.1 where TP and FP stand for true and false positives, TN and FN stand for true and false negatives, respectively.

$$\mathbf{MCC} = \frac{TP * TN - FP * FN}{\sqrt{(TP + FP)(TP + FN)(TN + FP)(TN + FN)}} \tag{8.1}$$

Table 8.6 gives the resulting MCC for training and validation predictions of each model. MCC for all the sag constraint model returned very high values for both the training and validation data. As a result of the goodness of the fit tests, this model was deemed acceptable to predict the sag voltage constraint violations.

The swell model also returned high MCC values and was deemed acceptable to carry forward. The validation MCC value of 0.839 is not a concern since it points to a reasonable correlation between the predicted and the observed data in the MCC scale. However, the caution made earlier about the scarceness of the Category-1 data must be reminded: had

there been more points which violated the voltage swell constraint, this model could have been improved further. With that being said, the low number of Category-1 cases observed in the design space of interest also implies that this constraint is violated only under some extreme cases, and thus should not be encountered often over the course of the actual flight mission.

Table 8.6: Matthews correlation coefficient for the training and validation confusion matrices of sag and swell constraint violation models.

Sag Constraint Model		*Swell Constraint Model*	
Training	**Validation**	**Training**	**Validation**
0.935	0.918	1.0	0.839

8.5.4 Establishing the Conditional Rule Set for Step Size Determination

The categorical ANN models created in the previous section were used to predict the probability of the respective constraint violations happening. If A is the event of constraint violation, then $P(A) = 1$ means a 100% probability of violating the constraint. Conversely, $P(A) = 0$ means 100% probability of *not* violating the constraint. Thus, the two categories established in the previous sections were used to predict the value $P(A)$ takes under varying operation scenarios based on the design factors.

Voltage Sag Transient

The models were first utilized to estimate variable importance and perform sensitivity analysis. The same method used in Section 8.4 to establish variable importance was used in these models. Figure 8.15 provides the distribution of the main and total effects of each design factor for the voltage sag. In this figure, the main effect is an indicator of the relative contribution of that factor alone, whereas total effect shows the variable importance of a

factor in terms of the relative contribution of the factor both alone and combined with the rest of the design factors. The bar charts in the figures illustrate the total effect.

Overall

Column	Main Effect	Total Effect
delta RPM ref	0.303	0.81
delta Tmech	0.128	0.605
RPM_ref_i	0.036	0.233
Tmech_i	0.02	0.116
SOC_i	0.016	0.078

P(Sag=0)

Column	Main Effect	Total Effect
delta RPM ref	0.303	0.81
delta Tmech	0.128	0.605
RPM_ref_i	0.036	0.233
Tmech_i	0.02	0.116
SOC_i	0.016	0.078

P(Sag=1)

Column	Main Effect	Total Effect
delta RPM ref	0.303	0.81
delta Tmech	0.128	0.605
RPM_ref_i	0.036	0.233
Tmech_i	0.02	0.116
SOC_i	0.016	0.078

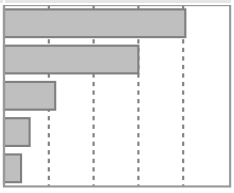

Figure 8.15: Variable importance assessment of the voltage sag model.

It can be seen from Figure 8.15 that the two most important design variables are the change in motor speed and mechanical torque inputs (shown with "delta RPM ref" and "delta Tmech" in the figure). These two factors drive the overall voltage sag constraint model. The third impact comes from the initial motor speed ("RPM_ref_i"). The impact of initial mechanical torque and initial battery SOC on the model results are rather unimportant compared to the other three factors.

Figure 8.15 also shows the variable importance for each category, where the table listed under $P(Sag = 1)$ assesses the design factors for the constraint violation category, and the table listed under $P(Sag = 0)$ does the same for the no violation category. The same distributions as the overall model can be seen in the individual models.

The variable importance assessment is also a means to validate the model, when the effect of the design factors are known or can be estimated by real life results. The fact that the voltage sag constraint model is driven mostly by the changes in the mission level behavior (i.e. simulation inputs) aligns well with the nature of this transient. Furthermore, it also shows that the initial conditions are at lesser importance compared to the absolute changes, which increases the confidence in the model when using for various mission level conditions.

The variable importance report provided how much impact each design factor has on the model predictions, but did not reveal *how*. The nature of the design factor impacts can be visualized with prediction profilers, which was previously explained and used in the sensitivity analysis performed in Section 7.3.

The prediction profiler is an interactive tool to see the impact of changing a single variable while keeping the other factors constant. The impact made on the prediction results depend heavily on what value the other factors are being kept fixed at. Although it is not possible to picture all of the scenarios simulated with the prediction profilers on paper, some important aspects are provided with snapshots from the multiple scenarios.

The first operation scenario is demonstrated with the prediction profiler in Figure 8.16. There are two profilers in this figure: one for each category. The top row demonstrates the probability of the event *(Sag=0)* happening, i.e. the probability of *not* violating the voltage sag constraint. Conversely, the bottom row demonstrates the probability of the event *(Sag=1)* happening, i.e. the probability of *violating* the voltage sag constraint. Because these probabilities are dependent on each other (since $P(Sag = 0) + P(Sag = 1) = 1$), the effect of the design factors which are displayed on the x-axis (or columns), will be the opposite of each other.

In this scenario, there is an initial mechanical torque input of 300 Nm on the motor shaft at a speed of 2200 RPM. This setting corresponds to a power draw of 69.1 kW. At this point, the battery SOC is 60%. These conditions correspond to the mission leg i. As a

result of the mission performance analysis, the load on the motor is raised to 96.3 kW by increasing the motor speed by 100 RPM and torque by 100 Nm.

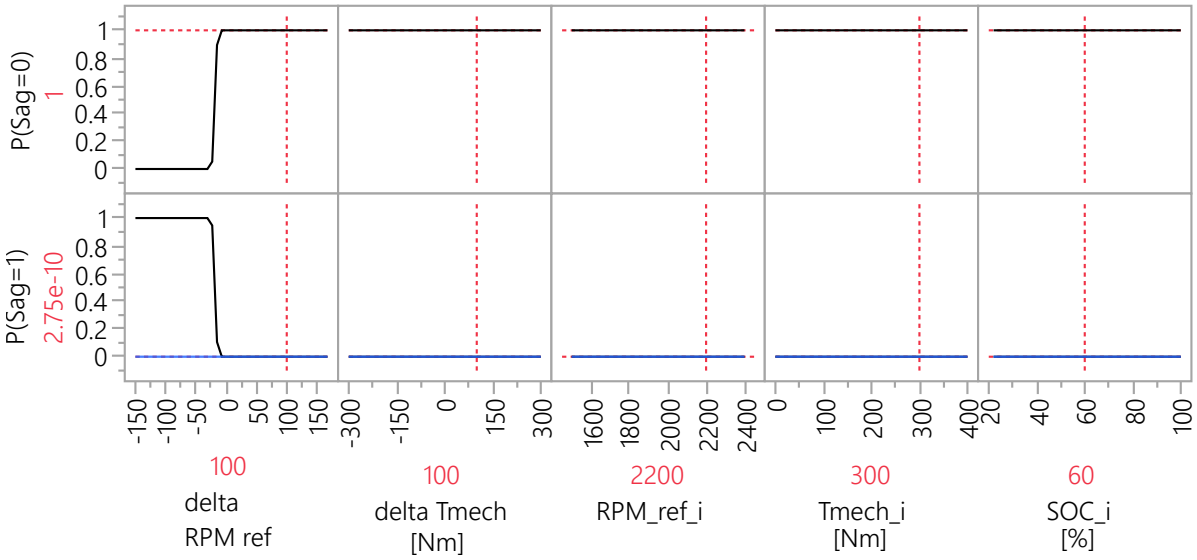

Figure 8.16: Prediction profiler of the voltage sag constraint violation predictions, Scenario 1.

At these conditions, the model predicts that the probability of a voltage sag not occurring is 1, which means that there is no need to perform transient analysis to decide whether a significant transient would occur that would cause a sag in the motor voltage outside the predefined tolerance limits. This is a very valuable information: although there was a change in the power requirement, the electric motor voltage is predicted to stay within the accepted boundaries, and thus the mission performance analysis can be continued without interruption.

Another interesting result of this scenario is that at the given operational conditions, the only factor that would affect this decision is the change in the motor speed. This can be seen from the flat trends of all of the design factors except the motor speed. The flat lines means that at the given conditions, if the design factor is varied while keeping the other factors constant, the outcome (in terms of the probability) would not change. The only factor that can increase the probability of violating the sag constraint is the absolute change in the motor speed. Moreover, it is not the magnitude of the speed that would cause such a

drastic change, but the direction of the angular velocity.

The motor RPM profile in Figure 8.16 shows that the probability of sag constraint violation increases if and only if the electric motor is decelerated from its initial condition. In fact, even a slight deceleration would be enough to increase the probability of a sag occurring to 100%. In fact, the impact of the absolute change in the motor speed is so dominant that the other factors, when individually varied while the other factors were kept constant at the shown values, had almost no impact on the outcome.

However, as explained previously, the impact of the design factors are not always as shown in Figure 8.16, and the trends can change when the conditions are changed. To illustrate, a second scenario with different operational conditions was given in Figure 8.17.

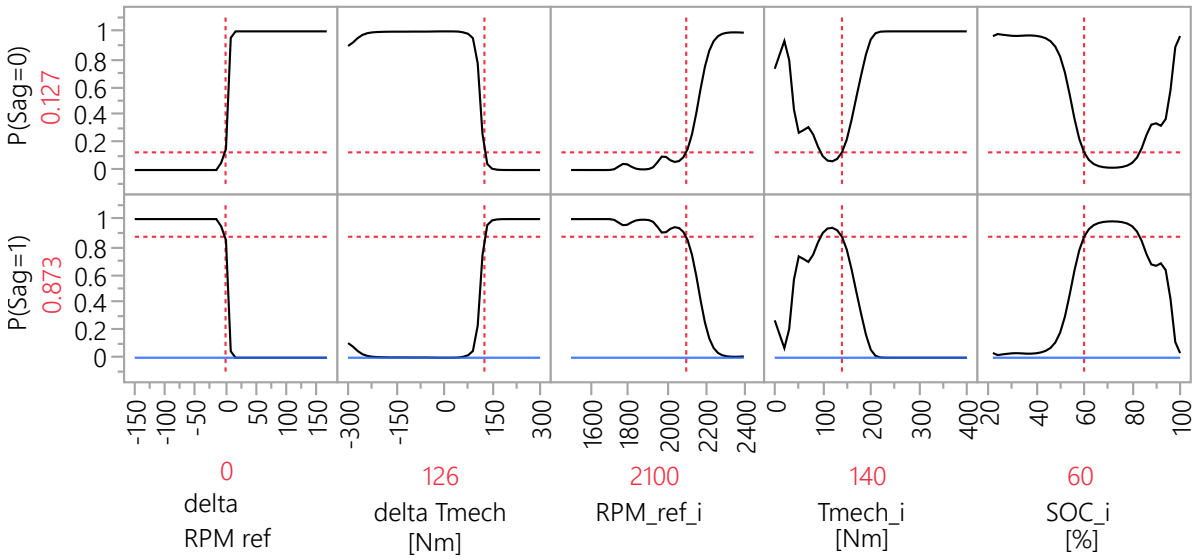

Figure 8.17: Prediction profiler of the voltage sag constraint violation predictions, Scenario 2.

In the second scenario shown in Figure 8.17, the motor speed remains constant at its initial speed of 2100 RPM. The battery is at the same state of charge of 60% as it was in the first scenario. This time, the mechanical torque requirement was increased from 140 Nm to 266 Nm, increasing the load on the motor from 30.8 kW to 58.5 kW at a constant speed. As it can be seen from the profiler, at the given conditions each design factor has a substantial impact on the predicted result, contrarily to the previous scenario.

At these conditions, the model predicts that there is a 87.3% probability of violating the electric motor voltage sag constraint. When these conditions are encountered at the mission level analysis, the step size should be decreased to the appropriate timescale to perform transient analysis due to the high probability of a constraint violation. Or as an alternative to performing transient analysis, the same power requirement could be met at different motor speed and torque settings based on the trends seen in the prediction profiler.

It should be noted that the trend seen in the initial mechanical torque in Figure 8.17 might seem peculiar due to the oscillation followed by a rapid change in the trend as the torque decreases. However, the increment in the probability of a violation *not* occurring as the mechanical torque is dropped is natural as the motor torque drops to zero and the load on the motor is removed. Same is true for the negative change in the torque.

An interesting relation between the battery SOC and the probability of constraint violation can also be seen in Figure 8.17. The up-and-down trend in $P(Sag = 0)$ due to the battery SOC reflects the response of the electrical system as a whole, and not only the electric motor. As the battery gets discharged, the battery voltage drops. As a result, the voltage conversion at the DC bus and thus the current carried through change. Thus, the dynamic response of the electrical system varies with the SOC.

Many different scenarios can be populated with the prediction profiler. As it can be seen from the two example scenarios provided above, even a slight variation in the design factors can change the electrical system characteristics and thus the probability of having a constraint violation. In complex systems such as these, it might be impossible to put boundaries on the design variables individually to express how the system would react as the impact might depend heavily on the state of the remaining design factors.

At this point, the strength of the surrogate model comes into play. The created categorical ANN model can be used to predict the probability of violating a constraint without sacrificing computational resources to conduct transient analysis at unnecessary conditions. The necessity can be established based on the confidence level on the surrogate model, and

how important a constraint violation is.

Hypothesis 4 proposed establishing a conditional rule set to determine when the temporal step size of the analysis should be changed to perform transient analysis. For this implementation, this conditional rule set was defined as the following mathematical expression in the light of the results obtained above:

$$\tau = \begin{cases} 2\,\mu s, & \text{if } P(Sag = 1)_i > 0.5 \\ \tau_i, & \text{if } 0 \leq P(Sag = 1)_i \leq 0.5 \end{cases} \tag{8.2}$$

where τ is the adaptive temporal step size, τ_i is the mission analysis step size for the mission leg i. τ_i is determined inherently by the mission analysis algorithm, but the order is minutes.

Eqn. 8.2 sets a conditional rule to change the step size τ based on the probability of a voltage sag constraint being violated. It reads as:

- If the probability of a sag voltage constraint violation is more than 50%, then change the time step to 2 microseconds to conduct transient analysis
- If the probability of a sag voltage constraint violation is 50% or less, carry on to mission performance analysis without changing the time step

The 50% limit was determined based on the model. Since the model passed the goodness of the fit tests, and there was enough data to represent both categories, the limit was set such that transient analysis would be done only when the model was indecisive, or confident about a constraint violation.

The probability of $P(Sag = 1)$ was determined based on the prediction function ζ_{sag} which the categorical ANN model produced as follows:

$$P(Sag = 1)_i = \zeta(\Delta\Phi_i)_{sag}$$

The prediction function ζ is a function of $\Delta\Phi_i$ which was earlier defined as the change in a subset of mission level requirements between the beginning of the mission leg i and the end of the mission leg $i+1$, given by:

$$\Delta\Phi_i = \Phi_{i+1} - \Phi_i;$$

For the categorical ANN model in this application, $\Delta\Phi_i$ consists of the relative change in motor speed (expressed by the initial motor RPM and absolute change in motor RPM), relative change in mechanical torque of the motor (expressed by the initial motor torque and absolute change in motor torque), and the initial condition of the battery state of charge.

Voltage Swell Transient

The same approach taken for predicting the probability of a voltage swell occurring was followed for the second voltage swell model. First, the variable importance was assessed to inspect whether the model was driven by a few or all of the design factors. The results are presented in Figure 8.18.

It can be seen by comparing Figure 8.18 to Figure 8.15 that the design variables of the voltage swell model have a more evenly distributed total effect on the predicted response than the voltage sag model. In Figure 8.15, it was seen that the trend in the main effects of the design factors aligned with their total effects, meaning if a factor had high importance by itself, it also had a high (even increased) importance when its effect was combined with the other factors.

In Figure 8.18, however, it can be seen that although the total effect of the absolute change in motor torque input is high, its main effect is rather low compared to the rest of the factors. This indicates to a significant interaction between this factor and the others. This is not unusual for a complex system like the one that is being studied.

The previously studied first operation scenario for the voltage sag model was revived

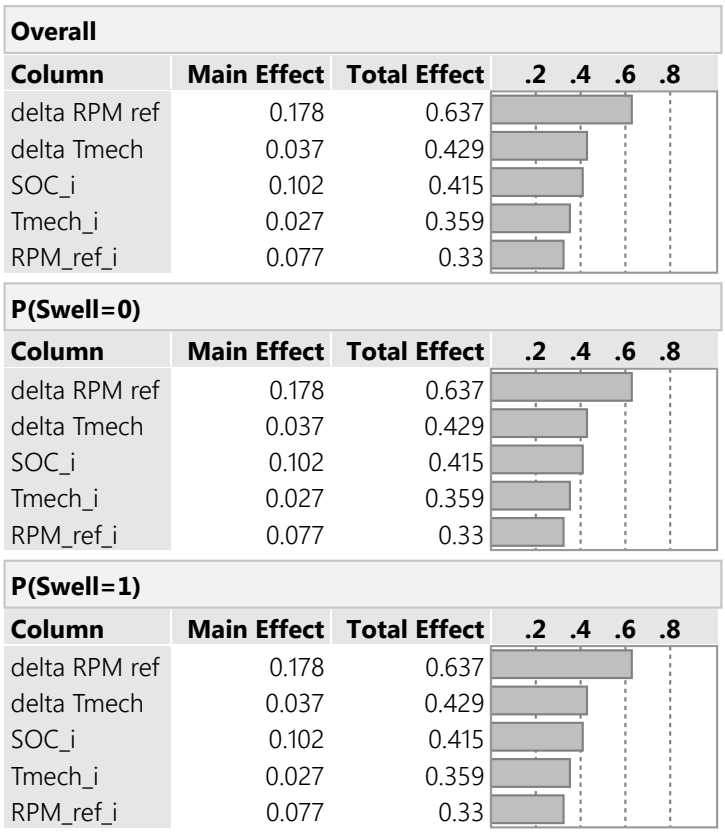

Figure 8.18: Variable importance assessment of the voltage swell model.

for the voltage swell model as well. The prediction profiler set up for Scenario 1 is demonstrated in Figure 8.19 for the voltage sag model.

For the current operation conditions given in Figure 8.19, the categorical model predicts that the probability of the electric motor dynamics violating the swell constraint is almost non-existing. Thus, the models predict that the conditions given in Scenario 1 do not trigger a significant transient in terms of voltage sags or swells.

The trends seen in Figure 8.19 for the swell constraint are somewhat different that those seen in Figure 8.16 for the sag constraint. At the given operation conditions, the main driver which can change the probability of a swell constraint violation drastically is the absolute change in motor speed. In fact, this trend is almost the same as the one seen in Figure 8.16 previously with the voltage sag model. In both cases, the probability of a constraint violation increases rapidly when the motor decelerates, provided that the other

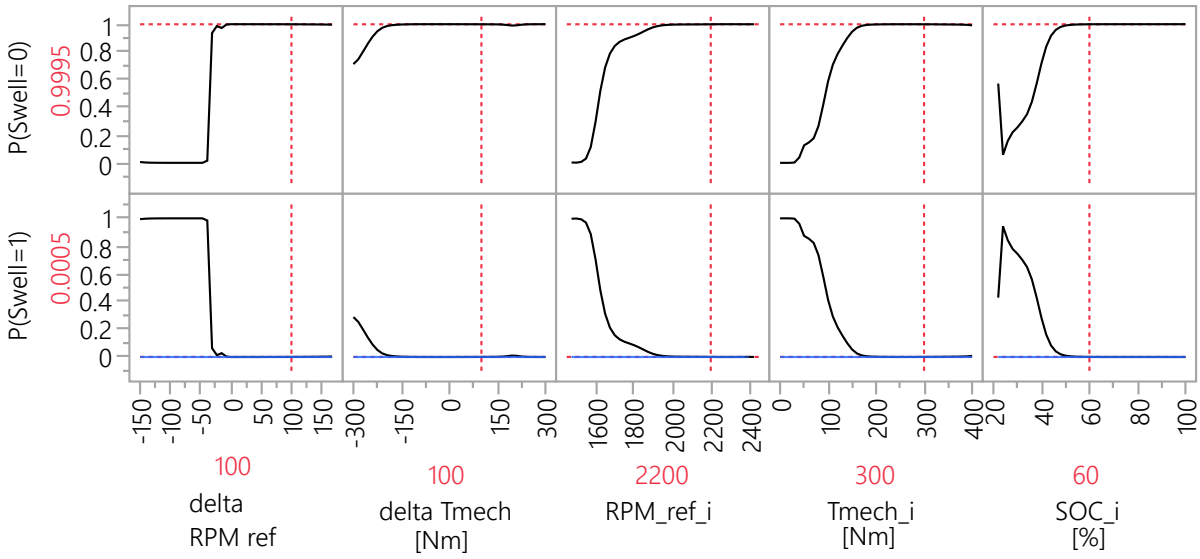

Figure 8.19: Prediction profiler of the voltage swell constraint violation predictions, Scenario 1.

factors remain constant.

Contrary to the sag model, the swell model predicts that a change in the other factors can also cause a swell voltage constraint violation. For instance, if the mechanical load is removed instantly (i.e. absolute change in mechanical torque is set to -300 Nm, which means a zero torque at the end of the mission leg since the initial torque is also 300 Nm), then the probability of a swell constraint occurring increases slightly. Similarly, if there were no load at the beginning of the mission leg i (which corresponds to a zero initial mechanical torque), then a sudden increase in the mechanical torque by 100 Nm is highly likely to cause a swell constraint violation, as P(Swell=1) increases to almost 1. Similar to the sag trends, these constraint violations due to a sudden change in the load align with the results from literature. [57]

A peculiar trend is seen at low SOC levels, since the probability of constraint violation first increases and then rapidly drops. This might have been caused by two things: first, because this drop is observed at such a low SOC level, i.e. the edge of the design space, there might not have been enough points to train the ANN model correctly. Second, the voltage drops rapidly as the battery is discharged close to its limit, which is in this case,

20% SOC. This sudden change in the voltage characteristics of the electrical system might have a positive impact on the voltage swell transient.

The second scenario was not replicated for the swell constraint, as the results turned out to be similar to the ones seen in Scenario 1. Instead, a rather rare case of voltage constraint violation was found at different mission conditions and demonstrated in the prediction profiler shown in Figure 8.20.

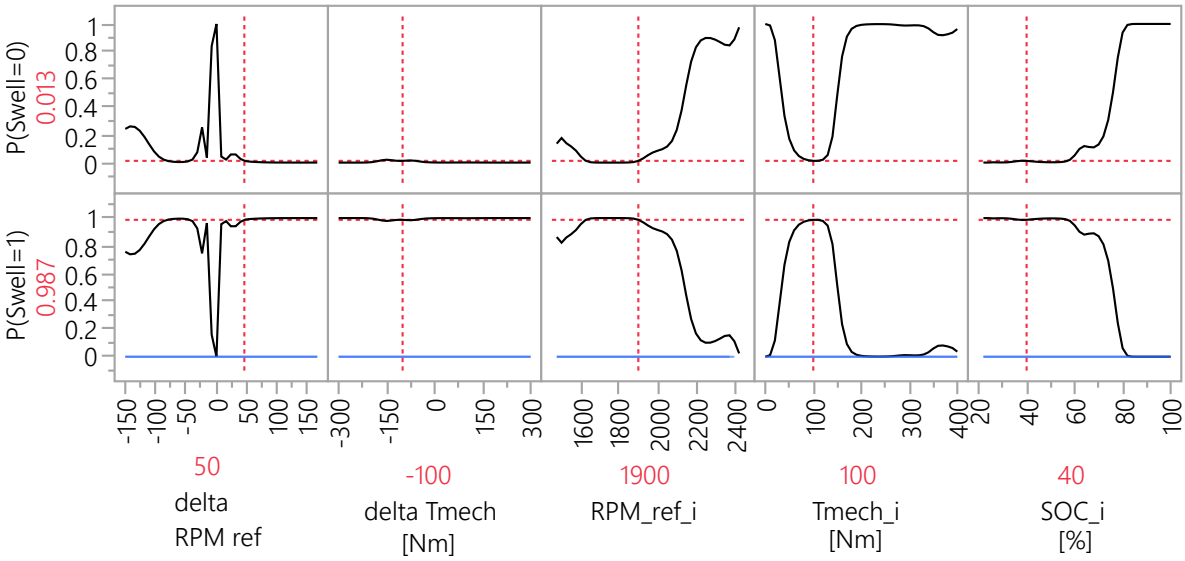

Figure 8.20: Prediction profiler of the voltage swell constraint violation predictions, Scenario 3.

The scenario shown in Figure 8.20 produces a high probability of voltage swell constraint violation, as P(Swell=1) was predicted to be 98.7%. In this scenario, the mechanical torque was decreased from 100 Nm to 0 Nm, while the motor speed was slightly increased from 1900 RPM to 1950 RPM at a battery SOC if 40%.

It can be seen from the trends that there are multiple ways of avoiding the constraint violation, such as having a higher initial motor speed, higher initial torque, a higher initial SOC, or not changing the motor speed. The latter one is an interesting result. In terms of the absolute change in the motor speed, the probability of not violating the swell constraint (i.e. $P(Swell = 0)$ spikes up only when there is no change for the given conditions. This can be explained by the following discussion: any change in motor speed is delivered by a change

in the motor voltage by the controllers. It is likely that the given conditions are not the best operational conditions for the motor and its controllers, and thus it is highly probable that even the slightest acceleration or deceleration could cause an undesired transient in terms of a voltage swell.

After studying the voltage swell model, a conditional rule set for this transient was written as given in Eqn. 8.3.

$$\tau = \begin{cases} 2\,\mu s, & \text{if } P(Sag = 1)_i > 0.4 \\ \tau_i, & \text{if } 0 \leq P(Sag = 1)_i \leq 0.6 \end{cases} \tag{8.3}$$

Eqn. 8.3 translates into:

- If the probability of a swell voltage constraint violation is more than 40%, then change the time step to 2 microseconds to conduct transient analysis
- If the probability of a swell voltage constraint violation is 40% or less, carry on to mission performance analysis without changing the time step

It can be seen that this rule set is slightly different than the sag constraint rule set given in Eqn. 8.2. There were two reasons that played an important role in this decision. First, it was seen that only the 7% of all observations violated the voltage swell constraint. This means that the number of times which the model would predict a 40% or higher probability of violating the swell constraint is expected to be low. Thus, because this scenario was not expected to be encountered as often, it was decided that a lower limit on whether the step size should be lowered to perform transient analysis could be afforded. Second, the low number of observations slightly reduced the confidence in the model's predictions. Thus, a lower limit was selected in order not to miss any probable constraint violations.

8.5.5 Summary of the Results of Experiment 4.3

Experiment 4.3 closes the loop for the methodology proposed in Hypothesis 4 by providing a proof of concept as to how a relationship can be established between the operational scenarios which might be encountered and the significant transients. This relationship was defined based on a set of intelligently designed experiments conducted a-priori to mission analysis, so that the computational burden could be minimized, As a result, two conditional rule sets were defined for two significant transients.

The conditional rule sets gave the probability of triggering a significant transient based on only the mission level factors. Thus, Experiment 4.3 proved that:

1. There is no need to perform transient analysis every time a mission level change occurs

2. The event of a constraint violation (i.e. triggering a significant transient) can be modeled by a categorical surrogate modeling technique

3. It is possible to predict where and when a significant transient could occur during a flight by performing sensitivity analysis using prediction profilers *before* conducting mission performance analysis

4. The predictions can be made based on only the operational conditions and very limited to no amount of knowledge about the electrical system dynamics during the mission analysis

Experiment 4.3 proves that the probability of a transient occurring can be established by a conditional rule set determined a-priori by fitting a categorical surrogate model to the transient signal at the neighborhood of the time at which the mission level change occurred.

8.6 Sizing and Performance Evaluation of a Novel Propulsion Architecture (Experiment 1)

This section brings all of the building blocks which make up the developed methodological framework, E-PASS, together. Furthermore, the methodological steps, revisited in Figure 8.21, are summarized and applied on a use case scenario.

As explained previously, E-PASS is suitable to size and evaluate the performance of novel architectures, including electric and hybrid-electric propulsion systems. Previous examples given in Chapter 7 demonstrated how the steps 1 to 6 are applied on different aircraft designs. Here, the loop is closed by continuing the design process with steps 7 to 9.

To this end, the parallel hybrid electric aircraft studied in Chapter 7.4 was revisited. This aircraft, previously called Design 1, was sized to fly a design mission range of 100 nautical miles and its power management schedule was optimized for minimum fuel burn. This was accomplished by applying the following steps of E-PASS:

1. Initialization

    - The process was started with a notional aircraft configuration, which was the baseline aircraft with the conventional propulsion system. The point performance requirements of the Cessna 172 aircraft were inherited by maintaining its wing and power loading. The mission performance requirements were defined by a climb-cruise-descent type of mission where the design range was set to 100 nautical miles, and the reserve mission duration to 15 minutes. The useful payload was 163.3 kg.

2. Subsystem Architecture Definition

    - The propulsion system was defined by two energy sources (battery and fuel), two power sources (IC engine and electric motor), and a single thrust source

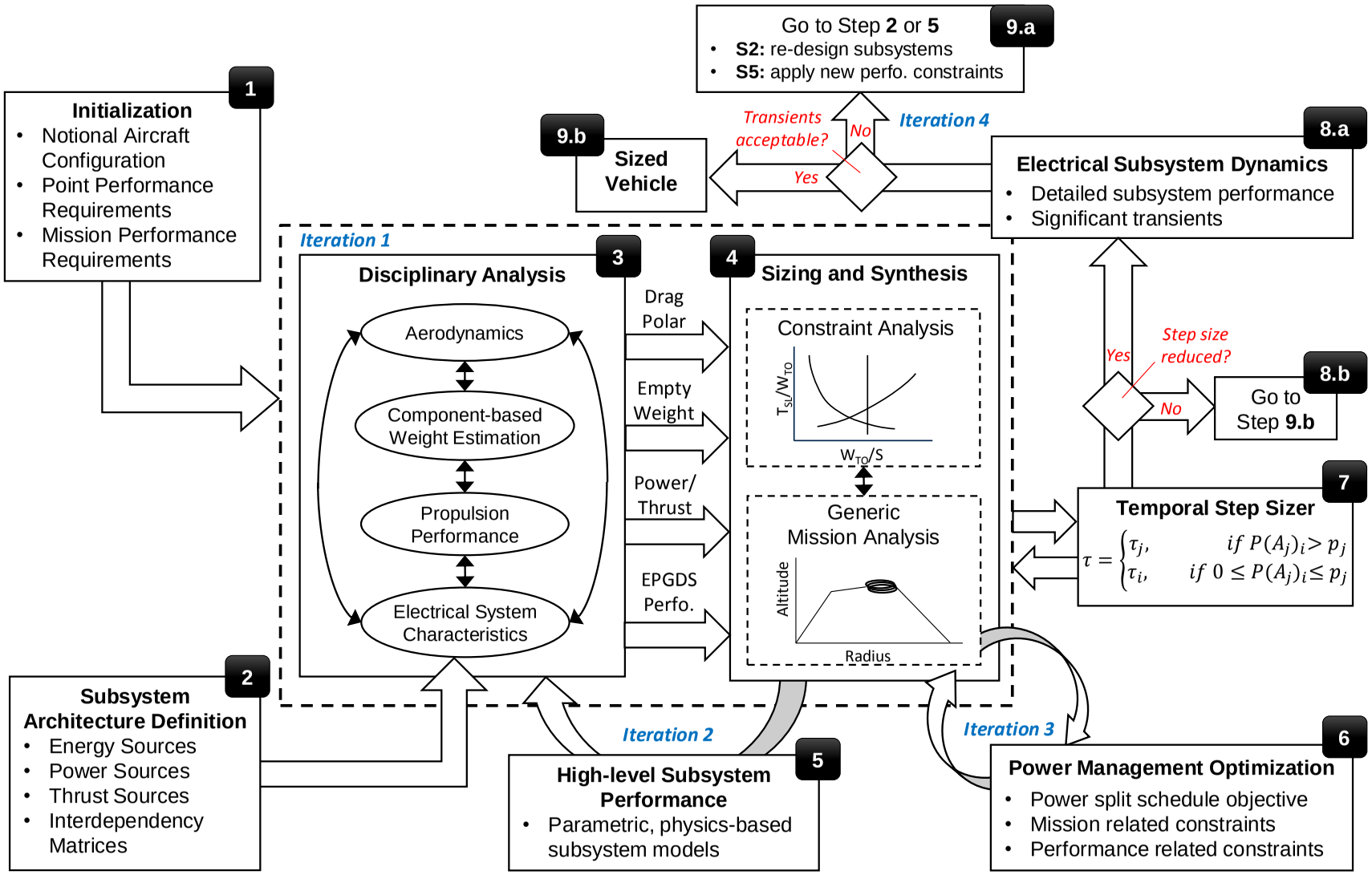

Figure 8.21: Revisiting the methodological steps of Electric Propulsion Architecture Sizing and Synthesis (E-PASS).

(propeller). The EPGDS architecture was chosen to be a parallel hybrid-electric one, where the relevant interrelationship matrices were given in Equations 5.55 and 5.56 in Chapter 5.5.

3. Disciplinary Analysis

   - The aerodynamics of the aircraft were computed using the drag polar of the baseline aircraft, as explained in Chapter 6.3. The empty weight of the aircraft was obtained by the component-based weight estimation technique using the equations given in Table 7.2. The propulsion performance was estimated by the propulsion system performance function Φ_{psp} described in Chapter 6.2. The electrical system characteristics were calculated using the high level EPGDS models developed in Chapter 5. The models were chosen and connected according to the architecture definition made in Step 2.
   - Initially, EPGDS weights were guessed and added onto the empty weight to calculate the takeoff gross weight. After the initial step, *Iteration 1* on empty weight took place every time the disciplinary analysis was performed. This is because the empty weight was initially estimated from the geometry, the new empty weight required different sizes of EPGDS which eventually changed the geometry in turn. *Iteration 1* continued until a convergence on empty weight is reached.

4. Sizing and Synthesis

   - The sizing and synthesis process was performed by maintaining the wing and power loading of the baseline aircraft (instead of explicitly performing constraint analysis), and flying the given design mission profile by utilizing the mission segment functions outlined in Chapter 6.4. The required energy to fly the given mission was calculated and budgeted between the two energy sources.

5. High-level Subsystem Performance

    - The energy sources were resized based on the required energy from each energy source. The new weight of the energy sources changed the takeoff gross weight of the aircraft. As a result, the aircraft was resized by going back to Step 3. The power and thrust sources were also resized using the high-level EPGDS models. *Iteration 2* on took place until the takeoff gross weight calculated at Step 3 agreed with the one calculated at Step 4.

6. Power Management Optimization

    - Once *Iteration 2* converged on a vehicle design, its design and mission performance were fed into the optimizer set up in Chapter 7.4 for the minimum fuel burn objective. Four control points were placed at the beginning and the end of climb and cruise segments. The control variables in between the control points were obtained by linear interpolation. The optimizer found the optimum power split schedule and sent them back to the Generic Mission Analysis block. According to the new energy requirement from energy sources, *Iteration 3* took place by returning back to Step 5. Iteration was continued until the weight of the energy sources converged under the optimum power schedule.
    - Note that the optimum schedule changes at each iteration of *Iteration 3* with changing aircraft design and mission performance. Also note that in this example, the power management optimizer was used within the design mission and thus was a big part of the sizing process. In an off-design mission, *Iteration 3* would not necessitate aircraft resizing.

The resulting design and its performance characteristics were shown in Table 7.8 and the mission profile in Figure 7.8. The next sections describe how the remaining steps were applied on the same aircraft design example. More specifically, Section 8.6.1 describes to the Temporal Step Sizer block in Step 7 and how the significant transients are captured in

Step 8.a, for various use-case scenarios. Section 8.6.2 corresponds to Step 9.a, discussing how capturing the significant transients impact the overall design.

8.6.1 Utilization of the Conditional Rule Set within the Mission

This section provides an example use case scenario for the conditional rule sets. The conditional rule set defined for the sag voltage in Eqn. 8.2 was tested on the parallel hybrid electric aircraft (called Design 1) which was previously sized to fly a design mission range of 100 nautical miles and its power management schedule was optimized for minimum fuel burn. The design and performance characteristics of this concept was shown in Table 7.8 and the mission profile in Figure 7.8.

First, the prediction formula obtained from the categorical ANN model created for voltage sag constraint violations was utilized to find the probability of encountering a significant voltage sag during the design mission. The results are shown in Figure 8.22 where the probability of a sag occurring was plotted against the mission time.

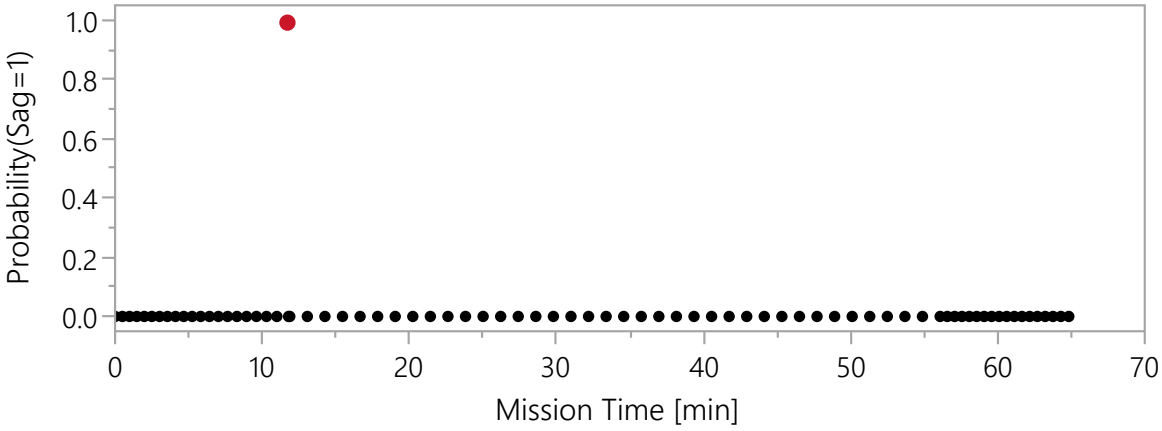

Figure 8.22: Probability of a sag occurring during the design mission of "Design 1 parallel hybrid electric aircraft with a 100 nautical miles of design range".

The points shown on the Figure 8.22 correspond to the mission legs. It can be seen from this figure that only a single point in the mission was predicted to trigger a significant transient response. When compared to the hybridization factor profile of this aircraft which was previous provided in Figure 7.8, it can be seen that this point corresponds to the

Table 8.7: Required performance from the electric motor before and during the critical mission leg.

	Motor Power [kW]	**Motor RPM**	**Mech. Torque [Nm]**	**Battery SOC**
Leg *i*	25.23	2100	114.74	99.05%
Leg *i+1*	49.44	2100	224.81	98.96%

beginning of the cruise segment where the power requirement was solely supplied by the electric motor, and the internal combustion engine was idle.

The required mechanical power, mechanical torque and the speed of the electric motor are listed in Table 8.7 at the initial conditions which were used to predict the voltage sag (mission leg *i*) as well as the instance the mission leg at which the sag was predicted to occur (leg *i+1*). It can be seen from this table that the power required from the electric motor increases by almost 96% during the transition between the climb and cruise segments.

According to the conditional rule set given in Eqn. 8.2, the transient analysis only need to be performed at the end of the climb segment where a constraint violation was predicted by the categorical ANN model. The results of the transient analysis is shown in Figure 8.23. The simulation was started 1 second before the change in the hybridization factor and thus the power required from the electric motor, thus the operational change occurs at exactly t=1s. As it can be seen in Figure 8.23, the categorical ANN model was correct in its prediction.

This provides a valuable information: the changes in the electrical power requirements during the climb segment (where the electric motor was utilized through varying hybridization factors, i.e. power split) did not cause the motor RMS voltage to go beyond the tolerance limit. It was only when the transition between the climb and the cruise segments had occurred that the sag was predicted to be encountered. If this information had been not known, then one would have to perform transient analysis for the whole course of a

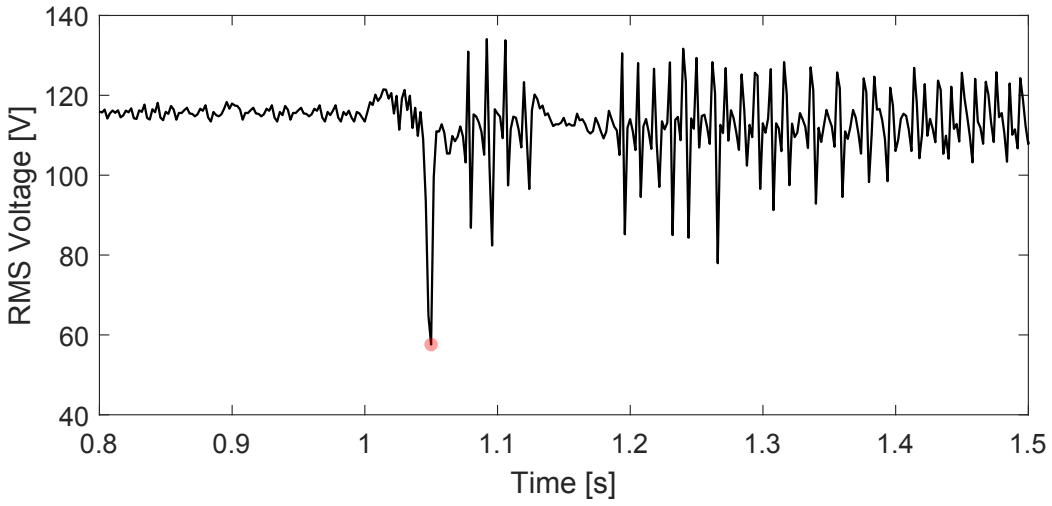

Figure 8.23: Transient analysis of Design 1 at the time of the sag constraint violation prediction.

mission and spend a considerable amount of computational resources.

As discussed before, this is a result of the optimized power split schedule. At the transition between the climb and the cruise segments, the engine was switched to the idle condition; leaving the electric motor to be responsible for supplying all of the operational power alone. This also corresponds to another critical condition where the engine goes out during the cruise segment. In fact, the use-cases can be populated to test the "engine inoperative" and "motor inoperative" scenarios at both the climb and cruise segments.

Engine Inoperative at Climb

The designed electrical system was tested for the case of an engine failure during the climb segment. Each mission leg of the climb segment was taken individually to be the initial condition of the voltage sag test, without any modifications on the flight or motor conditions. The subsequent mission leg, however, was altered such that the total power required to maintain the desired mission performance now comes from the electric motor alone. Then, the categorical ANN model was used to predict the probability of a voltage sag. The results are given in Figure 8.24. The points in this figure represent the probability of the sag constraint violation in case of an engine failure at each mission leg, *separately*.

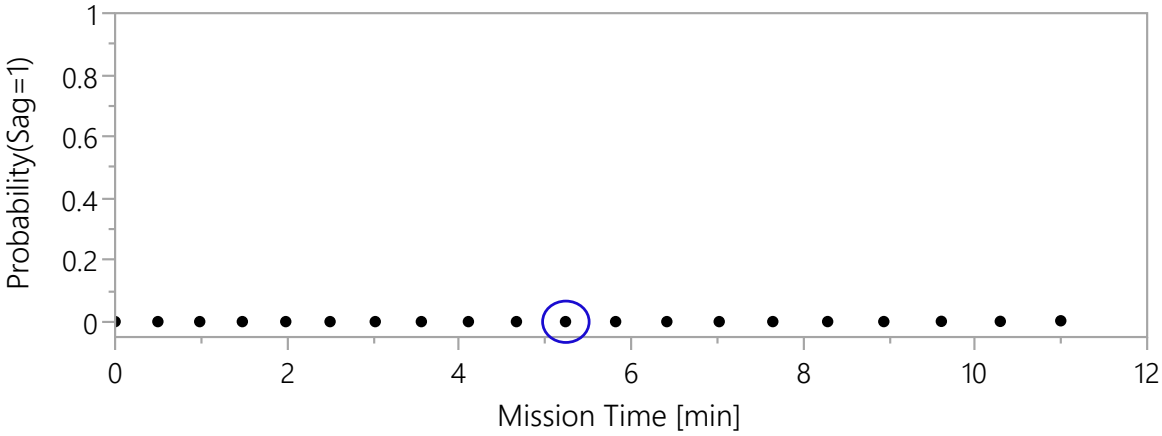

Figure 8.24: Probability of a sag occurring in the case of an engine failure during the climb segment.

Figure 8.24 shows that switching the power management such that the electric motor becomes solely responsible for all the power required to maintain the desired climb profile does not trigger a significant transient at any leg in the climb segment. This means that the designed electrical system is capable of bearing an engine failure during climb.

To validate the categorical ANN model, a random point (which was circled with blue in Figure 8.24) was selected at about the middle of the climb and the transient analysis was conducted in the same way as the previous example. The results of the transient analysis for this point is given in Figure 8.25.

As it can be seen in Figure 8.25, the transient behavior changes slightly shortly after the change in the power requirement takes place (at t = 1 s), but stays within the predetermined boundaries (20% of the steady-state voltage) which was shown with red dashed lines. Thus, this result validates the outcome of the categorical ANN model and the conditional rule set defined for the voltage sag constraint.

Electric Motor Inoperative at Climb

Figure 8.26 shows the same test performed this time for the case of an electric motor failure during the climb segment. Each point in this figure shows the probability of a voltage sag at each mission leg if the motor goes out.

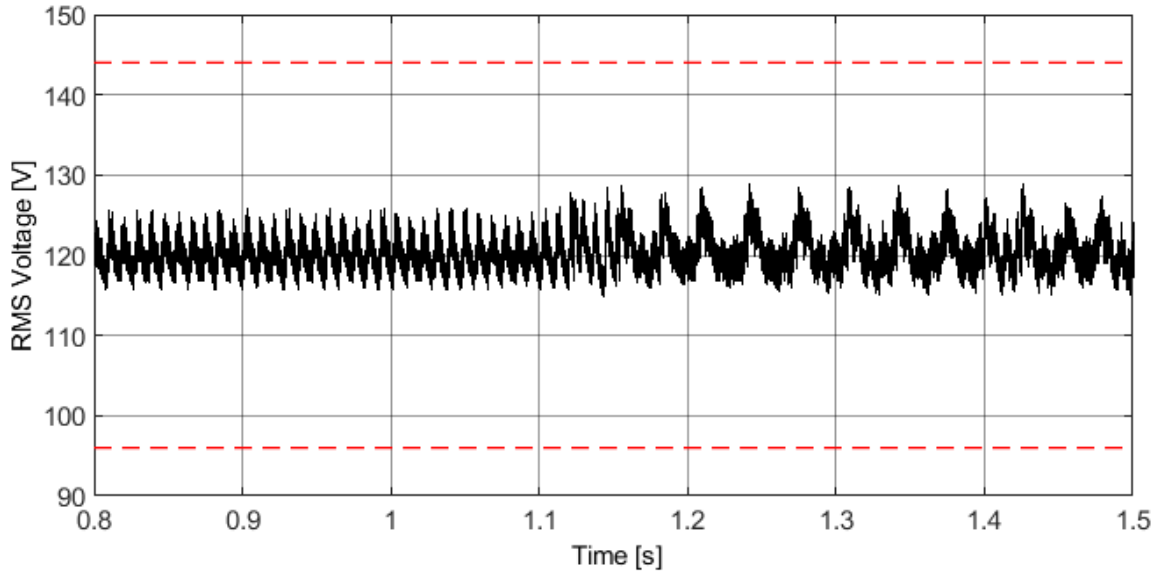

Figure 8.25: Transient analysis of Design 1 for the engine inoperative at about the middle of the climb scenario.

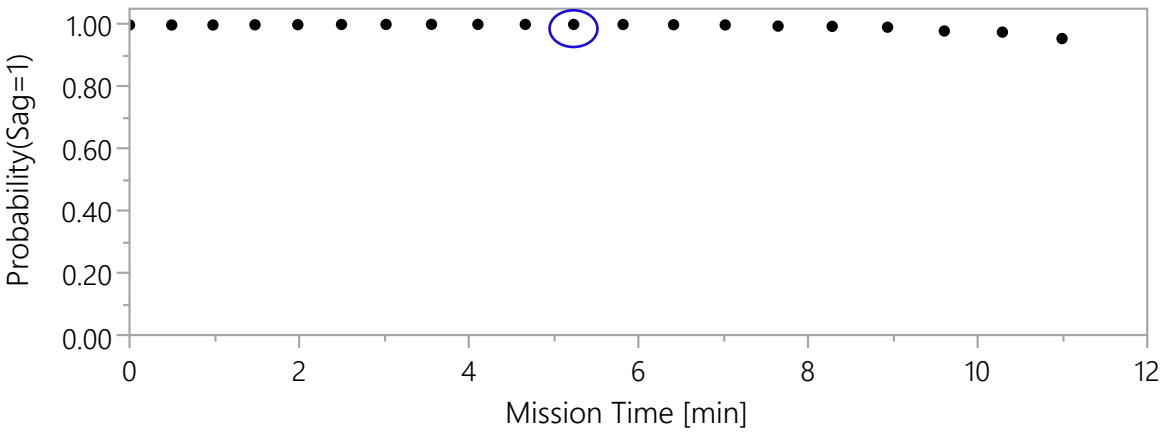

Figure 8.26: Probability of a sag occurring in the case of an electric motor failure during the climb segment.

As it can be seen from Figure 8.26, the categorical ANN model predicts that the probability of a sag constraint violation at each point of the climb segment to be higher than 95%. According to the conditional rule set, this means that if the electric motor goes out at any point during the climb segment, a significant voltage sag transient will occur at that moment of motor failure.

The transient analysis done at the same point in the climb segment as the previous

example, circled in blue, validates this result. The reaction window for this point was shown in Figure 8.27. As it can be seen from this figure, the transient response changes its behavior shortly after the electric motor goes out. The transient response exceeds the acceptable limits and violates the constraint multiple times.

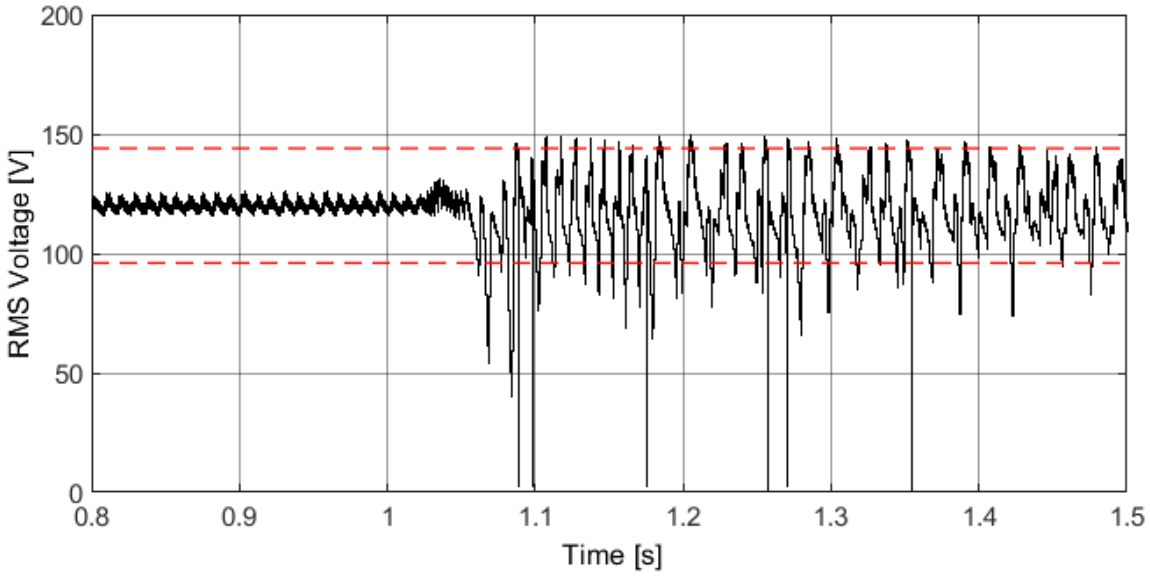

Figure 8.27: Transient analysis of Design 1 for the electric motor inoperative at about the middle of the climb scenario.

Electric Motor Inoperative at Cruise

Similar to the previous cases, Figure 8.28 shows the same test performed for an electric motor failure during this time at the cruise segment. Each point in this figure shows the probability of a voltage sag at each mission leg if the motor goes out during cruise.

The results are similar to the previous case. This is expected since the direction of change in terms of the electrical load is the same as the previous case. Moreover, the amount of change is even bigger due to the original power split schedule demanding 100% electric propulsion during cruise compared to the hybrid climb segment.

As discussed earlier, the conditional rule set deems all of the points shown in Figure8.28 to be constraint violations. Thus, if an electric motor failure occurs at any point of the cruise segment, the electrical system will experience an undesired voltage sag. Similar

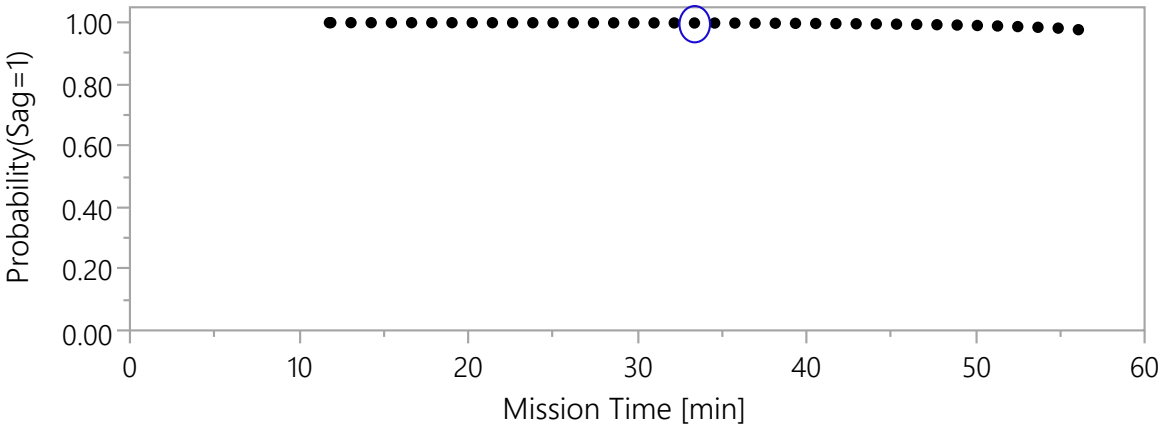

Figure 8.28: Probability of a sag occurring in the case of an electric motor failure during the cruise segment.

to the previous cases, the transient analysis was conducted for a randomly selected point, circled in blue in Figure 8.28. The transient behavior before and after the electric motor becomes inoperative is given in Figure 8.29.

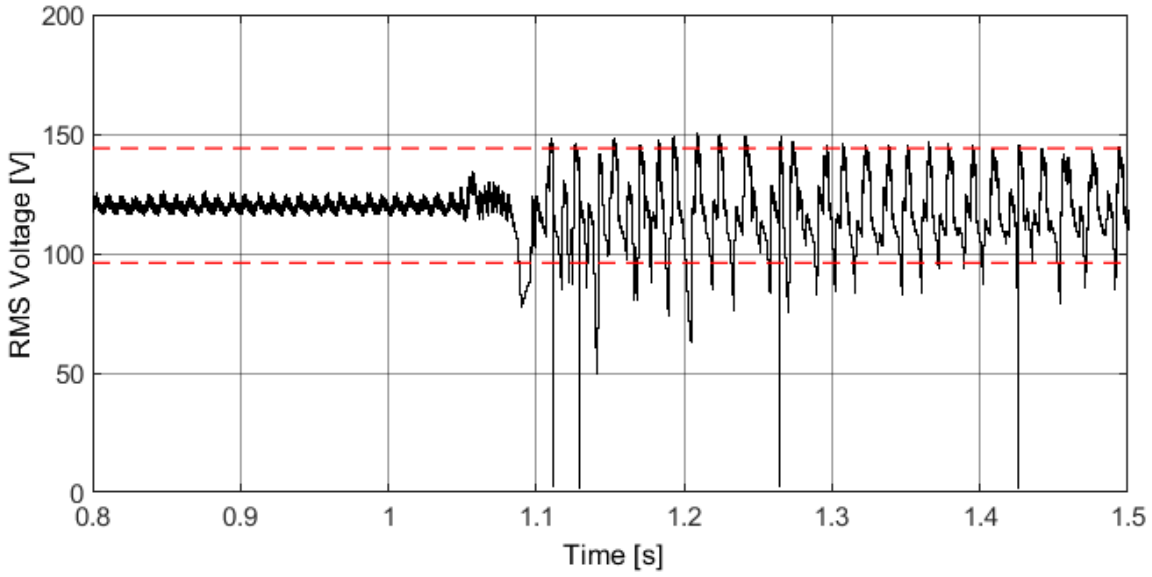

Figure 8.29: Transient analysis of Design 1 for the electric motor inoperative at about the middle of the cruise scenario.

Figure 8.29 shows that the dynamic RMS voltage exceeds the constraints shortly after the electric motor goes out. The results of the transient analysis are once again in agreement with the prediction made by the conditional rule set.

8.6.2 Implications of Capturing Transient Constraint Violations

Utilization of the conditional rule set for the previous example revealed an undesired voltage sag transient at one point of the mission during normal operations. The analyses were extended to capture abnormal operational conditions, including engine and electric motor inoperative cases, separately.

The results for the abnormal operation scenario were rather expected due to the sudden and drastic change in the amount of load carried by the electrical system. If the applied constraints are critical constraints which must not be violated at any point in the mission for both normal and abnormal operating conditions, then these results clearly imply that the designed electrical system is not suitable to be used with the given mission schedule.

There are two sides to solving this problem: manipulating the mission, and/or the EPGDS design. Changing the mission characteristics might be a quicker solution, but whether it can be afforded depends on the type of the problem. For instance, the constraint violation seen at the transition phase from the climb to the cruise segment in the normal operation example can be avoided by a simple change in the power management schedule.

Figure 8.30 shows how the probability of a sag constraint violation varies for a range of absolute changes in the mechanical torque of the electric motor during the transition from climb to cruise segments. The red dot in this figure corresponds to the constraint violation shown in Figure 8.22. As it can be seen from Figure 8.30, the probability of constraint violation drops below 50% as the absolute change in mechanical torque drops below 93 Nm. According to the conditional rule set for the sag voltage, any condition below 50% chance of constraint violation is considered to be within the constraint limits without necessitating transient analysis.

An example modification is shown in Table 8.8. The leg *i+1* was modified from its original which was previously given in Table 8.7. By changing the power split such that the electric motor supplies 43.98 kW of power at point *i+1* instead of 49.44 kW where the difference is taken over by the engine, the probability of a sag constraint violation drops

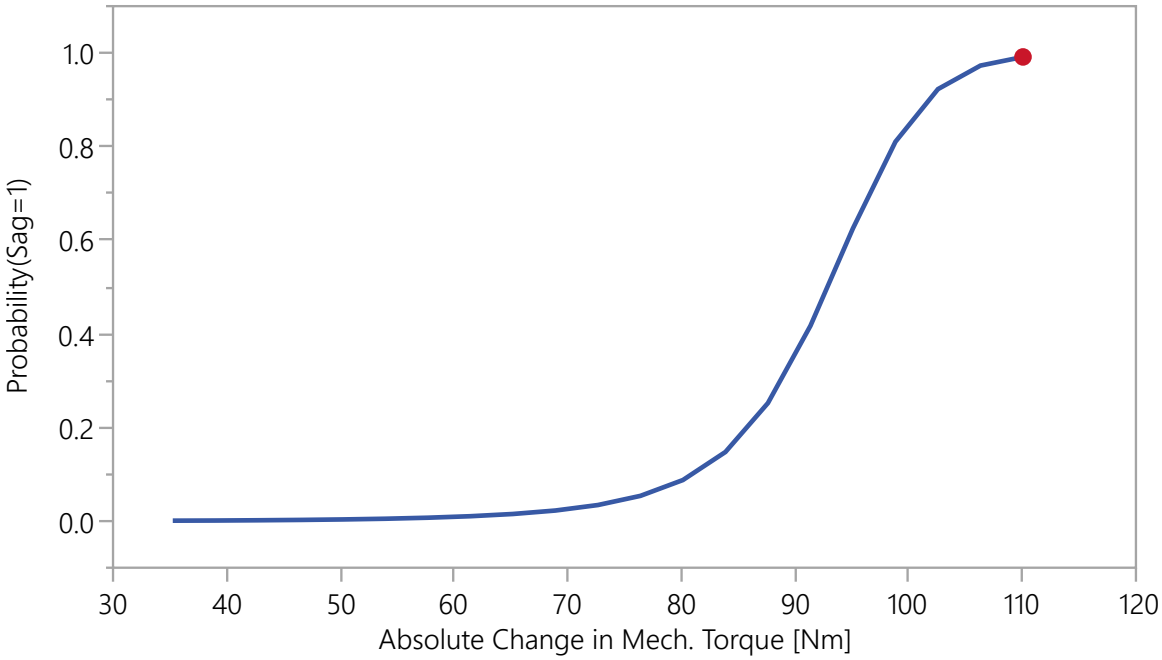

Figure 8.30: Probability of a sag occurring at the climb-cruise transition phase as a function of the absolute change in the mechanical torque of the electric motor.

Table 8.8: Modified performance required from the electric motor before and during the critical mission leg.

	Motor Power [kW]	**Motor RPM**	**Mech. Torque [Nm]**	**Battery SOC**
Leg *i*	25.23	2100	114.74	99.05%
Leg *i+1*	43.98	2100	200.00	98.96%

down from 99% to a striking 18%.

The transient analysis performed at this point confirm that a voltage sag has been avoided by this small change in the power split between the electric motor and the engine at the point of transition. Since it was the abrupt change in the mechanical torque of the electric motor rather that caused the sag, the optimum power management schedule can then be applied again for the rest of the points of the mission without encountering any significant voltage sag transients. This is because the optimum schedule do not require for such an increase in the mechanical torque ever again in the remaining parts of the mission.

However, such a quick and easy solution might not always be enough to avoid a constraint violation, such as is the case for the abnormal operations. In such cases, the second option is to change the design of the electrical system components, or on a greater scale its architecture. Although this could be costly due to the amount of subject matter expertise, computational work and analysis which need to be re-run, it is in many cases the ideal and sometimes the only solution.

In order to improve the power quality of the given electrical system under the aforementioned abnormal operations, the subsystems must be re-sized such that they are able to handle the expected abrupt changes in the electric load on the system. If the EPGDS design is fixed, then another solution could be to change the EPGDS architecture instead. As emphasized earlier, such efforts require subject-matter expertise and are not in the scope of this work. However, one way to utilize the information obtained from this work is to use the characteristics of the electric load experienced in the critical conditions as the targeted performance while re-designing the EPGDS and/or the architecture. These targets can be set as objectives in a multi-disciplinary optimization problem to solve for the design requirements for each component of the electrical network.

Moreover, the sensitivity analysis performed earlier shows which aspects of the electrical network needs to be improved. For instance, the prediction profilers shown in Figures 8.16 and 8.17 indicate that the main reason for a voltage sag constraint violation is the motor speed reduction. The components of the network can be re-sized to handle such changes in the motor speed, which translates into the change in the electrical current within the network.

If an architecture change is made on the EPGDS level, the subsystem architecture definition changes. This necessitates the design process outlined in Figure 8.21 must be re-initiated starting at Step 2. If the architecture is kept the same but an EPGDS is re-sized, then the design process must be re-initiated starting at Step 5. Since the new design generally means new mission performance and new dynamic responses, the transient analysis

approach must also be repeated, resulting in a final iteration process, *Iteration 4*. The iteration continues until the EPGDS dynamics remain within the acceptable region under all important conditions.

It can easily be seen that the aircraft design changes due to the requirements regarding the subsystem dynamics. What's more, because the impact of the significant transients were captured at the conceptual design stage, re-designing the aircraft now requires much less effort compared to the traditional way of performing the transient analysis in later design stages where the aircraft design might be more or less frozen.

As discussed previously, capturing the dynamic response of EPGDS in electric and hybrid electric aircraft are much more important than their conventional counterparts, because these subsystems must handle much greater electrical loads than secondary subsystems. Although a conventional, fuel-burning aircraft could have been sized with the traditional sizing approach, these novel designs could not have been properly sized without taking the dynamics into account.

8.7 Generalizability of the Approach

The transient analysis approach demonstrated in this chapter requires a bunch of cases to be run a-priori. The DoE approach maximizes the amount of knowledge about the design space with minimum effort. The upper and lower bounds selected for the design space vary depending on the nature of the problem, the region of interest and the availability of computational resources. Generally, the larger the design space, the more number of cases should be run to accurately describe it.

The confidence in the created surrogate models is limited by the chosen boundaries of the design variable space. In order to preserve generalizability of this approach, it is recommended to define the design space larger than the expected operational bounds. This way, the aforementioned DoEs can be designed and run only once in advance, while still enabling the use of the same surrogate models (both for gain tuning and constraint analysis)

in case the mission requirements or performance change.

Another limitation comes from the design of the components within the electrical system. If changes are made to the design of the related EPGDS or the architecture inside the control volume such that the performance of the electrical system also changes greatly, then both the constraint analysis model must be redone.

On the other hand, the gain tuning model may or may not be affected by the said changes, and must be checked to determine whether it can be used without any modifications or a new model is needed. This highly depends on the nature of the change made in the design, as well as on which subsystem it was made. It might also be the case that while some gain parameters do not need to be re-tuned, some do. In this case, the system design optimization approach enhanced by Monte Carlo simulations should be repeated only for the parameters which requires re-tuning.

To sum up, the initial design space definition should be done keeping in mind that the mission profile or the mission performance might change further down the road. Although a larger design space requires more cases to be run a-priori, it can minimize the efforts that might be required later on, keeping the approach generalizable for multiple mission scenarios. If a subsystem is re-sized or the architecture of the electrical network is changed, the gain tuning models must be checked before attempting to reuse. However, since the response of the system would change, the categorical model must be recreated.

8.8 Chapter Summary

This chapter provided a proof of concept for the methodology proposed in Hypothesis 4. The main motivation behind this hypothesis was to find a new way of integrating transient analysis into mission performance analysis without bringing the computational burden that comes with the drastically small time steps necessary to capture the transients. This was accomplished by utilizing the available information about the changes in the state of the aircraft and its propulsion requirements at the mission level.

This chapter demonstrated how the methodology can be implemented for the electric propulsion branch of a general aviation EA/HEA concept. The methodology explains how a conditional rule set can be written for any transient as a function of only mission level variables. Moreover, this chapter also provided a way of tuning the controllers of an electrical system for numerous design cases at only a few iterations.

The gain tuning and scheduling step is optional and could be skipped if subject-matter expertise is available. However, if such an expertise is not available, then tuning the controllers of even a rather simple system can be very expensive due to the considerable amount and variety of controller variables. In such cases, system design optimization techniques can be utilized to find the optimum gain settings that would minimize the controller error. However, when a large design space is to be investigated, a single controller gain set might not be enough to control the system response at every point of the design space.

Such a case was demonstrated in Section 8.4 of the current chapter. The immediate problem that was run into was that the design space was too big to try to optimize each and every case defined by the DoE. At this point, random cases could have been selected for the optimization problem with the intent of testing the optimized gain set with the remaining cases. However, two potential problems arose with this approach.

First, it was not known a-priori whether all the cases in the design space expressed by the DoE were physically realizable. Thus, an optimizer might not have been able to find a gain set to track the given signal for a randomly selected case if that case was outside the physical capabilities of the electrical system. Second, an initial condition assignment was necessary for most of the considered optimization techniques suitable for the dimensionality and the dynamic nature of the problem. Moreover, there usually are multiple and even distinct gain combinations that would optimize the system at a given condition. By setting up the optimization problem with a random initial condition, the optimization could have landed on a local minimum that would optimize the tested case, but most probably not the majority of the cases.

As a solution to these problems, the optimization was enhanced by the implementation of Monte Carlo simulations. A separate DoE was created to represent a larger design space of the simulation input variables and the controller gains. For these simulations the response metric was set to be the error between a previously defined reference signal and the actual response as a function of time. In the example application, this signal was the motor speed response in accordance with the chosen motor control approach. Then, an Artificial Neural Network model was fit to the response.

This ANN model was used to determine which cases were physically realizable; and of those cases which are realizable, which particular case could be used to represent the most common characteristics of the realizable cases. Moreover, the model was also utilized to make an *intelligent guess* for the initial conditions, so that the optimizer would produce the gain set which although was optimized for a single case, would also give acceptable results for the majority of cases.

By repeating this gain tuning procedure twice, two gain sets were identified for the majority of cases with a little optimization effort. The resulting gain sets were scheduled such that each time a particular combination of simulation inputs were given, an algorithm automatically selected the best gain set out of the two available.

Once the electrical system was tuned, transient analysis were conducted. Two examples were provided in terms of transient constraints: a voltage sag constraint and a voltage swell constraint, both for the electric motor in the electric propulsion branch. The literature provides some trends on when these transients might become significant, i.e. violate the established constraints. For instance, it is known that a voltage sag might occur when there is a sudden increase in the load. [57] However, the following questions could not have been answered without performing detailed, transient analysis: How much change is too much? How sudden is too sudden? What other conditions could increase the chances of having a voltage sag or a swell?

The answer to these questions depend on the characteristics of the electrical system at

hand, and thus there are no global boundaries on the operational conditions. This is where the strength of the proposed methodology lies: with this methodology, such boundaries can be discovered for a given electrical system by defining a big or small of a design space, adjusted based on the available computational resources and the desired level of detail.

The categorical surrogate modeling technique described in this chapter was found to be the most suitable surrogate modeling approach based on many experiments conducted with different techniques such as modeling the continuous signal of interest in the time-domain, modeling the continuous signal of interest in the frequency-domain, modeling the relative change in the transient, etc. None of these modeling approaches yielded acceptable results, because they demanded more information about the subsystem characteristics which could only be provided by transient analysis.

However, the main goal of this study was to find a way of predicting when a transient might occur solely based on mission level variables, so that maximum amount of knowledge could be gained with minimum amount of information on the subsystem dynamics. This methodology achieved this goal based on a bi-level categorical approach which provided a way of predicting the *probability* of a significant transient occurring based on the operational changes.

The methodology suits to various expertise levels by providing a flexibility in terms of the how a significant transient is defined, how the controllers of a system is tuned, and how the conditional rule set is determined.

Because the categorical surrogate modeling technique described in this methodology provides the probability of encountering a significant transient rather than absolute results, the resulting conditional rule set can be adjusted based on the knowledge and expertise about the electrical system, the relative importance of the significant transient compared to the other significant transient events, the amount of available computational resources, the amount of detail desired to bring to the conceptual design stage, and so on. Two examples on how the rule set can be adjusted for different transient events were provided in

the previous sections by the discussions made on how the two conditional rule sets were established.

Furthermore, the definition of a significant transient can be changed based on the specific implementation, research needs and computational resources. This flexibility was required due to the lack of standards established for electric propulsion. Thus, this methodology can be utilized for different standards and transients by simply changing the transient constraints put on the subsystem dynamics regardless of how a significant transient is defined.

To sum up, three experiments were conducted to test the validity of Hypothesis 4. The results of all three experiments proved that the methodology proposed in this hypothesis can be used to determine the probability of where and when a significant transient could occur, based only on mission level information, so that the transient analysis can be integrated into the mission performance analysis and thus the aircraft conceptual design stage while minimizing the computational burden that comes with it. Thus, Hypothesis 4 was substantiated by Experiments 4.1, 4.2 and 4.3.

After completing Experiment Set 4, all of the building blocks which make up the methodological framework were validated. Next, Experiment 1 which brought all of the other experiments was conducted. Experiment 1 demonstrated how each step of E-PASS was performed to size a parallel hybrid-electric aircraft, evaluate its mission performance, optimize its power management schedule, and capture any significant transients under the normal operation (i.e. design mission profile) as well as some abnormal operational scenarios.

Since undesired transient behaviors were captured using the categorical model, two possible actions to fix it were discussed. The first one was to change the power split between the power sources such that the electrical system in question did not have to deal with a sudden change in the load. Although this was a quick and easy fix, it might not always work. The first issue with this solution is that a change in the power split might not be

desired or even feasible in case of an electric aircraft. Secondly, it does not address the possibility of losing some or all of the other power sources, where the electrical system must be able to endure such a change.

The second option was to resize the components which make up the electrical system such that they were powerful or stable enough when faced with such conditions. Thanks to the sensitivity analysis which the surrogate modeling technique enabled, a connection between the dynamic response of the electrical system and the physical properties of its components could easily be obtained. This provided a strong point of reference in terms of which component(s) to resize, and the direction of change of the response relative to the change in the component and/or architecture choices.

It was pointed out how capturing the significant transient could impact the overall aircraft design, and why it is very important to include these additional analysis into the conceptual design stage. Without the approaches taken in E-PASS, capturing the dynamic response under various scenarios would have required much more effort, and might have not been practical at all with limited computational resources.

Thus, Experiment 1 substantiated the over-arching hypothesis of this dissertation, i.e. Hypothesis 1, by demonstrating that the aircraft sizing and synthesis process was generalized by the developed methodology, such that adequate comparisons between different types of primary power generation and distribution subsystems and candidate architectures are now possible thanks to E-PASS.

CHAPTER 9
CONCLUDING REMARKS

This chapter concludes the dissertation by providing a summary of conclusions, contributions, and recommendations for future work.

9.1 Conclusions

In this dissertation, a methodological framework was proposed for the sizing, integration and performance evaluation of dynamic electric power generation and distribution subsystems and architectures. The overarching hypothesis was divided into three parts, i.e. three hypotheses, based on the necessary capabilities developed to achieve the research objective. The methodology was applied on a modeling and simulation environment and as a result, an integrated electric and hybrid electric aircraft sizing and synthesis tool was built. This tool was then used to conduct a series of experiments to substantiate each hypothesis.

The development of the methodological framework started with the sizing and synthesis block defined by Hypothesis 2. This block was at the core of the framework, and built by modifying the traditional aircraft sizing and synthesis approach to perform electric and hybrid electric aircraft studies.

The sizing and synthesis block has the following capabilities:

- Component based weight estimations
- Generic and energy-based mission performance analysis
- Simultaneous sizing of EPGDS through parametric, physics-based models
- Flexible propulsion architectures

The component based weight estimation approach was needed to accommodate novel aircraft concepts such as urban air mobility type vehicles, or roadable flight vehicles, whose configuration may be expected to deviate from conventional designs. Thus, a database of weight estimation relationships and techniques to cover major vehicle components, including structural elements, power-train elements, and energy storage system elements were created based on methods documented in literature.

The traditional mission analysis approach was modified to be suitable for any type of aircraft design and propulsion architecture. This was accomplished by leveraging the energy reservoir analogy to replace the traditional approach which depends on the utilization of consumable fuel. An alternative energy expenditure bookkeeping method was proposed so that the modified mission analysis could be used with any sort of energy source.

Furthermore, a new method to establish the relationship among the main subsystems of any propulsion architecture was proposed. This capability provided flexibility in terms of architecture definitions and their use within the mission and propulsion performance characterizations.

These capabilities were tested with Experiment Set 2, the results of which were summarized below:

Experiment 2.1 tested the results of the sizing and synthesis tool by modeling a general aviation baseline aircraft with the sizing and synthesis tool and comparing its weight and mission characteristics to the manufacturer's data. Cessna 172R was chosen as the baseline aircraft. The same design mission profile, reserve mission requirements, wing loading and power loading properties were imposed.

The specifications of the sized aircraft resulted in an good match with the baseline aircraft (as shown in Table 7.4). The energy-based, generic mission analysis approach yielded very similar mission performance results to the actual aircraft. The component based weight estimation technique yielded only a 0.2% percent error relative to the baseline with an empty weight calibration factor of only 2.5%. Thus, Experiment 2.1 validated the

sizing and synthesis capabilities of the developed framework for a conventional aircraft and hence the related arguments of Hypothesis 2.

Experiment 2.2 tested the applicability of the sizing and synthesis tool to electric and hybrid electric aircraft. In this experiment, the conventional propulsion system of the baseline aircraft was replaced first by a parallel hybrid-electric architecture, and then a fully electric architecture. The developed EPGDS models were used in the electric propulsion branch of these two architectures. The architecture definitions and relationship establishment were made by a set of interrelationship matrices as proposed in Hypothesis 2.

The resulting designs were compared against a conventional aircraft which was sized for the same design mission and point performance requirements. The comparisons showed a significant increase in the takeoff gross weight of the hybrid and electric architectures. This was expected because of the drastically low specific energy of rechargeable batteries. In fact, the 50% hybrid architecture consumed 10 times more fuel than the conventional architecture with no electrification.

As a result, this experiment demonstrated that the developed methodological framework is generic and flexible enough to be used for unconventional aircraft designs, such as electric and hybrid-electric aircraft.

Experiment 2.3 tested whether technological projections could be made using the developed EPGDS models. To this end, a set of technology K-factors were defined to represent various subsystems within the electric propulsion architecture. This capability was made available by the parametric nature of the developed EPGDS models.

The baseline aircraft for this experiment was chosen to be a turboprop commuter, similar to Dornier 328. The propulsion architecture of this aircraft was replaced by a parallel hybrid electric one. Then, a design variable space was defined for the technology K-factors of the main EPGDS components. The design of experiments concept was utilized to explore the design space. Finally, prediction profilers were used to perform sensitivity analysis where each K-factor was varied from its corresponding technological state of the art

value. It was seen that the battery specific energy had the most significant impact on the mission performance compared to the specific power of electric motor and the power converter employed in the architecture, as expected.

This experiment demonstrated that the parametric nature and the increased dimensionality of the developed EPGDS models allowed for technology sensitivity studies, which is an important capability due to the ever-changing and improving subsystem characteristics.

Experiments 2.1, 2.2 and 2.3 proved that the proposed modifications to the traditional sizing and synthesis approach made it possible to size and evaluate the performance of notional aircraft with unconventional subsystems. Thus, Experiment Set 2 substantiated Hypothesis 2.

Hypothesis 3 proposed a power management schedule optimization technique based on a set of control points and variables, so that architectural comparisons could be made while the competing architectures operated at their best performance. The control variables were defined such that the potential performance degradation within the power sources were not neglected during the optimization process.

Experiment 3 was conducted to verify the applicability of this technique by setting up three optimization problems with different objectives. The optimization problem was then solved while the aircraft was being sized. Other than the power split variables, the mission segments were optimized based on a set of selected segment-wise objectives. Thus, the impact design changes were also captured on the resulting mission profiles.

Two design mission profiles were used in the sizing process. First, the aircraft were optimized to fly a design range of 100 nautical miles. Then, the design range was reduced to 50 nautical miles. The optimization results mostly favored the conventional architecture due to the low specific energy of rechargeable batteries compared to fossil fuels. Even when the objective function of the power management schedule optimization problem was selected to minimize the total fuel consumption, the electric aircraft architecture did not provide major benefits. On the contrary, the takeoff gross weight of the competing electric

and hybrid-electric architectures were substantially higher than the conventional one.

This experiment demonstrated the capability of optimization of the power management schedule within an on-design mission.

Hypothesis 4 proposed a methodology to bring transient analysis into the aircraft conceptual design stage by an adaptive step sizing capability. Experiment Set 4 followed the three-step approach described by Hypothesis 4 to test whether a relationship could be established between the subsystem dynamics and mission performance characteristics. To this end, the following capabilities were developed:

- Flexible definition of significant transients and transient constraint violations
- An aggregated controller gain tuning optimization technique enhanced by Monte Carlo simulations
- A categorical surrogate modeling approach to predict the probability of a constraint violation based on only mission level factors

Experiment 4.1 demonstrated that not all the changes made at the mission level trigger a significant transient response, and when they do, the significant transient can only be seen if the appropriate timescale is used. To this end, an electric propulsion architecture was built with detailed, dynamic EPGDS models. Then, the subsystem level response to a series of mission level step inputs were simulated under two timescales: one at the order of microseconds, and the other at the order of seconds.

The results of this experiment were two folds. First, it was seen that important information was lost when the time step size was raised from 2 microseconds to 2 seconds. Not only that the significant transients were not captured with the higher step size, but also the results were misleading. Second, it was observed that not all the changes made at the mission level inputs triggered a significant transient response. This supported the claim that to minimize the computational burden while maximizing the knowledge about the subsystem

design and dynamics at the conceptual design stage, the transient analysis should be performed only when necessary, where the necessity is defined by the likelihood of a transient constraint violation.

Experiment 4.2 verified that in order to tune the controllers of the electrical system, a gain scheduling technique could be established by an aggregated optimization approach where the optimization algorithm was directed based on variable importance estimated by Monte Carlo simulations.

The experiment was conducted by first defining the design space of the simulation inputs which represent the mission level changes by utilizing the design of experiments concept. Then, a larger design space of the simulation inputs combined with the controller gains was defined by a second design of experiments (DoE). Next, the second DoE was simulated to evaluate how well the controller gain set performed under the given circumstances (i.e. simulation inputs). An ANN model was fit to the response data and variable importance of the gain variables was assessed through Monte Carlo simulations. This step provided useful information regarding how to set up the optimization problem.

The optimization control variables were chosen based on the estimated variable importance, and the optimization was started at a specific initial condition such that a local minimum was guaranteed and that local minimum corresponded to a gain set which would not only tune the controllers at the given DoE case but would work with many other cases of the DoE. By tweaking the optimization algorithm this way, the optimization efforts were reduced and the cases which could not be controlled due to the physical constraints of the electrical system were identified and eliminated.

Experiment 4.3 showed that the probability of triggering a significant transient subsystem response can be predicted based solely on information which is readily available at the mission performance analysis. This was accomplished by establishing a conditional rule set determined a-priori by creating a categorical surrogate model based on transient constraint violation at the neighborhood of the time at which a mission level change occurred.

For this experiment, two significant transients were defined for the root mean square voltage of the electric motor: a voltage sag which is a momentary voltage decrease outside the tolerance level, and a voltage swell which is a momentary increase in the voltage outside the tolerance level. Two transient constraints were established to determine the tolerance level. The transients which violated the constraints were called significant transients.

The realizable cases of the DoE which were determined by the previous experiment were simulated where each case consisted of a step input in terms of motor speed and/or torque, as well as an initial battery SOC condition for 2 seconds at a time step of 2 microseconds. A reaction window of 0.1 seconds was determined based on the time of the change in the simulation inputs and the nature of the transients. The simulation results were divided into two categories for sag and swell constraints, separately: those which did not violate the constraint were gathered in Category 0, and those which did were gathered in Category 1. Category 1 included not just every single case that the related constraint was violated, but every instance within these cases.

A categorical ANN model was fit to the two categories of each transient type based on initial motor speed, torque, battery SOC, and the change in motor speed and torque inputs; that is, mission level information only. Both models passed several goodness of the fit tests and were deemed suitable to be used to predict the probability of the associated transient occurring under certain operational conditions. Finally, a conditional rule set was written for each transient type to be used during the mission performance analysis to determine whether the temporal step size should be changed to conduct transient analysis.

The results obtained from Experiment Set 4 substantiated Hypothesis 4 by verifying that a balanced time step size could be obtained by applying the three-step approach proposed in this hypothesis.

Experiment 1 tied experiments 2, 3 and 4 together to test the over-arching hypothesis. The methodology was applied on an example hybrid-electric architecture perform aircraft sizing, performance assessment, power management schedule optimization and subsystem

level response evaluation. The latter was repeated for multiple use-case scenarios. Capturing the significant transients at the conceptual design stage proved that it can change the overall aircraft design and its performance, resulting in an iteration process between the aircraft sizing and subsystem level response.

Experiment 1 proved that EA/HEA architectures can be properly sized and adequately compared using E-PASS, and substantiated the Hypothesis 1 which is over-arching hypothesis of this dissertation.

9.2 Contributions

The main contribution of this dissertation is the creation of a methodological framework for sizing, optimization and transient analysis of novel aircraft propulsion architectures. The most prominent feature of this framework is the flexibility and generality of the computational methods. As a result, the methodological framework enables the performance evaluation of and architectural comparisons among *any* aircraft and propulsion type.

The primary research objective was to develop a methodology to perform sizing, integration and performance evaluation of electric power generation and distribution subsystems and architectures within electric and hybrid electric aircraft concepts. This objective was achieved by the three main capabilities of the framework which were not available before:

The first one is the integrated aircraft sizing and synthesis capability which is based on modular weight estimation techniques, energy-based mission performance analysis, interchangeable propulsion architecture characteristics and parametric electric power generation and distribution subsystem models.

The literature review revealed that the first receivers of the electric propulsion technology will be the urban air mobility and general aviation type aircraft. Some of these aircraft, especially the urban air mobility concepts, have rather unconventional vehicle configurations. This poses a problem as the traditional weight estimation techniques which rely on

historical data. This approach might not be suitable to be applied directly to such vehicle concepts which do not conform to standard fixed-wing or rotary-wing vehicle configurations.

To overcome this problem, a weight build-up approach which consists of physics-based weight assessments and component weight look-ups was used within the sizing and synthesis block of the framework. The parametric nature of this weight estimation technique enabled the sizing of novel designs such as roadable aircraft, fixed-wing VTOL vehicles, and so on.

The traditional mission analysis approaches depend on the rate of change of fuel weight to calculate the weight fractions of each mission segment and thus the takeoff gross weight. This approach is obviously not suitable for non-consumable energy sources, such as rechargeable batteries whose weight may or may not changed during a mission.

There exist several other aircraft sizing tools which are capable of performing limited EA/HEA analysis. The limitations either come from the hybridization strategies, lack of flexibility and ease of use. For instance, although FLOPS is capable of evaluating the performance mission segments flown with 100% electric propulsion, it does not allow the use of multiple propulsion types at any given time, that is, hybridization.

The energy-based approach utilized in the mission analysis block of the proposed framework allowed for the performance evaluation of any propulsion system, energy source, desired power split, the number of propulsion types used at a given time, and the architecture definition. Moreover, no assumptions were made about the climb angle; which enabled vertical flight considerations. All these properties made the mission analysis generic enough to be used for any type of vehicle.

Furthermore, a new way of propulsion architecture characterization was introduced to enable rapid architectural changes to be made. The new approach relies on categorizing the most prominent subsystems into three main source groups (power, thrust and energy sources), as well as a set ofo interrelationship matrices to define the architectures and au-

tomatically establish the logical connections among the necessary subsystems. Then, these logical connections are mapped to the related first order principles during the propulsion performance evaluations. Thus, the analyst does not need to define separate calculation methods for diverse architectures.

Additionally, two levels of parametric, physics-based EPGDS models were developed to increase the dimensionality of the analysis: the high-level models suitable for rapid sizing and mission level analysis, and detailed models suitable for transient analysis. The impact of the EPGDS at the aircraft and mission levels was taken into account not only by their direct impact on the weight of the aircraft, but also by the individual power requirement they might impose. This brought increased dimensionality to the analysis compared to some other approaches in literature. Moreover, the ability to switch between the two types of models help reduce the epistemic uncertainty. Finally, the parametric nature of the models enabled performing sensitivity analysis to assess the sensitivity to modeling assumptions and technology advancements.

The second noteworthy capability of the methodological framework was the integration of a power management schedule optimization approach to the sizing and synthesis of hybrid electric aircraft. Due to the integrated optimization capability, various architectures can be compared under their optimum performance, allowing for a fair comparison to be made.

The optimization problem was set up with a set of control variables which do not depend on the potential performance degradation of the power sources. Furthermore, a strategic approach to determine the number of control variables and thus the extent of the resolution level of the analysis was introduced under the concept of control points. The control variables were then related to hybridization factors to impose the optimized power management schedule. What's more, new definitions for the level of hybridization were made based on mission segment characteristics. This way, the level of hybridization was made independent of the propulsion architecture as opposed to some other definitions seen in

literature.

Last but not least, the methodological framework brought the transient analysis of dynamic electric power generation and distribution subsystems to the aircraft conceptual design stage without exhausting computational resources.

The transient behavior of EPGDS is often neglected in aircraft design and mission performance analysis, but is crucial for the design of these subsystems. Traditionally, transient analysis are not performed until after the aircraft design is almost locked. However, the overall impact of EPGDS in terms of its changing design and performance characteristics is expected to be more strongly emphasized in EA/HEA concepts compared to the conventional ones due to the immense amount of electric power flow within the propulsion architecture and the increased sensitivity of the aircraft design to weight changes. Thus, the amount of epistemic uncertainty in the design and performance of these subsystems jeopardizes the design and performance of the aircraft.

The three most salient features of this capability is as follows: (i) the flexibility in the "significant transient" definition, (ii) the ability to tune the controllers of the electrical system for a large number usage scenarios, and (iii) the creation of a conditional rule set which determines when the temporal step size should be reduced to allow for transient analysis based on a very limited amount of knowledge available at the mission level.

A flexibility in terms of how the "significant transients" would be defined were needed because of the lack of established standards and transient constraints for EA/HEA concepts. With this feature, the analyst can decide on what kind of transients and which subsystem or subsystems to focus on, as well as the tolerance levels put on the transients.

The aggregated gain tuning technique was developed to be used when a subject-matter expertise is not available. An analytic solution is usually not an option due to the complexity and non-linearity of the electrical network. Instead, optimization methods can be utilized to find a local optimum solution for the controller gains in a given case. However, the number of controllers and therefore the gains to be tuned can quickly expand beyond

practical limits even in simple electrical systems.

The proposed gain tuning technique depends on variable importance assessment based on Monte Carlo simulations performed in advace of the optimization. First, the number of variables to be optimized are cut down by eliminating the variables which do not have a major impact on the optimum solution, if possible. Second, prediction profilers are utilized to examine the design space of the gains along with the simulation inputs so that a specific set of initial conditions to the optimization problem can be obtained. These initial conditions are selected such that the optimization would converge to a local solution which is expected to be an acceptable solution not only for the case being optimized, but for the majority of cases in the design space. This way, the optimization is strategically made "biased" to minimize the optimization efforts.

The resulting optimization solutions were used to create gain schedules for various cases defined by the design of experiments conducted to explore the design space of constraint violations. It was shown that not all of the mission level changes trigger an undesired transient response. More importantly, it was demonstrated that the time and place of the constraint violations can be estimated based only on variables which are calculated at mission performance analysis.

The constraint violations due to the mission level changes were modeled via categorical neural networks. These models predict the probability of a significant transient occurring under certain operational conditions. This capability was utilized to write a set of rules which determines during mission performance analysis whether the timescale should be decreased to conduct more detailed, transient analysis. This allows to perform the transient analysis only when necessary, so that the computational burden of simulating the whole mission is avoided. This capability is the key enabler for more accurate sizing and performance evaluation of EPGDS at the aircraft conceptual design stage.

This research was motivated by a list of questions posed in the very beginning of this dissertation, in Chapter 1. These questions were by no means the only questions which

drove this research, but the main ones which either did not have satisfactory answers in literature, or any answers at all, as the literature review provided in Chapter 2 showed. They were then formed into the overarching research question which was also revisited below.

The Overarching Research Question: How can the aircraft sizing and synthesis process be more generalized so that adequate comparisons between different types of primary power generation and distribution subsystems and candidate architectures are made available?

The answer to the main research question yielded the over-arching hypothesis of this thesis. The list of questions which made up the overarching research question were addressed by the subsequent hypothesis. Consequently, each question in this list was answered with a hypothesis and the answers were substantiated by the relevant experiments. The list of questions was revisited below. This time, the list includes the answers by mapping each question to a hypothesis of this dissertation.

- What modifications should be done on the aircraft sizing and mission analysis process so that it is inclusive of any type of aircraft design, propulsion system, architecture and the energy storage type? **- H.1, H.2**
  - The traditional mission analysis approach must be modified to an energy-based approach where the required energy to fly a mission profile is tracked and budgeted between different power sources of aircraft according to preset hybridization levels
  - A component based weight estimation technique must be used
  - Aircraft sizing and synthesis process must capture the sizing of EPGDS components based on required energy and/or power
  - The subsystem level impacts must be captured at aircraft and mission levels

- What capabilities are needed to enable rapid changes in the subsystem characteristics and architectures? **- H.1, H.2**
  - Flexible aircraft propulsion architecture definitions to account for various types for architectures and their impact on the vehicle and mission levels
  - Parametric, physics-based models to represent EPGDS performance characteristics
- How can EPGDS be represented to demonstrate various characteristics related to different types of subsystems? **- H.1, H.2, H.4**
  - By developing two levels of parametric, physics-based EPGDS models where high-level models are used for rapid sizing and performance evaluation analysis, and detailed models are used for transient analysis
- How can the dynamic EPGDS characteristics be integrated into the sizing process? **- H.1, H.2, H.4**
  - Vehicle and mission level requirements must be linked to EPGDS model parameters
  - Subsystem characteristics and dynamics must be computed by transitioning between the two levels of EPGDS models when and where necessary
  - The necessity must be determined by the occurrence of significant transients
- How can the technological sensitivities be captured? **- H.1, H.2**
  - Technology K-factors must be defined and linked to EPGDS model parameters
  - Subsystem level characteristics must be captured through aircraft and mission level measures of performance so that the impact of technological advances can then be seen on the overall design and mission performance

- How can the best performing hybrid electric architecture be determined under varying levels of hybridization? **- H.1, H.3**
  - If the competing architectures are being sized first, then the power management schedule must be optimized during the sizing process
  - If the design is frozen, then the architectures must be compared at their optimum schedule for the same off-design mission profile
  - The optimum schedule must be used to determine the best performing feasible architecture among the competing architectures by comparing their associated aircraft and mission level measures of performance
- How can the optimum operating conditions be obtained for different types of architectures? **- H.1, H.3**
  - The optimum power management schedule for an aircraft can be obtained by implementing a segment-wise optimization technique based on a set of control points and variables which do not depend on the type of the propulsion system
- What impact does the level of hybridization have on choosing the best performing architecture? **- H.1, H.3**
  - The level of hybridization throughout the mission (i.e. power management schedule) has a great impact on the vehicle design and mission performance and thus can be the driving factor in architectural comparisons
  - If the schedule is not optimized for the given objective at the design mission, then the vehicle cannot perform at its full potential
  - This would lead to an unfair competition and the wrong choice of architecture as the best performing one
- Does every operational change trigger a significant transient response in the electrical system of the aircraft? **- H.1, H.4**

  - No, only specific changes trigger a significant transient response. Such changes depend on the nature and magnitude of the change in the mission characteristics as well as the characteristics of the electrical system

- How can a balance between smaller and larger time steps be found so that significant transients at the subsystem level are captured at the conceptual design stage without bringing the associated computational burden? **- H.1, H.4**

  - By establishing a conditional rule set determined a-priori by fitting a categorical surrogate model to the transient signal at the neighborhood of the time at which the mission level change occurred, and then using this rule set to determine whether the transients are significant enough to require a reduction in the step size

- Can the transient behavior of an electrical system be related to the mission level parameters? If they are related, how can the relationship be captured between the significant transients of a given electrical system which could occur under a wide range of inputs which are expected to be given to the electrical system during a mission? **- H.1, H.4**

  - Yes, they can be related through sensitivity studies which can be performed by leveraging the design of experiments approach

- If they are related, can the relationship be generalized for the given electrical system so that the whether a significant transient occurs could be estimated with only the limited amount of information obtained from the mission performance analysis? **- H.1, H.4**

  - Yes, the relationship be generalized within the defined design variable space by creating a categorical surrogate modeling technique to estimate whether a

significant transient occurs using only a few variables related to the mission performance

As it can be seen from the short list of questions above, these questions and many more can now be answered thanks to the methodological framework developed in this dissertation.

To sum up, the developed methodological framework addresses the subsystem related problems in novel aircraft architectures which could not be solved with traditional sizing and synthesis approaches. By facilitating detailed subsystem level considerations within the aircraft conceptual design stage in a parametric and highly flexible manner, it enables more accurate yet still rapid architecture comparisons among various novel concepts, including electric and hybrid electric aircraft.

9.3 Recommendations for Future Work

This section lists some potential improvements that can be made on the developed framework to adjust the level of detail of the analysis desired to be performed.

First, further refinement can be done on the EPGDS models, specifically the high-level ones. Although being mentioned, the rechargeable battery sizing was done based only on it specific energy, without incorporating the specific power. This was due to the fact that the specific energy of the Lithium-Ion batteries used in electric propulsion concepts is more limiting than the specific power for the investigated aircraft types. Moreover, the rechargeable battery model can be replaced by other alternative energy sources, such as fuel cells.

Example applications of each step of the developed methodology were provided throughout this dissertation. Each example had different assumptions and boundary conditions to show the applicability of the methodology on different use-cases and different levels of detail. The examples covered majority of the main EPGDS, but left out some subsystems such as generators, other motor drive models instead of the induction motor drive, and so

on. The author plans on extending the architecture comparisons by including more EPGDS models within E-PASS in the upcoming studies.

Currently, the methodology does not include how the subsystems are located inside or on the aircraft, how the physical connection between them is established and how the distribution elements are sized. The placement of the subsystems and cabling were taken into account in only one application, Experiment 2.3. Previous work (Ref. [83]) addressed these issues, but the impact on the architectural decisions was not covered. The next step is to include a routing logic for the electric cables to widen the subsystem efforts.

Moreover, the mechanical and/or hydraulic subsystems were captured by their contribution to the empty weight only through the component-based weight estimation equations. Future efforts can include more detailed considerations for primary power generation and distribution subsystems other than the electrical once. For instance, a more detailed power split device can be modeled to account for more accurate sizing since such devices can introduce significant weight to the system.

Thermal management considerations were not in the scope of this research. However, one of the major concerns regarding the utilization of EPGDS with high electric loads is the heating problems. Detailed thermal models would prove useful for thermal management studies and could have a significant impact on the subsystem and vehicle design.

Because subject-matter expertise was not available at the time of this study, the impact of capturing the dynamic response of the subsystems on the vehicle design was not explicitly demonstrated, but explained through logical if-then type of scenarios. These studies can be expanded to resize the relevant subsystems, which would in turn change the vehicle design and performance, and result in different transient behaviors.

Finally, if more information regarding the nature of the transient is desired without conducting transient analysis during or after mission analysis, a continuous surrogate modeling approach can be attempted to fit a model to the signal itself, rather than the event of constraint violation. Although such modeling approaches to estimate the continuous transient

behavior within the reaction window were tried during the search for the best representation technique, the categorical model yielded more accurate results. However, more approaches can be populated; for instance, the signals can be filtered to reduce the inherent noise before modeling.

More areas can be populated to extend the capabilities and application areas of E-PASS. The parametric nature of the framework makes it easy to include additional properties, and there is definitely room for more improvement. With that said, the developed methodology in its current form was demonstrated to be sufficient to address the research questions and accomplish the over-arching research objective of this thesis by providing a framework to perform sizing, integration and performance evaluation of electric power generation and distribution subsystems and architectures within electric and hybrid electric aircraft concepts.

Appendices

APPENDIX A

DETAILED EPGDS MODELS IN SIMULINK

The detailed EPGDS models created in Simulink to be used in transient analysis are presented in this appendix. The main Simulink blocks which make up the overall electrical network are shown in Figure A.1. The electrical network consists of a rechargeable Lithium-Ion battery, a DC/DC converter (Figure A.2), and an induction motor drive (Figure A.4). The working principles and input/output parameters of each of these models are described in detail in Chapter 5.

The DC/DC converter consists of a two-quadrant converter model and a PWM controller (shown in Figure A.3). The induction motor drive consists of a braking chopper and a three-phase inverter to convert the DC current coming from the battery to AC current going to the induction machine. The motor drive also has a field oriented control system which incorporates a speed controller and a space vector modulation. Reference [98] presents the schematics for these motor controllers which are shown in Figures A.5 and A.6.

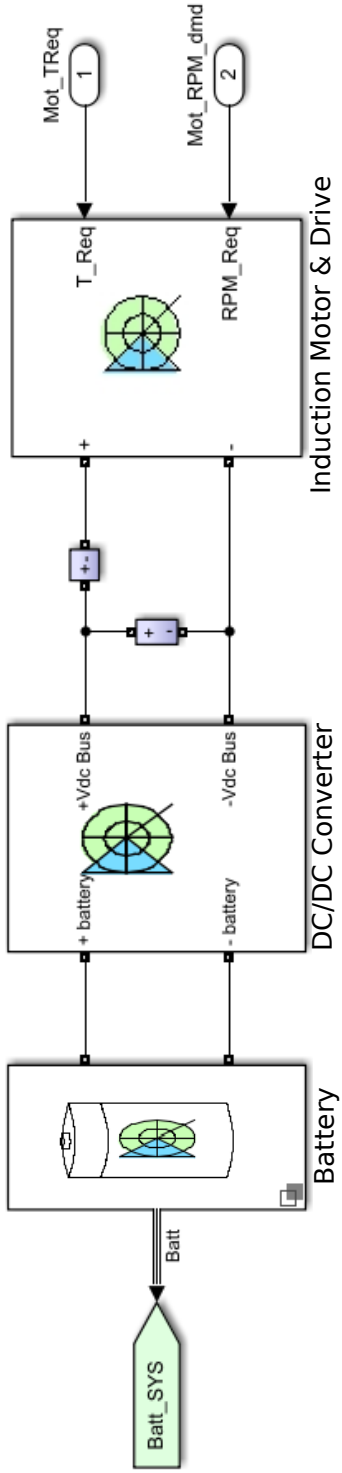

Figure A.1: Electric propulsion branch in Simulink.

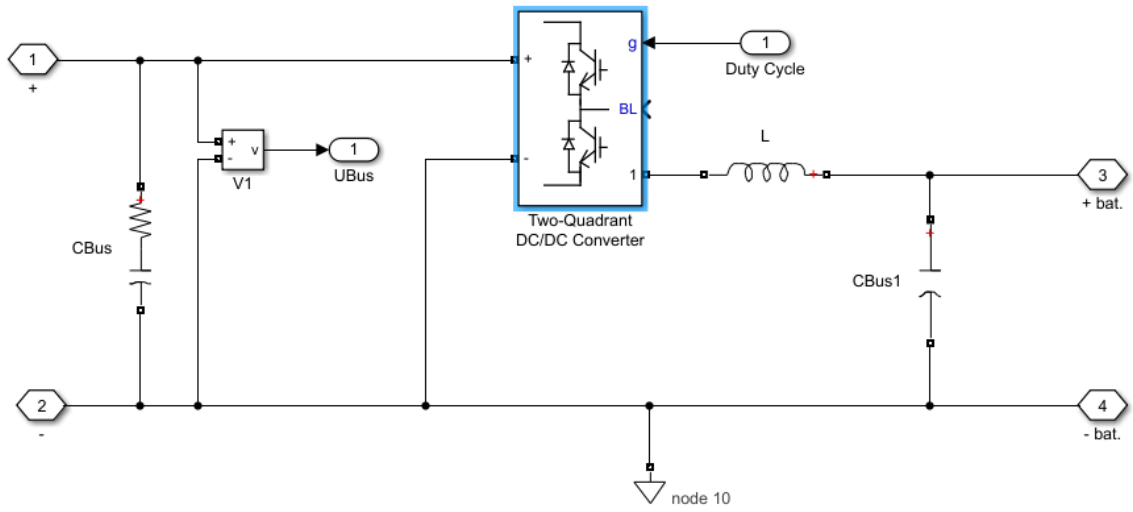

Figure A.2: DC-DC Converter (Bus) model in Simulink.

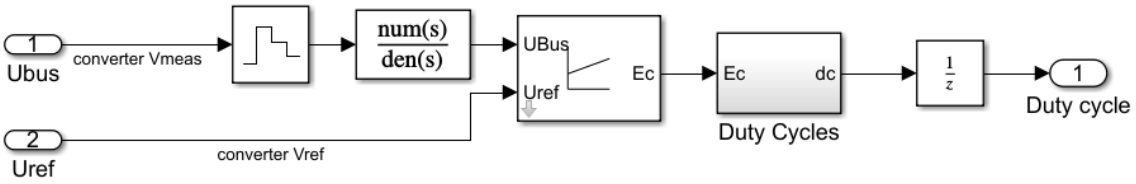

Figure A.3: Controller model for the DC bus in Simulink.

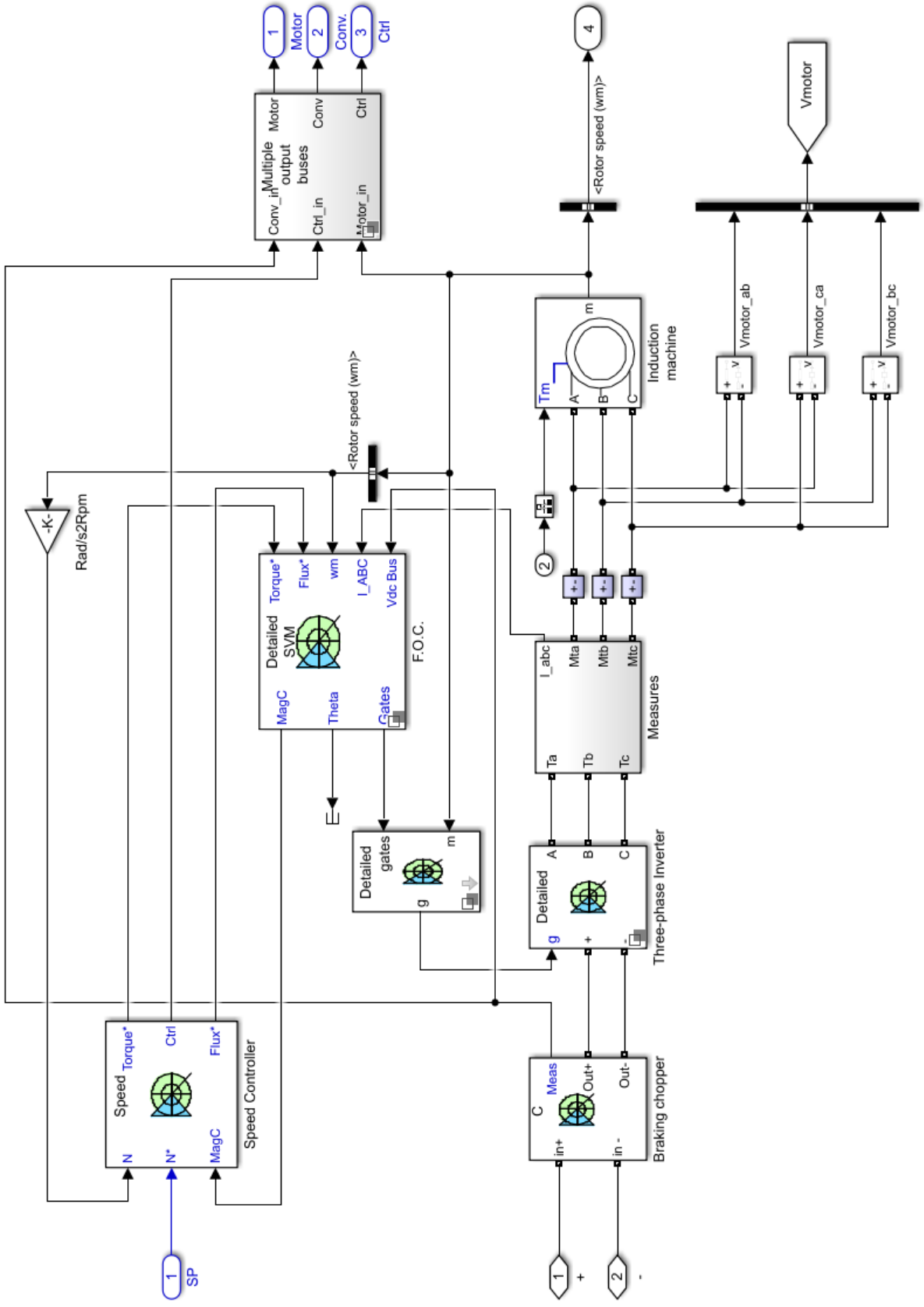

Figure A.4: Detailed model for the field-oriented control induction motor drive; modified from the "Field-Oriented Control Induction Motor Drive" block available in Electric Drives/AC drives library of Simulink.

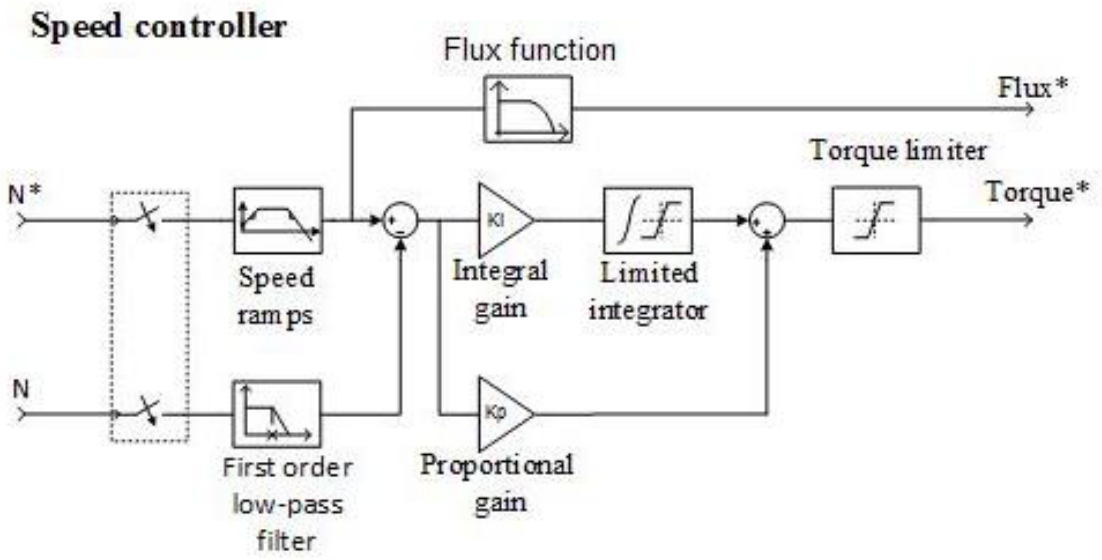

Figure A.5: Controller schematic for the speed controller of the motor drive [98].

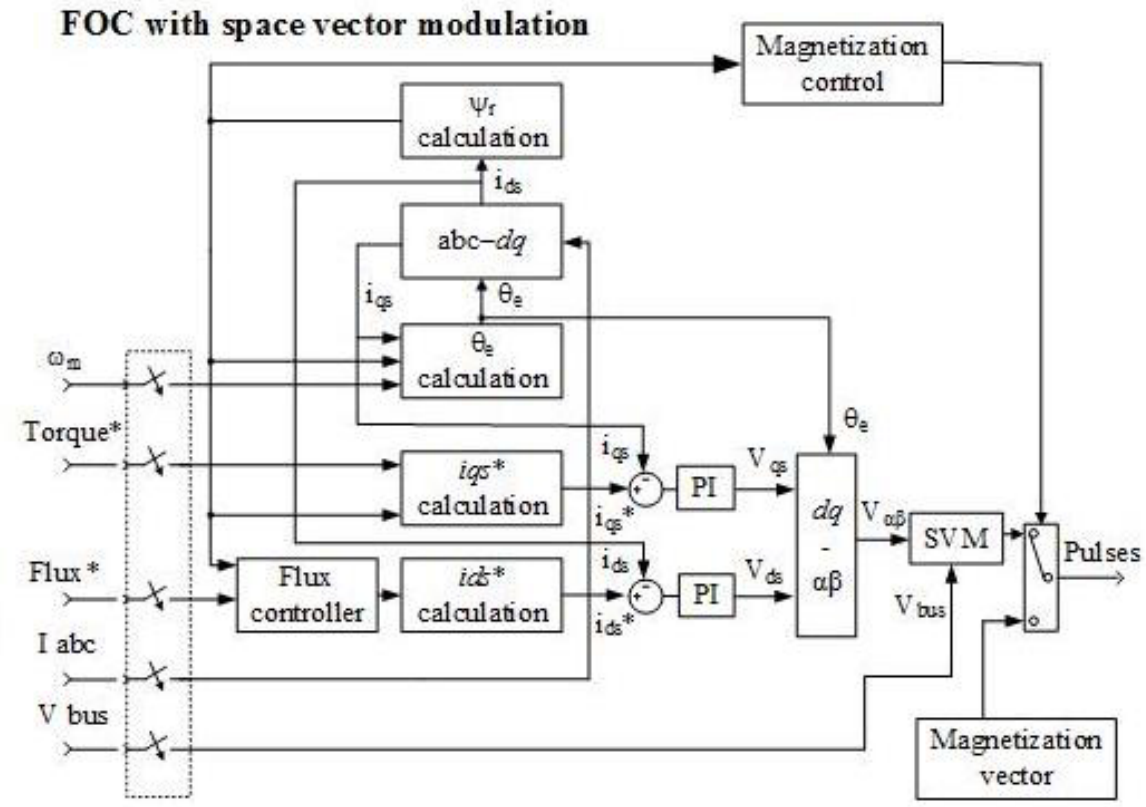

Figure A.6: Controller schematic for the field-oriented control with space vector modulation of the motor drive [98].

REFERENCES

[1] ICAO, *Environmental Report 2013: Aviation and Climate Change*.

[2] ICAO, "Resolution A37-19: Consolidated statement of continuing ICAO policies and practices related to environmental protection Climate change," Montreal, Tech. Rep., 2010.

[3] ICAO, *Environmental Report 2010: Aviation and Climate Change*.

[4] D. S. Lee, D. W. Fahey, P. M. Forster, P. J. Newton, R. C. Wit, L. L. Lim, B. Owen, and R. Sausen, "Aviation and Global Climate Change in the 21st Century," *Atmospheric Environment*, vol. 43, no. 22-23, 35203537, 2009.

[5] Air Transport Action Group (ATAG), *Facts and figures*, 2016.

[6] IATA, *Fact sheet: climate change & corsia*, 2016.

[7] ICAO, *Environmental Report 2016: Aviation and Climate Change*, 2016.

[8] IATA, "IATA Technology Roadmap," 4th Edition, 2013.

[9] NASA, *NASA Technology Roadmaps TA 15: Aeronautics*.

[10] M. Hornung, A. T. Isikveren, M. Cole, and A. Sizmann, "Ce-Liner Case Study for eMobility in Air Transportation," Los Angeles, CA: AIAA, 2013.

[11] M. K. Bradley and C. K. Droney, "Subsonic Ultra Green Aircraft Research: Phase II Volume II Hybrid Electric Design Exploration," Boeing Research and Technology, Huntington Beach, California, Tech. Rep., 2015.

[12] N. K. Madavan, R. D. Rosario, and A. L. Jankovsky, "Hybrid-Electric and Distributed Propulsion Technologies for Large Commercial Transports: A NASA Perspective," Special Session on Future Electric Aircraft Systems, Montreal, Canada: IEEE, 2015.

[13] I. Chakraborty, "Subsystem architecture sizing and analysis for aircraft conceptual design," PhD thesis, Georgia Institute of Technology, Atlanta, GA, 2015.

[14] National Academies of Sciences, Engineering, and Medicine, *Commercial Aircraft Propulsion and Energy Systems Research: Reducing Global Carbon Emissions*. Washington DC: The National Academies Press, 2016.

[15] A. T. Isikveren, C. Pornet, P. C. Vratny, and M. Schmidt, "Optimization of commercial aircraft using battery-based voltaic-joule/brayton propulsion," *Journal of Aircraft*, vol. 54, no. 1, pp. 246–261, 2017.

[16] R. Jansen, G. V. Brown, J. L. Felder, and K. P. Duffy, "Turboelectric aircraft drive key performance parameters and functional requirements," in *51st AIAA/SAE/ASEE Joint Propulsion Conference*, 2015.

[17] T. E. Noll, J. M. Brown, M. E. Perez-Davis, S. D. Ishmael, G. C. Tiffany, and M. Gaier, "Investigation of the helios prototype aircraft mishap volume i mishap report," *Downloaded on March 9*, 2004.

[18] N. K. Borer, C. L. Nickol, F. Jones, R. Yasky, K. Woodham, J. Fell, B. Litherland, P. Loyselle, A. Provenza, L. Kohlman, *et al.*, "Overcoming the adoption barrier to electric flight," 54th AIAA Aerospace Sciences Meeting, AIAA, 2016.

[19] Pipistrel, *Alpha Electro Overview*, [company website], URL: http://www.pipistrel.si/plane/alpha-electro/overview [cited on 13 Sep 2015].

[20] Airbus Group, *E-fan electric aircraft*, [company website], URL: http://www.airbusgroup.com/int/en/corporate-social-responsibility/airbus-e-fan-the-future-of-electric-aircraft.html [cited on 1 Mar 2017].

[21] K. Petermaier, "Electric propulsion components with high power densities for aviation," Transformative Vertical Flight Workshop, Siemens AG, 2015.

[22] Airbus Group, *Gaining valuable experience with E-Fan*, [company website], URL: http://www.airbusgroup.com/int/en/corporate-social-responsibility/latest-news/e-fan-plus-technology-improvements.html [cited on 9 Mar 2017], 2016.

[23] NASA, *NASA's X-57 Electric Research Plane*, [company website], URL: https://www.nasa.gov/image-feature/nasas-x-57-electric-research-plane [cited on 3 Mar. 2017], Jun. 2016.

[24] Boeing Company, *2014 environment report: future flight*, Company website, URL: http://www.boeing.com/aboutus/environment/environment_report_14/2.3_future_flight.html [cited on 3 Mar. 2017], 2014.

[25] NASA, *Hybrid wing body goes hybrid*, Company website, URL: https://www.nasa.gov/content/hybrid-wing-body-goes-hybrid [cited on 3 Mar. 2017], 2013.

[26] N. K. Borer, M. D. Patterson, J. K. Viken, M. D. Moore, J. Bevirt, A. M. Stoll, and A. R. Gibson, "Design and performance of the nasa sceptor distributed electric propulsion flight demonstrator," 16th AIAA Aviation Technology, Integration, and Operations Conference, Washington, D.C.: AIAA, 2016.

[27] M. D. Moore, "Misconceptions of electric aircraft and their emerging aviation markets," 52nd Aerospace Sciences Meeting, National Harbor, Maryland: AIAA, 2014.

[28] N. K. Borer, M. D. Moore, and A. Turnbull, "Tradespace Exploration of Distributed Propulsors for Advanced On-Demand Mobility Concepts," 14th AIAA Aviation Technology, Integration, and Operations Conference, Atlanta, GA: AIAA, 2014.

[29] N. K. Borer and M. D. Moore, "Integrated propeller-wing design exploration for distributed propulsion concepts," 53rd AIAA Aerospace Sciences Meeting, Kissimmee, FA: AIAA, 2015.

[30] M. D. Patterson, N. K. Borer, and B. German, "A simple method for high-lift propeller conceptual design," 54th AIAA Aerospace Sciences Meeting, San Diego, CA: AIAA, 2016.

[31] S. Clarke, K. Papathakis, A. Samuel, Y. Lin, and S. Ginn, "Nasa sceptor electric concept aircraft power system: x-plane electric propulsion system design and qualification for crewed flight testing," Transportation Electrification Conference and Expo (ITEC), IEEE, 2016.

[32] A. T. Isikveren, A. Seitz, P. C. Vratny, C. Pornet, K. O. Plötner, and M. Hornung, "Conceptual studies of universally-electric systems architectures suitable for transport aircraft," Deutscher Luft-und Raumfahrt Kongress, Germany: DLRK Berlin, 2012.

[33] M. K. Bradley and C. K. Droney, "Subsonic ultra green aircraft research - phase i final report," 2011.

[34] C. A. Perullo, D. R. Trawick, and D. N. Mavris, "Assessment of engine and vehicle performance using integrated hybrid-electric propulsion models," *Journal of Propulsion and Power*, vol. 32, no. 6, pp. 1305–1314, 2016.

[35] T. Nam, D. Soban, and D. Mavris, "Power based sizing method for aircraft consuming unconventional energy," 43rd AIAA Aerospace Sciences Meeting and Exhibit, Reno, NA: AIAA, 2005.

[36] T. Nam, and D. Soban, and D. Mavris, "A generalized aircraft sizing method and application to electric aircraft," 3rd International Energy Conversion Engineering Conference, San Francisco, CA: AIAA, 2005.

[37] C. Pornet, C. Gologan, P. C. Vratny, A. Seitz, O. Schmitz, A. T. Isikveren, and M. Hornung, "Methodology for sizing and performance assessment of hybrid energy aircraft," *Journal of Aircraft*, vol. 52, no. 1, pp. 341–352, 2014.

[38] C. Perullo and D. Mavris, "A review of hybrid-electric energy management and its inclusion in vehicle sizing," *Aircraft Engineering and Aerospace Technology: An International Journal*, vol. 86, no. 6, pp. 550–557, 2014.

[39] R. DelRosario, "Nasa fixed wing project: green technologies for future aircraft generation," 2014.

[40] J. Welstead and J. L. Felder, "Conceptual design of a single-aisle turboelectric commercial transport with fuselage boundary layer ingestion," 54th AIAA Aerospace Sciences Meeting, AIAA, 2016.

[41] Siemens AG, *World-record electric motor for aircraft*, [company website], URL: `http://www.siemens.com/press/en/feature/2015/corporate/2015-03-electromotor.php?content[]=Corp` [cited on 13 Sep. 2015], 2015.

[42] J. Lowry and J. Larminie, *Electric Vehicle Technology Explained*, 2nd ed. John Wiley & Sons, 2012.

[43] A. Emadi, Y. J. Lee, and K. Rajashekara, "Power Electronics and Motor Drives in Electric, Hybrid Electric, and Plug-In Hybrid Electric Vehicles," *IEEE Transactions On Industrial Electronics*, vol. 55, no. 6, pp. 2237–2245, 2008.

[44] K. Chau and Y. Wong, "Overview of power management in hybrid electric vehicles," *Energy Conversion and Management*, vol. 43, no. 15, pp. 1953–1968, 2002.

[45] D. Buecherl, I. Bolvashenkov, and H.-G. Herzog, "Verification of the optimum hybridization factor as design parameter of hybrid electric vehicles," 2009 IEEE Vehicle Power and Propulsion Conference, IEEE, 2009, pp. 847–851.

[46] A. Khajepour, M. S. Fallah, and A. Goodarzi, *Wiley Desktop Editions : Electric and Hybrid Vehicles : Technologies, Modeling and Control - A Mechatronic Approach*. Wiley, 2014.

[47] C. C. Chan, "The state of the art of electric, hybrid, and fuel cell vehicles," *Proceedings of the IEEE*, vol. 95, no. 4, pp. 704–718, Apr. 2007.

[48] J. Larminie, A. Dicks, and M. S. McDonald, *Fuel cell systems explained*. J. Wiley Chichester, UK, 2003.

[49] T. H. Bradley, B. A. Moffitt, D. N. Mavris, T. F. Fuller, and D. E. Parekh, "Hardware-in-the-loop testing of a fuel cell aircraft powerplant," *Journal of Propulsion and Power*, vol. 25, no. 6, pp. 1336–1344, 2009.

[50] G. Romeo, F. Borello, and G. Correa, "Enfica-fc: design, realization and flight test of all electric 2-seat aircraft powered by fuel cells," 27th International Congress of the Aeronautical Sciences (ICAS2010), 2010.

[51] A. Nishizawa, J. Kallo, O. Garrot, and J. Weiss-Ungethüm, "Fuel cell and li-ion battery direct hybridization system for aircraft applications," *Journal of Power Sources*, vol. 222, pp. 294–300, 2013.

[52] K. Friedrich, J. Kallo, J. Schirmer, and G. Schmitthals, "Fuel cell systems for aircraft application," *ECS Transactions*, vol. 25, no. 1, pp. 193–202, 2009.

[53] R. von Helmolt and U. Eberle, "Fuel cell vehicles: status 2007," *Journal of Power Sources*, vol. 165, no. 2, pp. 833–843, 2007.

[54] O. Tremblay and L. A. Dessaint, "Experimental validation of a battery dynamic model for ev applications," *World Electric Vehicle Journal*, vol. 3, no. 1, pp. 1–10, 2009.

[55] A. L. Shenkman, *Transient Analysis of Electric Power Circuits Handbook*. Springer Science & Business Media, 2006.

[56] L. L. Phan, D. N. Mavris, J.-J. Charrier, and E. Garcia, "Efficient integration of transient constraints in the design of aircraft dynamic systems," 27th Congress of the International Council of the Aeronautical Sciences, Nice, France: ICAS, Sep. 2010.

[57] W. E. Kazibwe and M. H. Sendaula, *Electric Power Quality Control Techniques*. Van Nostrand Reinhold, 1993.

[58] *Aircraft Electric Power Characteristics, MIL-STD-704F*, Department of Defense, Mar. 2004.

[59] C. J. Miller, A. C. Maser, E. Garcia, and D. N. Mavris, "Invent surrogate modeling and optimization of transient thermal responses," 50th AIAA Aerospace Sciences Meeting including the New Horizons Forum and Aerospace Exposition, Nashville, Tennessee: AIAA, 2012.

[60] J. I. Hileman, P. E. Donohoo, and R. W. Stratton, "Energy content and alternative jet fuel viability," *Journal of propulsion and Power*, vol. 26, no. 6, pp. 1184–1196, 2010.

[61] J.-M. Tarascon and P. Simon, *Electrochemical Energy Storage*. Somerset, US: Wiley-ISTE, 2015, vol. 1.

[62] K. G. Gallagher, S. Goebel, T. Greszler, M. Mathias, W. Oelerich, D. Eroglu, and V. Srinivasan, "Quantifying the promise of lithium–air batteries for electric vehicles," *Energy & Environmental Science*, vol. 7, no. 5, pp. 1555–1563, 2014.

[63] R. Wagner, N. Preschitschek, S. Passerini, J. Leker, and M. Winter, "Current research trends and prospects among the various materials and designs used in lithium-based batteries," *Journal of Applied Electrochemistry*, vol. 43, no. 5, pp. 481–496, 2013.

[64] M. M. Thackeray, C. Wolverton, and E. D. Isaacs, "Electrical energy storage for transportationapproaching the limits of, and going beyond, lithium-ion batteries," *Energy & Environmental Science*, vol. 5, no. 7, pp. 7854–7863, 2012.

[65] R. Slingerland, S. Zandstra, D. Scholz, and K. Seeckt, "Green freighter systems," 46th AIAA Aerospace Sciences Meeting and Exhibit, Reno, NV: AIAA, 2008.

[66] S. C. Hora, "Aleatory and epistemic uncertainty in probability elicitation with an example from hazardous waste management," *Reliability Engineering & System Safety*, vol. 54, no. 2-3, pp. 217–223, 1996.

[67] J. Roskam, *Airplane Design Part V - Component Weight Estimation*. Kansas: Design Analysis and Research Corporation, 1999.

[68] D. P. Raymer, *Aircraft Design: A Conceptual Approach*, 5th ed., ser. AIAA Education Series. Virginia: AIAA, 2012.

[69] J. D. Mattingly, W. H. Heiser, and D. T. Pratt, *Aircraft Engine Design*, 2nd edition, ser. AIAA Education Series. AIAA, 2002.

[70] I. Chakraborty and D. N. Mavris, "Heuristic definition, evaluation, and impact decomposition of aircraft subsystem architectures," 16th AIAA Aviation Technology, Integration, and Operations Conference, Washington, D.C.: AIAA, 2016.

[71] J. G. Coffin, "Study of airplane ranges and useful loads," NACA, Tustin, CA, Tech. Rep., 1920.

[72] D. P. Wells, B. L. Horvath, and L. A. McCullers, *The Flight Optimization System Weights Estimation Method*. NASA, Jun. 2017, vol. 1, NASA/TM?2017?219627.

[73] L. A. McCullers, *Flops user's guide*, 8.11, NASA Langley Research Center, Hampton, VA, 2009.

[74] K. R. Antcliff, M. D. Guynn, T. Marien, D. P. Wells, S. J. Schneider, and M. J. Tong, "Mission analysis and aircraft sizing of a hybrid-electric regional aircraft," in *54th AIAA Aerospace Sciences Meeting*, 2016, p. 1028.

[75] S. Gudmundsson, *General Aviation Aircraft Design: Applied Method and Procedures*, 1st ed. Oxford, UK: Elsevier, 2014.

[76] N. Kim, S. Cha, and H. Peng, "Optimal control of hybrid electric vehicles based on pontryagin's minimum principle," *IEEE Transactions on Control Systems Technology*, vol. 19, no. 5, pp. 1279–1287, 2011.

[77] P. Pisu and G. Rizzoni, "A comparative study of supervisory control strategies for hybrid electric vehicles," *IEEE Transactions on Control Systems Technology*, vol. 15, no. 3, pp. 506–518, 2007.

[78] C. Musardo, G. Rizzoni, Y. Guezennec, and B. Staccia, "A-ecms: an adaptive algorithm for hybrid electric vehicle energy management," *European Journal of Control*, vol. 11, no. 4-5, pp. 509–524, 2005.

[79] A. Sciarretta, M. Back, and L. Guzzella, "Optimal control of parallel hybrid electric vehicles," *IEEE Transactions on control systems technology*, vol. 12, no. 3, pp. 352–363, 2004.

[80] A. Saltelli, "Making best use of model evaluations to compute sensitivity indices," *Computer Physics Communications*, vol. 145, pp. 280–297, 2002.

[81] MathWorks, *MATLAB*, [company website], URL: `https://www.mathworks.com/products/matlab.html` [cited on July 30, 2018].

[82] F. Gaspari, L. Trainelli, A. Rolando, and I. Perkon, *D1.1: Concept of Modular Architecture for Hybrid Electric Propulsion of Aircraft*, Dec. 2017.

[83] G. Cinar, D. N. Mavris, M. Emeneth, A. Schneegans, and Y. Fefermann, "Development of parametric power generation and distribution subsystem models at the conceptual aircraft design stage," 55th AIAA Aerospace Sciences Meeting, Grapevine, TX: AIAA, 2017.

[84] G. Cinar, D. N. Mavris, M. Emeneth, A. Schneegans, C. Riediger, Y. Fefermann, and A. Isikveren, "Sizing, integration and performance evaluation of hybrid electric propulsion subsystem architectures," 55th AIAA Aerospace Sciences Meeting, Grapevine, TX: AIAA, Jan. 2017.

[85] M. Chen and G. A. Rincon-Mora, "Accurate electrical battery model capable of predicting runtime and iv performance," *IEEE Transactions on Energy Conversion*, vol. 21, no. 2, pp. 504–511, 2006.

[86] V. Ramadesigan, P. W. C. Northrop, S. De, S. Santhanagopalan, R. D. Braatz, and V. R. Subramanian, "Modeling and simulation of lithium-ion batteries from a systems engineering perspective," *Journal of The Electrochemical Society*, vol. 159, no. 3, R31–R45, 2012.

[87] M. R. Jongerden and B. R. Haverkort, "Which battery model to use?" *IET Software*, vol. 3, no. 6, pp. 445–457, 2009.

[88] H. He, R. Xiong, and J. Fan, "Evaluation of lithium-ion battery equivalent circuit models for state of charge estimation by an experimental approach," *Energies*, vol. 4, pp. 582–598, 2011.

[89] K. W. E. Cheng, B. Divakar, H. Wu, K. Ding, and H. F. Ho, "Battery-management system (bms) and soc development for electrical vehicles," *IEEE Transactions on Vehicular Technology*, vol. 60, no. 1, pp. 76–88, 2011.

[90] H. Rahimi-Eichi, U. Ojha, F. Baronti, and M.-Y. Chow, "Battery management system: an overview of its application in the smart grid and electric vehicles," *IEEE Industrial Electronics Magazine*, vol. 7, no. 2, pp. 4–16, 2013.

[91] IEEE, "IEEE Guide for Synchronous Generator Modeling Practices and Applications in Power System Stability Analyses," *IEEE Std 1110-2002, Revision of IEEE Std 1110-1991*, pp. 1–72, 2003.

[92] K. Metcalf, "Power Management and Distribution (PMAD) Model Development," Boeing Corporation, Canoga Park, CA, Tech. Rep. NASA/CR2011-217268, 2011.

[93] B. K. Bose, *Modern Power Electronics and AC Drives*, 1st ed. Prentice Hall, Oct. 2001.

[94] M. Ehsani, K. M. Rahman, and H. A. Toliyat, "Propulsion system design of electric and hybrid vehicles," *IEEE Transactions on industrial electronics*, vol. 44, no. 1, pp. 19–27, 1997.

[95] C. T. Faria, F. Chauvicourt, R. Hallez, C. Colangeli, J. Cuenca, H. V. der Auweraer, T. Olbrechts, D. Toure, and O. Broca, "Early-stages comfort simulation of an e-aircraft," AIAA Propulsion and Energy Forum, Cincinnati, Ohio: AIAA, Jul. 2018.

[96] R. Vepa, *Dynamic Modeling, Simulation and Control of Energy Generation*. Springer, 2013, vol. 20.

[97] M. Ahmad, *High Performance AC Drives*. Springer, 2010.

[98] H.Blanchette and L.-A. Dessaint, *Ac3 - field-oriented control induction 200 hp motor drive*, [company website], URL: `https://www.mathworks.com/`

help/physmod/sps/examples/ac3-field-oriented-control-induction-200-hp-motor-drive.html [cited on 30 July 2018].

[99] E. Hendricks and M. Tong, "Performance and weight estimates for an advanced open rotor engine," 48th AIAA/ASME/SAE/ASEE Joint Propulsion Conference & Exhibit, Joint Propulsion Conferences, Atlanta, GA: AIAA, 2012.

[100] J. Liu and H. Peng, "A systematic design approach for two planetary gear split hybrid vehicles," *Vehicle System Dynamics*, vol. 48, no. 11, pp. 1395–1412, Oct. 2010.

[101] B. Mashadi and S. A. M. Emadi, "Dual-mode power-split transmission for hybrid electric vehicles," *IEEE Transactions on Vehicular Technology*, vol. 59, no. 7, pp. 3223 –3232, Sep. 2010.

[102] J. Liu and H. Peng, "Modeling and control of a power-split hybrid vehicle," *IEEE Transactions On Control Systems Technology*, vol. 16, no. 6, pp. 1242–1251, Nov. 2008.

[103] C. A. Perullo, D. Trawick, W. Clifton, T. J. C.M., and D. N. Mavris, "Development of a suite of hybrid electric propulsion modeling elements using npss," Proceedings of ASME Turbo Expo 2014: Turbine Technical Conference and Exposition, Germany, Jun. 2014.

[104] R. W. Claus, A. Evans, J. Lylte, and L. Nichols, "Numerical propulsion system simulation," *Computing Systems in Engineering*, vol. 2, no. 4, pp. 357–364, 1991.

[105] M. Drela, "Xfoil: an analysis and ddesign system for low reynolds number airfoils," *Low Reynolds number aerodynamics*, pp. 1–12, 1989.

[106] T. G. Puranik, E. D. Harrison, S. Min, I. Chakraborty, and D. N. Mavris, "A framework for general aviation aircraft performance model calibration and validation," AIAA AVIATION Forum, Atlanta, GA: AIAA, Jun. 2018.

[107] M. H. Amelink, M. Mulder, M. Van Paassen, and J. Flach, "Theoretical foundations for a total energy-based perspective flightpath display," *International Journal of Aviation Psychology*, vol. 15, no. 3, pp. 205–231, 2005.

[108] T. Puranik, H. Jimenez, and D. Mavris, "Energy-based metrics for safety analysis of general aviation operations," *Journal of Aircraft*, vol. 54, no. 6, pp. 2285–2297, 2017.

[109] B. Kumar, D. DeRemer, and D. Marshall, Eds., *An Illustrated Dictionary of Aviation*. The McGraw-Hill Companies, Inc., 2005.

[110] J. D. Anderson, *Aircraft Performance and Design*. The McGraw-Hill Companies, Inc., 1999.

[111] Cessna, *Cessna model 172r*, Dec. 1996.

[112] G. Cinar, Y. Cai, I. Chakraborty, and D. Mavris, "Sizing and optimization of novel general aviation vehicles and propulsion system architectures," 2018 Aviation Technology, Integration, and Operations Conference, AIAA AVIATION Forum, Atlanta, GA: AIAA, Jun. 2018.

[113] Lycoming, *Operator's Manual: O-360, HO-360, IO-360, AIO-360, HIO-360 and TIO-360 Series*, 8th ed., Williamsport, PA.

[114] SHELL, *Shell avgas 100ll piston engine aircraft fuel*, company website.

[115] M. D. Moore, "The Third Wave of Aeronautics: On-Demand Mobility," *SAE Technical Paper*, 2006, https://doi.org/10.4271/2006-01-2429.

[116] M. D. Moore, "Aviation Frontiers: On-Demand Aircraft," 10th AIAA Aviation Technology, Integration, and Operations (ATIO) Conference, Fort Worth, TX: AIAA, Sep. 2010.

[117] UBER, *Uber elevate mission and vehicle requirements*, [company website], URL: `https://www.uber.com/info/elevate/` [cited on 17 May 2018].

[118] Cessna Aircraft Company, *Pilot's Operating Handbook: Skyhawk Cessna Model 172N*, 1978.

[119] 328 Design GmbH, *Dornier 328-100 tp*, Company website, URL: http://328.eu/wp-content/uploads/2013/06/328-100-turboprop.pdf [cited 22 Nov 2016], 2013.

[120] R. Slingerland and S. Zandstra, "Green freighter systems," 46th AIAA Aerospace Sciences Meeting and Exhibit, Reno, Nevada, 2008.

[121] SAS, *Assess variable importance*, [user manual].

[122] M. Felix and J.-Y. Routex, "A copper bird for aircraft equipment systems integration and electrical network characterization," 45th AIAA Aerospace Sciences Meeting and Exhibit, Reno, Nevada: AIAA, Jan. 2007.

[123] B. W. Matthews, "Comparison of the predicted and observed secondary structure of t4 phage lysozyme," *Biochimica et Biophysica Acta (BBA) - Protein Structure*, vol. 405, no. 2, pp. 442–451,

[124] P. Baldi, S. B. Y. Chauvin, C. Andersen, and H. Nielsen, "Assessing the accuracy of prediction algorithms for classification: an overview," *Bioinformatics*, vol. 16, no. 5, pp. 412–424, 2000.

VITA

Gökçin Çınar was born in Ankara in 1990 and grew up in Izmir, Turkey. She received her Bachelor's of Science degree in Aerospace Engineering with high honors from the Middle East Technical University (METU) in June 2012. Upon graduation, she enrolled in the Doctor of Philosophy (Ph.D.) program and joined the Aerospace Systems Design Laboratory (ASDL) in the Daniel Guggenheim School of Aerospace Engineering at the Georgia Institute of Technology (Georgia Tech) in August 2012. She earned her Master of Science degree in Aerospace Engineering in December 2015. During her time as a graduate research assistant and then as a senior graduate researcher at ASDL, she worked on many projects including but not limited to system of systems analysis for fleet level assessment of NASA's Environmentally Responsible Aviation technologies, on-demand mobility studies, and thermal management systems for turboelectric aircraft. Her research interests include the conceptual and architectural design and performance optimization of novel vehicles, specifically electric, hybrid-electric and urban air mobility type aircraft. She was a member of the Georgia Tech-METU team which won the 29th Annual AHS/Industry Student Design Competition in the undergraduate category. She is a member of the American Institute of Aeronautics and Astronautics (AIAA) since 2010.